University of Southampton
School of Civil Engineering and the Environment

THE MECHANICS OF CONTINUOUS FLIGHT AUGERS IN CLAY

by
Martin Rust

A Thesis Submitted in Fulfillment of the Degree of Doctor of Philosophy
in the School of Civil Engineering and the Environment of the
University of Southampton

October 2003

Aan God, Michelle en ons families.

Acknowledgements

A special thanks and all my love to Michelle for joining me abroad and generally just putting up with me, and of course all the coffee (all the best with your own PhD). To my family and her family for support and understanding, especially dad for reading a lot of my work when it was still pretty much unreadable and giving so much advice. Katrien, for all the pap to make me strong.

The sponsors STENT foundations and the EPSRC, Norman, Jason and now Toby as well. Thanks for all the support and advice, enjoy the read.

Thanks Chris for being more than a supervisor and taking care of us (and for putting up with the Afrikanerisms). Harvey and Dave for the tremendous amount of work spent on building the rig. All the friends: Jo and Jon (for letting us stay at your place), Hennie (it all started one new-years morning whilst walking on the beach with a terrible hangover, teach your children well), Hannes, Toby, Joel, Jeff, Geoff, Yann, Ching-Li, Chris, Ming, Morgan and Irene, Sharach, Dominique, Teit, Abdullah, Siavash, Morris and everyone I've not mentioned and of course the loyal friends at home. You're always welcome at my place, especially if you have not yet tried the curry.

Rod and the running squad for helping me escape the computer screen enough to retain my sanity, get some miles in those legs!

"en iewers skyn die somer son op die velde van Transvaal"
Koos du Plessis

UNIVERSITY OF SOUTHAMPTON

ABSTRACT

FACULTY OF ENGINEERING
CIVIL AND ENVIRONMENTAL ENGINEERING

Doctor of Philosophy

THE MECHANICS OF CONTINUOUS FLIGHT AUGERS IN CLAY

by Martin Rust

By the late 1980's the method of Continuous Flight Auger (CFA) piling was the most popular method of manufacturing small diameter piles in the UK. The growth of this industry could mainly be attributed to its small environmental impact and speed of the procedure. The main disadvantage of CFA piles was the lack of predictability of their performance. This research has been concerned with improving the predictability of CFA pile behaviour in clay by using measurements made on a CFA auger penetrating into clay to gain information on the subsoil conditions. To achieve this aim, a thorough understanding of the mechanics of a CFA auger penetrating clay was required.

A small-scale CFA model was designed, built and instrumented to measure torque and axial load on several different augers in the laboratory. The design of the model was such that close control of the auger movement could be achieved. A technique was developed to prepare a stiff clay sample in the laboratory with uniform and repeatable properties. The model rig was then used to advance the augers into these clay samples. A valuable understanding of the mechanics of augers penetrating clay was gained from the analysis of the results obtained on the model rig. Results from the model tests were then used to recommend techniques of pile capacity prediction using improved instrumentation on the full-scale CFA rigs.

Contents

List of Tables

List of Figures

List of Symbols

Roman symbols

A_{aug}	surface area of the auger
A_b	surface area of the base of the pile
A_{fl}	surface area of one side of the auger flight for one pitch of the auger
A_p	surface area of the auger for one pitch of the auger
A_s	surface area of the shaft of the pile
A_{st}	surface area of the stem of the auger for one pitch of the auger
c_a	peak adhesion between clay and other materials
$c_{a(res)}$	residual adhesion between clay and other materials
c_b	undrained shear strength at the base of the pile
c_s	ultimate skin friction when using effective stress design
c_u	undrained shear strength
C_b	describes correlation between CPT tip resistance and pile base capacity
C_s	describes correlation between CPT tip resistance and pile shaft capacity
C_{sf}	describes correlation between CPT sleeve resistance and pile shaft capacity
$\overline{d}$	vector of vertical distance moved by the auger
d	depth below soil surface, or effective depth (Skempton, 1959)
d	auger stem (inner) diameter
D	auger outer diameter
E_{Ax}	energy dissipated by vertical movement of the auger

E_{Rot}	energy dissipated by rotational movement of the auger
E_{Tot}	total energy dissipated by the auger
f	resistance at the tip of the auger taking into account the cutting action at the tip of the auger flight, and the resistance to the penetration of the solid inner stem
f_{cut}	resistance to the cutting action at the tip of the auger flight
f_s	cone sleeve resistance
f_{st}	resistance to penetration of the inner stem of the auger
F	axial load applied to the auger
F_R	flighting force ratio (Fleming, 1995)
G_s	specific gravity of soil grains
I_z	first moment of area of the auger around the polar axis z
K	earth pressure coefficient
K_o	earth pressure coefficient at rest
K_p	earth pressure coefficient after pile installation
l	depth of the auger tip below the soil surface
L_0	circumference of the auger at radius r_0
L_{ave}	average auger lead as a percentage of the physical auger pitch
L_{full}	lead value required to ensure that the auger is totally filled with soil
$L_{\%}$	lead value of the auger as a percentage of the auger pitch
n_b	describes the correlation between SPT N value and pile base resistance
n_s	describes the correlation between SPT N value and pile shaft resistance
m	coefficient used to describe the relationship between auger energy dissipation and pile capacity
M	moment applied to the auger
N	bearing capacity factor (Skempton, 1959)
N	SPT N value

N	'stability number' (Taylor, 1948)
OCR	over consolidation ratio
p	auger pitch
p'	mean principal effective stress
P	the pitch of the auger (vertical distance between consecutive auger flight blades of a single helix)
q	shear stress invariant
q_c'	cone tip resistance
Q_b	pile base capacity
Q_s	pile shaft capacity
r	radius of the auger
r	coefficient used to describe the relationship between auger energy dissipation and pile capacity
r_t	weighted average of the distance of area of the auger from the polar axis
R	total number of revolutions of the auger
T	torque applied to the auger in the direction of auger rotation
V_{aug}	volume of the auger
V_{bore}	volume of the bore
W	weight of the auger
W	weight of the soil on the auger

Greek symbols

α	a reduction factor taking into account the difference between the undrained shear strength of the in-situ soil and the adhesion between the pile and clay shaft (Skempton, 1959)
α	angle of movement of soil on the auger with horizontal
β	angle of the auger flight with horizontal
γ	soil unit weight
δ	effective angle of friction between the soil and the pile shaft

$\overline{\theta}$	vector of angle of rotation of the auger in radians
ν	Poisson's ratio
σ'_h	horizontal effective stress
σ'_v	vertical effective stress
τ_m	shear stress on the bore wall caused by moment M
τ_f	shear stress on the bore wall caused by force F
τ_{aug}	shear stress on the auger surface
τ_{so}	shear stress between soil on the auger flight and soil surrounding the bore
τ_{tot}	total shear stress on the bore wall
ϕ	angle of internal friction of the soil
ϕ_{res}	residual angle of friction
ϕ_{rem}	effective residual angle of friction
ψ	angle representing the ratio of axial to rotational movement of the auger
ω	soil moisture content

Prefixes

μ	micro ($\times 10^{-6}$)
m	milli ($\times 10^{-3}$)
k	kilo ($\times 10^{3}$)
M	mega ($\times 10^{6}$)

Chapter 1

INTRODUCTION

1.1 Background

The American company "Intrusion Prepact" introduced augered cast-in-place (ACIP) piles to the market in the 1940's. The early system used a pipe to place grout in an open augered hole. At this stage pile depth was limited to 6m and diameters to 305mm. Raymond Patterson was granted a patent for the technique of placing grout through a hollow stem in the auger in 1956 (Lacy, Moskowitz and Merjan, 1994). Basically piles were formed by drilling a continuously flighted auger into the ground and, on reaching the required depth, pumping concrete down a hollow stem in the auger as the auger was steadily withdrawn. This basic methodology is still used today and is commonly referred to as Continuous Flight Auger (CFA) piling.

Today CFA piling is one of the fastest growing industries under the banner of geotechnical engineering. The use of CFA piles has increased to such an extent that it is now the most widely used method of constructing small diameter bored piles in the UK (Derbishire, Turner and Wain, 1989).

The growth of CFA piling may be attributed to several advantages that this method of piling has to offer over other traditional piling methods. The following advantages are listed in the literature (O'Neill, 1994) :

- The environmental impact of construction is much less than that of a

driven pile, both in terms of noise pollution and vibration.

- Speed of construction is greater than that of other bored cast in-situ piles, and as a consequence the cost of construction is often lower.
- In situations where the pile is to rely solely on skin friction, pile capacity is greater than that of bored cast in-situ piles for a given diameter pile.

Of these advantages the small environmental impact of CFA piling is the most important factor, as a very high proportion of piling projects is carried out in populated areas (Lacy et al., 1994).

The drawback of this method of pile installation however is the lack of reliability of the piles for load bearing capacity and serviceability limits, and the difficulty in predicting the pile performance (Fleming and Simpson, 1988; Lizzi, 1988; Modhorst, 1988; Neely, 1991). Currently defective piles can only be detected long after pile installation has been completed. Remediation has to be carried out and the cost thereof is often more than that of the original piling. If defective piles could be detected earlier the cost of remediation would be much less.

This project has been dubbed Just-In-Time pile design (JIT pile) and has been carried out jointly with Stent Foundations, a British company specializing in all types of deep foundation methods, and Lancaster University who have been involved in the instrumentation and data capture on the auger rig.

1.2 Objectives of the research

The research in this project is concerned with the gathering of data during the construction of a CFA pile and using this data for the prediction of pile performance. An understanding of the mechanics of an auger penetrating into soil is a crucial part of the development of such a system. The design and manufacture of a model rig to investigate these mechanics was therefore one of the aims of the project.

The following key aims were identified early on in the project:

1. A study of methods currently used to predict CFA pile capacity.

2. Analysis of data currently recorded on CFA rigs to establish if this data could be used to assess pile performance.

3. The development of a model CFA rig with good control of boring and the capability to accurately measure chosen parameters.

4. Assessment of the applicability of data recorded on the model CFA rig to providing information on pile performance.

5. Suggested instrumentation requirements and subsequent data analysis for a full-scale CFA rig.

1.3 Scope of the research

Initially a thorough literature review of all aspects of CFA piling was conducted, and time was spent on site studying CFA rigs in operation. Data gathered on these rigs was then analysed and compared to site investigation data.

The design of a small-scale model CFA rig was conducted using preliminary laboratory tests to obtain design values for forces likely to be applied to the auger and knowledge of the working of a full-scale CFA rig. An investigation into the soil to be used in the experiment (Speswhite kaolin clay) was carried out to determine material properties. Auger tests in the soil samples were then conducted to investigate the effect of the following variables on measurements taken whilst augering:

- rate of rotation of the auger,
- vertical penetration per revolution (lead) of the auger and
- size of the auger.

The data gathered were then analysed and recommendations were made as to which parameters would be useful if measured on the full-scale CFA rig.

1.4 Organization of the thesis

Chapter 2 is a literature review of bored and CFA piling with emphasis on pile design methods. A review on the development of specifications for CFA piling is also included.

Chapter 3 describes the CFA process in detail. Information for this chapter was gained both in the field and during the literature review. The analysis of the data currently recorded by the CFA rigs is discussed.

Chapter 4 details the experimental setup used to simulate CFA augering in the laboratory. Properties of the soil used in the experiments are given, the preliminary auger tests are discussed as well as the design of the model CFA rig. This chapter also contains a summary of the test results obtained from the model CFA rig. The results are not discussed or manipulated, only presented.

Chapter 5 is a discussion of all the work done during the project. Data from the model rig is discussed, and comparisons between test results are made. Methods are proposed for the estimation of pile performance and compared to methods currently in use in industry.

Chapter 6 draws conclusions from the test results and data analysis and a set of recommendations are made.

Two appendices are included in the thesis. Appendix A, wherein all the model CFA test results are given individually. Appendix B, wherein detailed derivations of all the formulae used in the thesis are given.

Chapter 2

LITERATURE REVIEW

As this research is aimed at improving predictability of CFA pile performance, a review of the current methods of pile design is included as well as a discussion of pile load test procedures used to check these design methods. A review of recent piling specifications with particular reference to the boring and monitoring of CFA piles is presented. Furthermore a detailed discussion of the paper published by Fleming in 1995 on the understanding of CFA piling is included. Certain case histories found in the literature are briefly discussed to illustrate particular points.

Chapter 3, "The CFA process", includes the part of the literature review relevant to that chapter.

2.1 Continuous Flight Auger pile design

The majority of design methods used for CFA piles were originally developed for more traditional bored pile design. There is some reason to believe that traditional bored pile design will yield a realistic estimation of CFA pile performance because of the similarity in construction methods. Both CFA and bored piles are classed as "replacement" piles by BS8004 (1986) however, several authors have commented on differences in the performance of traditional bored and CFA piles. van Weele (1988) found the base stiffness of CFA

piles greater than that of other bored piles, but less than that of driven piles. He concluded however that the prediction of a CFA pile's capacity was "not yet possible with sufficient accuracy". Part of the reason for this was thought to be the influence of the quality of the method of construction on the ultimate capacity. Fleming (1995) has provided the following remarks on the comparison between bored and CFA pile capacity based on his experience:

- On end bearing capacity: "Provided good construction techniques are used the end resistance of CFA piles is consistently good."... "The performance is generally better than found by similar means in other bored piles."
- On the shaft friction of CFA piles in sand: "Shaft friction in sand can be less than might be expected"... "This feature is inconsistent in the sense that when machines with higher power have been used and construction carried out as rapidly as possible, the results appear to become similar to those for other bored piles."
- On the shaft friction of CFA piles in stiff clay: "In stiff clays the shaft friction results appear to be marginally better than those for conventional bored piles"

These comments suggest that, except for the case of shaft friction in sandy material, the use of bored pile design for CFA piles will yield a conservative estimate of capacity. For the case of CFA piles in sand, potential sideloading onto the auger may reduce capacity (and in severe cases cause subsidence of adjacent structures, some case histories are discussed later in the chapter). Several methods for prediction of the capacity of bored piles have been developed and these will now be discussed. Three schools of thought are distinguished:

- total stress design,
- effective stress design and
- design based on in-situ test results.

The choice of design method is generally as described by Tomlinson (1994). In clay a total stress design, usually based on triaxial undrained shear strength or SPT data, is the most frequently used method. In cohesionless soil an effective stress design is usually employed. The required soil parameters and design calculations for the methods listed above will be discussed in this section.

2.1.1 *Total stress design*

The use of the undrained shear strength (c_u) for the prediction of pile capacity is a relatively simple method used commonly around the world, particularly for clays. Several authors have encouraged this method of design (Golder and Leonard, 1954; Skempton, 1959; Wright, 1979; Tomlinson, 1994; Bandini and Saldago, 1998) as well as BS8004 (1986). The method as described by Skempton (1959) developed for use in London Clay is still widely accepted. Authors such as Mohan and Chandra (1961) have shown that this method is applicable to some other parts of the world.

Soil parameters required for total stress design

The c_u versus depth profile of a site is required for total stress design. In his 1984 Rankine Lecture Wroth discussed the interpretation of in-situ soil tests. The following in-situ soil tests were rated as having a high applicability to measuring c_u:

- vane shear (for soft soils),
- self boring pressuremeter and
- self boring shear vane (an instrument no longer used in industry).

In the laboratory the unconsolidated undrained triaxial test is the standard test for measuring undrained shear strength. Wroth (1984) explained how the tests were fundamentally different. Differences such as the directions and freedom of rotation of the three principal stresses were highlighted. He

described the different test results as a hierarchy of undrained shear strengths, and concluded that "it is imperative for a designer to recognize this hierarchy, and to select a strength which is appropriate to the analysis or the design procedure being used". The pile capacity prediction developed by Skempton (1959) used c_u values measured by the unconsolidated undrained triaxial test. Burland, Butler and Dunican (1966) showed that laboratory triaxial tests yield up to 50% higher values for c_u than in-situ plate bearing tests. Furthermore Clayton, Matthews and Simons (1995) show that values of c_u determined from 38mm triaxial samples yield values of c_u that are 50% to 100% higher than those found from 100mm triaxial samples. For CFA pile design industry relies mostly on the unconsolidated undrained triaxial and/or the Standard Penetration Test (SPT) to obtain the c_u with depth profile.

The calculation of pile bearing capacity using total stress design

The end bearing capacity and shaft bearing capacity of the pile are calculated separately. The sum of these gives the ultimate bearing capacity of the pile. Two factors are applied to the ultimate bearing capacity in order to calculate the working load to ensure that the pile head displacement is within serviceability limits. These are the factor of safety and a factor that takes into account the interaction of piles in a group. The ultimate base bearing capacity Q_b is calculated using:

$$Q_b = NA_b c_b \tag{2.1}$$

Where A_b is the base area, c_b is the undrained shear strength at the base of the pile and N is a bearing capacity factor, usually taken as 9.

The shaft bearing capacity Q_s is calculated using:

$$Q_s = A_s c_a \tag{2.2}$$

Where A_s is the area of the shaft and c_a is the average adhesion between the clay and the pile shaft. It is appreciated that c_a will be less than c_u,

where c_u is the average undisturbed undrained shear strength along the pile of the shaft, therefore:

$$c_a = \alpha c_u \tag{2.3}$$

in which α is a reduction factor taking into account the difference between the undrained shear strength of the in-situ soil and the adhesion between the pile and clay shaft ($0 < \alpha < 1$).

Using case histories from several sites in London, Skempton (1959) established α to be 0.45 with a maximum variation of 30% for bored cast-in-situ piles. He advised the use of α equal to 0.3 for short piles with poor quality control and 0.6 under favourable conditions. The value of c_a should be kept below 2000lb/sq.ft. (96kPa). Mohan and Chandra (1961) found similar values for α from a series of tests conducted at four different sites in India. Bjerrum (1973) collated estimations of α values from several authors and showed that α is a function of c_u. He found that for soft clays (values of c_u less than 100kPa) α is in the order of 1, and as the clay gets stronger α decreases to a value of approximately 0.45 for c_u between 200kPa and 300kPa. For the case of CFA piles where quality control is of a high standard α may be somewhat higher than for bored piles (Fleming, 1995).

2.1.2 *Effective stress design*

The use of effective stress design for bored piles has been proposed by several authors (Chandler, 1968; Burland, 1973; Parry and Swain, 1977; Anderson, 1988). For clays the method is more complex than the total stress design, and therefore is only applied to contracts where detailed site investigation data is available. Effective stress design is generally used for the prediction of pile capacity in cohesionless soil because the concept of undrained shear strength is not applicable.

Soil parameters required for effective stress design

A profile of the effective angle of friction between the soil and the pile shaft (δ') with depth is required. For clays δ' is assumed to be equal to ϕ'_{res}, the remoulded angle of friction of the soil (Chandler, 1968; Burland, 1973; Parry and Swain, 1977) or ϕ'_{rem}, the angle of effective residual shear strength (Anderson, 1988; Burland and Twine, 1988). ϕ'_{res} can be measured in a shearbox or triaxial test apparatus using remoulded samples and effective stress soil testing and ϕ'_{rem} can be measured in a Bromhead ring shear apparatus.

The horizontal effective stress acting on the pile (σ'_h) is also required. As the vertical effective stress (σ'_v) is easily obtainable from the bulk density and hydrostatic profile of the soil, σ'_h is usually expressed as a ratio to σ'_v using the earth pressure coefficient K where:

$$K = \sigma'_h/\sigma'_v \tag{2.4}$$

The value of the earth pressure coefficient at rest, K_0, may be measured using the self boring pressuremeter. The pile installation will alter the value of K_0, and an assumption of how much the value has changed has to be made. Back analysis of carefully performed pile load tests provide a means of calculating the coefficient of lateral earth pressure on the pile (K_s), which has given an empirical basis for this assumption (Meyerhof, 1976; Burland and Twine, 1988).

The calculation of the shaft bearing capacity of piles using effective stress design

No effective stress method has been developed to predict the base resistance of a pile, the method discussed in Section 2.1.1 is often used in conjunction with the effective stress method discussed in this section. The following equation is used to calculate the shaft friction on a pile:

$$Q_s = A_s c_s = A_s \beta \sigma'_{vo} \tag{2.5}$$

where c_s is the ultimate skin friction, σ'_{vo} is the in-situ vertical effective stress, A_s is the shaft area, and

$$\beta = K_s tan\phi'_{res}{}^{1} \tag{2.6}$$

Values of K_s for bored piles in stiff clays vary from approximately $0.7K_0$ to $1.2K_0$ (values found for stiff fissured London clay by Meyerhof (1976)). Values of K_0 for normally consolidated soils (soft clays) may be estimated using the modified Jaky (1944) equation (Burland, 1973; Meyerhof, 1976; Parry and Swain, 1977):

$$K_0 = 1 - sin\phi'_{res}{}^{1} \tag{2.7}$$

and for overconsolidated soils the empirical equation suggested by Meyerhof (1976):

$$K_0 = 1 - sin\phi'_{res}{}^{1}\sqrt{OCR} \tag{2.8}$$

For bored piles Parry and Swain (1977) suggest using $K_s = 0.75K_0$, and thus β may be estimated using the equation:

$$\beta = 0.75 tan\phi'_{res}(1 - sin\phi'_{res}{}^{1})\sqrt{OCR} \tag{2.9}$$

Figure 2.1 is an illustration of the differences between the angles ϕ'_{res} and ϕ'_{rem}. ϕ'_{rem} is the value measured by the triaxial test at the point where no more volume change is measured in the sample. ϕ'_{res} is the value measured in the ring shear apparatus at large strain values. ϕ'_{res} is less than ϕ'_{rem} due to particle alignment parallel to the shear plane at large strain levels.

2.1.3 *Design using in-situ test results*

The use of the Cone Penetration Test (CPT) and Standard Penetration Test (SPT) results to predict pile capacity is commonplace throughout industry. "Penetration test results (SPT and CPT) are almost invariably the sole

[1] Anderson (1988) and Burland and Twine (1988) suggest replacing ϕ'_{res} with ϕ'_{rem}

data available to the design engineer" (Lopes and Laprovitera, 1988). Empirical relationships between in-situ measurements and pile capacity should be applied only under conditions similar to those under which they were determined. Bandini and Saldago (1998) compiled a review of correlations proposed to estimate the performance of piles using CPT and SPT tests. Other in-situ tests such as the vane, plate bearing and pressuremeter tests have also been used for bored pile design but not as frequently as CPT and SPT tests.

Cone Penetration Test (CPT)

The CPT test can be used to derive soil shear strength parameters and these values can be used to calculate pile capacity as described before (Meigh, 1987). Direct correlation between the cone resistance value (q_c') and both shaft and base pile resistance has been attempted by several authors (Meyerhof, 1956; Aoki and de Alencar, 1975; Schmertmann, 1978; Ruiter and Beringen, 1979; Philipponnat, 1980; Bustamente and Gianeselli, 1982; Lopes and Laprovitera, 1988), as well as direct correlation between cone sleeve friction (f_s) and shaft resistance (Schmertmann, 1978; Price and Wardle, 1982).

In general the ultimate base capacity (Q_b) of a pile may be directly related to the average cone tip resistance q_c' over a depth representative of the pile base.

$$Q_b = C_b q_c' A_b \tag{2.10}$$

The value of C_b correlates the cone resistance to pile base capacity and is principally governed by the pile type.

The ultimate shaft capacity (Q_s) of bored piles is related to the cone resistance q_c' along the pile shaft.

$$Q_s = \sum_{i=1}^{n} C_{si} q_{ci}' A_{si} \tag{2.11}$$

where C_{si} is a factor to convert from q_{ci} to shaft resistance for layer i.

The value of C_{si} is once again governed by the pile type and installation technique.

Schmertmann (1978) and Price and Wardle (1982) proposed expressions for relating shaft resistance (Q_s) to cone sleeve friction (f_s) as follows:

$$Q_s = \sum_{i=1}^{n} C_{sfi} f_s A_{si} \tag{2.12}$$

where C_{sfi} is a factor to convert f_s to shaft resistance for soil layer i.

Standard Penetration Test (SPT)

Because of its simplicity the SPT is possibly the most widely used in-situ test for predicting pile capacity. The test will generally provide a conservative estimate since poor execution of the test will generally under predict the in-situ soil strength (Byrne, Everett and Schwartz, 1995). The SPT N-value can be used to estimate the undrained shear strength profile. There are however methods of direct correlation of the SPT N-value with the ultimate base and shaft capacity. Several authors proposed correlation equations (Meyerhof, 1956; Aoki and de Alencar, 1975; Decourt, 1982; Meyerhof, 1983; Bazaraa and Kurkur, 1986; Lopes and Laprovitera, 1988; Hirayama, 1990). Bandini and Saldago (1998) have compiled a review of these. This section will give the general form of the equations used for pile design from SPT results. For numerical values of the correlation factors the original publications need to be consulted. As with the case of CPT correlations, these empirical correlations should only be used in conditions similar to those in which they were determined. Q_b and Q_s are usually predicted using the following equations:

$$Q_b = n_b N_b A_b \tag{2.13}$$

and

$$Q_{si} = \sum n_{si} N_{si} A_{si} \tag{2.14}$$

where n_b is a factor to convert the SPT N-value to base resistance, and n_{si} is a factor to convert the SPT N-value to shaft resistance for layer i.

In an attempt to produce CPT to pile capacity correlations, authors such as Lopes and Laprovitera (1988) have used the results obtained from the SPT and converted these to CPT q_c and f_s values using correlations available in the literature. This procedure adds uncertainty to the interpretation and derived correlations should be used with care, if at all.

2.1.4 *Factors of safety*

Different factors of safety are applied to piles to take into account the different uncertainties involved. Two classes of factors of safety are distinguished, those applied to calculate the maximum safe working load (ultimate load) and those applied to limit the settlement of the pile. The factors of safety prescribed in Eurocode 7 are also summarized.

Factors of safety applied to calculate the ultimate load

Jamiolkowski and Lancellotta (1988) state that partial factors of safety should be used to address:

- the importance of the structure,
- the consequence of a possible collapse,
- the nature of loads and their recurrence over the life-time of the structure,
- the reliability of the relevant soil parameters and
- the uncertainties in the analytical model(s) used to predict the performance of the design foundation.

Table 2.1 contains partial factors of safety for soil parameters for use in the design of bored piles (Jamiolkowski and Lancellotta, 1988). Wright (1979) compiled Table 2.2 showing the probability of failure of a bored pile foundation under normal design conditions for a given total factor of safety. The total factor of safety is the multiple of all the partial factors of safety.

Factors of safety applied to limit settlement

In order to satisfy the serviceability limit for pile settlement a factor of safety is applied to the ultimate load to calculate a safe working load where the pile will not settle more than is specified. Skempton (1959) advised the use of 2.5 for the factor of safety on the ultimate load of bored piles if group effects do not have to be taken into account. BS8004 (1986) states that this factor of safety should be between 2 and 3 depending on the following factors:

- quality and quantity of load test data and
- amount of local experience.

Slender piles have more elastic settlement and therefore a higher factor of safety is required. The structure itself may also influence this safety factor. A rigid structure will be able to redistribute the load between the piles, decreasing differential settlement, whereas a non-rigid structure will be subject to more differential settlement.

Other authors such as Bustamente and Gianeselli (1982), Decourt (1982) and Price and Wardle (1982) suggest the use of separate factors of safety for shaft resistance and end bearing, as end bearing on a bored pile is usually only mobilized after serviceability limits have been exceeded (for example Bustamente and Gianeselli (1982) recommend a factor of safety of 2 for shaft resistance and 3 for end bearing). Whitaker and Cooke (1966) conducted tests on bored piles in London Clay. They found that a settlement of between 0.5% and 1.0% of the pile diameter was required to fully mobilize the pile shaft capacity, and between 10% and 20% to mobilize base resistance.

van Weele (1988) compared load settlement characteristics at the bases of driven and CFA piles as well as piles cast under bentonite. He normalized base displacement with base diameter and found that, to mobilize 50% of the base capacity, the following displacements were required (the soil type was not specified):

- 0.8% to 1.0% for displacement piles,

- 2% to 3% for CFA piles and
- 3% to 5% for piles cast under bentonite.

Factors of safety in Eurocode 7 (1997)

Eurocode 7 specifies factors of safety specifically for CFA piling. These factors of safety are used to calculate the "ultimate bearing resistance" and are separated in two groups, those based on pile test results and those based on soil test results. The factors of safety derived from pile test results reduce with increase in the number of pile tests, whereas the factors of safety based on soil test results are fixed. An additional factor of safety is required to limit the settlement of the pile.

Ultimate bearing resistance based on pile load tests

The "ultimate characteristic bearing resistance" (R_{ck}) is derived from the values of one or more pile load tests (R_{cm}) where:

$$R_{ck} = R_{cm}/\xi \tag{2.15}$$

Values for ξ are given in Table 2.3.

In order to derive the "ultimate design bearing resistance" (R_{cd}), the characteristic value should be divided into shaft (R_{sk}) and base resistance (R_{bk}) components:

$$R_{ck} = R_{bk} + R_{sk} \tag{2.16}$$

Partial factors of safety are then introduced to calculate R_{cd}:

$$R_{cd} = R_{bk}/\gamma_b + R_{sk}/\gamma_s \tag{2.17}$$

Values for γ_b and γ_s are 1.45 and 1.30 respectively for the case of CFA piling . In cases where the shaft and end resistance have not been measured separately the total characteristic value should be divided by factor γ_t which is 1.40 for CFA piling.

Ultimate bearing resistance based on ground test results

The ultimate design bearing resistance, R_{cd} is again split up into shaft resistance and base resistance as in Equation 2.17. The shaft and base resistances are then divided by γ_b and γ_s which are 1.45 and 1.30 respectively as before. The ground test results referred to in Eurocode 7 are penetration tests such as the SPT or CPT.

2.2 Pile load tests

Bustamente and Gianeselli (1982) state that in their experience prediction of pile bearing capacity within 20% of the measured load is difficult. Therefore load testing of piles on site is essential to verify the design calculations and assumptions. Although most pile tests are designed to measure the pile capacity, careful testing procedures and monitoring can yield good approximations for the stiffness of the pile response. Pile load tests will be split into three groups for discussion:

- static pile load tests,
- dynamic pile load tests and
- non-destructive testing.

2.2.1 *Static pile load tests*

BS8004 (1986) states that preliminary piles should be installed in all cases except when extensive local experience is available or high factors of safety are employed. A large variety of different static pile load tests are offered by the industry, and different tests can produce significantly differing results. The ideal load test would be one that closely simulated the actual loading of the pile during and after construction. However, for practical reasons it is desirable to carry out tests in a shorter time than the construction period. Several methods of increasing the rate of loading of a pile in a load test have been suggested. A brief discussion of some of these tests will be given, as

well as a more detailed discussion of more recent advances in pile testing as described by England and Fleming (1994).

The ASTM designation D-1143 (ASTM, 1974) describes a "standard loading procedure" (which has also been known as the maintained load test) in which the pile is loaded in eight equal increments up to a maximum load, usually twice the predetermined allowable load. Each increment is maintained until "zero" settlement is reached, defined as 0.25mm/hr. The final load is maintained for 24 hours. This load testing method is time consuming, requiring from 30 to 70 hours to complete.

Mohan, Jain and Jain (1967) proposed a method of speeding up this procedure by allowing the pressure in the jack to drop rather than being maintained by pumping. The equilibrium load is taken as the applied load. Hounsel (1966) proposed that each of the eight increments be maintained for one hour exactly regardless of settlement. This greatly reduces the time required to complete the test. From this philosophy the "quick maintained load" (quick ML) test was developed by Butler and Hoy (1977). In this method one should aim for up to 40 increments at short but constant time intervals. Fellenius (1980) states that where drained conditions are desirable the duration of load tests should be "measured in weeks, months or even years" which is not a viable option. He then adds that while the piles are being loaded undrained the procedure might as well be speeded up even more.

A quick test which is popular in Europe is the Constant Rate of Penetration test (CRP test), proposed by Whitaker (1957), Whitaker and Cooke (1961) and Whitaker (1963). The pile is forced into the ground at a constant rate while the load is monitored. Whitaker (1963) proposed a rate of 0.76mm/min (0.03in./min) for friction piles in clay, and 1.52mm/min (0.06in/min) for end bearing piles in sand or gravel. Current ICE specifications (ICE, 1996) prescribe a rate of 0.6mm/min in clays and 1.2mm/min in cohesionless soils. The test is terminated if the pile head movement is 50mm to 75mm (ideally when an asymptote parallel to the settlement axis on the load settlement graph is reached). BS8004 (1986) describes the test as good

for determining the ultimate pile bearing capacity, but not the stress-strain behaviour of the pile.

It has been shown by Whitaker and Cooke (1966), Bjerrum (1973), Burland and Twine (1988), Patel (1992) and others that the effect of increase of the rate of penetration is to enhance pile shaft capacities in clay soils, and the same result is likely for a wider range of soils and also for pile base capacities. "All rapid pile testing methods".. "suffer from similar problems in trying to relate true static and enhanced resistances" (England and Fleming, 1994).

Cyclic testing of piles has been discouraged by authors such as Fellenius (1980) and England and Fleming (1994). They argue that the ultimate load settlement behaviour of the pile will be severely influenced, making it impossible to predict the load settlement behaviour of the pile. England and Fleming (1994) recommend the use of cyclic testing only in special cases such as silo foundations.

The current ICE specification (ICE, 1996) calls for the loads to be applied in stages of 25% of the design verification load (DVL[1]) to a load of $DVL + 50\%\ SWL$, where SWL[2] is the safe working load. There is provision for the load to be extended to higher load when appropriate. Minimum holding times for increase of load vary from 30 minutes to 6 hours.

England and Fleming (1994) and England (1994) have developed refinements to be used with the ICE specifications to enhance the quality of the test results. Computerized load control through a feedback loop, as well as computerized load and settlement monitoring increases the accuracy of the load settlement graph. The need for constant supervision is diminished, and data are produced in electronic format. This enables extrapolation of the load-settlement response to infinite time, representing fully drained conditions. Formulae based on accurate test results have been developed to separate the

[1]a load which will be substituted for the Specified Working Load for the purpose of a test and which may be applied to an isolated or singly loaded pile at the time of testing in the given conditions of the site

[2]the specified load at the head of the pile as stated in the relevant particular specification

shaft friction and end bearing capacity on the basis that each component can be represented by a hyperbolic function. The elastic shortening of the pile, which may be significant in slender piles, is also taken into account by these formulae. Test results of this quality enable the engineer to make an estimation of the load-settlement response of a pile.

The definition of the ultimate load of a pile is a source of confusion as different authors have produced their own definitions. According to England and Fleming (1994) and Fleming (1995), Terzaghi advocated the definition of the ultimate load as an asymptote parallel to the settlement axis on the load-settlement diagram. Other definitions usually define the ultimate load as a load at a given settlement, such as 10% of the base diameter as specified in BS8004 (1986). Friction piles usually reach their ultimate load before this point but end bearing piles often require more settlement to reach an asymptotic load. The difficulty in straining a pile more than 10% of its base diameter has led to the establishment of this empirical value. Several methods have been proposed for the interpretation of static load test data. A review of these has been carried out by Fellenius (1980) and will not form part of this thesis.

Tension load tests may be of use where the shaft capacity of a pile is required, or where a pile may be subjected to uplift. In some compression test cases, piles are installed to provide the reaction to the compressive load. These piles are in tension and provide useful information if monitored. Care has to be taken to install reinforcement to the tip of the pile for tension tests.

2.2.2 *Dynamic pile load tests*

Dynamic pile load tests have their origin in the field of preformed driven piles. The hammer used for driving the pile provides a convenient means of generating large input forces on the pile. Similar systems have been developed for bored piles. Wave equations developed from Smith (1960) are used to interpret the results.

Dynamic tests suffer from the same disadvantages as quick static load

tests. England (1994) and England and Fleming (1994) reasonably state that dynamic tests do not reveal the unique long-term pile behaviour or a pile's ultimate capacity. The application of these tests have however been the subject of extensive debate. Chiesura (1998) argues that the larger number of test results adequately compensate for the inaccuracy of the results. Svinkin and Woods (1998) argue that the disparity in static and dynamic test results is a result of the time delay between the respective tests causing consolidation in the surrounding soil, altering the pile capacity. ENV1997-1 (1997) states that "The design shall be based on one of the following approaches":

- the results of static load tests,
- empirical or analytical calculation methods or
- the results of dynamic load tests whose validity has been demonstrated by static load tests in comparable situations.

2.2.3 *Non-destructive (integrity) pile load testing*

Due to the limitations, both from a logistic and economic point of view, of testing a representative sample of working piles using static load testing as described above, non-destructive integrity test methods have been developed to aid in the detection of defects in the structural integrity of pile shafts. The results from integrity tests are subject to interpretation and should only be used to provide an initial assessment of pile integrity. If any defects are detected they should be investigated further using load testing procedures.

The sonic impact test is carried out by propagating a sonic wave down the pile while a transducer, capable of measuring sonic wave reflection, is held to the head of the pile. The sonic wave will be reflected by the toe of the pile or by any intermediate structural defects of the pile. The reflected wave is logged (referred to as a reflectogram) and analysed. Any major structural defects in the pile should show on this record as these will reflect the sonic wave. If no defects are detected, a clear response from the base will enable

the engineer to check the length of the pile. The ideal condition to use this test in is a short pile with high end bearing capacity. If however the pile is slender (length/diameter > 45) and/or has high shaft friction the wave will be damped and a clear reflection will not be obtained.

Other methods of integrity testing involve lowering a transmitter and receiver down separate tubes in the pile. This method is particularly popular in France Fenoux and de Buysere (1988). A minimum of 2 tubes of 50mm diameter are lowered into the pile with the reinforcement. According to Fenoux and de Buysere (1988) it is difficult to install the tubes into small diameter piles.

2.3 Stress distribution along a pile shaft

Snow (Fall 1965) described the use of "telltales" in piles. These are rods inserted in one or more tubes down to different depths in the pile. Accurate measurement of the differential settlement of these will yield information of the stress distribution along the pile shaft and base. Alteratively vibrating wire or electrical resistance strain gauges can be used. These are fixed to the reinforcement cage. The top gauge is placed close to the top of the pile, and the output of this gauge is then used as a reference to which the other straingauge outputs are compared. Barker and Reese (1970) have developed a cell specifically for internal instrumentation of a bored pile. Such cells are designed to give high electrical output at small strains.

Figure 2.2 after Reese and O'Neill (1988) shows a typical set of load distribution curves from internally instrumented pile test results conducted on bored cast in-situ piles. Results from a suite of tests conducted on CFA piles by ?) show that the shape of the stress distribution on CFA piles is similar to that found on traditional bored piles. The authors show that the pile stiffness response is influenced by installation procedures and conclude that the behaviour of CFA piles is intermediate between traditional bored and driven piles.

By analysis of this data, and the load settlement response of the pile cap, the load transfer characteristics of any point on the pile shaft, as well as the base, may be obtained. This information is invaluable for the understanding of the working of piles. However it is not used in any of the pile design methods discussed earlier in the chapter. Consideration of the stress distribution along a pile shaft of a pile should increase the accuracy of pile performance prediction.

2.4 Pile load-settlement characteristics

The pile design formulae described at the beginning of this chapter have been developed to estimate the total capacity of a pile. Serviceability limits on the settlement however necessitate the use of high factors of safety as discussed in Section 2.1.4, as the total pile capacity will only be mobilized at high strain levels. A pile design method which uses soil stiffness has not been developed. This is because commonly used site investigation equipment cannot measure soil stiffness accurately, and also because the stiffness is affected severely by the pile installation. Burland et al. (1966) have shown that settlement can only be predicted within broad bands.

According to Fleming and England (2001) attempts to relate soil stiffness to shear strength are common. For the case of overconsolidated clay, soil stiffness is commonly quoted as 150 to 400 times the undrained shear strength. They have proposed the values in Table 2.4 for use as a first estimate of pile base stiffness (defined as the settlement at 25% of the ultimate (asymptotic) load). These values were determined from a significant number of results of tests on CFA and other piles and are also valid for bored piles. Fleming and England (2001) also add some values for the ratio of base stiffness to ultimate pile capacity given in Table 2.5.

2.5 A review of recent piling specifications with specific reference to boring and monitoring phases of CFA pile construction

The following recent specifications have been reviewed:

- BS8004 (1986), British standard code of practice for foundations,
- ICE (1988), Institution of Civil Engineers, specification for piling,
- ICE (1996), Institution of Civil Engineers specification for piling and embedded retaining walls and
- ENV1997-1 (1997), Eurocode 7: Geotechnical design (1997) .

Amongst these ICE (1996) has the most detailed specification on CFA piling. It is interesting to note how the specifications for CFA piling have developed over the relatively short period of approximately 10 years.
The following recommendations are made in BS8004 (1986):

- CFA piling requires continuous supervision and good site investigation (SI) data because the borehole cannot be inspected.
- Care should be taken when boring in loose sand to prevent the inflow of loose sand into the bore.
- Valuable information on site conditions may be obtained by monitoring the boring phase.

The ICE Specifications for Piling, published in 1988, provided a standard document for the range of different piling construction techniques commonly used in the UK. The updated specification released in 1996 includes retaining walls and new developments in piling practice. The following guidelines for the boring phase of CFA construction were given in the 1988 specification (ICE, 1988):

- Vibration and noise caused by piling should be kept within current environmental legislation.

- Possible damage to adjacent structures and piles is to be monitored.
- Augers shall not be extracted from the ground in such a way as to leave an open unsupported bore.
- Piles shall be bored using "suitable" equipment, capable of penetrating the ground without drawing in soil adjacent to the bore.
- Any failure of a pile to reach the required depth shall be reported with a full statement of reasons.
- The base of the auger should be fitted with a suitable means of sealing against ingress of water and soil until boring commences. This device is to be removed by concrete pressure and care should be taken to ensure that the auger is lifted only enough to initiate flow of concrete.
- The rate of withdrawal of the auger, injection pressures and the rate of supply of concrete should be measured. Care should be taken that the rate of concrete supply is enough to fill the bore and create a monolithic shaft.

The following guidelines were then added in the 1996 edition of the ICE specifications (ICE, 1996).

- The maximum permitted deviation of the finished pile from the vertical is 1:75.
- The contractor shall make a record of when flighting of soil up the auger is excessive.
- Lengths of auger shall not be joined together during boring, nor split during extraction.
- If rotation of the auger occurs during auger extraction it shall be positive (i.e. in the same direction as the auger was rotated during penetration).
- An automated system for monitoring the construction of piles shall be provided.
- The following parameters are to be measured:
  - auger penetration rate (in incremental time steps),

  - rate of extraction of the auger (time taken for every 0.5m extraction),
  - relative injection pressure of concrete,
  - rate of supply of concrete or grout (volume injected every 0.5m),
  - time from start to end of construction including any delays and
  - the direction of drilling during extraction.

- The rig operator shall be competent and experienced in the construction of CFA piles.
- A full-time experienced supervisor shall be devoted to pile construction.
- The automated monitoring system must be operational at the start of every pile.
- If the number of auger revolutions relative to the auger penetration becomes abnormally high this fact shall be recorded, as well as excessive flighting.

Eurocode 7 (ENV1997-1, 1997) is a general geotechnical design guideline and does not have any section specifically intended for CFA piling. The following quote is intended for all methods of pile construction and has particular relevance to CFA pile construction: "The records of the installation of the test pile(s) should be checked, and any deviation from the normal execution conditions should be accounted for."

2.6 Possible capacity reducing effects due to the augering phase of CFA pile construction

Installation of piles may affect the integrity of the pile itself or soften/loosen of the in-situ soil surrounding the auger. Cases of pile integrity defects are well documented and will not be discussed in this thesis (Hodgon, 1991; Tomlinson, 1994; Fleming, 1995).

Defects that occur in the surrounding soil strata are not as well documented or understood. Three mechanisms causing softening/loosening in the surrounding soil are discussed:

- stress relief in the surrounding soil,
- remoulding of a thin layer of soil directly in contact with the pile shaft and
- softening the surrounding soil due to water migration from the fresh concrete.

Figure 2.3 is a diagram showing where weakening of the soil might occur.

2.6.1 *Stress relief in the surrounding soil*

CFA rigs do not have the torque capacity to advance the auger at one pitch per revolution (van Weele, 1988; Fleming, 1995). Neely (1991) suggests 1.5 to 2.0 revolutions per pitch penetration, whilst Lacy et al. (1994) have described a case history where a significant decrease in displacement of an adjacent structure was achieved by reducing the rotation per pitch penetration of the auger from 20 to 2 (discussed in detail in Section 2.10). As far as the author is aware there exists no guideline on how much torque and winch capacity a rig should have for a given diameter auger and soil type. Therefore the engineer will only find out what the maximum vertical penetration per revolution (lead) of a rig is when it is on site and augering commences. The low capacity rigs however are cheaper to buy and have lower running costs, therefore a contractor with a low capacity rig can tender a lower price. This has resulted in the low capacity of CFA rigs throughout industry (van Weele, 1988). Fleming (1995) concludes from case histories and a mathematical model of the auger transport mechanism (Section 2.8) in a cohesionless soil, that the penetration rate of the auger should be such that maximum available torque on the CFA rig is mobilized. He adds that "low powered machines are not suitable for many sandy ground conditions".

Ground conditions where an unstable layer overlies a hard layer are particularly hazardous. Stress relief in the unstable material will occur when the auger is rotated excessively whilst penetrating the harder layer due to the weaker material being transported to the surface. In severe cases material from the side of the bore may then fall onto the auger (known as sideloading) causing further stress relief in the surrounding soil (van Weele, 1988). Additionally sideloading may cause subsidence of the soil surrounding the auger, possibly damaging adjacent structures. Rotation on withdrawal of the auger is another disputed issue as more sideloading could occur at this stage but rotation may also help keep the spoil on the auger flights. van Weele (1988) discourages any rotation of the auger on withdrawal.

Stress relief in the surrounding soil strata can also take place without sideloading, especially in highly overconsolidated fissured clay such as London clay, as the reduction in in-situ stress allows the opening of fissures in the clay. The fact that the hole is never totally unsupported and that the CFA pile manufacturing process is fast, decreases the stress relief in soils with low permeability compared to the stress relief caused by bored cast-in-situ piling in similar soils where the hole may sometimes be left open and unsupported for some time. There is evidence that the soil strata will reestablish some or all of the initial horizontal effective stress with time (Milititsky, 1983; Anderson, 1988).

In cases of severe potential sideloading (usually in granular soils with a high horizontal effective stress), a system where a casing is advanced just behind the tip of the auger has been developed. This procedure is discussed by Brons and Kool (1988) and others.

2.6.2 *Remoulding of a thin layer of soil surrounding the pile*

Remoulding of a thin layer of soil as result of the auger reworking the soil surrounding the hole whilst augering may affect the performance of the pile (Figure 2.3). If thin intermittent layers of sand and clay are present in the

strata this effect is more severe as wet sandy clay forms when the two layers mix (Milititsky, 1983). Excessive rotation of the auger should be prevented as doing so would increase this effect.

2.6.3 *Water migration from the concrete to the surrounding soil*

When the concrete is placed the water from the concrete migrates into the surrounding soil, softening the soil. Meyerhof and Murdock (1952) found an increase in moisture content for up to two inches (51mm) away from the edge of the concrete. An increase in moisture content of up to 7% in the London clay was measured. A significant decrease in strength of in-situ soil has been measured as result of the water migration from the concrete to the soil (Milititsky, 1983; van Weele, 1988).

2.7 Physico-Chemical effect of cement on clay

The addition of cement to clay changes the physio-chemical properties of the clay. These changes are brought about by the lime (CaO) present in the cement. Two processes are commonly distinguished (Boardman, Glendinning and Rogers, 2001), an immediate (modification) and a long term (solidification) effect.

The hydration process between clay and lime is highly exothermic and utilizes water, which results in a decrease in moisture content of the clay. High concentrations of calcium (Ca^2) and hydroxide (OH^-) ions are present in the pore water of clay that is in contact with concrete. Modification of the clay occurs due to a cation exchange between the calcium ions present in the pore water and cations at the negative charge sites on the clay mineral lattice. At the same time, the hydroxide ions increase the pH of the pore water, which further promotes this reaction. Flocculation of clay minerals occurs and the plasticity properties of the clay are changed. As the lime content of the clay

increases the plasticity of the clay decreases (Rogers, Glendinning and Roff, 1997).

Solidification of the clay occurs as a result of pozzolanic reactions. The alkaline nature of the pore water (due to the presence of the hydroxide ions) causes the silica and aluminum ions to dissociate from the edge sites of the clay plates (Sherwood, 1993). These then react with the dissolved calcium ions in the pore water to form calcium silicate hydrate (CSH) and calcium aluminate hydrate (CAH) compounds which crystallize over a period of time. Solidification of the clay is characterized by an increase in shear strength, decrease in permeability and further changes in the plasticity of the material.

Both of these processes, should result in an increase of pile capacity.

2.8 Review of Fleming (1995), "The understanding of continuous flight auger piling, its monitoring and control"

Augers are used for several applications throughout industry. Their main use is as screw conveyers in the mining, agricultural and materials (mainly plastics and ceramics) industries. Mathematical models on how these screw conveyers work have been under development for some time.

Fleming (1995) studied several of these models and proposed a mathematical model more suitable to an auger advancing into soil, taking into account the bulking of soil and displacement of the auger in the soil matrix. The model was specifically developed to estimate when flighting (the transport of soil up the auger flight) would occur on an auger in a cohesionless soil (soil with an insignificant clay content). A "flighting force ratio (F_R)" is calculated as the ratio between forces inducing and forces resisting flighting of soil up the auger. If F_R exceeds unity, flighting of soil will occur.

Forces are calculated for the situation when no flighting of soil occurs, and the penetration of the auger per revolution (lead) of the auger is equal

to the auger pitch. In this situation soil will move upward on the auger flight as a result of the displacement of the auger volume into the soil and as a result of bulking of the in-situ soil. Soil is assumed to act as a continuous ribbon and the following three forces acting on the soil ribbon are calculated:

1. the self weight of the soil,
2. the force due to friction on the auger flight and
3. the force at the bore wall between soil on the auger flight and soil outside.

The first two forces impede the transportation of soil up the auger flight and the third force is the only force attempting to force soil upwards on the auger flight (i.e. friction caused on the boundary between soil on the auger flight and soil surrounding the auger may cause soil on the auger to slip on the auger surface and in severe cases move upward on the auger). In order to calculate the force between soil on the auger flight and outside the auger flight, the lateral earth pressure is required. Fleming (1995) used work by Terzaghi (1944) for estimating the lateral earth pressure necessary to maintain a stable bore wall. The following general findings are listed:

1. The occurrence of excessive flighting is more likely with large than with small diameter augers.
2. Flighting of soil becomes more difficult as the flight angle is steepened.
3. Excessive flighting becomes less probable as the angle of friction of the soil external to the auger increases.

Terzaghi (1944) showed that as the size of the bore increases, the force required to stabilize the bore increases. This is due to more effective arching in smaller diameter bores. Because of this phenomenon the lateral earth pressure on the bore wall increases as the auger size increases, causing an increase of the force between the bore wall and soil on the auger flight (the

force attempting to force soil up the auger flight). Flighting is therefore more likely in large diameter bores.

The finding that flighting becomes more difficult as the flight angle steepens was reached because a smaller pitch length used in the calculation of F_R, keeping all the other variables constant, reduces F_R. However the analysis does not take into account the fact that fewer turns per pitch penetration of the auger will be required, another variable required in the calculation. If the ratio of auger pitch to the number of turns per pitch penetration is kept constant, F_R remains constant. This finding is therefore incorrect and should read "Flighting of soil becomes more difficult as the ratio of the auger pitch to the number of penetrations required for one pitch penetration increases".

The third finding also stems from work by Terzaghi (1944) as he found that a bore would be more stable if the angle of friction of the soil outside the bore increased.

2.9 Modification of Fleming (1995) for undrained conditions

The model proposed by Fleming is a valuable addition to the literature and adds to the understanding of the mechanics of CFA augers however, inaccurate the assumptions and basic the model. The application of the theory to a soil of low permeability is relatively simple. If the same forces are calculated by using the remoulded undrained shear strength behaviour of a clay some understanding may be gained on the mechanics of a CFA auger in clay.

The first observation when doing the calculation is that the stability of the bore does not influence the magnitude of the force at the bore wall between soil on the auger and the surrounding soil. This is due to the fact that the soil shear stress in an undrained case is independent of normal stress.

As the area of the bore wall is a function of the auger diameter (D) and the area on the auger flight is a function of the square of the auger diameter (D^2), the force resulting from friction on the auger flight increases more

rapidly than the force resulting from friction on the bore wall as the auger diameter increases. An increase in diameter in this case will thus decrease the amount of flighting up the auger.

When the auger pitch reduces, the surface area on the auger increases however, the area of the bore wall stays constant. A lower pitch angle will therefore cause less flighting.

The following general comments summarize the findings found by modifying the model proposed by Fleming (1995) to represent an auger in clay.

- The stability of the bore wall does not affect the potential for the flighting of soil.
- An increase in auger diameter reduces the likelihood of soil flighting.
- A lower flight angle reduces the likelihood of the flighting of soil up the auger.

We may conclude from a comparison of the results from the two cases of an auger penetrating in sand and clay:

on increasing the auger diameter: more flighting in sand, less flighting in clay;

on increasing the flight angle: less flighting in sand, more flighting in clay.

2.10 CFA pile case histories

Some case histories have been extracted from the literature to highlight some of the common characteristics and problems associated with CFA piles. If available, details of the method of construction and soil profile are given as well as remarks made by the original authors

Couldery and Fleming (1986): Continuous flight auger piling at St. Enoch square, Glasgow

Couldery and Fleming (1986) describe a case history at a site in Glasgow. Two trial piles were constructed at the site and both failed at less than 1.75 times the working load. It was concluded by the authors that poor control during the concreting phase was one of the main reasons for the defects. To remedy the situation a target over-supply of 26% was specified and a single start auger was used instead of a double start auger to stop 'choking' of the auger. The following seven trial piles performed adequately. Authors advise the use of an experienced contractor.

Case 1: Site in Glasgow, U.K.
Soil profile:

Depth	**Soil description**
0 - 2.5m	Fill
2.5 - 6.0m	medium dense fine to medium Sand (SPT N = 16 - 26)
6.0 - 16.0m	firm or stiff silty Clay, laminated
16.0 - 30.0m	Sand and Gravel (SPT N = 20-60)
30.0 to 32.0m	very stiff sandy Clay, some gravel
32.0 to 35m	bedrock

Remarks: The rig used to construct the trial piles was only capable of 5.6tm (50kNm, an 8tm machine working at 70% of its capacity). The rig was not capable of penetrating to the design pile depth for a 750mm diameter pile (refusal at 23m). Although the pile failures were structural, over-rotation in the laminated silty clay and sand and gravel layers may have decreased the shaft bearing capacity as well.

Fleming (1995): Two examples to show reduced shaft capacity of CFA piles in sand

Fleming (1995) describes the back analysis of two piles in sand (Case 2 and 3). These cases are specifically used to show that CFA piles may have a low shaft friction in sand if construction is not carried out carefully. A normal value for K_s after construction of bored piles is in the region of 0.7.

Case 2: Site in Stafford, U.K.
Soil profile:

Depth	**Soil description**
0 - 4.5m	made ground
4.5 - 8.0m	silty clayey Sand (SPT N = 10 blows per 300mm)
8.0 - 24.0m	clayey silty Sand (SPT N = 10 - 20 blows per 300mm)

Remarks: K_s was determined through back analysis of load test results and a value of 0.3 was obtained. The reason for K_s being as small is believed to be excessive rotation of the auger in the sand.

Case 3: Site in Belfast, U.K.
Soil profile:

Depth	**Soil description**
0 - 4.3m	made ground
4.3 - 7.0m	soft organic clayey Silt
7.0 - 14.7m	Sand and Gravel (SPT N = 17 - 32 blows per 300mm)
14.7 - 17.0m	stiff laminated sandy silty Clay
17.0 to 19.5m	stiff sandy silty Clay with cobbles

Remarks: The value for K_s was determined through back analysis to be of the order of 0.45. Again the disturbance of the sand and gravel by excessive rotation of the auger is the reason for the low value of K_s.

Lacy, Moskowitz and Merjan (1994): Effect of workmanship on pile performance and the impact of CFA piles on adjacent structures

Lacy et al. (1994) discuss several case histories around New York city. Cases 4 and 5 have been selected from the original publication:

Case 4: Two nearby sites in Southern Brooklyn, New York city, USA
At the first site a pile was installed 15m into the bearing stratum and tested to 150t (1334kN), 3 times the design load without failure. At the second site a different contractor was used. Piles were constructed to reach 12m and 15m into the bearing stratum respectively. The piles extending 12m into the bearing stratum failed at 90t to 125t (801kN to 1112kN). The pile extending 15m into the bearing stratum failed at 110t (979kN).

Remarks: The authors concluded that "a contractor's technique for installing this type of pile is more important than small variations in soil density and grain size of the soil in which the pile is installed".

Case 5: "Protecting an old sewer", New York city, USA
Soil profile:

Depth	**Soil description**
0-4m	compact fine Sand
4-17m	compact Silt
17-20m	varved Silt

Groundwater 1m above pile cap (piling in an excavation)

Remarks: Inclinometers were installed next to the sewer that was to be protected. Production started using a "low-torque, high rotation-rate gear box" on the piling rig. Augers were rotating "as many as 20 times per advance of 1 auger pitch". The grout volumes pumped into the piles were in the region of 200% of the nominal augered hole. Significant movements were recorded in inclinometers installed nearby as shown in Figure 2.4 (redrawn

after Lacy et al. (1994)). Piling was stopped and a turntable with a larger torque capacity (43kNm) was provided. Rotation was reduced to less than 2 revolutions per advance of one pitch. The grout take decreased to 160% of the nominal augered hole. The movement as recorded by the inclinometers was significantly less (Figure 2.4).

Lacy et al. (1994) compiled a list of case histories specifically to show the reduction in the settlement of adjacent structures when using CFA instead of several types of driven piles. In all the cases presented the settlement of the structure was significantly less than that due to pile driving. The reason for settlement of adjacent structures due to pile driving was that the "vibrations from the pile driving densified the sand". The soil in every case was silt or sand with an average SPT N-value of between 20 and 45.

Table 2.1: Partial factors of safety for soil parameters (after Jamiolkowsy and Lancellotta (1988))

Partial factor for:	Level of confidence [1]		
	Good	Normal	Poor
Angle of shear resistance	1.15	1.15	1.25
Undrained shear strength	1.50	1.60	1.66
Unit side resistance of piles	1.60	1.70	1.85
End bearing resistance of piles	1.54	1.62	1.77

Table 2.2: Probability of failure of bored piles under normal design conditions (after Wright (1979))

Probability of failure (%)	Factor of safety	Structure classification
0.005	2.50	monumental
0.01	2.20	permanent
0.05	2.00	permanent
0.1	1.85	temporary
0.5	1.65	temporary

Table 2.3: Factors ξ to derive R_{ck} (ENV1997-1 (1997))

Number of load tests	1	2	>2
(a) Factor ξ on mean R_{ck}	1.50	1.35	1.30
(b) Factor ξ on lowest R_{ck}	1.50	1.25	1.10

[1]Depending on both the quality of the tests and the control during the installation of piles

Table 2.4: Estimation of CFA pile base stiffness, defined as settlement at 25% of the ultimate load (after Fleming and England (2001))

Description (Grade)	Stiffness (MN/m^2)
Clays	
Very soft	3
Soft	3 to 6
Firm	6 to 15
Stiff	15 to 25
Very stiff	25 to 40
Hard	>40
Marls, shales or mudstones	
Zone I	150 to 300
Zone II	100 to 200
Zone III	50 to 100
Zone IV	20 to 75
Sands and gravels	
Very loose	<15
Loose	15 to 30
Medium dense	30 to 150
Dense	100 to 300
Very dense	250 to 300
Chalk	
D (structureless)	< 100
C (apertures > 3mm)	100 to 200
B (apertures < 3mm)	150 to 250
A (discontinuities closed)	> 250

Table 2.5: Ratio of the base stiffness to the ultimate pile capacity (after Fleming and England (2001))

Soil	Base stiffness/Ultimate capacity
Clays	25
Mudstone	10
Sands and gravels	10

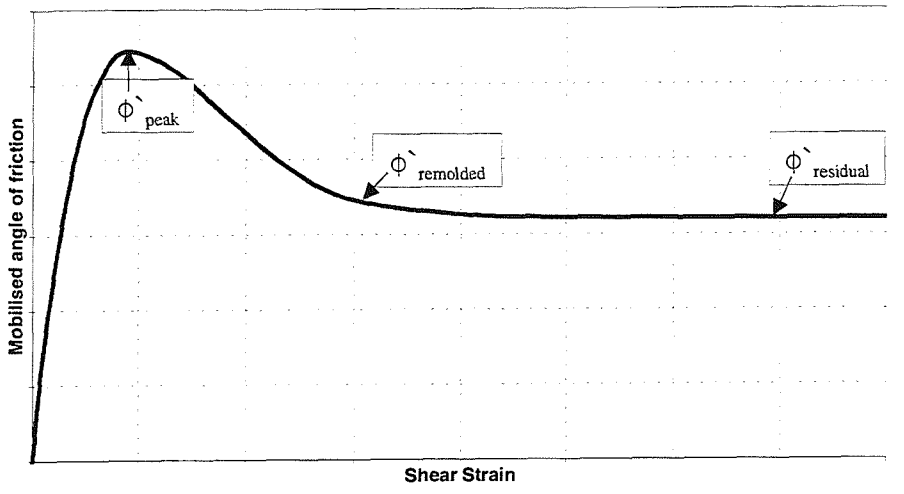

Figure 2.1: The mobilized effective internal angle of friction of soil

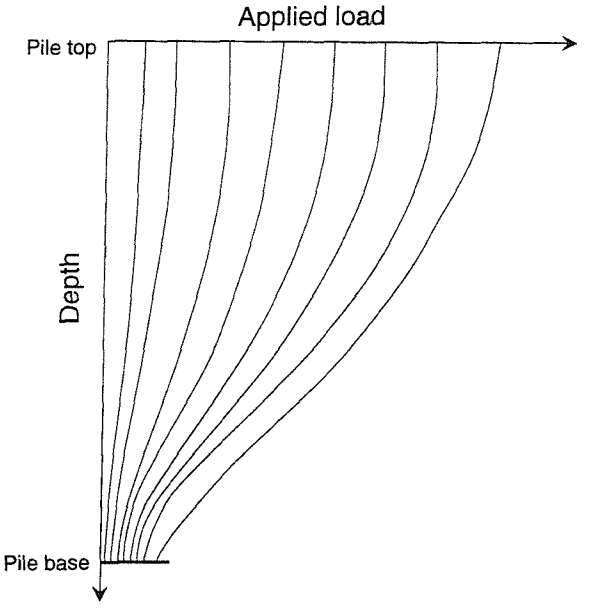

Figure 2.2: Typical stress distribution along a pile shaft (after Reese and O'Neill (1988))

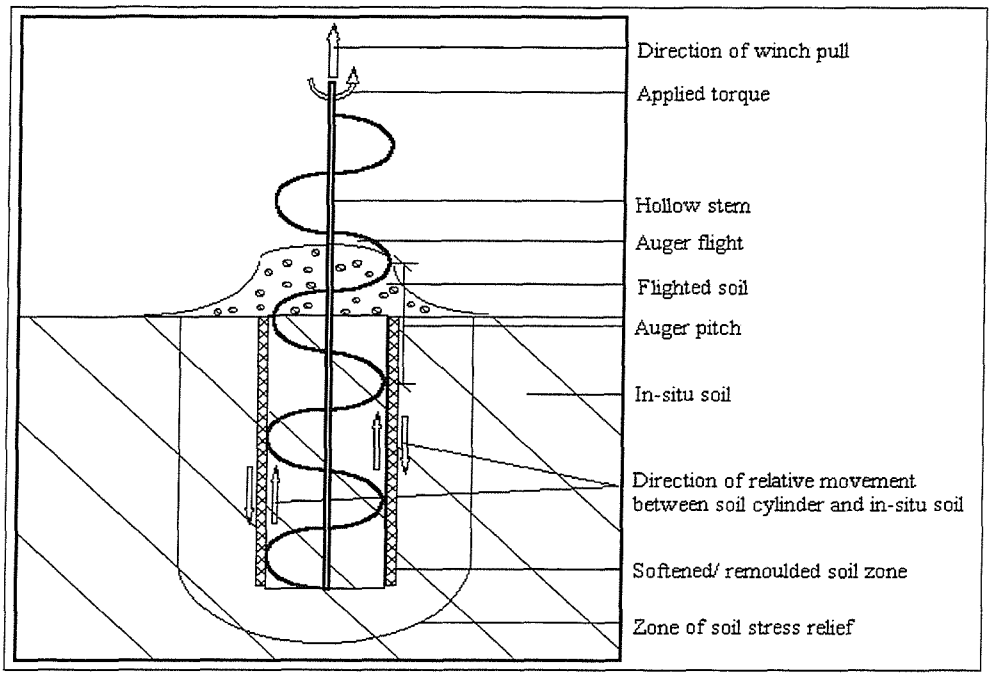

Figure 2.3: An illustration of the augering process

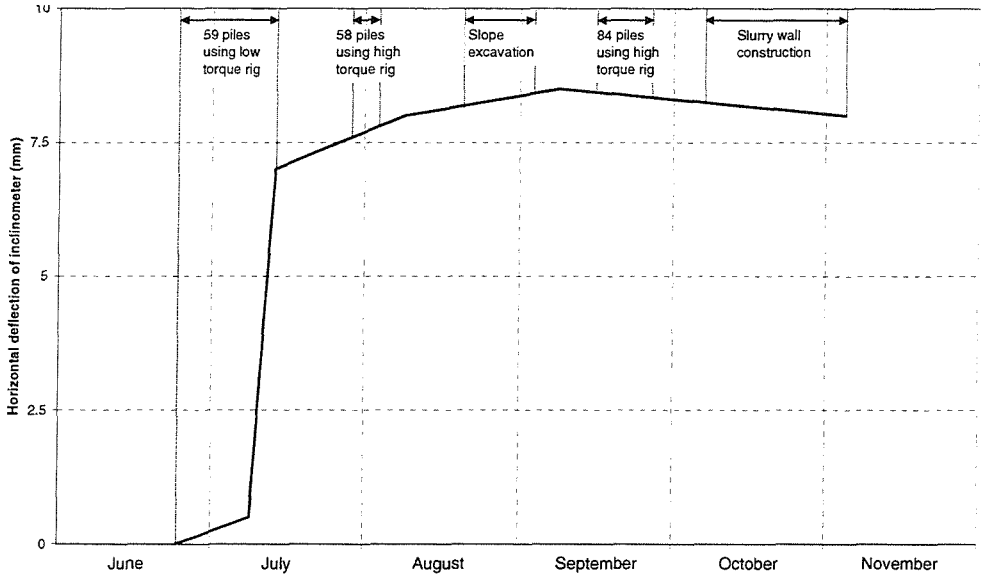

Figure 2.4: Deflection of an inclinometer installed close to the construction of CFA piles (after Lacy et al. (1994))

Chapter 3

THE CFA PROCESS

This chapter describes the CFA rig and the CFA pile construction process. Sources of information for this chapter have been the observation of CFA rigs during pile construction, discussions with piling specialists and rig operators and articles from the literature. Analysis of the data recorded on a CFA rig is included, using data supplied by Stent Foundations, UK.

3.1 CFA piling equipment

CFA equipment available from different manufacturers may differ somewhat in design however, all have the same basic components. These components will be split up into two sections in this chapter; the basic mechanical and hydraulic equipment and the rig instrumentation system. The CM48 CFA rig is used as an example, as data from this rig will be analysed in the chapter.

3.1.1 *Basic mechanical and hydraulic equipment common to CFA rigs*

Figure 3.1(a) is an illustration of the basic mechanical and hydraulic equipment used in the construction of CFA piles. Two separate systems may be distinguished; the auger drive system and concrete supply system.

The power for the auger drive system is supplied by a diesel engine on the CFA rig. This diesel engine drives the hydraulic pump, which in turn drives both the winch and the rotary table on the rig. The winch cable is connected to the top of the auger to enable it to pull the auger upwards. The rotary table is a hydraulic motor driven by the pressure and flow of hydraulic fluid supplied by the hydraulic pump through the high-pressure hoses. The rig thus has the capacity for turning the auger and pulling it upwards. In some cases CFA rigs have the capability of pulling the auger downwards (often referred to as 'crud' in the industry) however, this is more the exception than the rule.

A concrete pump separated from the main rig drives the concrete supply system (Figure 3.2). The concrete is pumped through a pump line up to the swan neck and down through a hollow stem in the auger. A 'clack' is used to block the hollow stem of the auger when the auger is being advanced into the soil (Figure 3.3). When the auger reaches the required depth, concrete pressure from within the stem forces the clack open which allows concrete out of the auger stem. Some contractors prefer the use of a watertight rubber bung instead of a clack. Positioning of this bung at the side of the auger is sometimes employed to help prevent blockages in the auger stem.

Values for CFA rig torque in the literature

As the CFA rig torque capacity is widely believed to be important in the assurance of quality of the pile, values of rig torque quoted in the literature were noted and listed in Table 3.1. The list was included to draw attention to the wide variation in torque capacities of the different rigs.

3.1.2 *CFA rig instrumentation systems*

According to Fleming and Simpson (1988) the development of CFA instrumentation systems has been driven by a lack of reliability of CFA piles. After the development of instrumentation, CFA piles have had improved reliability

and cases of pile failures could be investigated to help prevent similar occurrences in the future. Several different manufacturers have developed their own rig instrumentation systems, and some piling contractors their own in-house designs. The different systems however have similar characteristics. A general instrumentation description common to most instrumented CFA rigs follows (Fenoux and de Buysere, 1988; Derbishire et al., 1989; England, 1994; O'Neill, 1994; van Impe, van Impe, Viggiani, Russo and Bottiau, 1998).

In Figure 3.1(a) numbers have been added to indicate the various positions where measurement devices are usually situated and these will be referred to in the following two paragraphs. Instrumentation is usually installed on the CFA rig to measure the amount of concrete pumped through the stem of the auger. This is done either by counting the strokes of the concrete pump (by counting the pressure surges in the concrete pump line) or by installing a flow meter on this pump line (No. 1 in Figure 3.1(a)). Non-invasive flow meters are used (i.e. a device that does not require contact with the flowing material) which rely on either Doppler or electromagnetic techniques. As the flow of concrete in the pipeline is complex an accuracy of $\pm 3\%$ is expected when using a flow meter (Derbishire et al., 1989). The flow meter is believed to be more accurate in its measurement as the pump does not always deliver the same amount of concrete per stroke and the pressure transducer sometimes misses the pressure surge and thus does not count every stroke. The advantage of the stroke counting method however is the robust nature of the equipment, making it more reliable. Another pressure transducer may be installed in the concrete line at the top of the swan neck (No. 2) since contract specifications often require the pressure measured by this transducer to remain positive in order to ensure a continuous pile shaft (Couldery and Fleming, 1986).

In addition the depth of the auger (No. 3) and the amount of revolutions made by the auger are measured (No. 4). The revolution counter usually records every quarter revolution. The oil pressure supplied by the hydraulic pump is also measured (No. 5). The torque transmitted to the auger will have

some relationship with this pressure measurement however, measurement of flow in the hydraulic system is also required to obtain an accurate estimate of torque applied by the hydraulic table.

Brons and Kool (1988) have suggested additional instrumentation for a CFA rig. This includes pressure measurement at the tip of the auger, combined with an electronic feedback loop, to ensure a given target pressure is achieved at the tip of the auger. They also discuss the insertion of a CPT inside the hollow stem of the auger to get pile specific data at the tip of the pile.

Derbishire et al. (1989) describe the development of a series of probes to be attached to the auger to check the continuity of concrete in the stem of the auger. These probes can give an output of "concrete present" indicating a continuous concrete column, with "concrete passing" indicating a discontinuous stream of falling concrete, and an output of "no concrete" indicating a void in the auger stem. Another recent development is aimed at controlling the penetration rate of the auger through feedback of the torque being applied (Fleming, 1995).

England (1994) shows how instrumentation and data logging is an invaluable management tool whereby the performance of a particular rig or crew may be assessed in terms of productivity, materials wastage, etc.

As a part of the research project, direct measurement of torque and axial load on the auger was developed at Lancaster University. This development was still in progress at the time of submission of this thesis.

3.1.3 *The CM48 CFA rig*

The CM48 CFA rig is used by Stent Foundations with their SIRIS (Stent Integrated Rig Instrumentation System) program aimed at developing their own in-house CFA instrumentation system. The power rating for this rig is discussed, as the data captured on this rig will be analysed later in this chapter.

The engine on the CM48 rig is a 5.9 litre Cummins diesel, the 6BTA5.9C

'Elite'. The setting power of an engine is the power supplied at the lowest fuel consumption, achieved at an optimum rpm. The setting power rating for this engine is 116kW @ 2100rpm, and the maximum power output is 134kW @ 2500rpm. Usual practice is to run the motor at its setting power as this will require the least maintenance and fuel.

The hydraulic pump on the rig has a constant power rating of 93kW, a maximum pressure rating of 350bar and 250bar when in gear. This suggests an efficiency of 80% from the engine to the pump. The pump is geared but the same constant power rating is given for all three of the available gears, indicating that the pressure increases as the flow is decreased. The rig operator has control of gear changes.

The torque available from the rotary table for different rotational speeds in one of the gears of the rotary table is shown in Figure 3.4. This figure has been redrawn from a figure supplied by Soilmec, the manufacturers of the CM48 auger rig. The upper boundary for the torque supply is assumed to be a pressure limit, and the upper boundary on the rotational speed is assumed to be a flow limit in the system. The non-linear part of the curve has been drawn for a constant power supply of 73.3kW. If constant power output is assumed then the rate of rotation must decrease as the torque increases and vice versa, hence the non-linear shape of the curve. The efficiency from the hydraulic pump to the rotary table is approximately 79%. The torque from the rotary table is directly transmitted to the auger.

3.2 CFA construction procedure

The CFA piling procedure has become popular because it is less time consuming than other methods of pile construction and has low noise and vibration levels. This construction procedure will now be discussed. Two phases are distinguished, the augering and the concreting phase.

3.2.1 *Augering phase*

Advanced instrumentation systems ensure that the auger is in the right position to start drilling, and that the auger is vertical (Seward, Scott, Dixon, Findlay and Kinniburgh, 1997). The auger guide (Figure 3.1(a) and Figure 3.5) is closed to ensure the auger does not deviate from this position when drilling commences. The hydraulic pump is engaged in low gear and the auger is slowly advanced 1m to 2m into the soil. The auger guide is opened and the hydraulic pump is engaged in a higher gear. The auger is then advanced into the soil until the torque required to turn the auger reaches a target torque (or rather the pressure in the hydraulic line reaches a target system pressure). At this point the winch is activated to hold the auger back, allowing the auger to rotate without penetration. This action ensures that the soil on the flights and directly adjacent to the bore is remoulded (Figure 2.3), the required torque will decrease and the auger is allowed to penetrate further. This process is repeated until the auger reaches the required depth. In this way an underpowered CFA rig may drill a hole sufficiently deep for the pile manufacturing requirements (model auger tests discussed later in the thesis show the reduced torque requirement when augering by this method). The operator dependence of the pile capacity is partially due to the technique employed during augering, as some operators will remould the soil to a lesser extent than others.

3.2.2 *Concreting phase*

Once the auger has reached the required depth the concrete pump is started. Usually concrete pressure forces the clack open. Some operators lift the auger slightly to help the clack open. This procedure has been discouraged by van Weele (1988) and others as it may influence the pile base stiffness and bearing capacity. They suggest that if the auger must be raised to open the clack, the resulting void below the auger should be filled with concrete and the auger advanced back to its maximum depth with the clack open.

Next the auger is steadily withdrawn and slowly rotated in the direction it was rotated during auger advance in an effort to keep the spoil on the auger flight (referred to as positive rotation in the industry). This procedure has however been discouraged by van Weele (1988) and Fleming (1995), especially in sandy soils, so as to avoid sideloading during extraction (Section 2.6.1). These authors suggest a single 360° rotation of the auger before it is withdrawn to ensure a clean pile base, and then the withdrawal of the auger without rotation. ICE (1996) requires the rotation of the auger to be positive during extraction or not at all and measurement of the number of rotations per half metre extraction is required.

Using knowledge of the diameter and the depth of the auger the theoretical volume of concrete required to fill the void below the auger is calculated. This is compared with the volume of concrete pumped through the stem measured by flow meter or pump stroke count and shown on a monitor within the rig cab (Figure 3.6). The auger is withdrawn at a rate slow enough to ensure that the volume of concrete pumped through the stem is greater than the theoretical volume required. The proportion of the excess concrete to the theoretical volume is termed the concrete oversupply. On most contracts the oversupply is specified to be in the order of 20% (Fleming, 1995), depending on the soil properties. The excavation of CFA piles after construction often show that concrete flowed laterally into the surrounding soil[1]. Furthermore the pressure measured by the pressure transducer at the swan neck is kept positive in an attempt to prevent voids and defects being formed as a result of the undersupply concrete in a particular part of the pile (often referred to as 'pile necking' in the industry). In soft clays this pressure may be excessive, causing expansion of the auger hole. When the auger tip is close to the surface concrete may start flowing up the auger flights to the surface. Pressure measurement at this stage is of no use and the pile is constructed using concrete flow as the only indicator.

[1]This is due to the mechanism described as hydrofracture, which occurs when the concrete fluid pressure exceeds the smallest total principle stress in the soil matrix

When the tip of the auger reaches the soil surface the CFA rig moves away and a back actor removes the spoil generated by the process (Figure 3.7). A reinforcement cage is lowered into the concrete-filled hole by hand, except in the cases of large diameter piles where the back actor lowers the reinforcement cage into the concrete-filled hole and pushes the reinforcement into the pile (Figure 3.8). During a single shift a CFA rig can produce 10 to 25 piles depending on pile size, soil conditions and the experience of the operator.

Wastage of a significant amount of concrete because of a lack of communication between the rig and the pump operator is a common problem on CFA piling projects. A possible improvement to the rig would be to give the CFA rig operator the control of the concrete pump.

3.3 Analysis of existing data

Data captured on site on the CM48 rig as described in Section 3.1.3, have been analysed to gain a better understanding of how CFA rigs operate on site as well as investigating whether the feedback from the transducers installed at present may be producing useful information on subsoil conditions. Data recorded during the augering phase (Section 3.2.1) of pile construction were analysed.

The output recorded during the augering phase was obtained from a revolution counter, depth monitor and pressure gauge on the hydraulic hose. Data were recorded as comma separated values containing measurements of:

- depth (m),
- hydraulic system pressure (bar),
- number of revolutions (no., the sign indicating the direction of rotation) and
- time (s).

A program was written in Visual Basic to analyze large numbers of pile construction records. The data were filtered to remove pauses in excess of 10s in the augering process (for example the opening of the auger guide). The following parameters were calculated:

- rate of penetration (m/min),
- rate of rotation (rpm) and
- lead of the auger (as % of auger pitch advanced per revolution).

An assumption was made to obtain a rough estimate of the rig power consumption. It was assumed that 93kW of power is utilized when the measured pressure is 250bar, as described in Section 3.1.3, and that power and pressure are directly proportional. The fact that flow in the hydraulic hose was not measured makes an accurate estimation of the rig power consumption impossible however, given the data available this was the best estimate.

Furthermore, using site investigation data a rough estimate of pile capacity versus depth was made using pile design techniques described in the previous chapter. Total stress design was used in clays and effective stress design in cohesionless soils. The design values and assumptions are documented under the respective case histories.

A discussion of the results obtained will be conducted in Chapter 5.

3.3.1 *ExCel site in the London dockyards*

The following simplified soil profile of the site has been obtained from cross sections of borehole records produced during the site investigation. Depth of soil layers varied considerably in different trial pits, but the depth of the top of the London clay at 13.3m remained constant.

Depth	**Soil description**
0 to 10.0m:	Sand and Gravel with some clay zones (made ground)

10.0 to 13.3m:	Gravel (River terrace deposits)
13.3 to 21.5m:	stiff becoming very stiff fissured Clay (London Clay)
21.5 to 35.0m:	very stiff sandy Clay or very dense Sand (Woolwich and Reading beds)

Because of the wide scatter found in the site investigation data as shown on Figure 3.9, the simplified soil profile was used to estimate pile shaft capacity with depth (attempts at design lines on the graphs illustrate the difficulty in the analysis of the site investigation data). An effective stress design calculation was used to a depth of 13.3m (Section 2.1.2), and a total stress design below this depth (Section 2.1.1). The following values were assumed for the effective stress calculation:

- bulk density $= 18kNm^{-3}$,
- $K_0 = 1$,
- $K_s = 0.75K_0$ and
- $\phi = 30^o$.

For the total stress calculation values of c_u for London clay from Skempton (1959) were used to produce a second order polynomial of c_u versus depth. The polynomial used was:

$$c_u = -0.13d^2 + 13.2d + 55.8 \tag{3.1}$$

where d is the 'effective depth' in metres as described by Skempton (1959) and c_u is measured in kPa. The value of α was assumed to be 0.45 (Equation 2.3). Figure 3.10 shows how the pile capacity prediction for a 350mm diameter pile varies with depth.

Energy dissipated by the auger rotation was estimated using measurements of the hydraulic system pressure. Figure 3.11 shows the energy dissipation with depth profile obtained from the construction records of several 350mm piles. Note that there is an increase in the rate of energy dissipation with depth at approximately 14m, which corresponds to the soil profile changing from medium dense sand and gravel to stiff London clay.

If pile capacity prediction and auger energy graphs are combined, a pile capacity versus auger energy use graph can be obtained as shown on Figure 3.12. This graph contains the data from 8 pile construction records. The distribution of the energy-depth data is shown on Figure 3.13, created using all of the 350mm records available on ExCel site (a total of 53). The pile capacity value predicted when 8MJ of energy had been used by the rig was used to produce the histogram. Characteristics of this distribution and the reliability of using this method are discussed in Section 5.3.3.

Using revolution and time data recorded on the rig, an average rate of rotation was calculated for every 3 rotations of the auger as shown in Figure 3.14(a). The wide scatter of data suggests that either the rate of rotation of the auger varies rapidly during augering, and/or the recorded data were not reliable. It is apparent from Figure 3.14(a) that the rate of rotation of the auger on this site decreased with depth. Between depths of 5m and 20m, the rate of rotation decreased from approximately 29rpm to 24rpm on the 350mm auger, and from 32rpm to 20rpm on the 450mm auger.

Depth and time measurements recorded on the rig were used to calculate the rate of penetration of the auger at 0.5m intervals as shown in Figure 3.14(b). Again a wide scatter of data was found, especially at the start of penetration. The scatter becomes less with depth, suggesting that the measurements are accurate because the scatter would have remained constant if it was a result of inaccurate data. Figure 3.14(b) shows that the rate of penetration of both the 350mm and 450mm augers at this site reduced with depth however, a change in the data trend seems apparent at approximately 14m depth. This depth coincides with a change in soil strata. It seems that

the auger penetrates slower into the clay matrix, and the rate of penetration is more constant.

By using the rotation and depth measurements the leads of the augers were calculated. As a result of the resolution of both sensors being low (1rpm and 125mm) the lead calculated using these two measurements yields a low resolution (approximately 10% of the physical auger pitch). The average lead over three revolutions of the auger was calculated and is shown in Figure 3.14(c). Lead values for both augers decline with depth, and it seems as if the 350mm auger initially penetrates at a larger lead value. The rate of decline of the lead value for the 350mm auger seems to greater than for the 450mm auger.

3.3.2 *Brentford site in West London*

The following simplified soil profile of the site has been obtained from cross sections of borehole records produced during the site investigation.

Depth	**Soil description**
0 to 2.0m:	made ground including Clay and Gravel
2.0 to 3.5m:	Firm brown silty sandy Clay (London Clay)
3.5 to 20.0m:	Stiff to very stiff slightly silty Clay (London Clay)

As the profile consists almost entirely of London clay, a total stress design was employed to predict the pile capacity on the site (see Section 2.1.1). The second order polynomial derived in the previous section to describe the relationship between depth and undrained shear strength in the London Clay from data by Skempton (1959) was again used (Equation 3.1). The value of α was assumed to be 0.45. Figure 3.15 shows how pile capacity prediction varies with depth on the Brentford site.

Energy dissipated by the auger rotation was estimated using measurements of the hydraulic system pressure. Figure 3.16 shows the energy dissipation with depth profile obtained from the construction records of several

350mm piles. Eleven pile construction records are shown, 8 of which seem to have used a similar amount of energy during augering, while 3 of the piles seemed to have required more energy. It is not clear what caused this increase in energy use, it may have been due to local variations in soil conditions or the auger might have been penetrating at a very low lead value (¡15% of the pitch), at which the auger model results in Chapter 4 show that energy use increases.

If pile capacity prediction and auger energy use graphs are combined, we can plot a graph of pile capacity versus auger energy use as shown in Figure 3.17. This graph contains the data from 8 pile construction records. The distribution of the energy-depth data as shown by Figure 3.18, created using all of the 350mm records available on the Brentford site (a total of 114). The pile capacity value predicted when 8MJ of energy had been used by the rig was used to produce the histogram.

The same methods as in the previous section were used to produce graphs of:

- the rate of rotation with depth (Figure 3.19(a)),
- the rate of penetration with depth (Figure 3.19(b)) and
- the lead values with depth (Figure 3.19(c))

for the 300mm, 350mm and 450mm augers used on this site.

The data from the Brentford site shows a similar scatter to that found on the ExCel site. Again it is not clear whether this scatter is a result of unreliable data or a rapid variation in the auger rate of penetration and rotation during auger penetration.

Figure 3.19(a) shows that the rate of rotation of the augers decreased with depth, and that the larger augers were rotated at greater speed. The rate of rotation of the augers decreased from 28rpm to 24rpm and 18rpm for the 450mm and 350mm augers respectively, and from 26rpm to 13rpm for the 300mm auger between 5m and 19m. The rate of penetration of the augers

on the Brentford site remained fairly constant with depth at approximately 1.8m/min as shown on Figure 3.19(b).

Auger lead values calculated from the logged data show significantly higher lead values for the smaller augers used on the site, and interestingly the auger lead values for the small diameter augers increased with depth. The 350mm and 300mm auger lead values increased from 17% and 21% to 21% and 33% respectively between 5m and 15m. The 450mm auger lead seemed to remain relatively constant at 13%. As the rate of penetration (m/min) of the auger did not vary significantly the increase in lead of the smaller augers is attributable to the decrease in the rate of rotation of the augers.

Table 3.1: Values of CFA rig torque in the literature

Author	Description	Rig torque (kNm)
1	Maximum torque available in 1988	226
2	Starsol Enbesol (French system)	88
3	Early rigs	9.8
	Common in 1995	78 - 98
	Large in 1995	147 - 196
4	Large inner diameter auger	100 - 150
5	Rotation less than 2 revolutions per pitch for 457mm auger (c_u between 25kPa and 90kPa)	43

1 Derbishire et al. (1989)

2 Fenoux and de Buysere (1988)

3 Fleming (1995)

4 van Weele (1988)

5 Lacy et al. (1994)

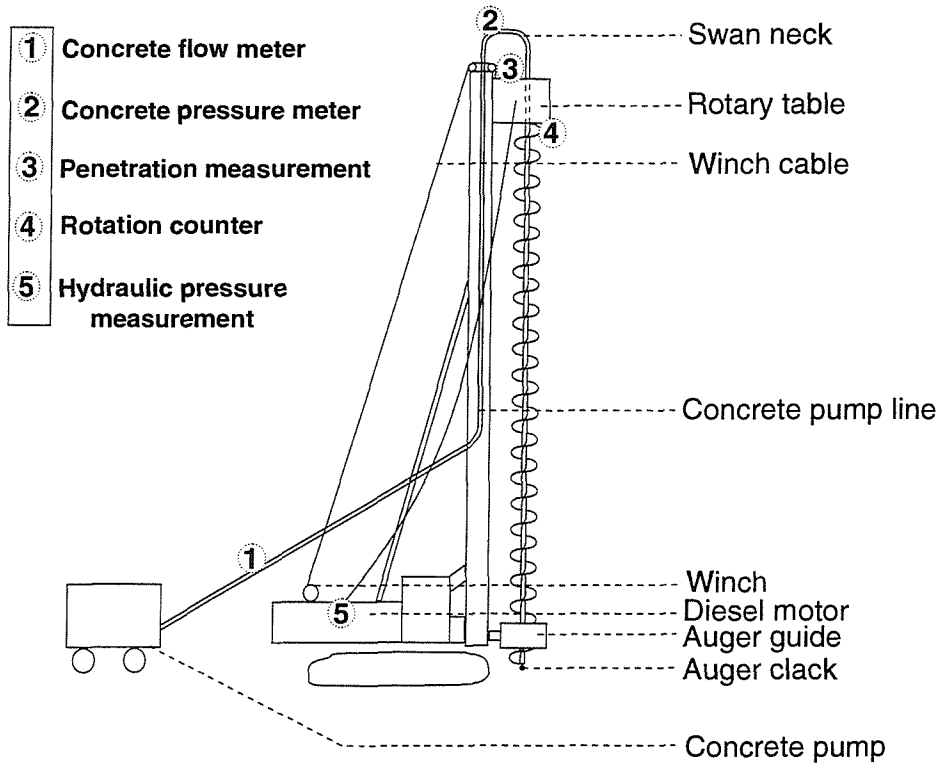

(a) Illustration of a CFA rig

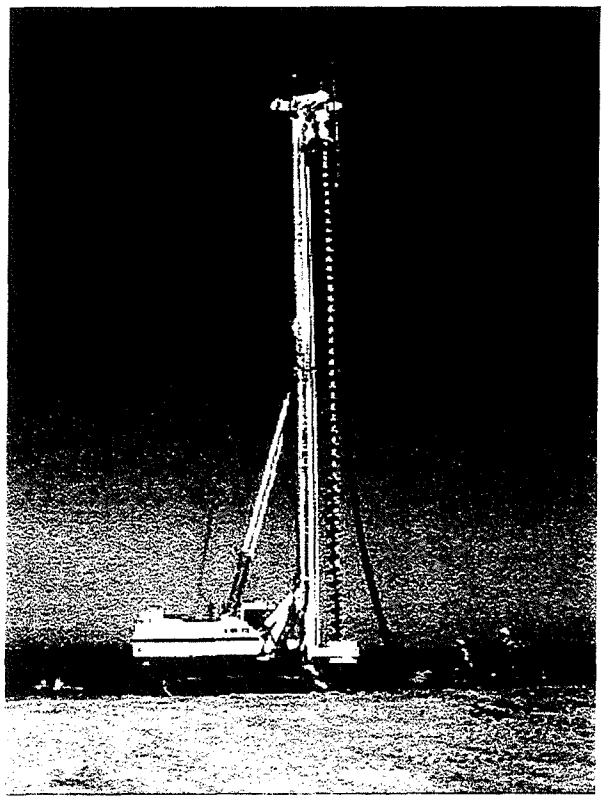

(b) Photograph of a CFA rig

Figure 3.1: The CFA rig

Figure 3.2: The concrete pump which pumps concrete to the base of the auger

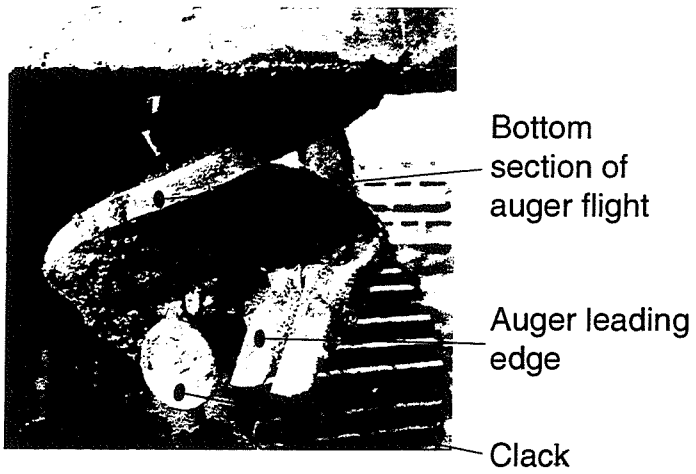

Figure 3.3: Tip of a continuously flighted auger showing the clack used to prevent soil from entering the hollow stem

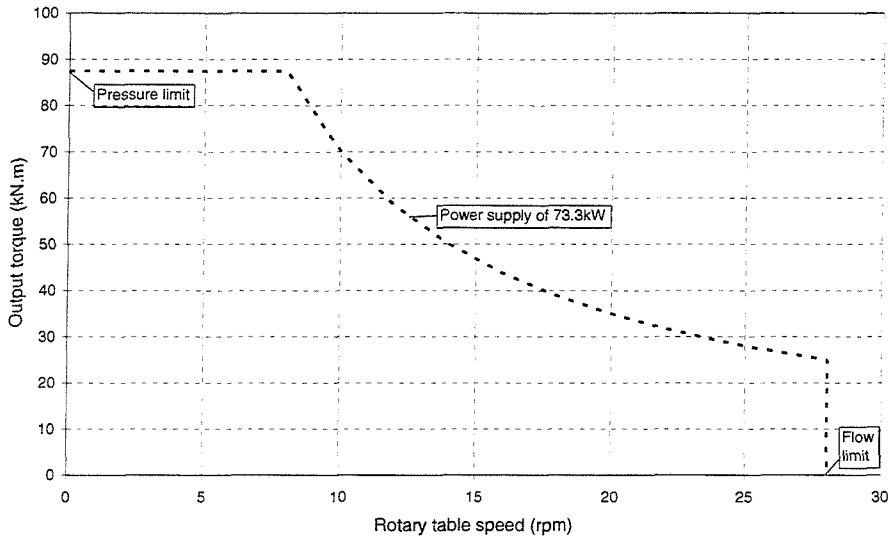

Figure 3.4: Torque available on a CM48 CFA rig

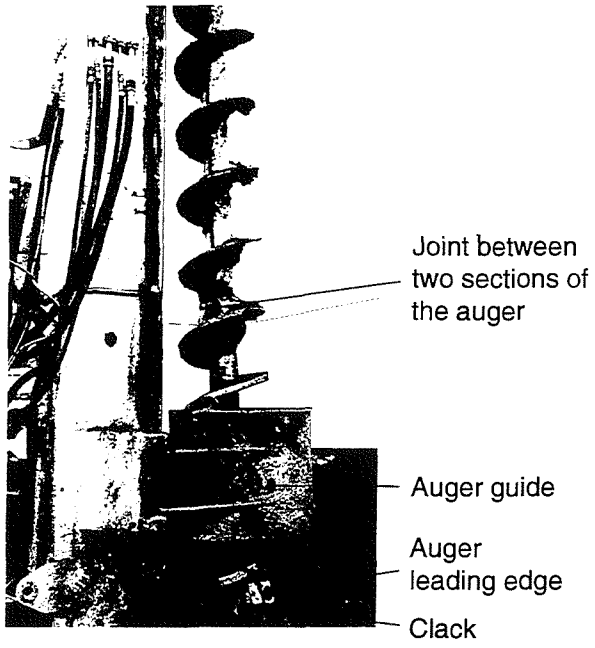

Figure 3.5: Bottom section of a continuously flighted auger

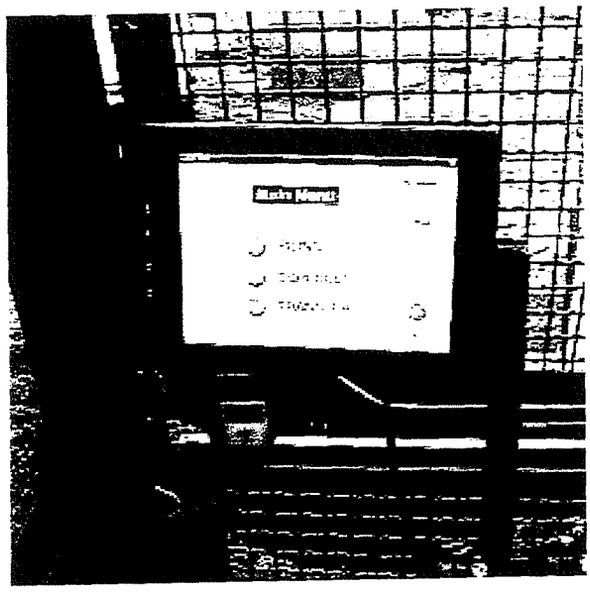

Figure 3.6: Monitor in the CFA rig to give information to the operator

Figure 3.7: Removal of spoil generated by the CFA process by a back actor

Figure 3.8: Reinforcement lowered into the fluid concrete by hand, helped by the back actor when necessary

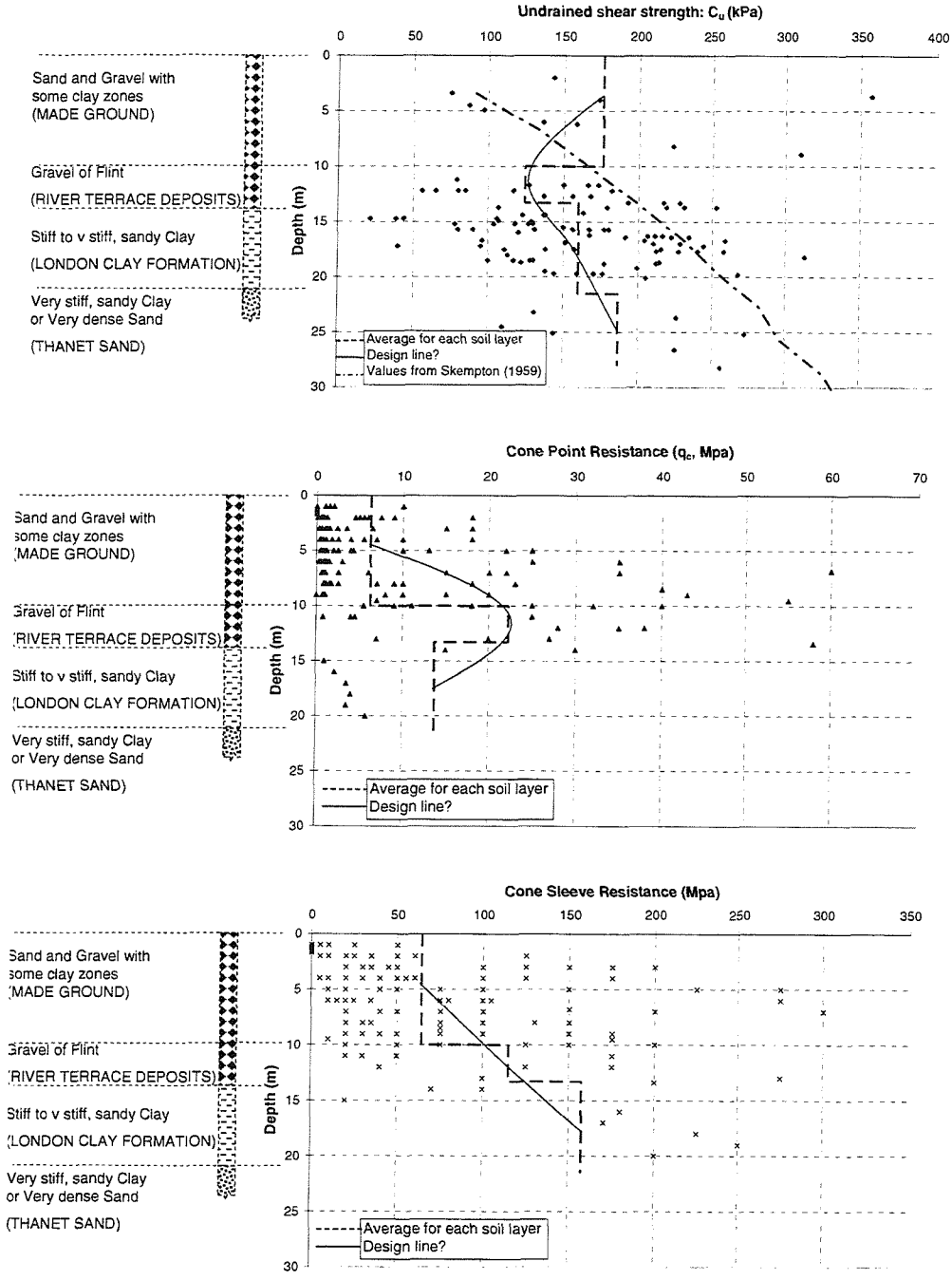

Figure 3.9: Site investigation data from the ExCel site in the Royal Victoria docks, London

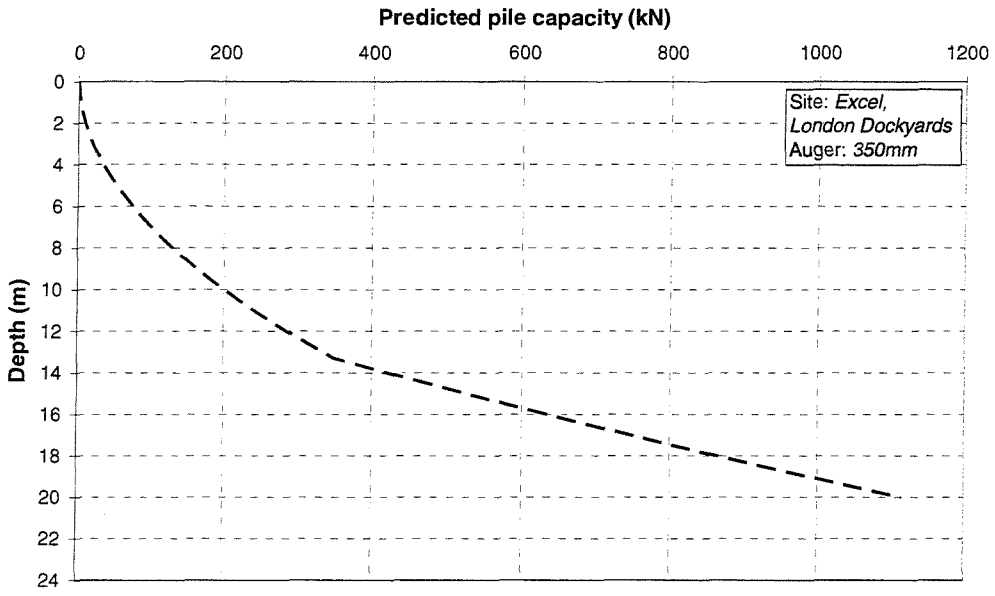

Figure 3.10: A prediction of the capacity of a 350mm diameter pile on the ExCel site

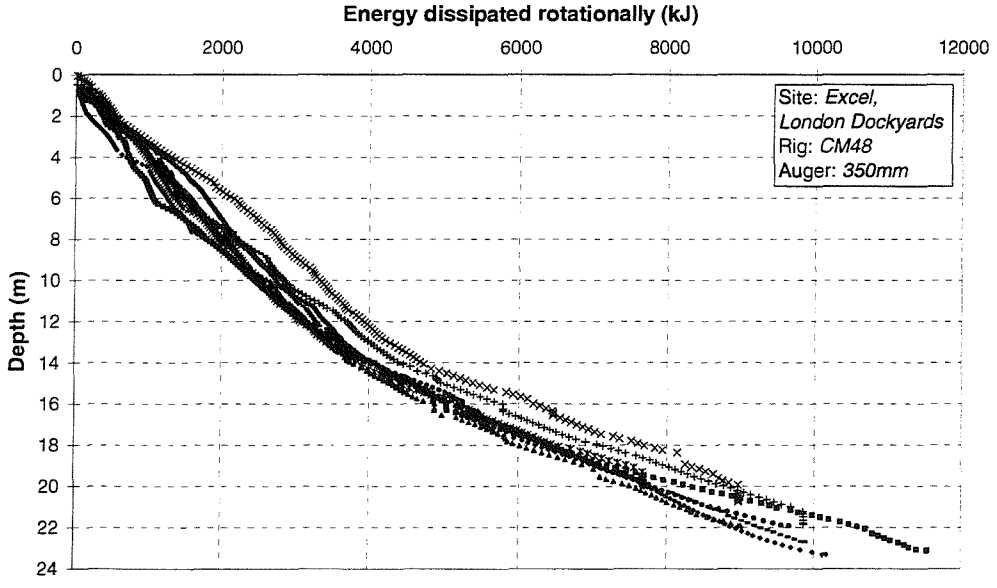

Figure 3.11: Energy used rotationally by the 350mm auger on the ExCel site

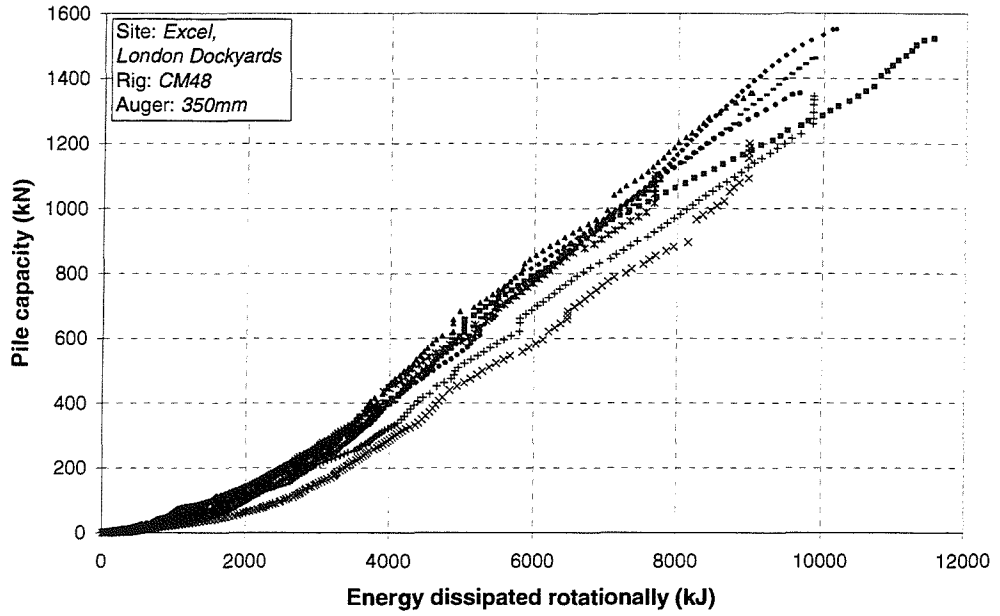

Figure 3.12: The relationship between pile capacity and energy used by the rotation of the 350mm auger found on the ExCel site

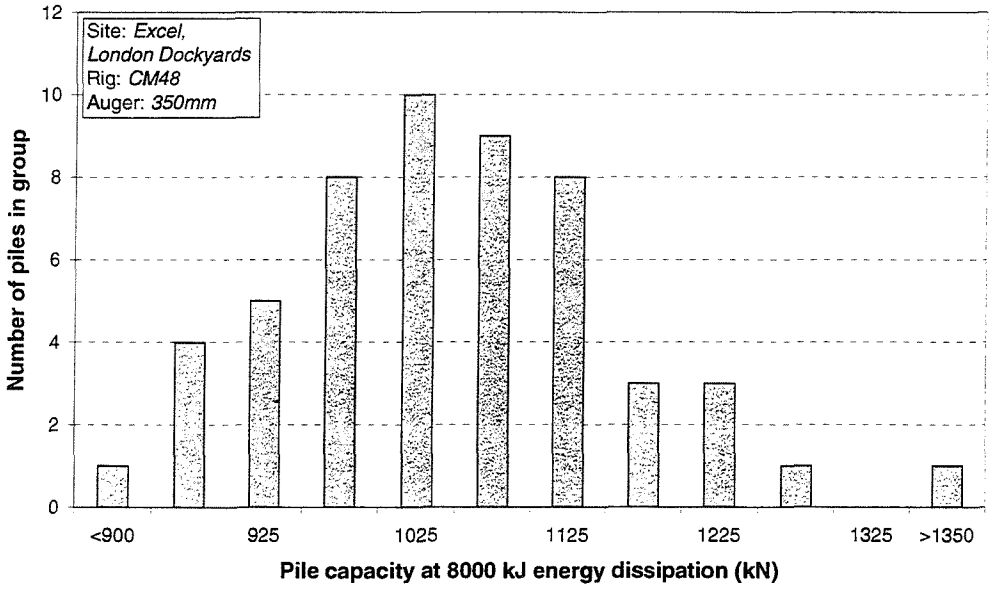

Figure 3.13: The distribution of pile capacity predictions using the 350mm auger on the ExCel site in the London dockyards for 8MJ energy dissipation

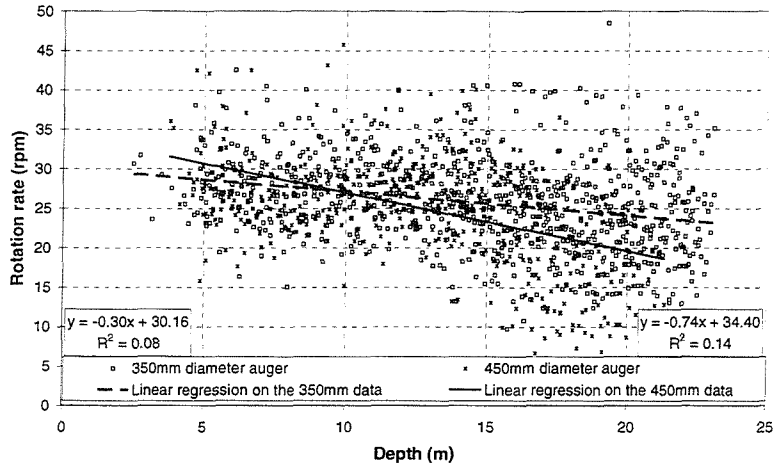

(a) Rate of rotation

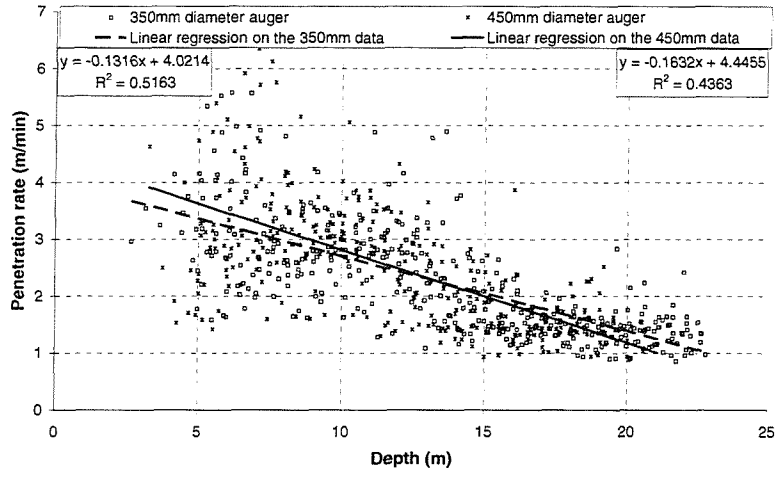

(b) Rate of penetration

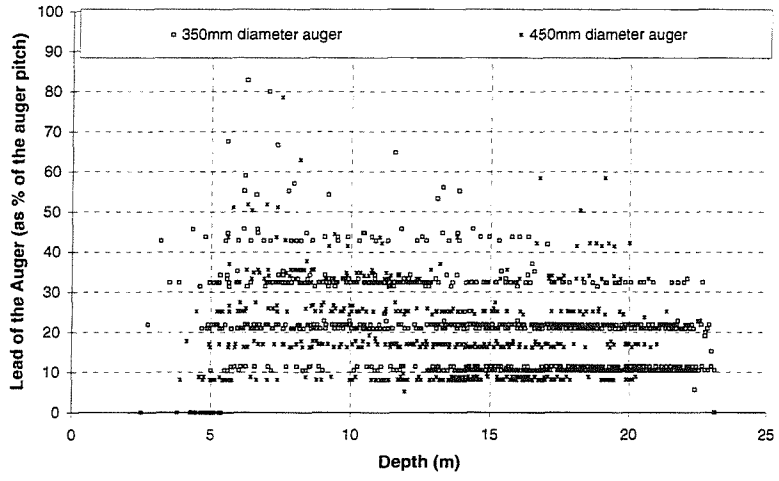

(c) Auger lead values

Figure 3.14: Data recorded on the CM48 rig on the ExCel site

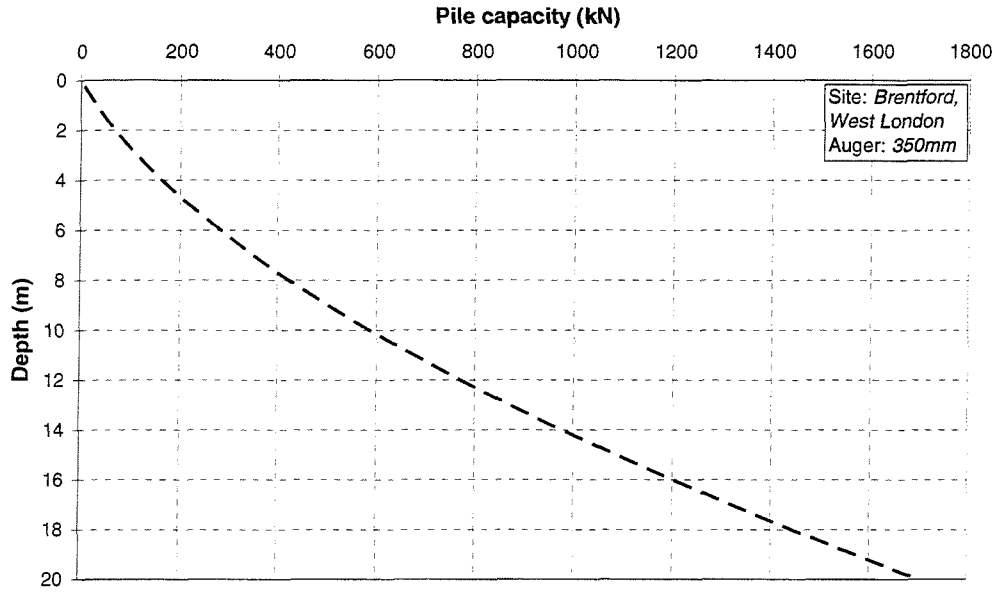

Figure 3.15: A prediction of the capacity of a 350mm diameter pile on the Brentford site

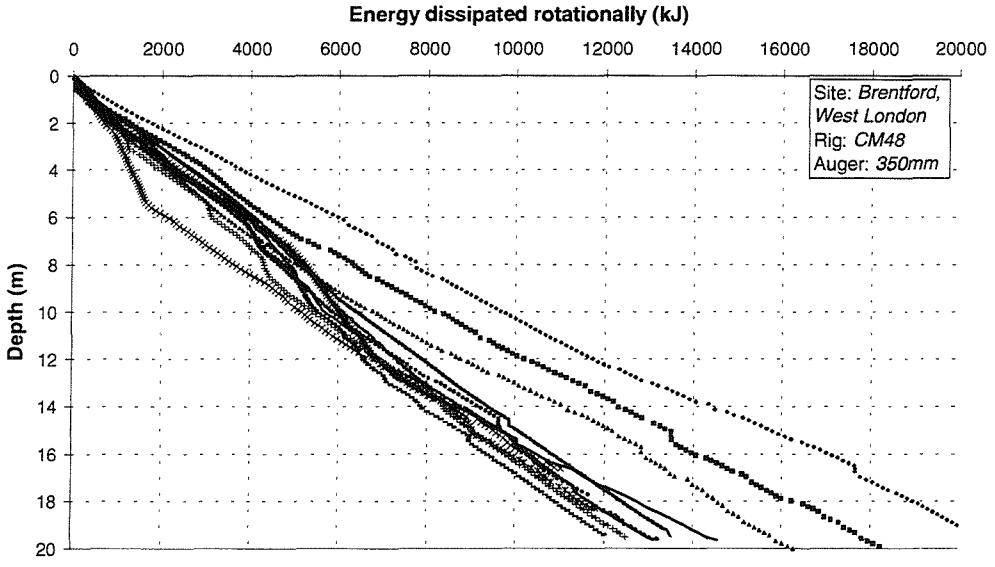

Figure 3.16: Energy used rotationally by the 350mm auger on the Brentford site

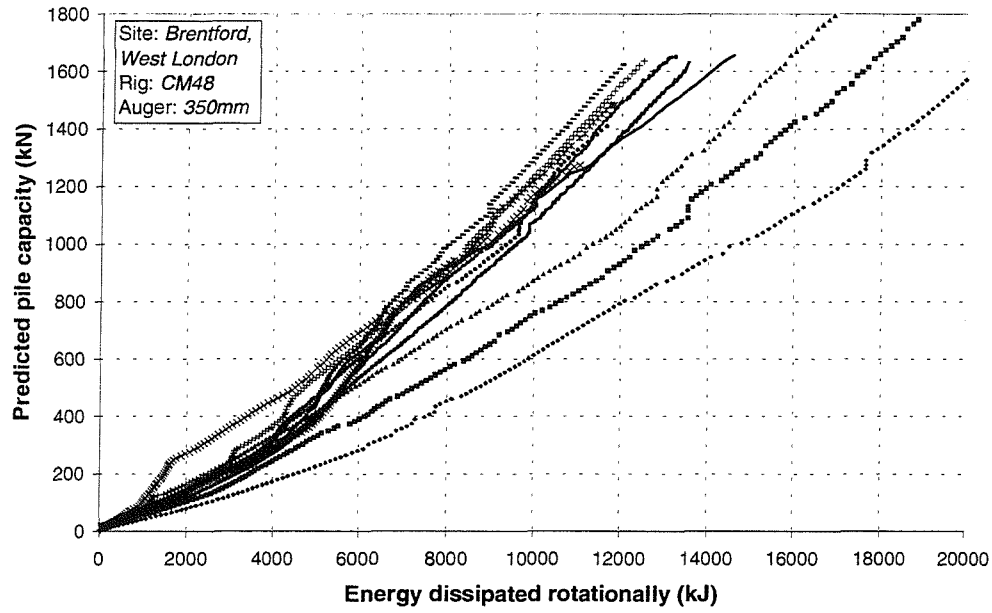

Figure 3.17: The relationship between pile capacity and energy used by the rotation of the 350mm auger

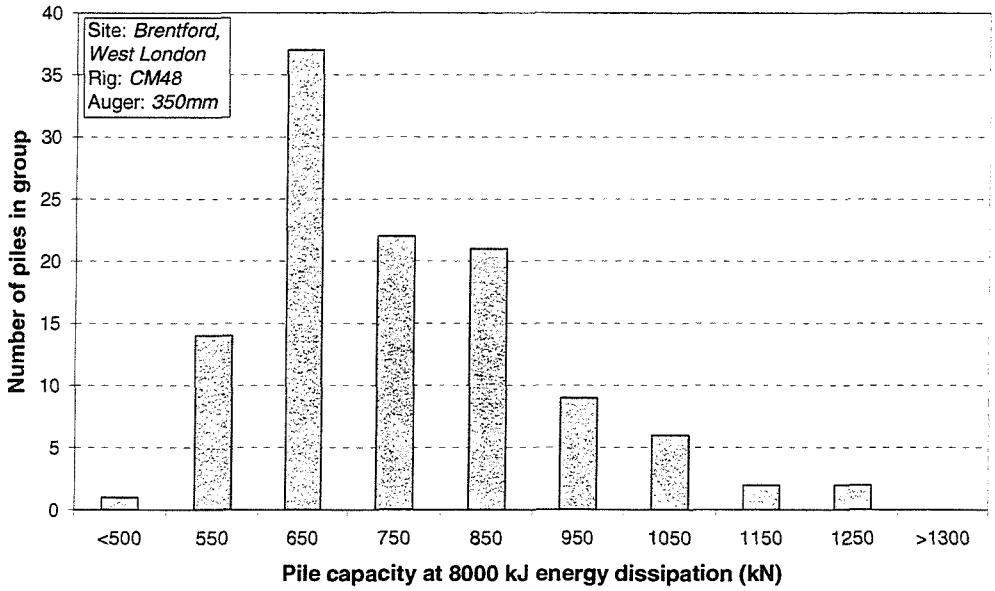

Figure 3.18: The distribution of pile capacity predictions using the 350mm auger on the Brentford site in West London for 8MJ energy dissipation

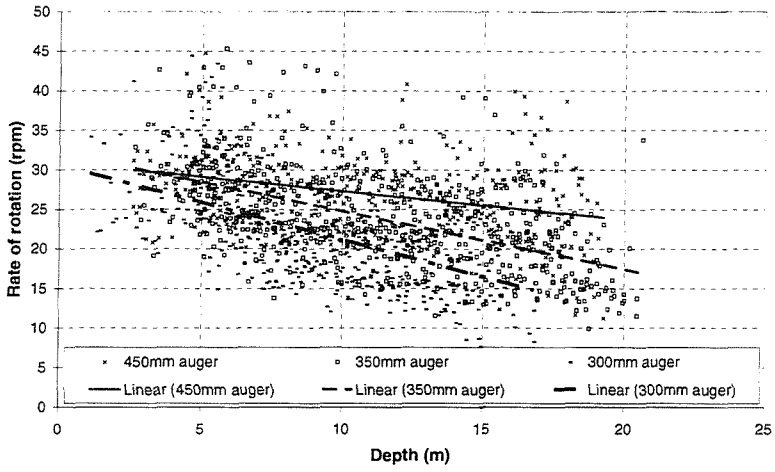

(a) Rate of rotation

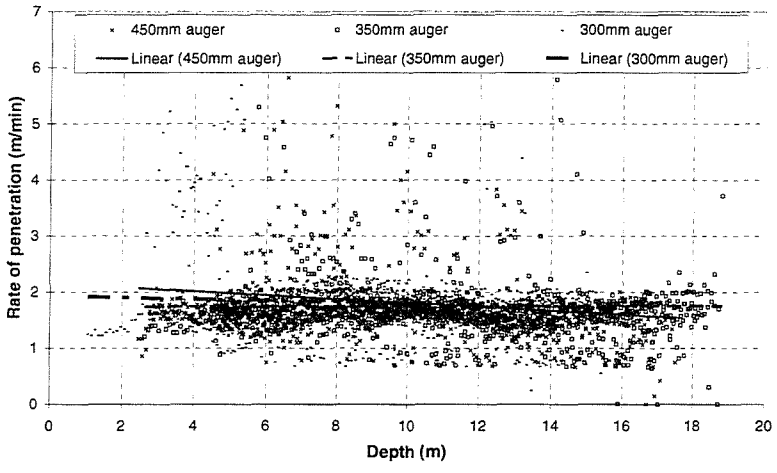

(b) Rate of penetration

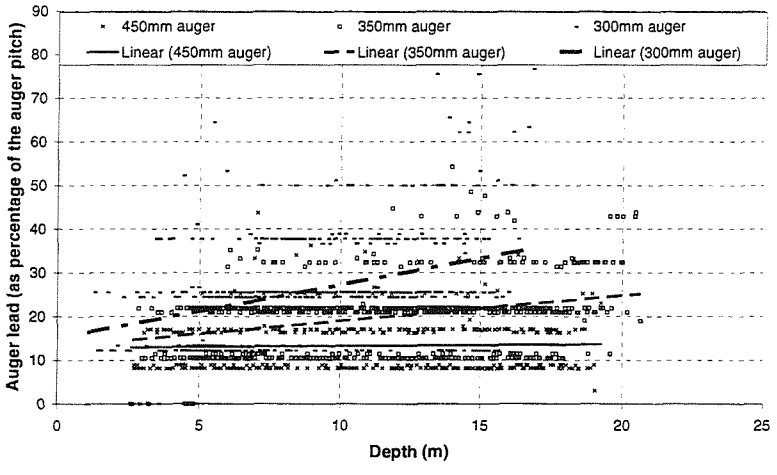

(c) Auger lead values

Figure 3.19: Data recorded on the CM48 rig on the Brentford site

Chapter 4

EXPERIMENTAL SET-UP AND TEST RESULTS

4.1 Introduction

A small-scale simulation of a CFA rig was developed to conduct the set of experiments. Other options considered were using a full-scale CFA rig, using a mini-pile rig or adapting a bench drill.

A design using instrumented electric servo motors was chosen as it would facilitate accurate control of speed and displacement of the auger. Another advantage was that the instrumentation could be included in the original design of the model rather than doing a modification to an existing set-up such as a bench drill. As the equipment used for sample preparation for scale model tests in a centrifuge was readily available in the laboratory it was decided to use this established method of sample preparation. Some modification was applied to produce repeatable samples under normal gravity conditions.

In this chapter the sample preparation technique and subsequent sample properties will be discussed and the design and instrumentation of the model CFA rig described.

4.2 Kaolin sample preparation

The research was aimed at investigating auger mechanics in a stiff clay. Speswhite kaolin clay was therefore used as the test material. The advantages of using kaolin are that it is a material which has been extensively used for modelling by other researchers, and much work has been done in characterising the material, see for example Al-Tabaa (1987). In order to produce repeatable samples, each sample was prepared strictly in the following manner.

Kaolin was delivered in powder form. This powder was mixed with de-aired water under a vacuum in an industrial mixer built for the purpose. The target moisture content (ω) was 100% (a liquidity index of 2.3). Each batch contained 60kg of kaolin and 60kg of de-aired water. This mixture was viscous enough to flow out of a tap in the bottom of the mixer and into the sample box to achieve a uniform placement.

The sample box (also known as the centrifuge strong box) is a container manufactured to contain samples in a centrifuge. Figure 4.1 shows a cross section of the sample box containing the kaolin sample. The sample box had a 300mm extension to accommodate the water that was displaced during consolidation. A sand drainage layer was placed at the bottom of the box, covered by a porous plastic sheet. The kaolin slurry was placed on top of this porous plastic sheet and a second porous plastic sheet was then placed on top of the kaolin. The sample box was well greased on the inside using silicone grease to minimise the adhesion of the kaolin to the box.

The sample box was placed in a consolidation press, and drainage was supplied to the top and bottom of the sample. A settling stress of 7.5kPa was applied and left for 24 hours. Thereafter the applied stress was doubled every 24 hours until it reached a constant 960kPa for 24 hours. The stress was then increased to 1250kPa and left for 48 hours to ensure that primary consolidation had been completed. The load was then lowered from 1250kPa to 960kPa and halved every 24 hours until a stress of 100kPa was reached. During this time water was supplied to the top and bottom of the sample

to facilitate swelling without the sample becoming unsaturated. The load of 100kPa was kept on for 48 hours to enable the sample to swell to 100kPa vertical effective stress. 100kPa was chosen because it would ensure a high OCR, but the material should retain enough strength to supply measurable resistance to the auger penetrating it. It was assumed that 100kPa was below the air entry value of the sample. All excess water was carefully removed and the load was taken off the sample completely. The sample was sealed and left for 7 days to ensure all the pore water pressures had reached equilibrium.

4.2.1 *Development of kaolin preparation procedure*

The sample preparation procedure as described above has often been used in preparing samples for centrifuge tests (Kantartzi, 1993), except for some of the finer details required to make a uniform and somewhat repeatable sample under normal gravity conditions.

The numbering of boxes was as follows: Boxes 1 to 5 were prepared for preliminary auger tests, refinement of the sample preparation procedure and characterization of the kaolin samples. Boxes A to E were prepared for the auger model CFA testing. A Geonor hand vane was routinely used to investigate the samples.

The importance of leaving the sample for several days after swelling is illustrated in Figure 4.2, which shows a plot of hand vane tests carried out on Sample Box 2. The first two hand vane tests were carried out immediately after the box was taken off the consolidation press and the rest of the tests were carried out 2, 3 and 4 days later. There was a dramatic initial drop in c_u which seemed to stabilize after 4 days. This may have been due to the soil swelling because of the absorbtion of excess water in the sand filter below the sample as well as excess water that may not have been completely removed from the clay surface (although every effort was made). It was decided that it would be safest to leave the box for 7 days after consolidation had been completed.

Usual practice for centrifuge sample preparation was to seal off the bot-

tom drainage layer during swelling as the standpipe would require regular refilling (Figure 4.1). Sample Box 2 was prepared in this manner and the moisture content with depth shows a general decrease of approximately 1% (Figure 4.3(a)). Furthermore, hand vane tests showed an increase of c_u with depth of approximately 20kPa (Figure 4.3(b)) even though this sample was left in excess of 7 days before these tests were carried out. In Sample Box 3 water was supplied to the bottom drainage layer during swelling. The moisture content with depth variation (Figure 4.4) was of the order of 0.5%, which may have been within the accuracy of the test or due to the sample drying out from the top as the other soil tests were conducted (the moisture content with depth profile was only measured after all other tests on the sample had been completed and the sample box dismantled). It therefore seems that the supply of water to the bottom drain during swelling of the sample was crucial to obtaining a uniform sample.

There was a concern that adhesion of the clay to the side of the box would cause a variation in sample properties in a horizontal direction in the sample. Horizontal sections of hand vane tests showed little variation of strength over the width and length of the box (Figure 4.5), indicating that adhesion to the greased sides of the box had a small effect on the sample properties.

Although the measurement of stress on the consolidation press was reasonably accurate, the control thereof was not. A range of $\pm$ 20kPa around the desired stress value was the best that could be achieved. This issue did not have great significance at the maximum consolidation pressure (1250kPa), but at the 100kPa pressure, at the end of the sample swelling stage, it was difficult to maintain the correct stress on the sample. Some of the variation in sample properties may be attributed to this.

4.3 Kaolin sample properties

A standard set of soil classification tests were carried out on every sample box after the auger tests had been completed. These included hand vane tests,

moisture content with depth profile and unconsolidated undrained triaxial tests, in that order. It was assumed that the tests would not influence the results of the other tests significantly. Other tests were also carried out on the kaolin but not routinely. These included Atterberg limits, effective stress triaxial tests (consolidated undrained), ring shear and machine vane tests.

4.3.1 *Atterberg limits*

A set of Atterberg limit tests was conducted on the Speswhite kaolin used in the project (BS1377, 1990). The plastic limit was found to be 33% and the liquid limit 67%. Plotted on the Casagrande classification chart the sample plots directly onto the A-line, and is therefore classified as CH-MH (Casagrande, 1948).

4.3.2 *Moisture content with depth*

Once the auger model and hand vane tests had been completed one side of the strongbox was removed. Moisture content samples were carefully taken at predetermined depths and tested according to BS1377 (1990). For most of the sample boxes the variation in moisture content with depth was less than the presumed accuracy of the test of 1% (BS1377 (1990) recommends moisture content results to be given to the nearest whole number if in excess of 10%). A summary of the test results is given in Table 4.1. Tests on the saturation of the samples showed that the samples were indeed saturated (test results follow later in the chapter).

4.3.3 *Hand vane tests*

A Geonor hand-vane was used to measure the undrained shear strength of the samples. A summary of the results is given in Table 4.1. Sample Box A dried out considerably as it was left for 4 months before testing and showed a much higher undrained shear strength than the other boxes. Note that the strength variation in Boxes B to E was small (between 72kPa and 91kPa).

Auger model tests results obtained in Sample Box A were not compared to results from other sample boxes.

Figure 4.6 shows the relationship between moisture content and undrained shear strength as measured by the hand vane. The trend of results suggests a 29kPa drop in undrained shear strength for every 1% increase in moisture content of kaolin with this particular stress history. The figure also shows the reliability of both the moisture content and hand vane test results as the tests are totally independent but show a clear relationship.

4.3.4 *Unconsolidated undrained triaxial tests*

Samples were taken from boxes using a thin walled 38mm diameter sampling tube with a sharpened leading edge. These samples were extruded and tested in a triaxial cell at 2% strain per minute at cell pressures of 100, 200 and 400kPa. Six samples were taken from every box. A test was carried out at 100, 200 and 400kPa confining pressures respectively. If the results of any of these tests seemed unreliable they were repeated, otherwise the remaining three samples were tested at 200kPa.

To check the saturation of the samples, a set of unconsolidated undrained triaxial tests were carried out with multi staging (the cell pressure was ramped up in steps as the test progressed (Figure 4.8)). The fact that the stress-strain response of the sample followed the same curve as the cell pressure increased shows that the sample was saturated. A set of tests was carried out on samples from box 5 over a wide range of cell pressures (100 to 800kPa) and c_u remained constant with increase of cell pressure (Figure 4.9).

Barden (1972) and Kirkpatrick and Rennie (1973) observed a structure of horizontally aligned particles in one dimensionally consolidated kaolin using an electron microscope. Kirkpatrick and Rennie (1972) concluded that the samples were anisotropic in stiffness terms but not in strength. Triaxial samples were taken in vertical and horizontal directions from the sample box and no variation in c_u with sampling direction was found.

Figure 4.7 shows the relationship between moisture content and undrained

shear strength as measured by the unconsolidated undrained triaxial test. The relationship is less well defined than that shown with the hand vane test, and is reflected in the lower R^2 value of the linear regression which is 0.88 for the hand vane results and 0.62 for the triaxial test results. On these grounds the hand vane test seemed to be more dependable than the unconsolidated undrained triaxial test.

Considerable time was spent improving the technique used during the unconsolidated undrained triaxial tests however, the results were consistently more variable than those obtained by the hand vane. According to both the moisture content and the hand vane test results samples B to E were similar (Table 4.1), yet the triaxial tests show a variability in the undrained shear strength (c_u). A possible reason for this may be that there was a variation in the delay between sampling and testing, however data to support this claim was not logged. In some cases samples were tested immediately after sampling, and in other cases the samples were stored for up to 3 weeks before testing. Consequently the hand vane test results will be used in the discussion of auger test results and not the triaxial test results.

Figure 4.10 is a plot of a series of unconsolidated undrained triaxial tests carried out on samples taken from Sample Box 5. An initial stiff response of the kaolin was observed in these tests and in all other samples taken from the sample boxes. An investigation into the cause of this phenomenon was conducted. The conclusion of the investigation was that it was the result of the one dimensional consolidation of the sample in the sample box. Samples consolidated isotropically did not exhibit the same behaviour.

4.4 Preliminary auger tests

To obtain design values for the laboratory CFA model rig, preliminary tests using augers in sample boxes 1 to 4 were carried out.

4.4.1 *Equipment*

A digital torque wrench was used to turn in the augers (Figure 4.12), to establish what the torque requirements would be. The range of the torque wrench was 5Nm to 50Nm. Examination of the axial loads on the rig were also required, and a system using cables and a swivel was used to connect the auger to a proving ring (Figure 4.14) to measure the axial load.

The ratio of outer diameter, pitch and inner diameter on the 400mm CFA auger was used as a template and a set of augers was manufactured accordingly. The ratios were:

- outer diameter equal to pitch and
- inner diameter = 20% to 25% of the outer diameter.

Model augers were made by welding a helix to an inner shaft of the correct diameter (Figure 4.11). The outer diameters of the augers were 50mm, 40mm, 35mm and 25mm. The augers were made with a single cutting tip and helix. Excess metal from the welding process was removed by angle grinder.

4.4.2 *Test description and results*

Two different types of tests were carried out. In the first test no axial loads were imposed on the auger (except for the first pitch penetration, where the auger had to be pushed into the ground) and the auger was allowed to penetrate freely as it was rotated (Figure 4.12). Once the full length of the auger had penetrated the kaolin the direction of rotation was reversed and the auger was turned out of the clay. The torque and depth was recorded every quarter turn. The results from this test were repeatable, as shown in Figure 4.13. Verticality of the auger was not deemed important, therefore no great care was taken to ensure that augers penetrated the sample vertically.

The second test method entailed allowing the auger to penetrate freely for a certain distance, connecting the auger to a cable which held the auger back stopping penetration, but allowing rotation through a swivel in the cable (Figure 4.14). This caused the soil at the side of the bore to shear.

The amount of tension in the cable was measured using a proving ring and recorded as well as the torque and depth. A typical result from such a test is shown on Figure 4.15. Note that the torque wrench only gave an output when a minimum of 5Nm was applied. The hole and auger was then cleared of loose material and the next test was carried out below the previous test until the bottom of the box was reached. Three to four tests were typically made in each hole.

If it is assumed that a cylinder of soil of length equal to the depth that the auger was allowed to penetrate freely is sheared on the side and bottom surface, then the undrained shear strength of the soil can be estimated. Both the moment and the axial force contribute to the shear stress in the soil and they act in perpendicular directions. The shear stress on the soil boundary caused by the moment and axial load are calculated separately.

If it was assumed that shear stress on the cylinder was uniformly distributed over the sides and bottom of the cylinder, then when taking moments about the axis of the cylinder the following equation was found:

$$M = \tau_m \pi D l \frac{D}{2} + \int_0^{D/2} \tau_m 2\pi r^2 dr$$

which simplifies to:

$$\tau_m = \frac{M}{\pi l D^2/2 + \pi D^3/12} \tag{4.1}$$

where τ_m is the shear stress caused on the soil boundary by the applied moment.

However, experience in the field of vane testing has shown that it is very important to take into account the non-uniform stress distribution at the ends of the cylinder (only the bottom end in this case). Wroth (1984) suggested using the following polynomial expression to represent the shear stress at the bottom of the cylinder:

$$\tau = \left(\frac{r}{D/2}\right)^n \tau_m \tag{4.2}$$

where n is an exponent describing the ratio between τ and r (the simplified case above is the case where n = 0). In order to calculate the contribution of the bottom surface to the moment required to turn the auger (M_{bot}) the following expression is integrated:

$$M_{bot} = \int_0^{D/2} 2\pi r^2 \left(\frac{r}{D/2}\right)^n \tau_m dr$$

which simplifies to

$$M_{bot} = \frac{\pi \tau_m D^3}{4(3+n)} \tag{4.3}$$

and therefore

$$\tau_m = \frac{M}{\pi l D^2/2 + \pi D^3/(4(3+n))} \tag{4.4}$$

where l is the length of the cylinder and D is the diameter of the cylinder (or the auger). Menzies and Merrifield (1980) found that $n = 5$ for the London Clay. In the absence of data for Kaolin, this value was used in Equation 4.4. Note that the bottom surface therefore requires a very small proportion of the applied torque to shear the soil on that boundary. The shear stress on the cylinder (τ_f) caused by the axial force F may be calculated by:

$$\tau_f = \frac{F}{\pi D l} \tag{4.5}$$

Note that the bottom surface is not taken into account when calculating τ_f as doing so would imply that soil had a tensile strength. The resultant of the two stresses (τ_{tot}) is simply the root of the sum of the squares (Equation 4.6) as they are perpendicular:

$$\tau_{tot} = \sqrt{\tau_m^2 + \tau_f^2} \tag{4.6}$$

The undrained shear strength (c_u) was then assumed to be equal to the maximum shear stress imposed on the soil cylinder (τ_{tot}). Figure 4.16 shows a comparison between c_u by hand vane, unconsolidated undrained triaxial

test and the auger test as described above. The auger test appeared to yield an undrained shear strength close to that measured by the hand vane and triaxial test, and the repeatability of the test was encouraging. An increase of strength with depth measured by the auger was believed to be a result of the test technique. As the hole became deeper the auger touched the sides on the way down which increased the torque and load on the auger.

4.5 Laboratory model design

This section describes the development of the laboratory CFA model rig that has been used to simulate the augering process of the full-scale CFA rig in the laboratory.

4.5.1 *Design values*

From the preliminary tests the torque and axial load capabilities required for the laboratory auger rig were estimated. The design torque was found to be 25Nm and the design axial load 1000N.

The rate of penetration of the model rig could not be set to a particular design value because of the range of auger sizes that were to be tested and because the rate of penetration of the auger was one of the variables to be investigated by the model. Therefore a system in which the rate of penetration could be varied considerably was required.

For the rate of rotation of the auger an upper bound of 100rpm was decided on, although the apparatus also had to be able to run at much lower speeds to accommodate the different auger sizes and test variables.

It was crucially important to have accurate control of the rate of rotation and penetration of the auger to ensure that the auger accelerated, rotated and decelerated at a precise lead value.

4.5.2 *Mechanics of the model*

The completed model is shown in Figures 4.17 and 4.18. To describe development of the model in a structured manner, it has been divided up into sections which will be discussed separately.

Model augers

The augers used in the preliminary tests were adapted to work on the laboratory model by adding a shear pin arrangement (Figure 4.19).

Platform

The platform that attached the model to the sample box needed to be stiff enough to hold the model in place rigidly and yet have the capacity to be moved to different locations on the box for successive tests. For this purpose a platform which could slide along the top of a centrifuge strong box was built with the ability to clamp onto the box at any position (Figure 4.20). A hole for the auger to drill through was made off-center to enable two rows of holes to be drilled in one sample box. The auger guides shown in Figure 4.19 were made of HDPE to fit into this hole in the platform to guide the augers. Attached to the platform was a large rectangular section on which the linear motion system was fixed.

A system to control the penetration of the auger

The KR33A linear motion system manufactured by THK co., Ltd (Tokyo, Japan) was chosen as it could withstand large forces and had a stroke length of 400mm (Figure 4.21). The critical design load on the ballscrew was the moment produced by the axial force on the auger, on the linear motion system. The maximum permissible moment in this plane was 166Nm. With the design load equal to 1000N, the lever arm (centreline of the auger to the centreline of the ballscrew on the linear guide) could not be greater than 166mm as illustrated in Figure 4.18. A rigid platform to fit onto the linear

motion system was manufactured, with the aforementioned lever arm equal to 100mm, increasing the permissible axial load to 1660N. The ballscrew on the linear motion system had a lead of 6mm (i.e. one revolution of the ballscrew moved the platform by 6mm).

The large variance and high accuracy in the required rate of penetration of the augers necessitated a versatile motor. A 100W brushless servomotor from Mitsubishi Electric Corporation (Tokyo, Japan) was used (model: HA-FF13C-UE), controlled by a PM600 PC controller card supplied by McLennan Servo Supplies Ltd (Camberley, Surrey, UK.). A brake system on the servomotor comes as standard. The maximum speed of this motor was 3000rpm, and this connected to a Alpha 1:50 ratio gearbox (model: SP 075-MF2-10-031-000, manufactured by Alpha getriebebau Ltd., Germany) provided a maximum rate of penetration of 6mm per second. The motor provided 8192 feedback pulses per revolution to aid in positioning of the motor. Commands were given to the motor to go to a particular feedback pulse using a preset acceleration, deceleration and travel velocity. The accuracy of the motor positioning could be set using the 'window' command on the PM600 PC controller card. The window is the number of feedback pulses that the motor is allowed to be from the target feedback pulse when it stops. For extremely accurate positioning the window can be set to 0, so that the feedback loop positioning the motor will only be exited when the motor is at the correct feedback pulse out of the available 8192. The drawback of high accuracy positioning is the time delay experienced when setting the motor to such a small window value. It was found that a window value of 400 ($\pm$ 200) was the minimum value at which no noticeable time delay was required to position the auger. This window value resulted in an accuracy of $\pm$ 6μm on the auger penetration due to motor inaccuracy.

The physical size of the motor was important to ensure that the auger centreline was as close as possible to the linear motion system. This motor, mounted correctly, was small enough not to be an obstruction to the motor turning the auger as shown in Figure 4.18.

To protect the model a coupling (type: Huco-Oldham) built by Huco Engineering Industries Ltd. was used to connect the servo motor to the linear motion system (Figure 4.22). A plastic flange was incorporated into the coupling that would shear if excessive torque was applied by the servo motor.

A system to control the rotation of the auger

Another Mitsubishi brushless servomotor was used for the rotation of the auger (power: 600W, model: HA-FF63C-UE). A 1:16 ratio Alpha gearbox was mounted on the motor (model: SP 075-MF2-16-031-000). This motor and gearbox combination could supply a torque of 28Nm, and the Alpha gearbox was designed in such a way as to transmit the axial load directly to the platform, thereby protecting the motor. The motor was also controlled through a PM600 PC card. The accuracy of this motor was set to $\pm$ 1.1 degrees using a window of 400.

Both motor amplifiers were mounted in a box, which provided a Faraday shield to reduce the intensive electrical noise generated by these amplifiers on the load and torque measurement transducers (crosstalk[1], Figure 4.23). The amplifier power supply was also kept separate from the instrumentation to further limit the noise on the transducer signal.

4.5.3 *Instrumentation*

Torque and load measurement were not made directly on the auger itself because of the difficulty of such instrumentation. The instrumentation was placed below the gearbox of the motor turning the auger (Figure 4.18).

As servo motors apply more torque they use more current. The current output from both motors was measured as a backup of the torque and load measurement by instrumentation. This measurement of torque proved to be accurate however, the derivation of axial load on the auger by measurement

[1]electrical noise caused by mutual inductance and capacitance between lines due to their proximity

of the current in the motor controlling vertical movement was inaccurate (noise on the signal seemed to exceed the signal itself). Possible reasons for this may have been friction in the system as well as losses in the 1:50 gearbox.

An attempt was made to manufacture a transducer to measure torque and axial load on the model. The desired accuracy could not be achieved and commercial sources were sought for the transducers.

The torque measurement transducer was the HBM TB1A acquired from Hottinger Baldwin Messtechnik (Darmstadt, Germany) with a full-scale of 200Nm (Figure 4.24). This transducer was chosen because of its excellent load and bending moment compensation characteristics. No standard load measurement transducer was available to fit onto the rig. A 2kN transducer was designed and build by Proctor Chester Measurements Ltd. to fit onto the rig where the previous transducer had been removed (Figure 4.26). This figure also shows the sliding pin arrangement used to isolate torque from axial load.

Torque transducer The torque transducer required a 10V excitation. The sensitivity of the transducer was 1.5003mV/V at full-scale. The DC amplifier was set to amplify the signal as close as possible to 1000 times using a voltage divider and voltmeter. An output voltage of 15V at full-scale was thus expected. The 16 bit A to D card was set to $\pm 10V$ input range. An output of 245 bits/Nm was therefore expected. The calibration achieved an output of 251 bits/Nm (Figure 4.29).

Load transducer The load transducer required a 10V excitation. The sensitivity of the transducer was 0.569mV/V at full-scale. The amplifier was set to amplify the signal as close as possible to 1000 times, to achieve an output of 5.69V at full-scale. The 16 bit A to D card was set to $\pm 10V$ input range. An output of 7.46 bits/N was expected. The calibration showed an output of 7.17 bits/Nm (Figure 4.30).

As the load transducer was not compensated for torque, torque and axial load had to be separated mechanically to enable accurate load measurement.

A flange was built to connect the torque transducer to the load transducer which would transmit the torque through pins to the outer ring of the load transducer where it could not influence the load measurement, but the load to the inner ring of the load transducer (Figure 4.26(c)). The pins ran in linear ball bearings (type LBBR 5 from SKF (Göteborg, Sweden), Figure 4.26(a)) to ensure they did not transmit any of the load to the outer ring of the load transducer. A pin roller bearing was inserted on top of the inner ring to ensure no torque was applied to the inner ring of the load transducer (Figure 4.26(b)). Figure 4.27 shows the transducers assembled on the model rig.

4.5.4 *Calibration of the model CFA rig*

For torque calibration a frame was built which applied a moment to the fully assembled model through a dead weight system (Figure 4.28). This enabled regular calibration to be carried out on the torque transducer. Calibration using the calibration frame suffered from hysteresis due to friction in the bearings, as well as inaccuracies in the alignment of the transducer, lever arm and weights. The calibration supplied by the manufacturer was therefore used during data analysis. The calibration data from the frame was used to check on this calibration constant.

For load calibration the load transducer was calibrated on a Budenberg dead weight tester, and to check the transducer between tests dead weights were put on top of the motor controlling rotation of the auger. The calibration obtained by using the Budenberg dead weight tester was used in the data analysis.

Both the calibration systems achieved a calibration constant close to that supplied by the manufacturers (within 0.8% for torque measurement and 3.8% for axial load measurement), showing that the amplification and data logging was correctly set up and the transducers were working as expected.

4.5.5 *Software interface*

A software interface was developed to control the motors using the software package Test Point (an interface to Visual Basic specifically developed for laboratory use). The motion control cards communicate with the PC through an RS232 interface. As testing progressed the interface was continually changed and upgraded.

Data logging was carried out using separate software specifically developed for the A to D card (PC super). Data was stored to file and imported into a spreadsheet for manipulation.

4.6 Model auger test procedures

Two model auger test procedures were employed, the first procedure was designed to investigate the influence of auger rate of rotation and lead on the torque and load measured on the auger and the second procedure was an attempt to measure c_u using the model auger rig. These two procedures will be referred to as the *'auger penetration'* and *'auger shear tests'* respectively.

The procedure followed during the auger penetration test was to advance an auger at a fixed rate of rotation and lead into the soil. Once the auger had reached the maximum penetration depth of the model set-up, the direction of movement (axial and rotational) was reversed so as to extract the auger from the soil. The variables altered were:

- the rate of auger rotation,
- the auger lead and
- the auger diameter.

The first variable investigated was the rate of rotation of the auger. This was a priority because it had been found that there was a large variation in the rate of rotation of full-scale augers as shown in Figures 3.14(a) and 3.19(a). If the rate of rotation influenced torque on the auger then this would need to be taken into account in the next set of tests. The results from this

set of tests were required before the rates at which the other tests were to be conducted were decided on.

The auger shear tests were set up to mimic the procedure often followed by full-scale CFA rigs. It was observed on site that CFA rig drivers allow the auger to penetrate freely into the soil for some distance, then apply the winch so as to stop the auger penetration whilst continuing auger rotation. The following procedure was used in the auger shear tests:

1. the auger was advanced into the soil to a depth which was chosen such that the point where no (or as close as possible to zero) axial load was imposed on the auger was reached at this depth (described as the *'zero load contour line'* in Chapter 5);

2. auger penetration was then stopped, but rotation continued so as to shear the soil on the boundary between soil on the auger flight and the soil surrounding the bore (this boundary will be referred to as the *'soil boundary'* in the remainder of the chapter) and

3. auger penetration was then restarted, and steps 1 and 2 repeated until the maximum penetration depth of the model was reached.

Completion of steps 1 and 2 constituted one auger shear test and several of these could be conducted below one another in a single hole. The depth described in the first step was chosen as twice the auger lead.

The variables altered during the tests were:

- the lead of the auger during the penetration phase (this was an iterative procedure to reach the *'zero load contour line'* at the predetermined depth) and
- the auger diameter.

As the tests were carried out results were analysed continuously and the testing schedule was reassessed according to the findings.

4.7 Model auger test results

This section contains a summary of all the test results obtained using the model auger rig. Results are plotted in such a way that comparisons may be made in the discussion chapter (Chapter 5).

4.7.1 *The influence of the rate of rotation on required torque*

The first set of experiments were conducted when only torque measurement using feedback of from the motor current was available. The 25mm outer diameter auger was used for this set of experiments (detailed auger dimensions are given in Table 4.2), and tests were conducted in Sample Box A. Table 4.5 contains the variables altered during the tests. Figure 4.31 shows the torque required at 250mm depth for the different rates of rotation.

4.7.2 *The influence of auger lead on the torque and load measurements (Auger penetration tests)*

Two augers were used during this set of experiments. The augers will be referred to by their outer diameters (40mm and 50mm respectively). The exact dimensions of the augers employed in the tests are given in Tables 4.3 and 4.4. Sample boxes C, D and E were used for this set of experiments. Undrained shear strengths measured in these boxes varied from 72kPa to 91kPa and moisture contents from 40.4% to 41.2% as shown in Table 3.2 in Chapter 3. Note that positive torque was defined as the torque applied in the direction that the auger was rotating and positive force was defined as the force applied in the direction that the auger was penetrating (downwards). Individual test results for this set of experiments have been included in Appendix A. The measurement of load could only be made to a maximum of 300N and therefore a plateau of this value is seen in some tests.

Results from the 40mm auger

Table 4.6 gives a list of the auger penetration tests carried out using the 40mm auger. Figures 4.32(a) and 4.32(b) contain a summary of torque measurements made by the torque transducer during this set of tests. Figures 4.33(a) and 4.33(b) contain a summary of the load measurements made by the load transducer during this set of tests. Figures 4.32(a) and 4.33(a) contain results from auger lead values greater than 90% of the auger pitch and Figures 4.33(b) and 4.32(b) contain results from auger lead values lower than 95% of the auger pitch. The results were split up in such a manner because a marked change in the correlation between auger pitch and both torque and load measured on the auger occurred at a lead value of approximately 92% of the pitch of the auger as can be seen on the graphs. Figures 4.34 and 4.35 have been drawn from the same set of results, only the torque and axial loads at specific depths have been plotted for the different rates of advance of the auger. These graphs are vertical sections of Figures 4.32 and 4.33 and show clearly that a maximum value for both torque and load was obtained at auger lead values slightly greater than 90% of the auger pitch.

Results from the 50mm auger

Results from the 50mm diameter auger have been plotted in exactly the same manner and order as those of the 40mm auger. Table 4.7 gives a list of the auger penetration tests using the 50mm auger. Figures 4.36(a) and 4.36(b) contain a summary of torque measurements made during this set of tests. Figures 4.37(a) and 4.37(b) contain a summary of the load measurements during this set of tests. Figures 4.36(a) and 4.37(a) contain results from auger lead values greater than 90% of the auger pitch and Figures 4.37(b) and 4.36(b) contain results from auger lead values lower than 95% of the auger pitch. The same reversal in direction of the correlation between auger pitch and both torque and load measured on the auger occurred at a lead value of approximately 92% of the auger pitch. Figures 4.38 and 4.39 have been drawn from the same set of results, only the torque and axial loads at

specific depths have been plotted for the different rates of advance of the auger.

4.7.3 *Simulation of the stop-start procedure observed on full-scale CFA rigs (Auger shear tests)*

The 40mm auger, the dimensions of which are given in Table 4.3, was used in this set of experiments. The tests were conducted in Sample Box F. The test procedure followed was as described in Section 4.6. Table 4.8 shows the variables altered during the test procedure. Figures 4.40 and 4.41 show the torque and load measurement results of three auger shear tests where a 40mm diameter auger was allowed to penetrate for 74mm at 37mm per revolution (penetration phase), penetration was then stopped and rotation was continued for one more revolution. Also in Figures 4.40 and 4.41 is the result of the 40mm diameter auger penetrating the soil at 37mm per revolution into the same sample box, but without the shearing phase. A graph of the torque and load measurement during the shearing phase is shown in Figure 4.42.

Table 4.9 shows back calculated undrained shear strengths deduced from the auger shear test results as well as hand vane test results from the same sample box (Sample Box F). The formulas used in the back calculation were those given in Section 4.4.2. The average of the undrained shear strengths deduced from all the auger tests was 81kPa with a standard deviation of 9kPa. For comparison the average undrained shear strength obtained from the vane test result was 82kPa with a standard deviation of 5kPa.

Table 4.1: Summary of the routine test results on Boxes 1 to 5 and A to E

Box no.	Moisture content (%)		Undrained shear strength (c_u, kPa)			
			Hand vane		Quick undrained triaxial	
	Mean	St Dev	Mean	St Dev	Mean	St Dev
1	40.0	n.a.	112.0	n.a.	69.3	6.2
2	40.1	0.5	71.0	8.0	41.7	8.8
3	40.0	0.4	74.0	6.4	39.5	7.2
4	41.3	0.6	56.8	4.5	53.9	3.6
5	41.4	0.5	43.6	7.2	27.8	2.7
A	38.0	0.5	156.3	14.3	121.5	n.a.
B	40.0	0.8	86.4	9.7	73.2	12.0
C	40.4	0.5	83.1	4.1	47.0	3.4
D	41.2	0.5	71.8	1.3	59.3	7.7
E	40.2	0.6	91.1	5.8	49.5	3.2
F	41.5	0.3	82.0	4.8	81.1[1]	n.a
Box B to F	40.7		82.9		62.0	

[1] 100mm sample (as opposed to 38mm for the other triaxial tests)

Table 4.2: Dimensions of the 25mm auger

Outer Diameter	25mm
Inner Diameter	8mm
Pitch	25.6mm
Auger volume	$86mm^3/mm$

Table 4.3: Dimensions of the 40mm auger

Outer Diameter	40mm
Inner Diameter	10mm
Pitch	39.1mm
Auger volume	$167mm^3/mm$

Table 4.4: Dimensions of the 50mm auger

Outer Diameter	50mm
Inner Diameter	10mm
Pitch	40mm
Auger volume	$191mm^3/mm$

Table 4.5: Variables altered in experiment set to investigate the effect of the rate of rotation of the auger on required torque using the 25mm auger

Sample Box and test no.	Auger lead values		Rate of rotation (rpm)
	(mm/rev.)	(% of pitch/rev.)	
A4	25.6	100	13.67
A1	25.6	100	10
A6	25.6	100	7.5
A3	25.6	100	5
A7	25.6	100	5
A8	25.6	100	5
A9	25.6	100	5
A2	25.6	100	2.5
A5	25.6	100	1.25

Table 4.6: Variables altered in experiments designed to investigate the effect of the rate of penetration of the auger using the 40mm auger

Sample Box and test no.	Auger lead values		Rate of rotation (rpm)
	(mm/rev.)	(% of pitch/rev.)	
C1	39.5	101	1
C2	39.0	99.7	1
C5	38.5	99.7	1
C4	38.75	99.1	1
C3	38.5	98.5	1
C6	38.0	97.2	1
C8	37.0	94.6	1
C9	34.0	87.0	1
C10	30.0	77	1
C11	26.0	67	1
C14	18.0	46	1
D1	39.0	99.7	1
D2	39.0	99.7	1
D7	22.0	56	1
D4	14.0	36	1
D5	10.0	26	1
D6	6.0	15	1
E9	6.0	15	1

Table 4.7: Variables altered in experiments designed to investigate the effect of the rate of penetration of the auger using the 50mm auger

Sample Box and test no.	Auger lead values		Rate of rotation (rpm)
	(mm/rev.)	(% of pitch/rev.)	
D9	40.0	100	0.8
D10	39.0	97.5	0.8
D11	38.0	95	0.8
E1	39.5	98.75	0.8
E2	37.0	92.5	0.8
E3	36.0	90	0.8
E4	33.0	82.5	0.8
E5	30.0	75	0.8
E6	20.0	50	0.8
E7	10.0	25	0.8
E8	5.0	12.5	0.8

Table 4.8: Variables altered in experiments designed to measure the undrained shear strength of the soil on the 40mm auger

Sample Box and test no.	Auger lead values		Rate of rotation (rpm)	Length of sheared cylinder
	(mm/rev.)	(% of pitch/rev.)		
F1a	36	90	1	72
F1b	36	90	1	72
F1c	36	90	1	72
F2a	36	90	1	72
F2b	36	90	1	72
F2c	36	90	1	72
F3a	37	92.5	1	74
F3b	37	92.5	1	74
F3c	37	92.5	1	74

Table 4.9: Results from the auger shearing tests compared to values measured by hand vane

Auger test	c_u(kPa)	Vane test	c_u(kPa)
F1a	69	1	91
F1b	63	2	82
F1c	55	3	83
F2a	66	4	86
F2b	65	5	78
F2c	54	6	75
F3a	69	7	82
F3b	72	8	78
F3c	72	9	80
		10	78
Average	65	Average	82
Std. dev.	6.7	Std. dev.	4.8

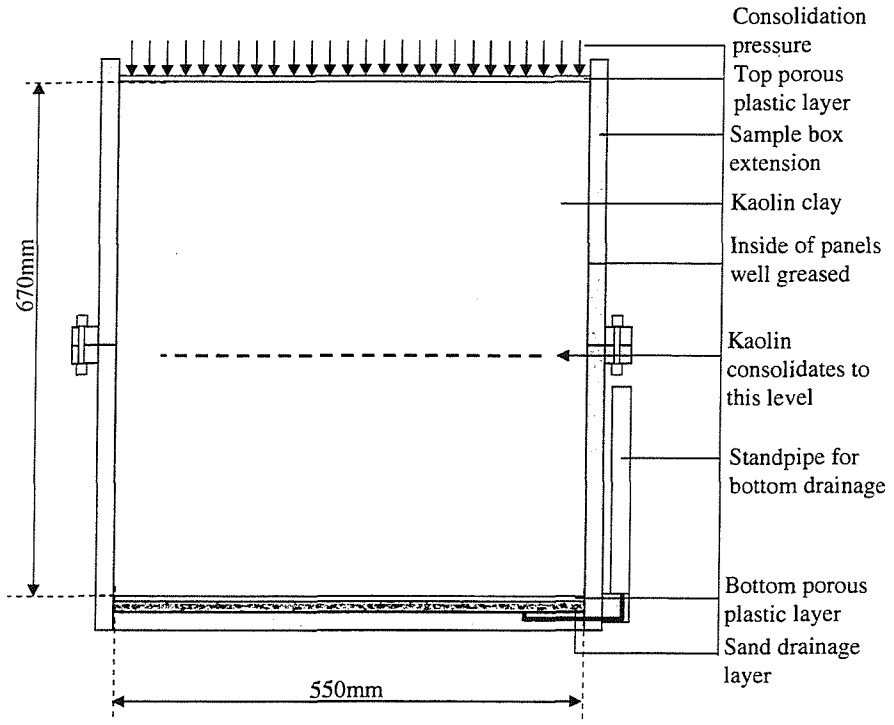

Figure 4.1: Cross section of the sample box (a centrifuge strong box, width of clay is 200mm)

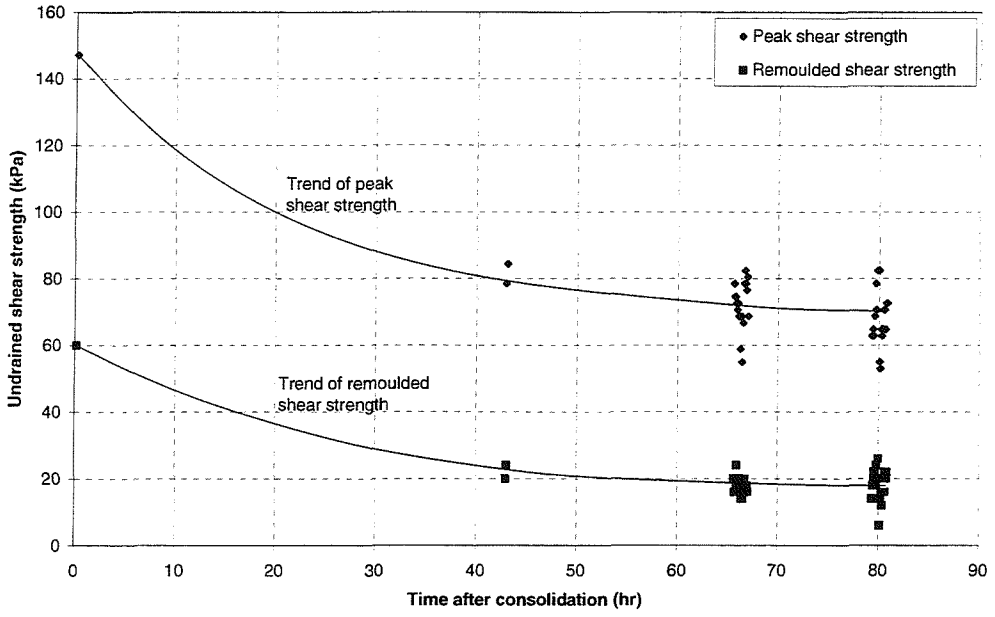

Figure 4.2: Effect of the time after consolidation on the undrained shear strength as measured by hand vane

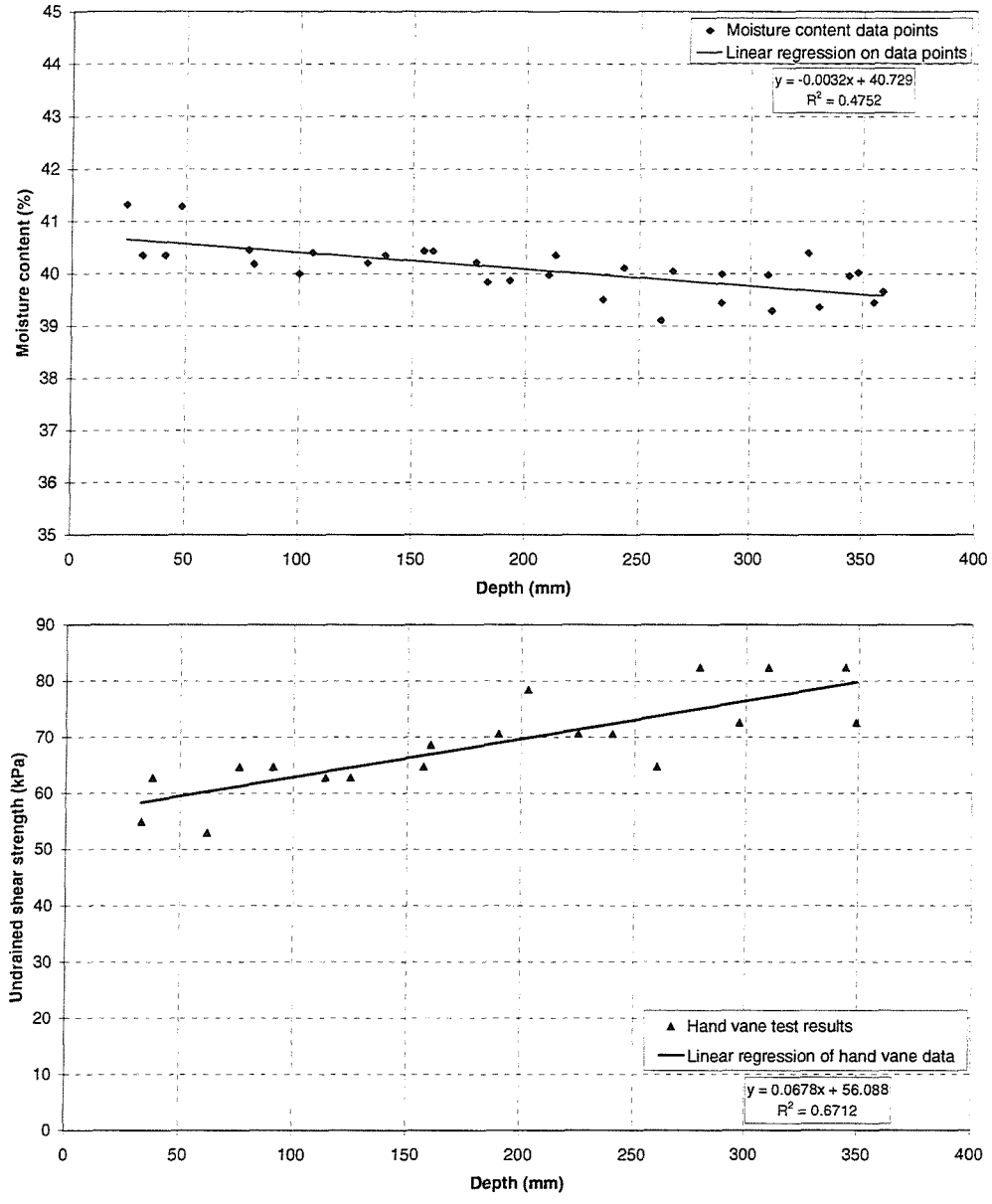

Figure 4.3: Moisture content and undrained shear strength with depth profile of Sample Box 2 swelled with bottom drainage sealed off

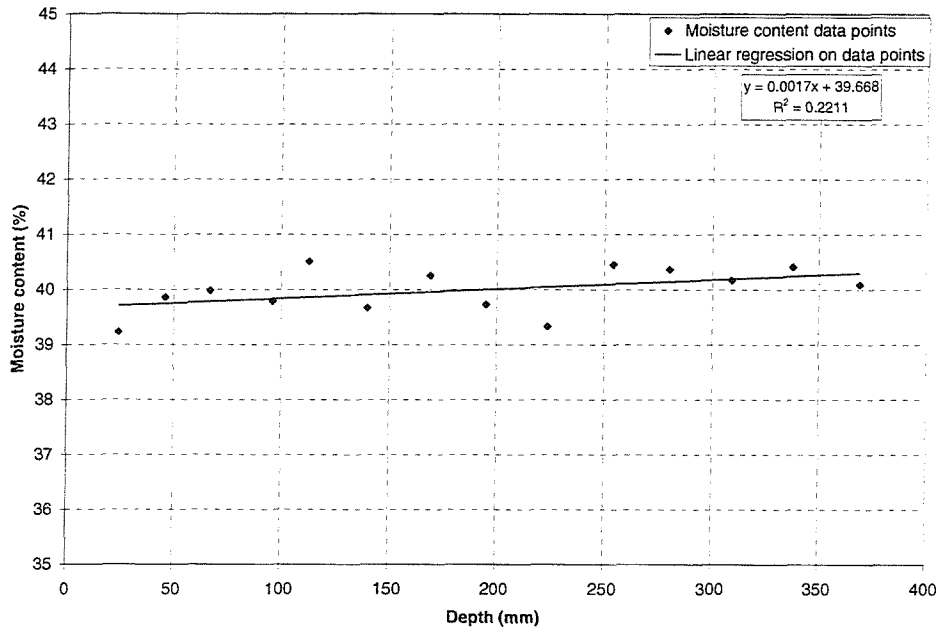

Figure 4.4: Moisture content with depth profile of Sample Box 3 swelled with water supply to bottom drainage

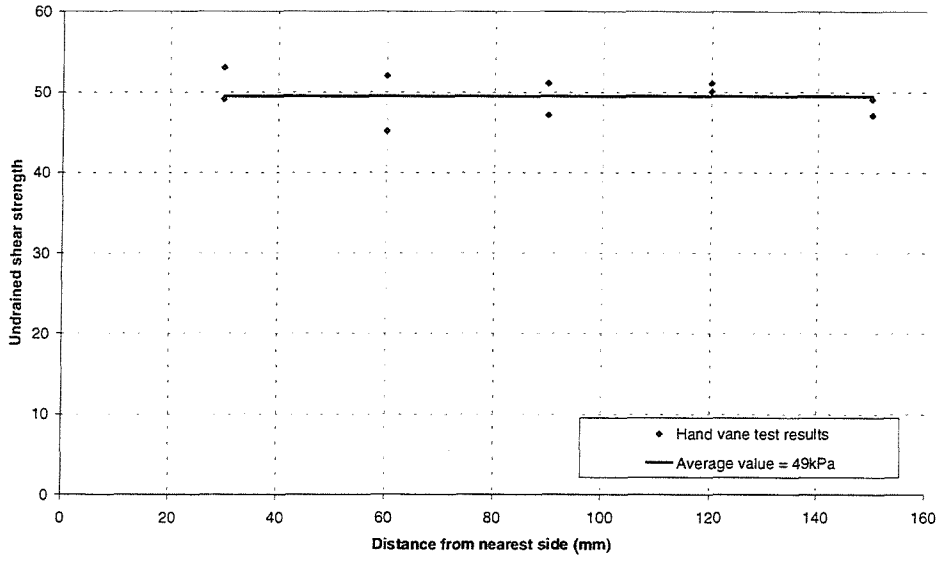

Figure 4.5: Horisontal strength variation over the length of the sample box (done in Sample Box 5)

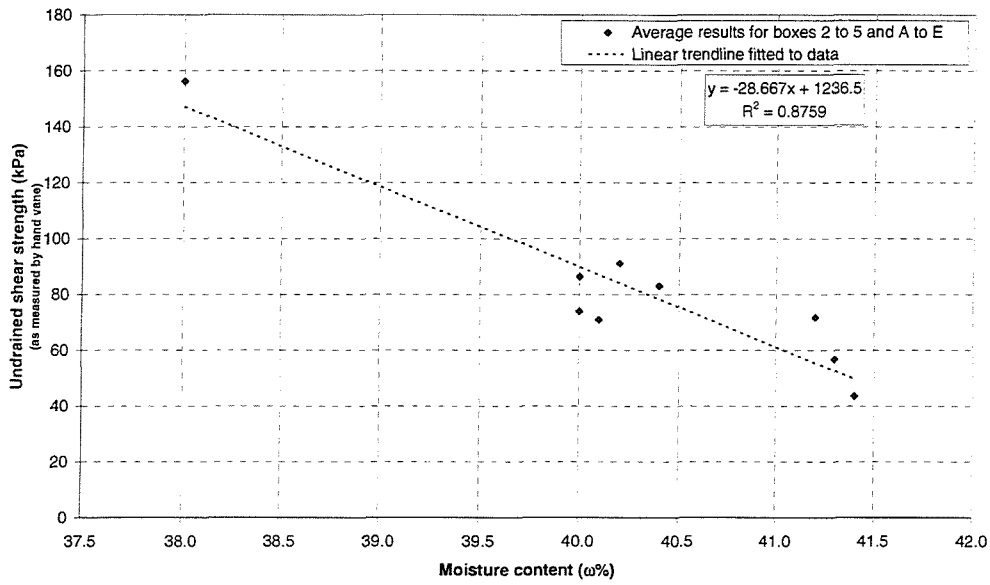

Figure 4.6: Variation in undrained shear strength as measured by the hand vane with a change in moisture content

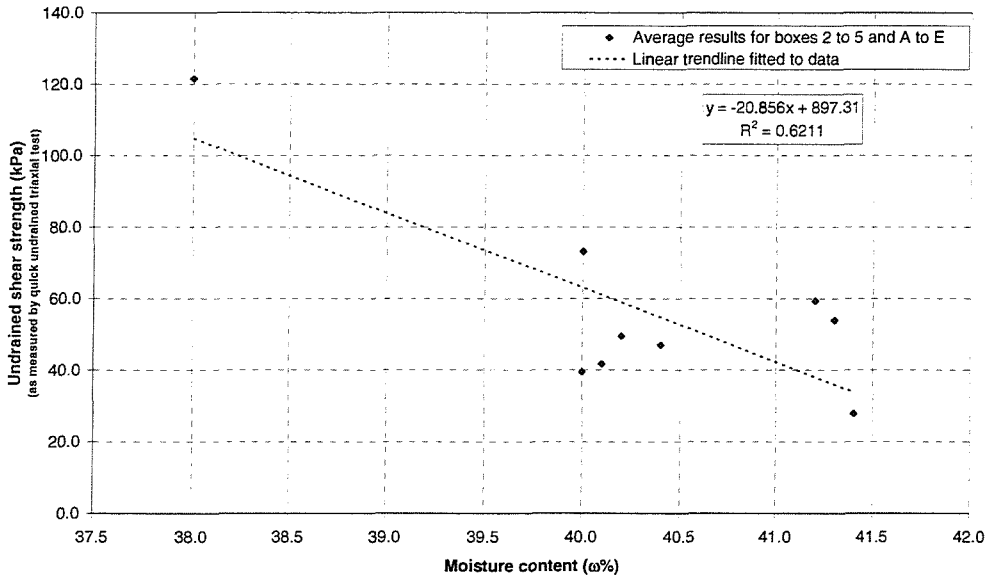

Figure 4.7: Variation in undrained shear strength as measured by the unconsolidated undrained triaxial test with a change in moisture content

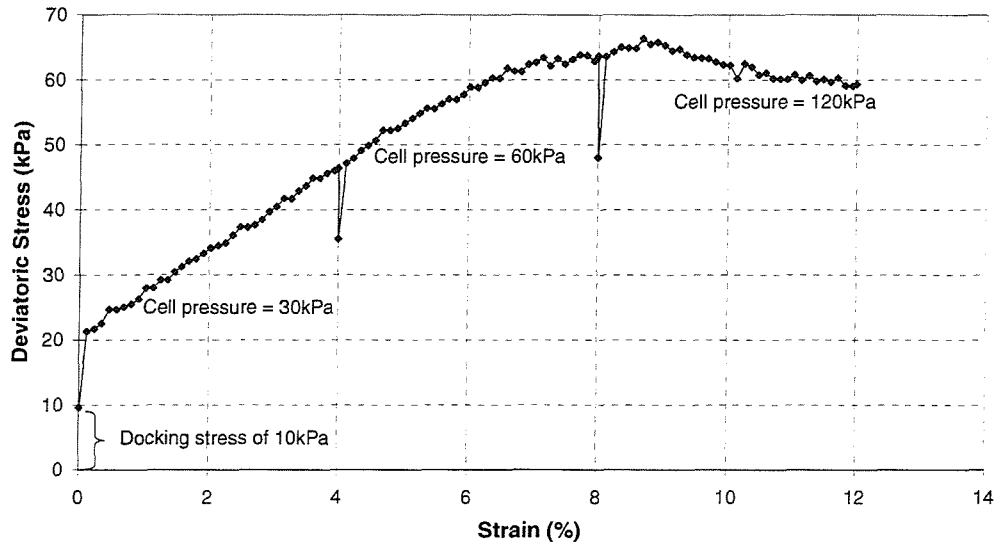

Figure 4.8: Multi-stage unconsolidated undrained triaxial result to test sample saturation

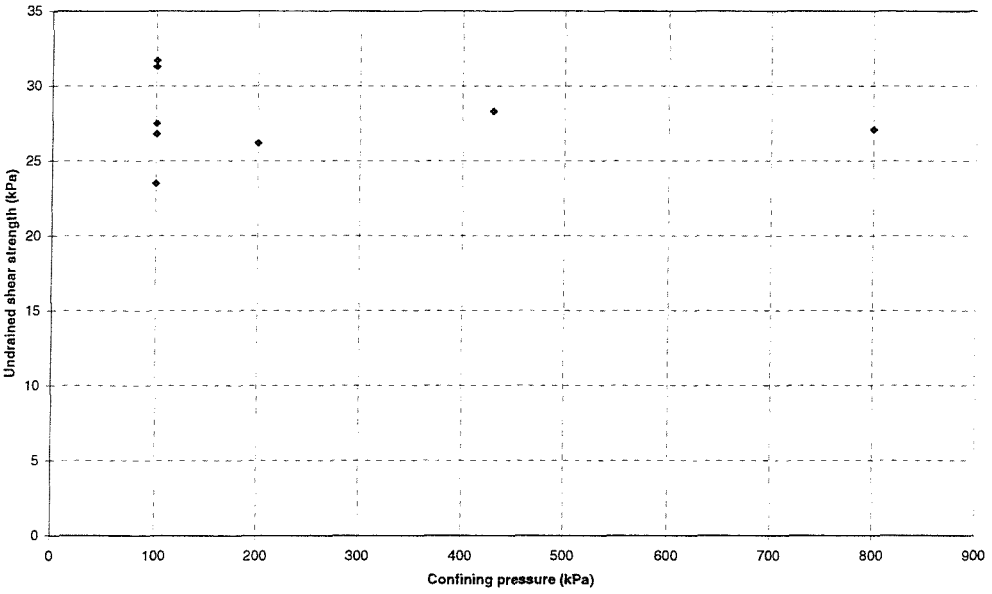

Figure 4.9: Undrained shear strength variation as a function of confining pressure

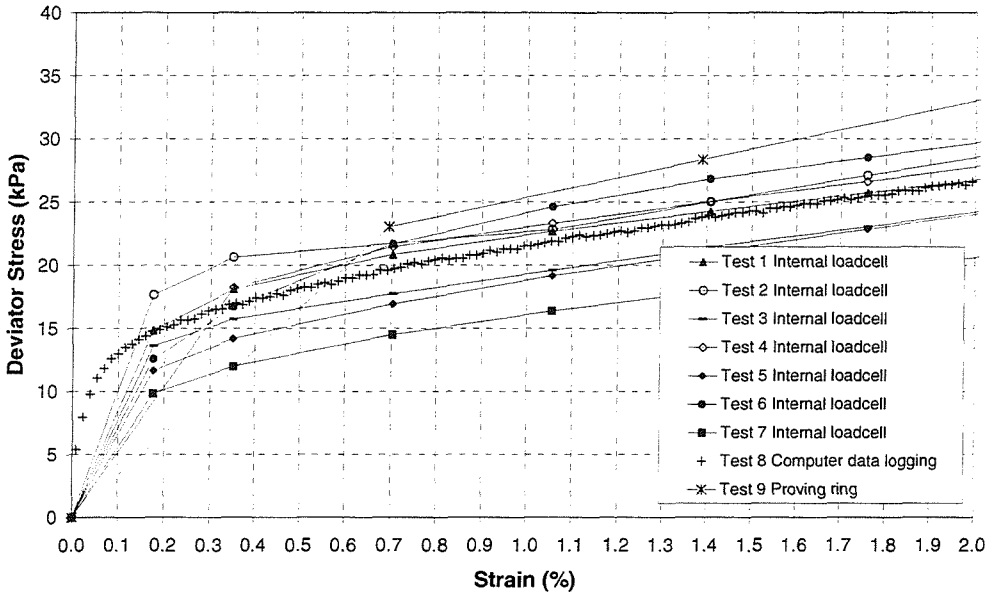

Figure 4.10: A set of unconsolidated undrained triaxial tests showing the repeatability of the initial stiff response

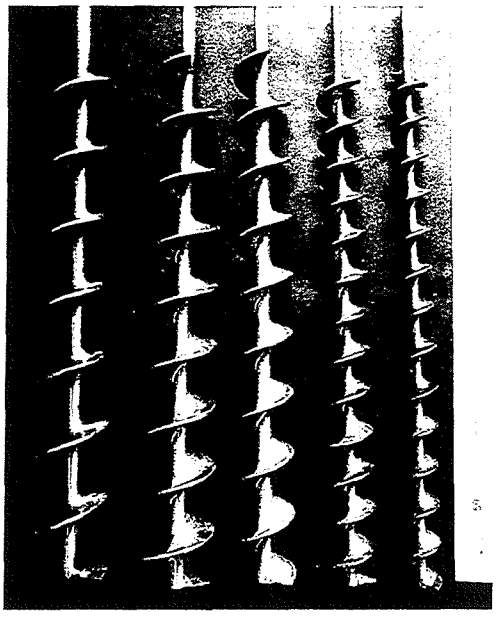

Figure 4.11: Model augers used in the preliminary auger tests

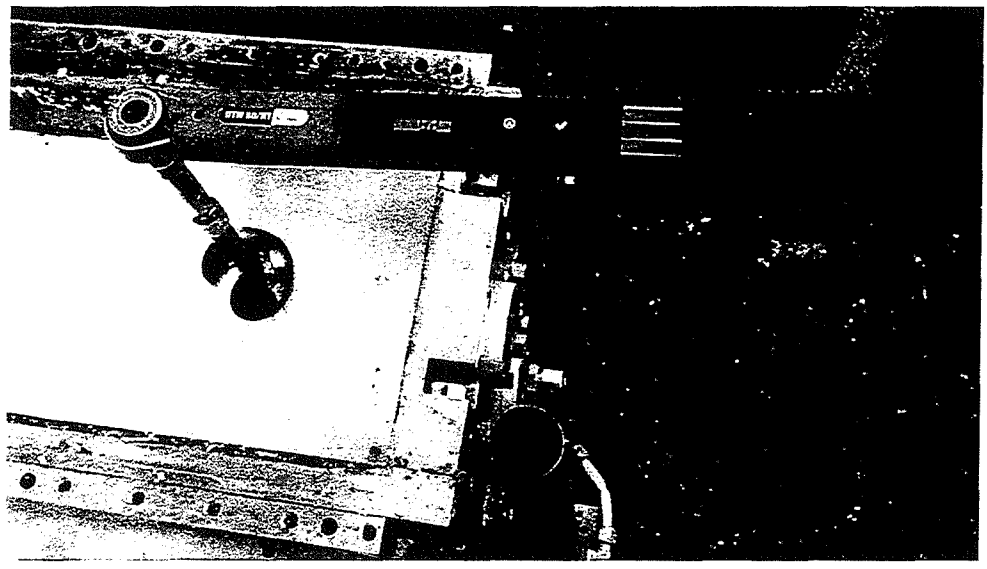

Figure 4.12: Preliminary auger test showing the torque wrench used in the preliminary auger tests

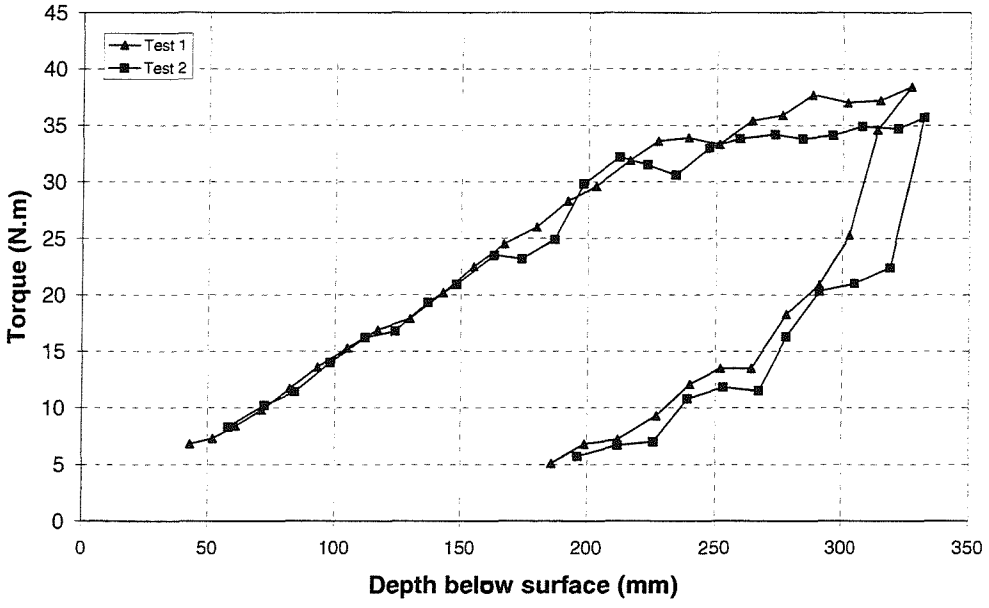

Figure 4.13: Results from two preliminary tests carried out with no axial restraint imposed on the auger

Figure 4.14: Preliminary auger test showing the proving ring set-up used to measure the axial load on the auger

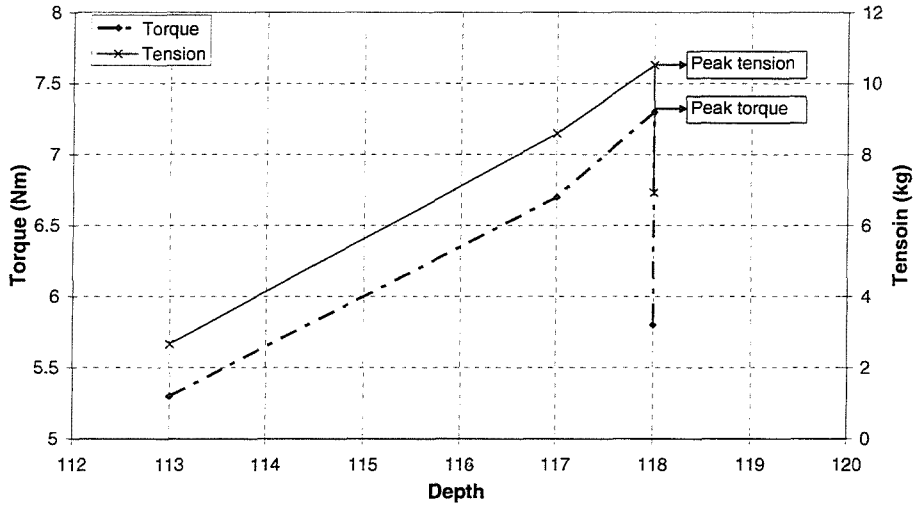

Figure 4.15: Typical result from a preliminary auger test where an axial restraint was imposed on the auger

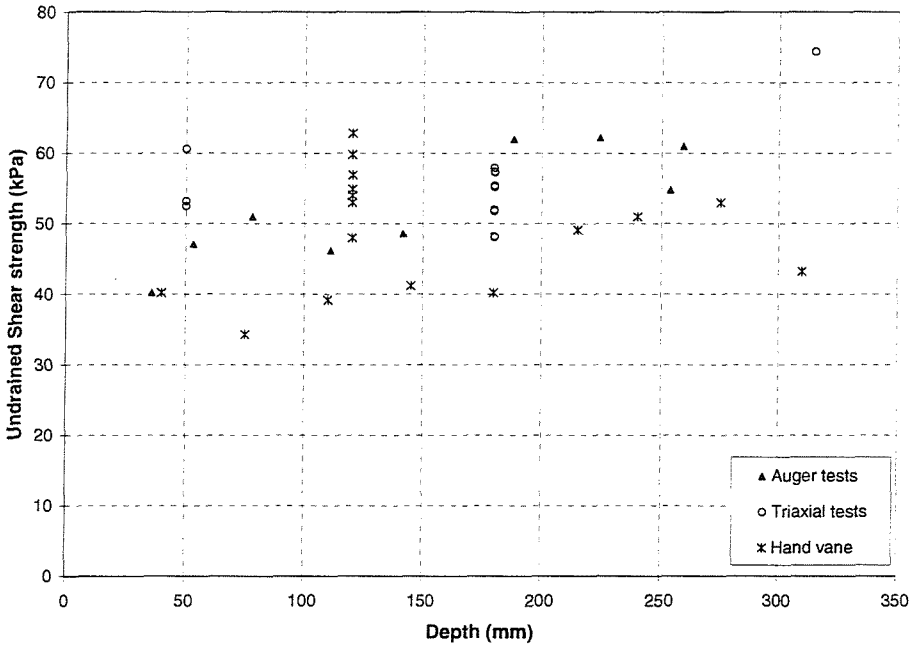

Figure 4.16: Comparison between undrained shear strength (c_u) as measured by preliminary auger test, hand vane and triaxial

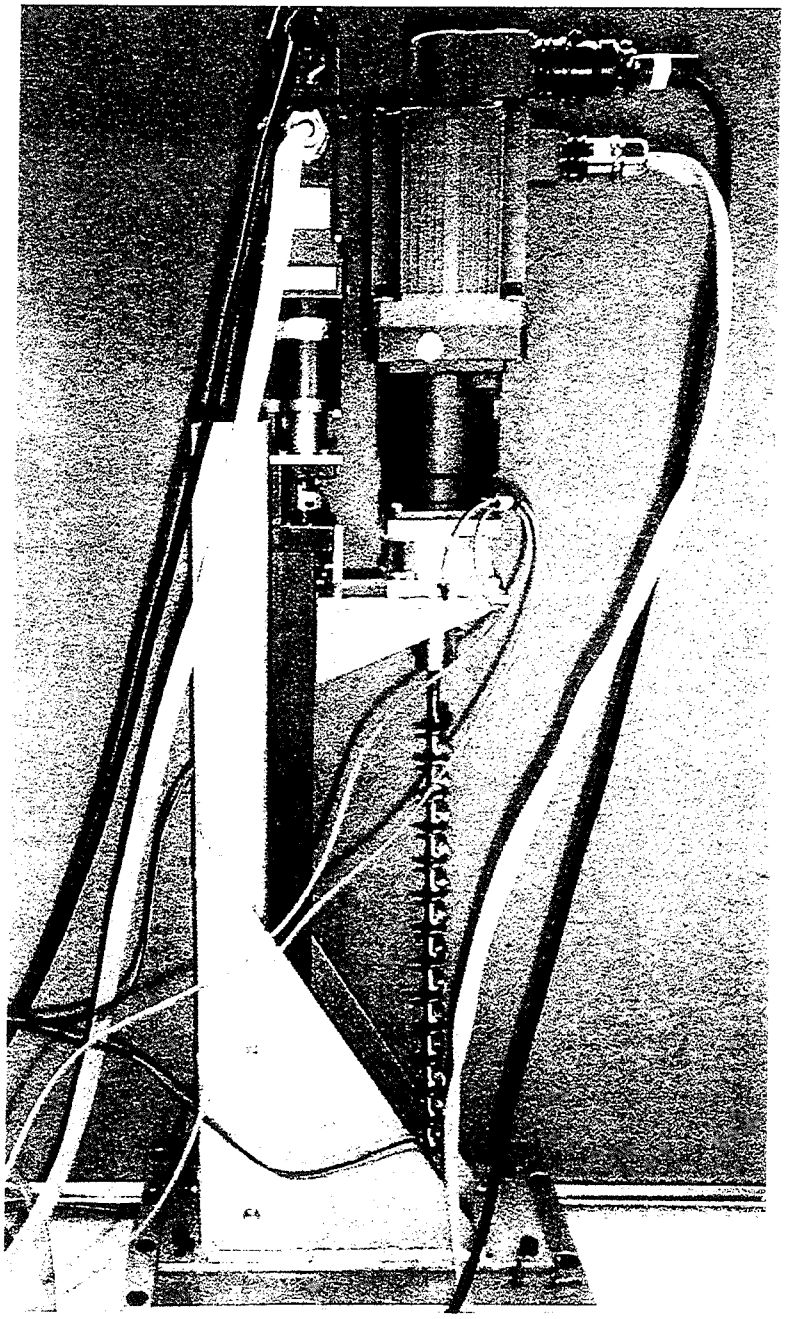

Figure 4.17: The model CFA rig

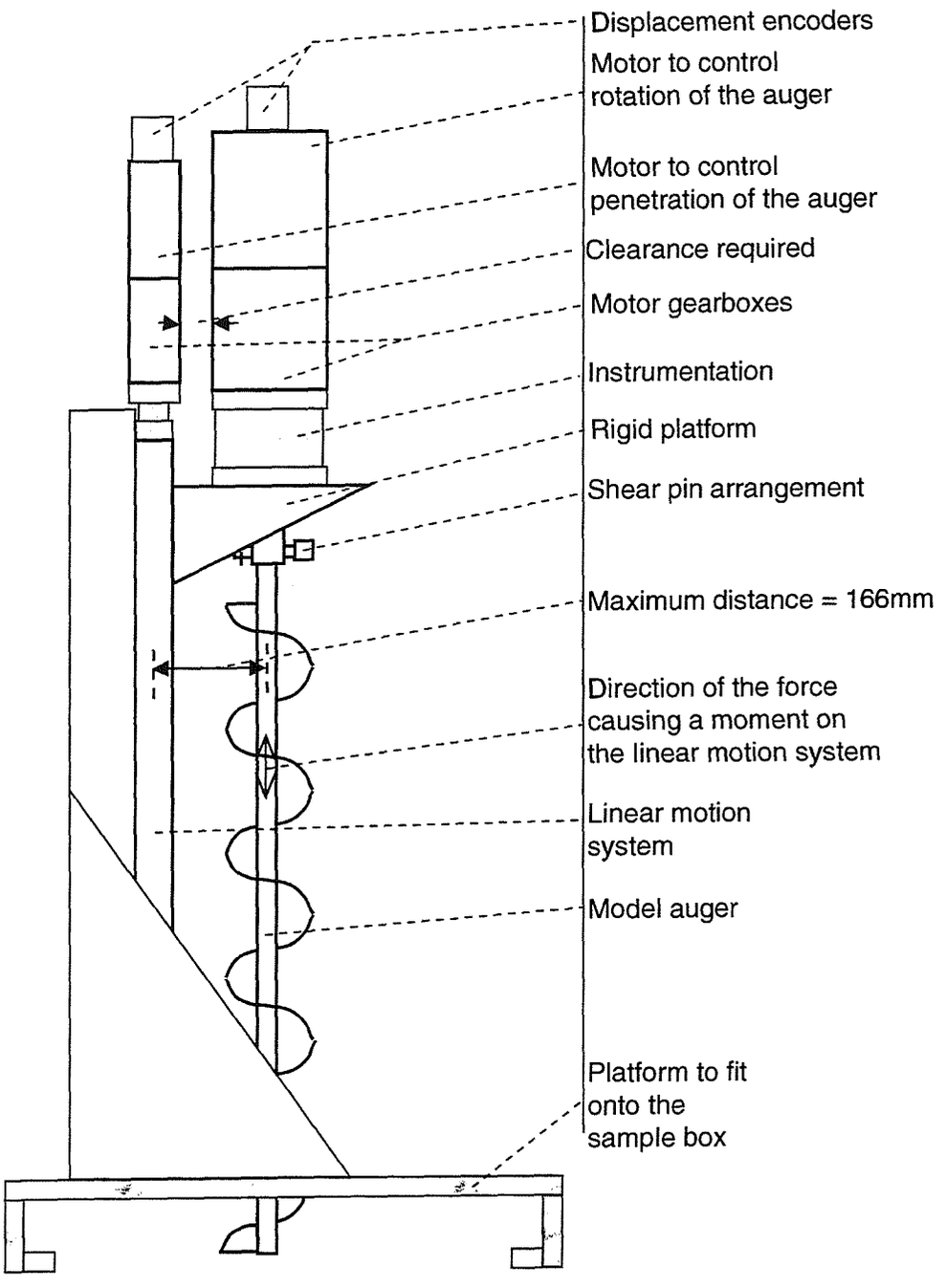

Figure 4.18: A diagram of the model CFA rig

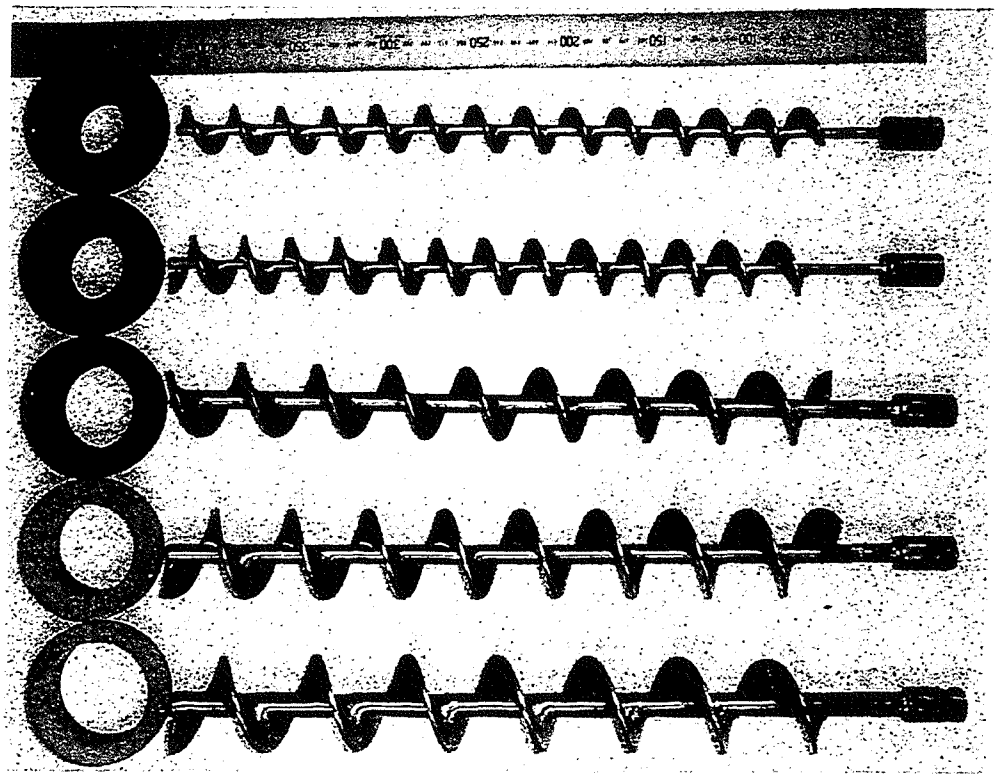

Figure 4.19: Augers with added shear pin arrangement, and auger guides for the model CFA rig

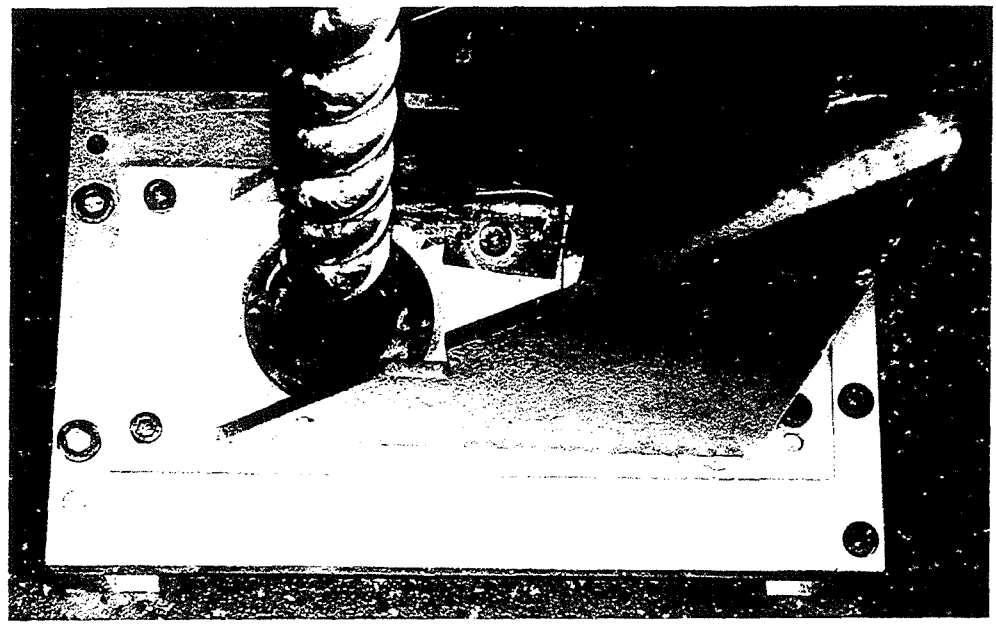

(a) Off-center hole in the platform

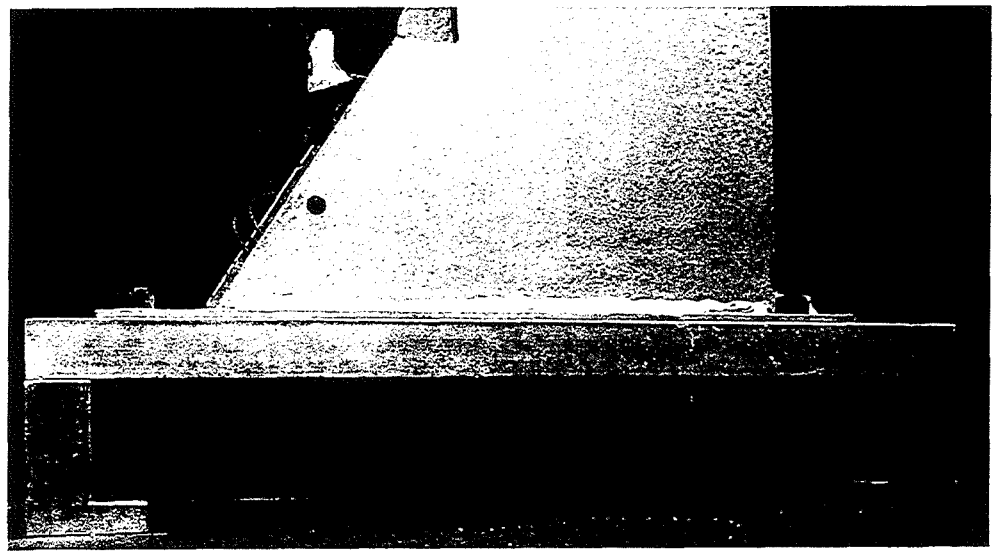

(b) Clamp configuration of the platform

Figure 4.20: The platform made to clamp onto the sample box

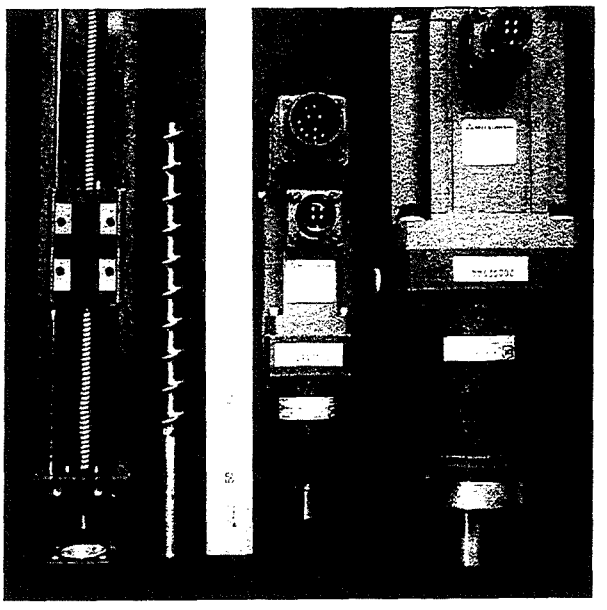

Figure 4.21: THK KR33A linear motion system, the Mitsubishi servo motors with Alpha gearboxes fitted and a model auger

Figure 4.22: The coupling with shear flange arrangement designed to protect the model from excessive forces

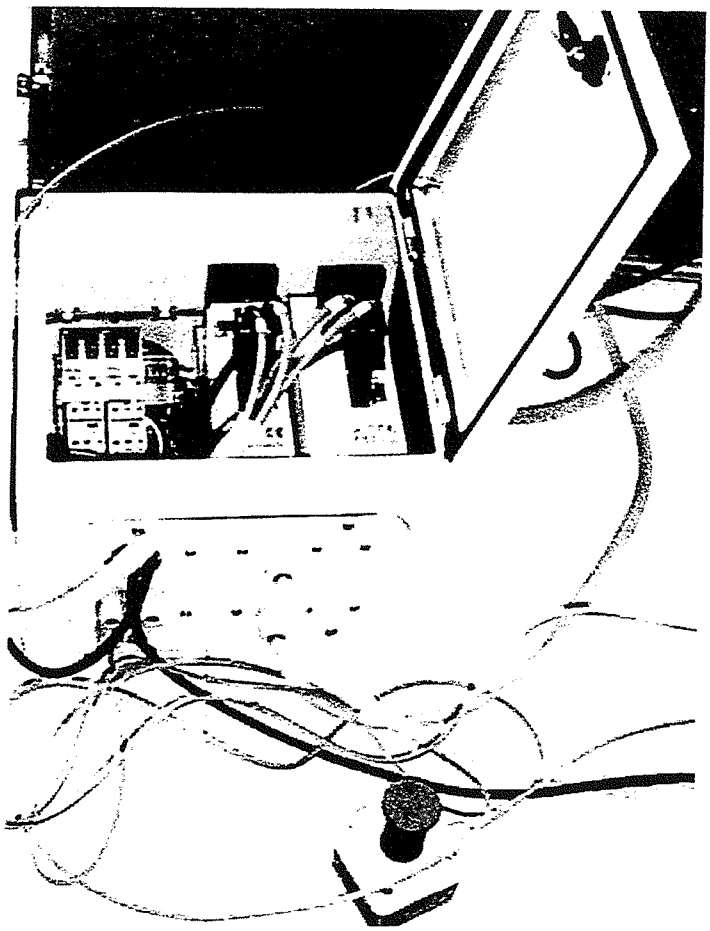

Figure 4.23: The motor amplifiers in their box to minimize interference. Emergency stop switch also shown

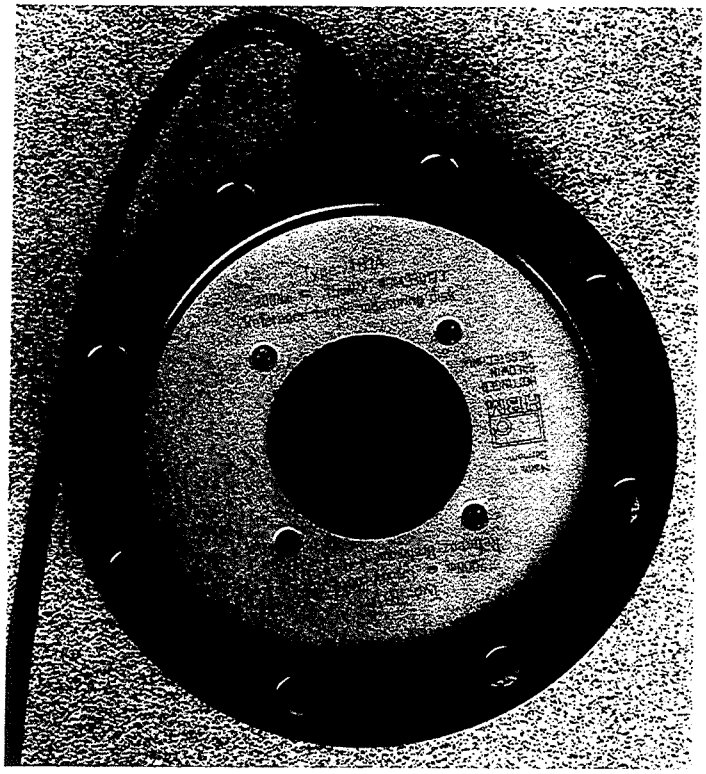

(a) Top of the transducer

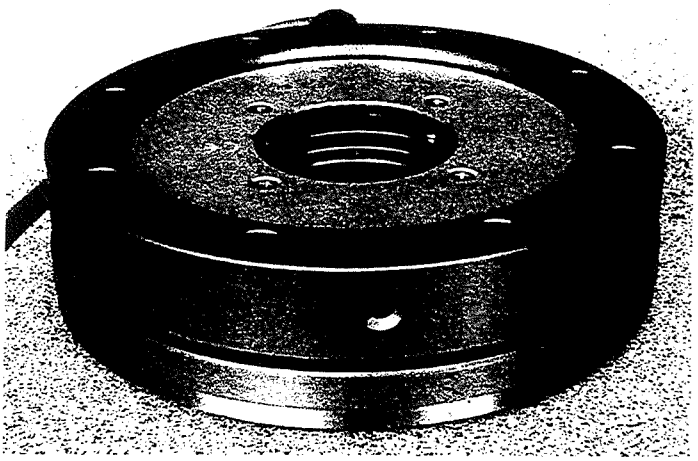

(b) Side view showing two flanges between which torque is measured

Figure 4.24: The HBM TB1A torque measurement transducer

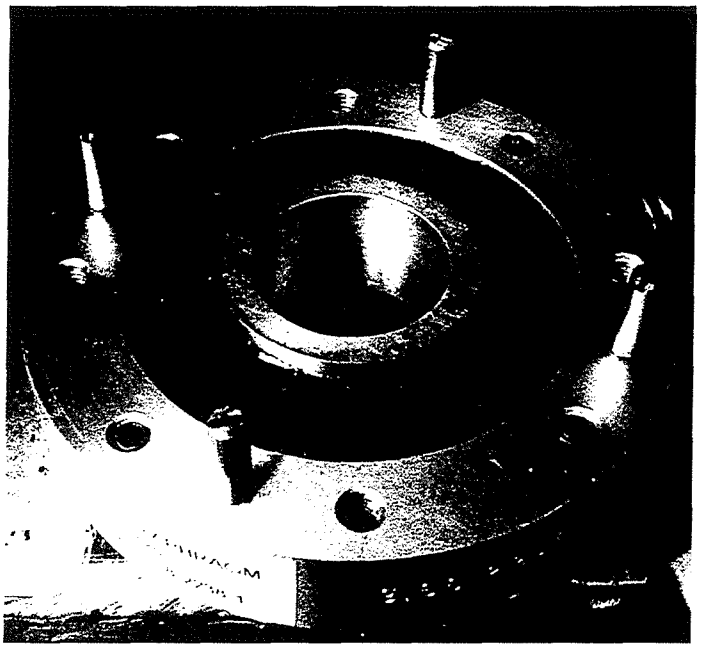

(a) The load transducer with sliding pin arrangement

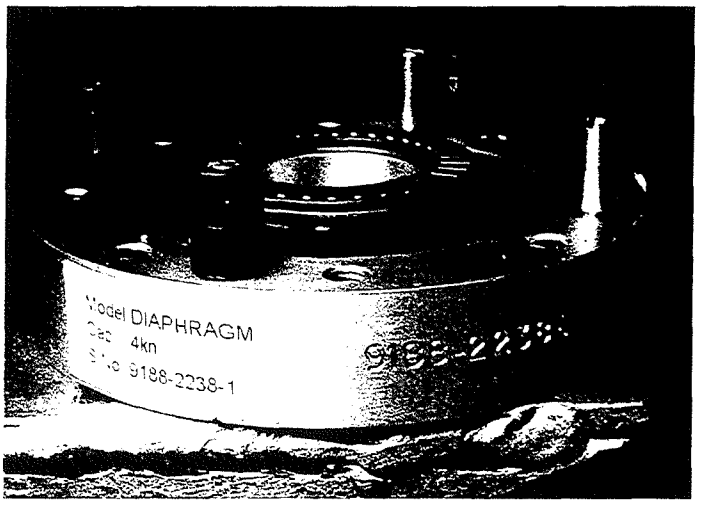

(b) The load transducer as well as the linear ball bearings and the roller bearing

Figure 4.25: Custom made 4kN transducer to measure axial load on the auger and transmit torque away from the measurement system

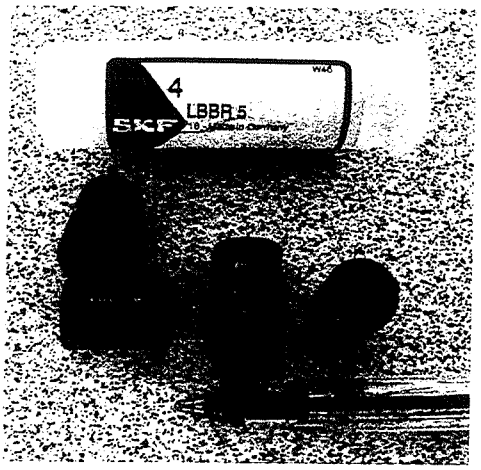

(a) The SKF LBBR5 linear ball bearings

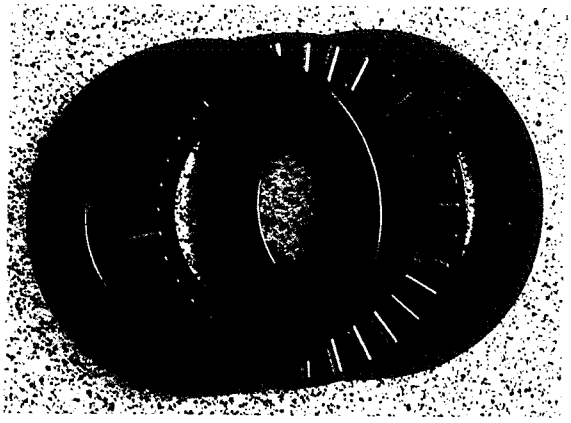

(b) The pin roller bearing

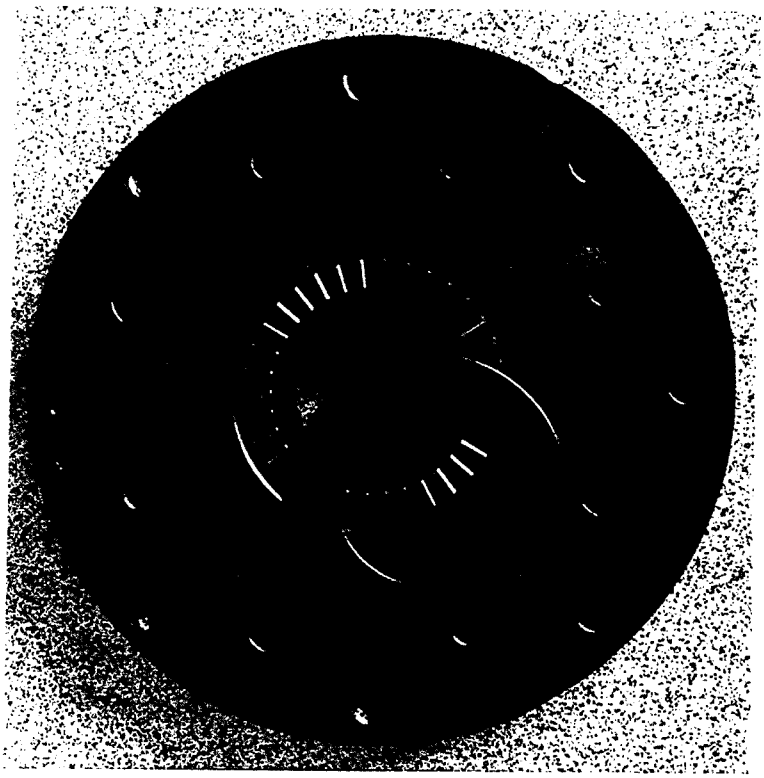

(c) Flange built to accommodate the bearings

Figure 4.26: Components used to separate torque from load to enable accurate measurement of axial load on the auger

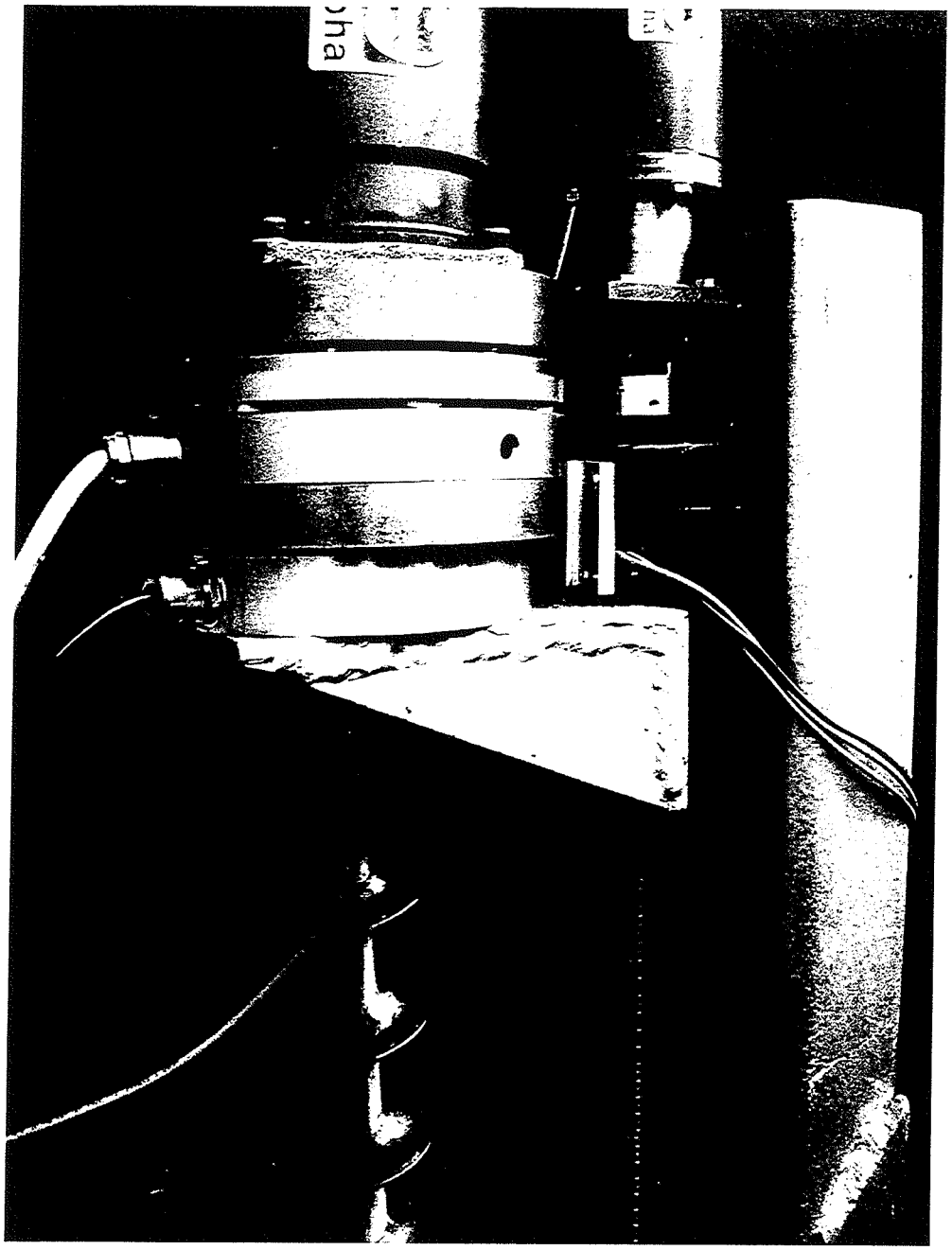

Figure 4.27: The new instruments assembled on the model CFA rig. Also note the upper end of travel switch to the right of the transducers.

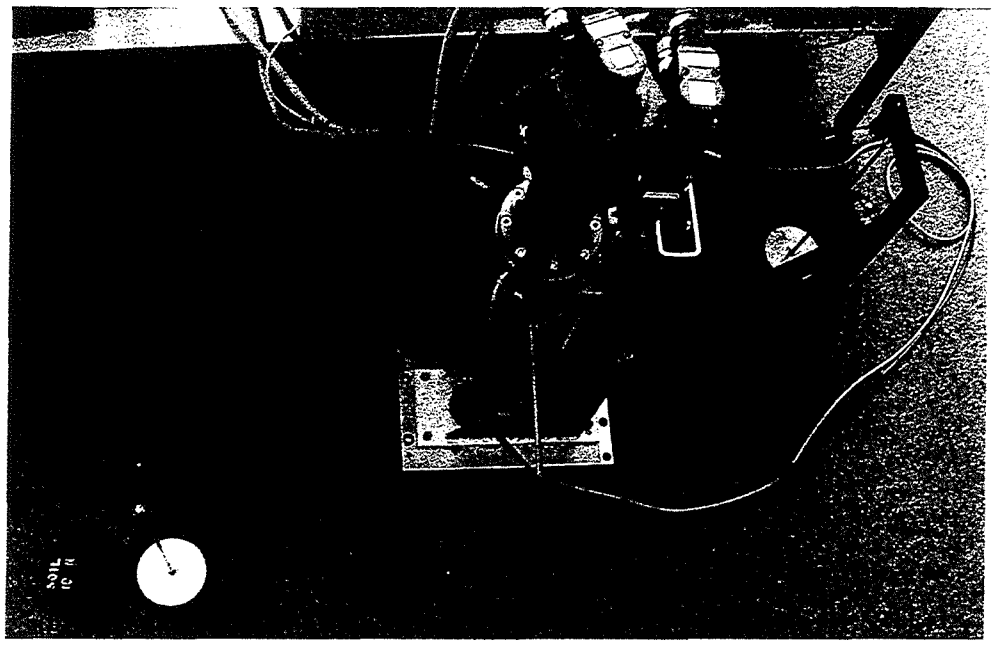

Figure 4.28: Loading frame built to calibrate the torque transducer

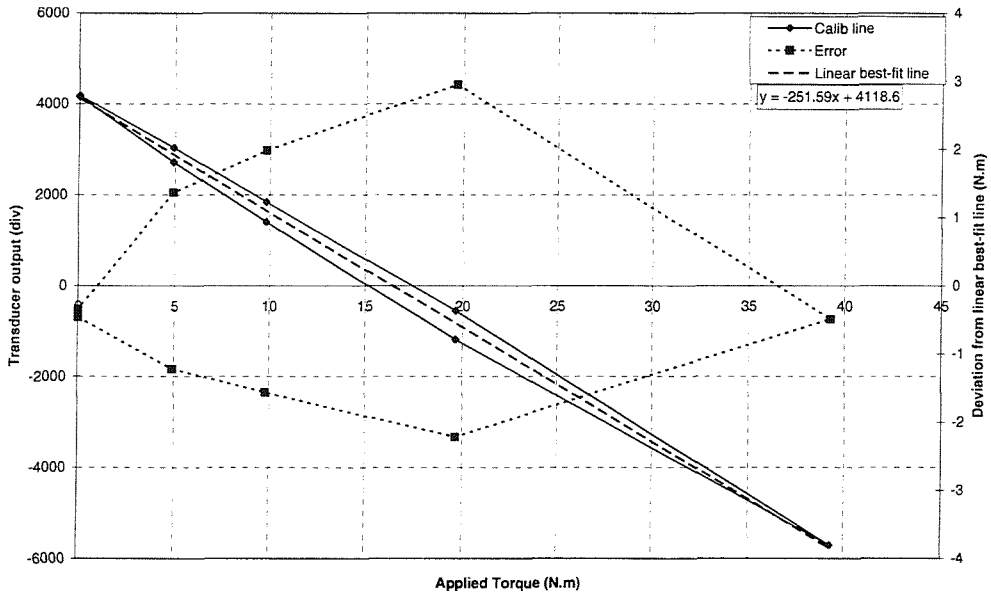

Figure 4.29: Calibration of the torque transducer

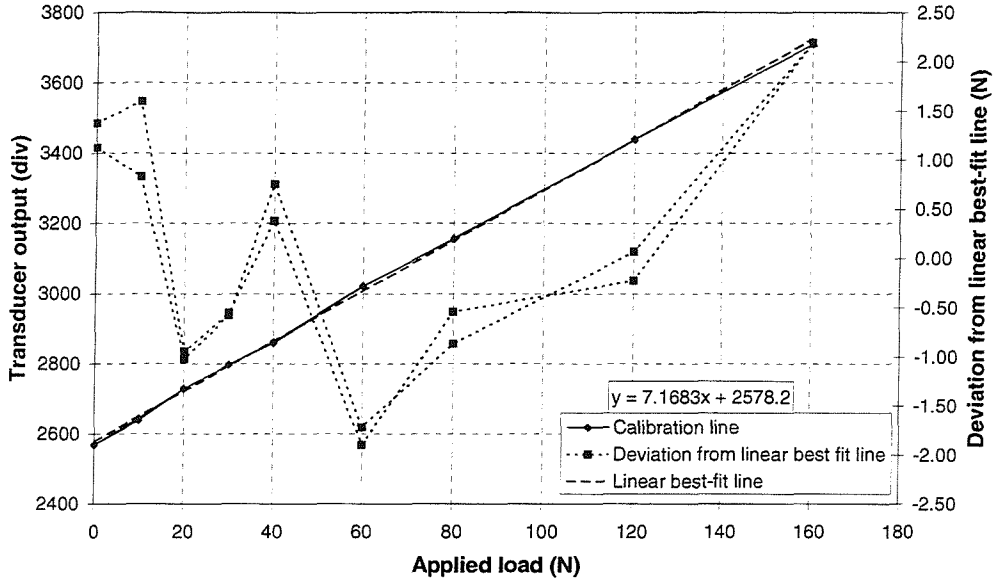

Figure 4.30: Calibration of the load transducer

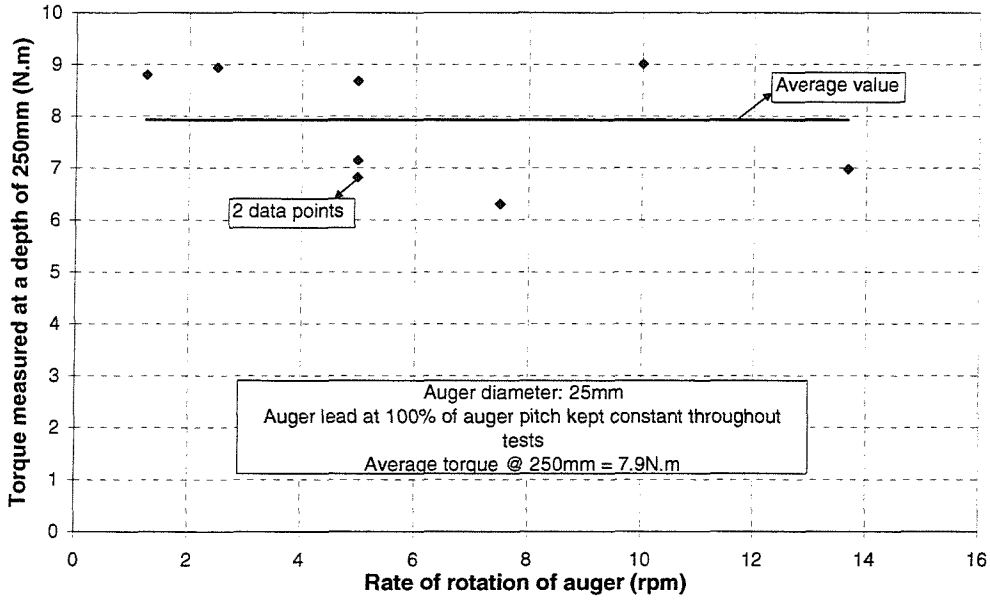

Figure 4.31: The influence of the rate of penetration on torque required to turn the 25mm auger

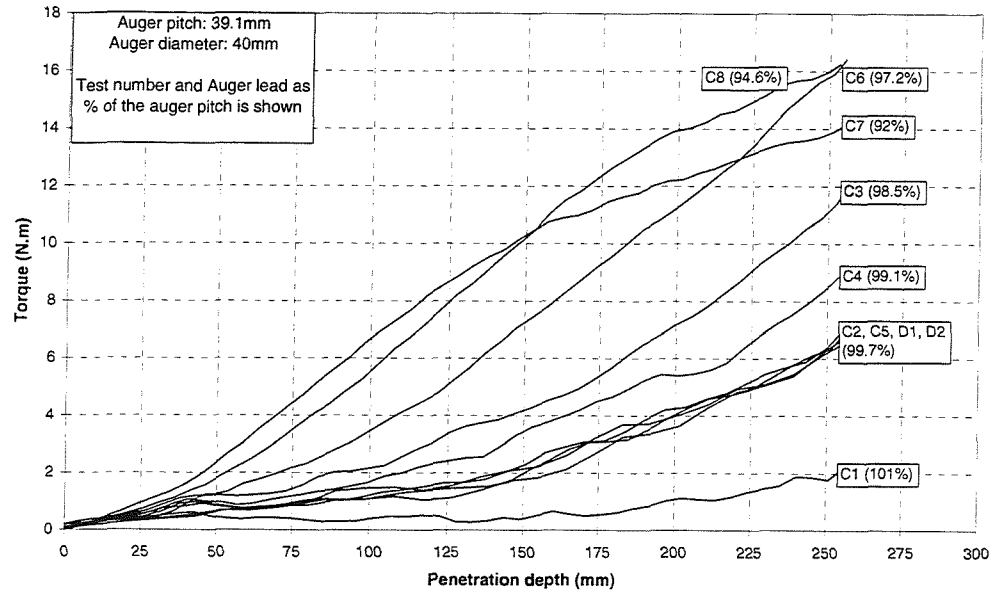

(a) Lead values ranging from 92% to 101% of pitch

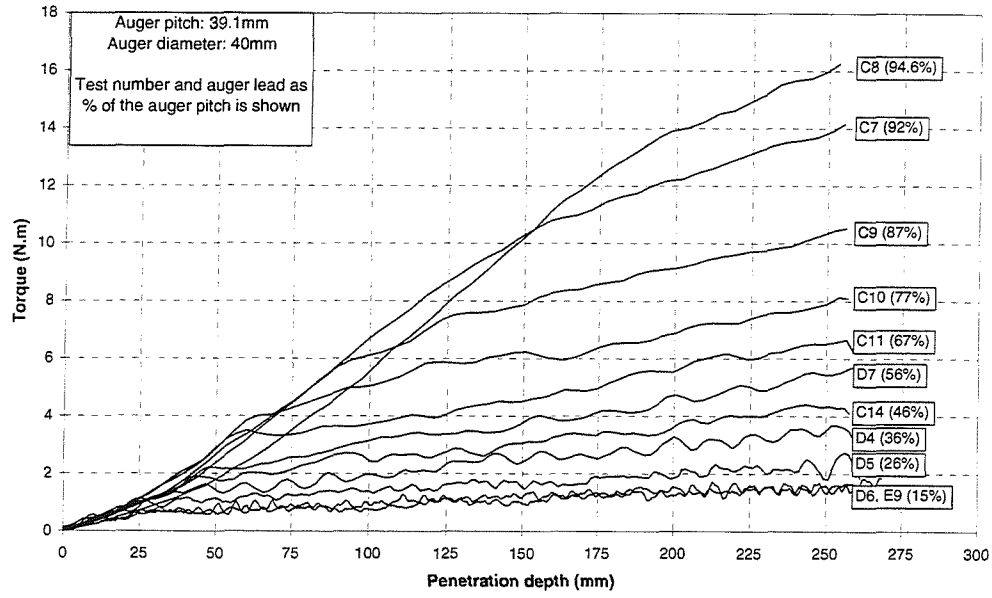

(b) Lead values ranging from 15% to 94.6% of pitch

Figure 4.32: Summary of torque measured on the 40mm auger

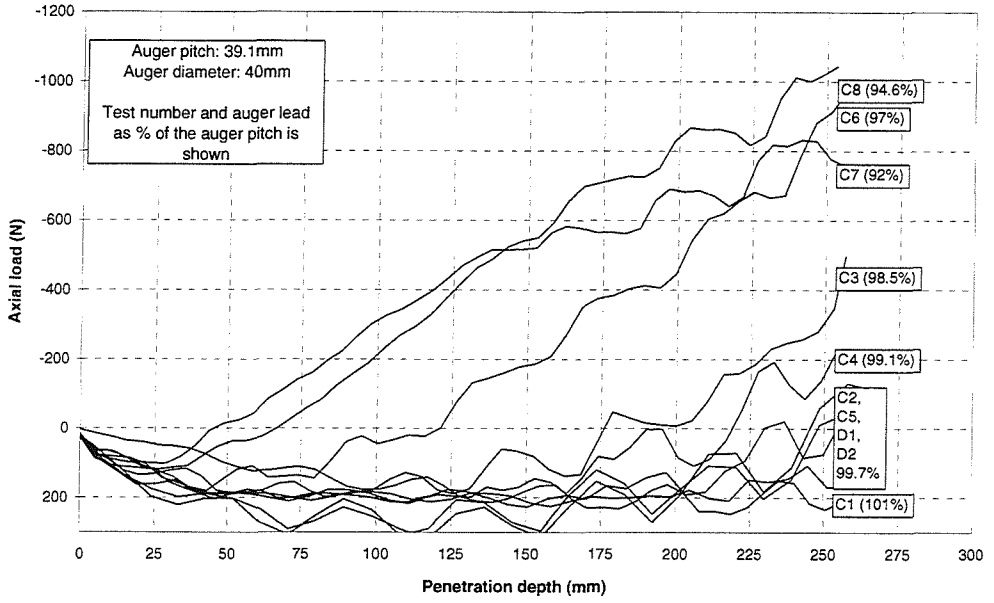

(a) Lead values ranging from 92% to 101% of pitch

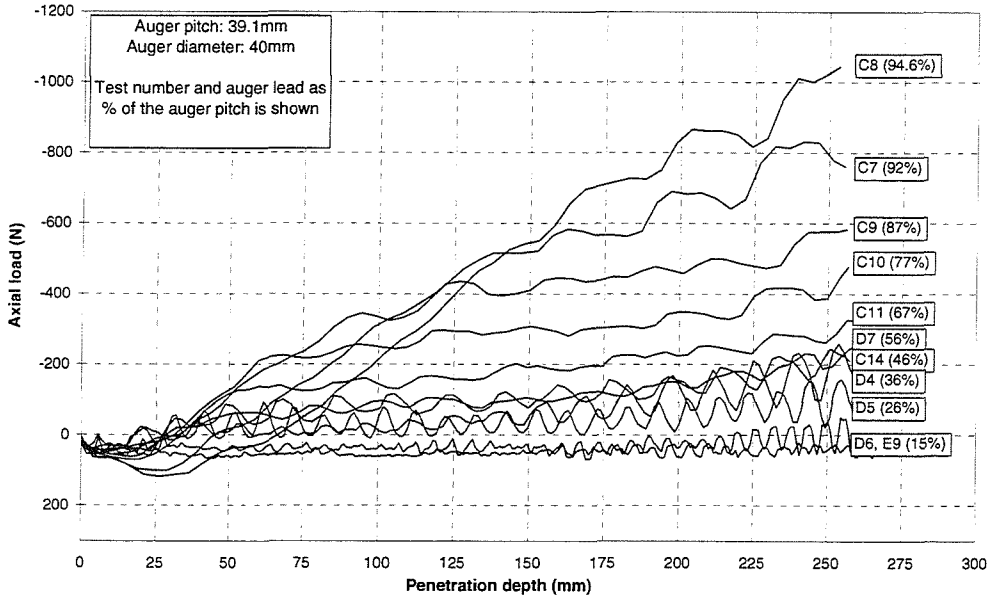

(b) Lead values ranging from 15% to 94.6% of pitch

Figure 4.33: Summary of axial load measured on the 40mm auger

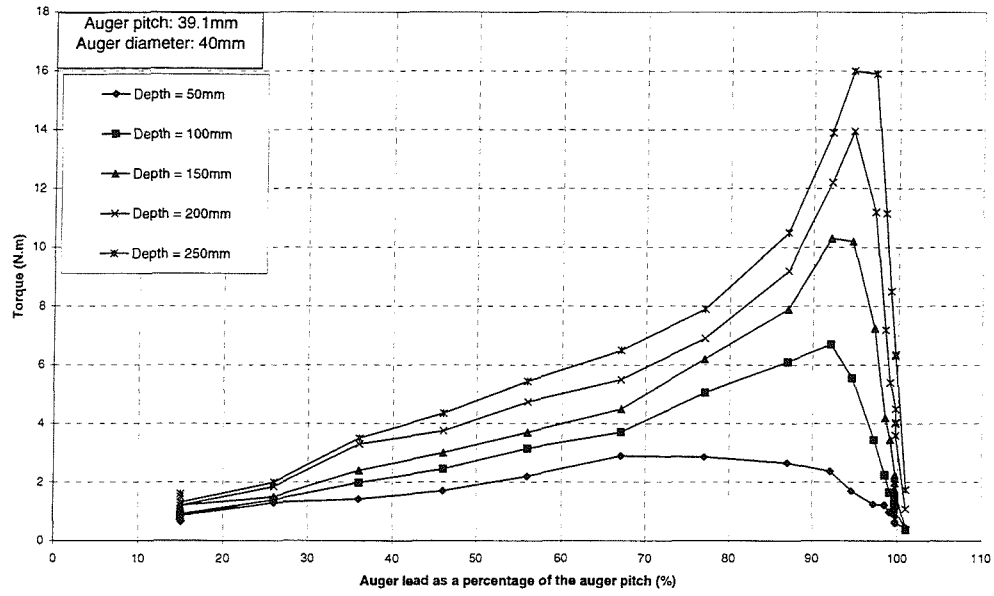

Figure 4.34: Torque recorded at certain depth intervals on the 40mm auger

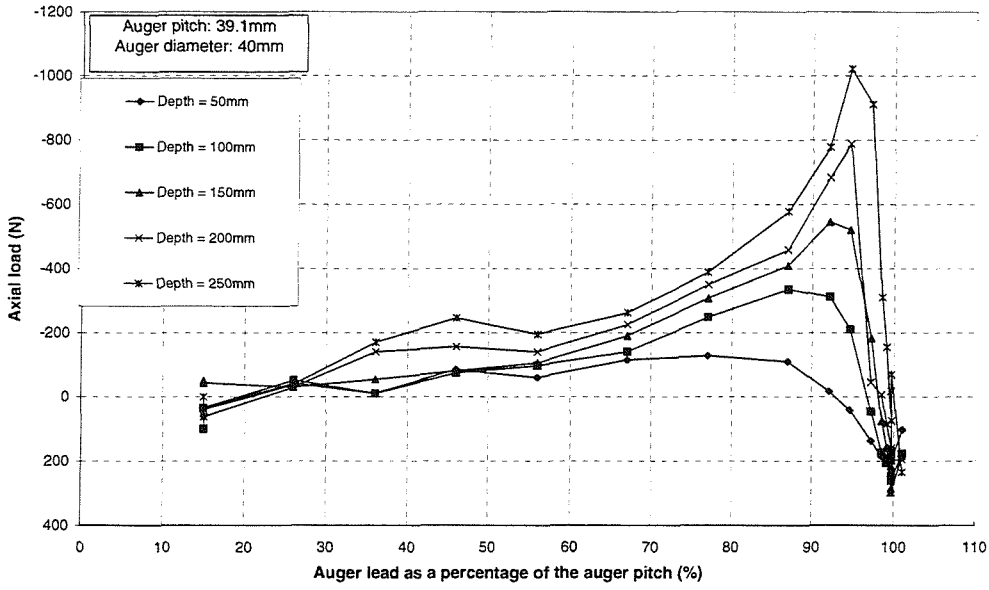

Figure 4.35: Axial loads recorded at certain depth intervals on the 40mm auger

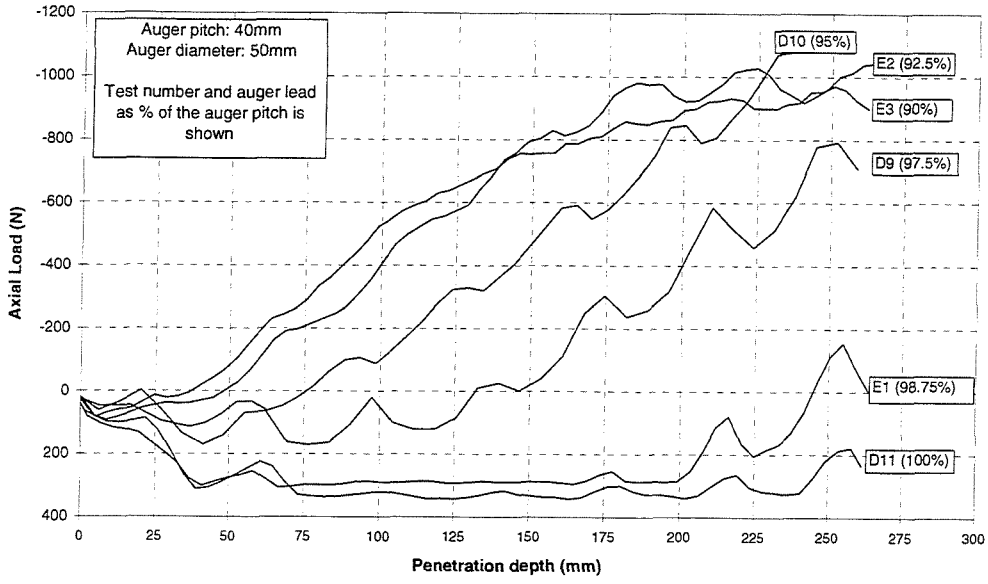

(a) Lead values ranging from 90% to 100% of pitch

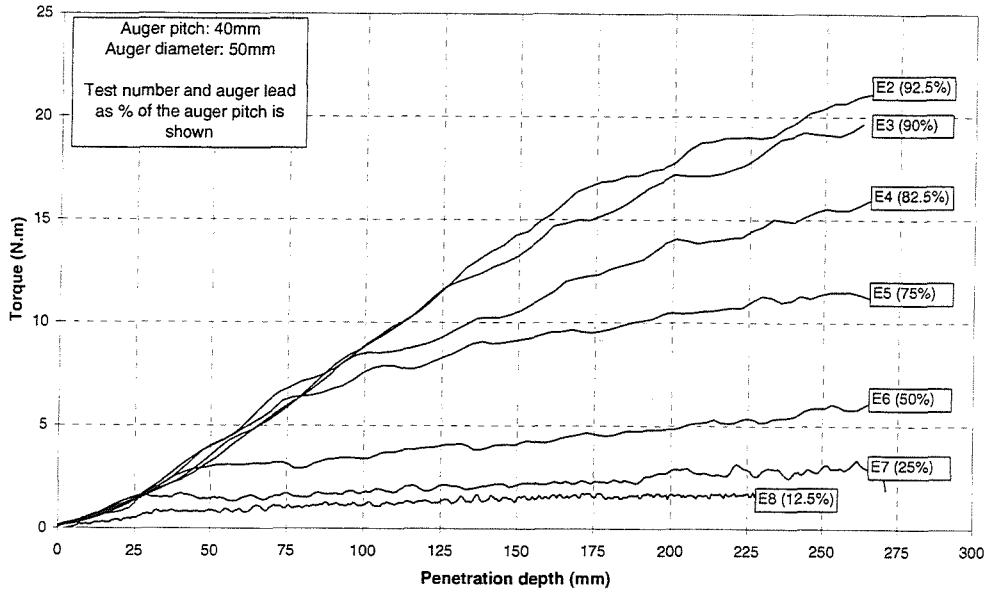

(b) Lead values ranging from 15% to 92.5% of pitch

Figure 4.36: Summary of torque measured on the 50mm auger

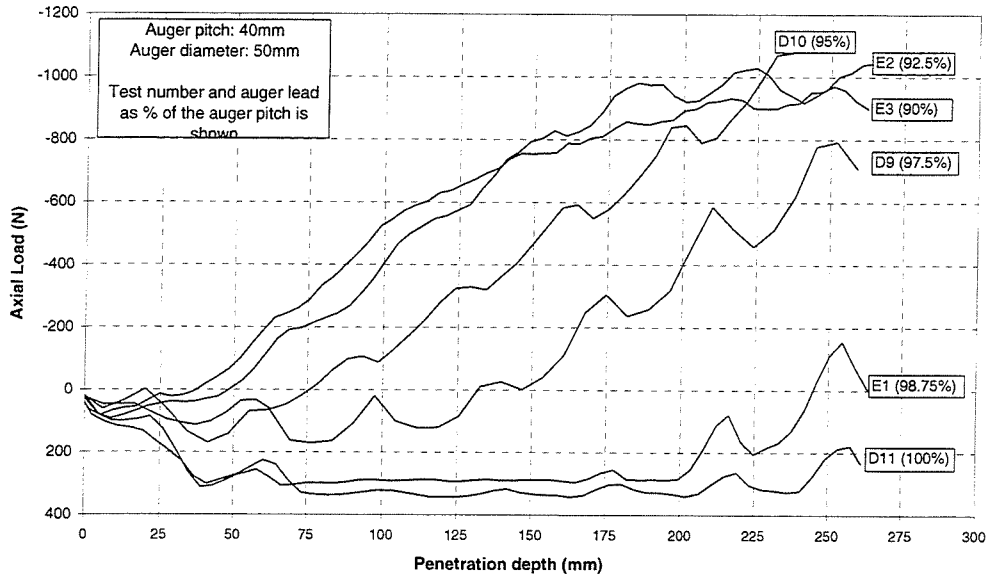

(a) Lead values ranging from 90% to 100% of pitch

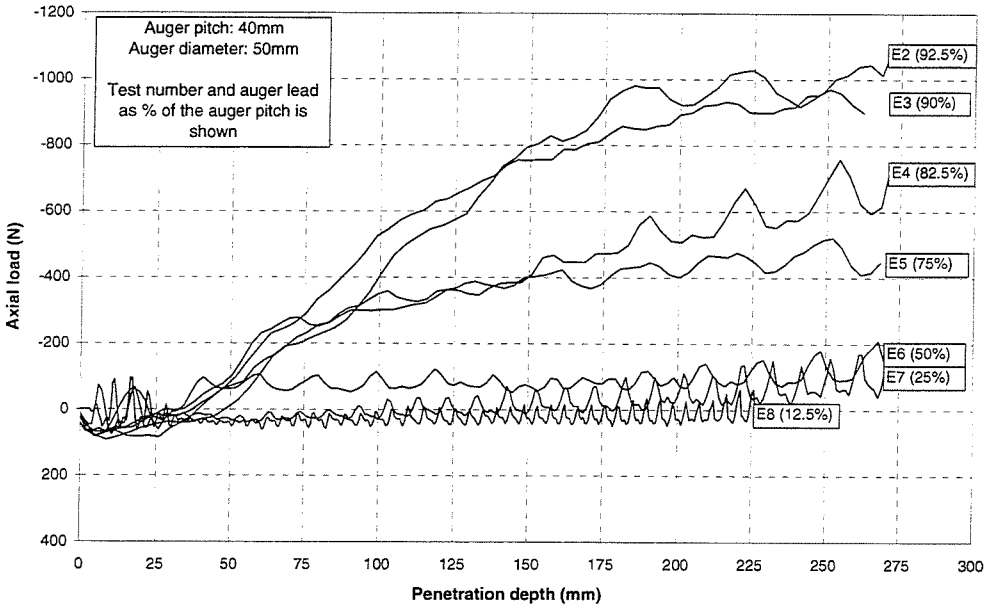

(b) Lead values ranging from 15% to 92.5% of pitch

Figure 4.37: Summary of axial load measured on the 50mm auger

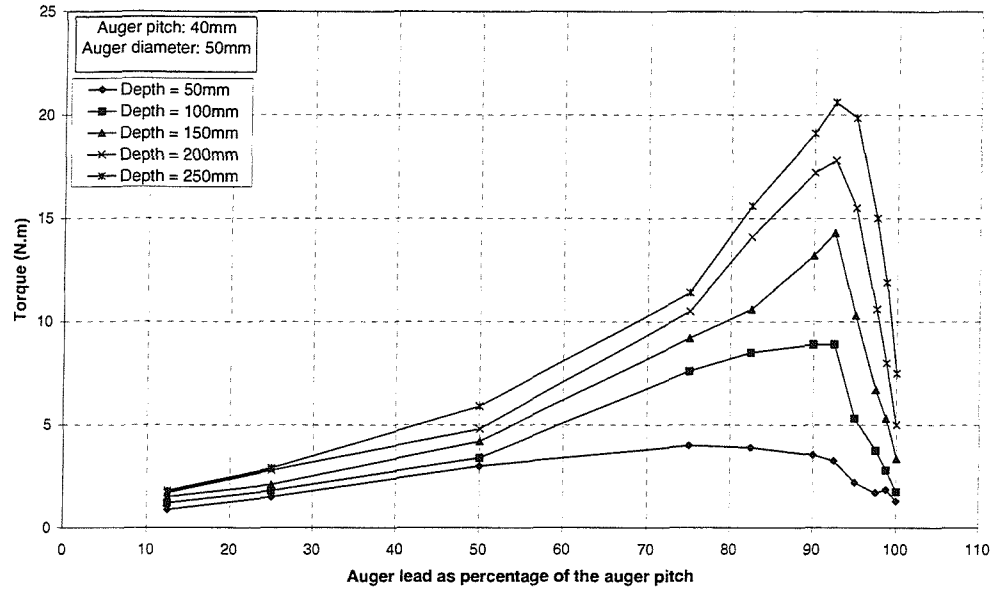

Figure 4.38: Torque recorded at certain depth intervals on the 50mm auger

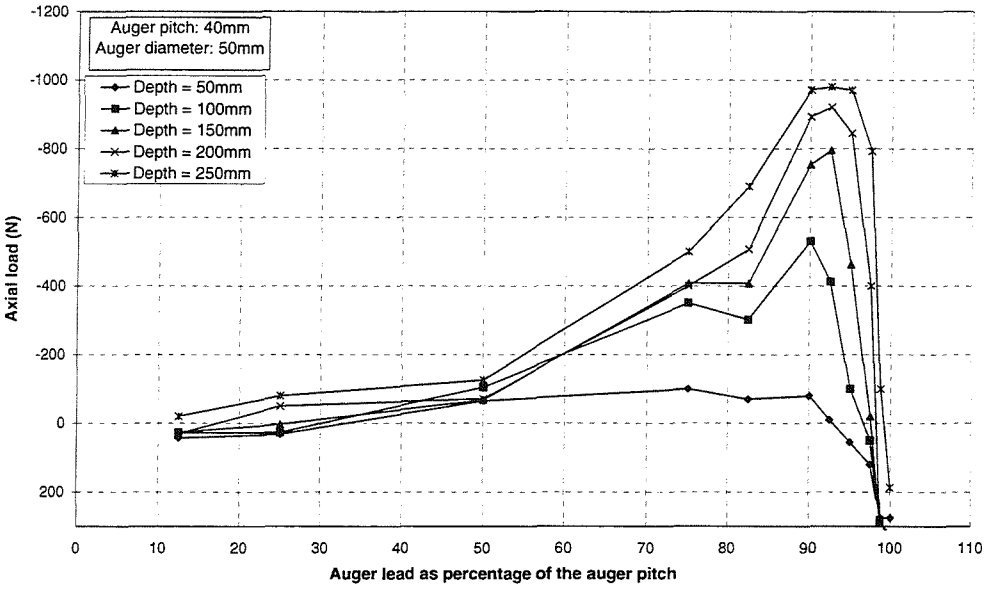

Figure 4.39: Axial loads recorded at certain depth intervals on the 50mm auger

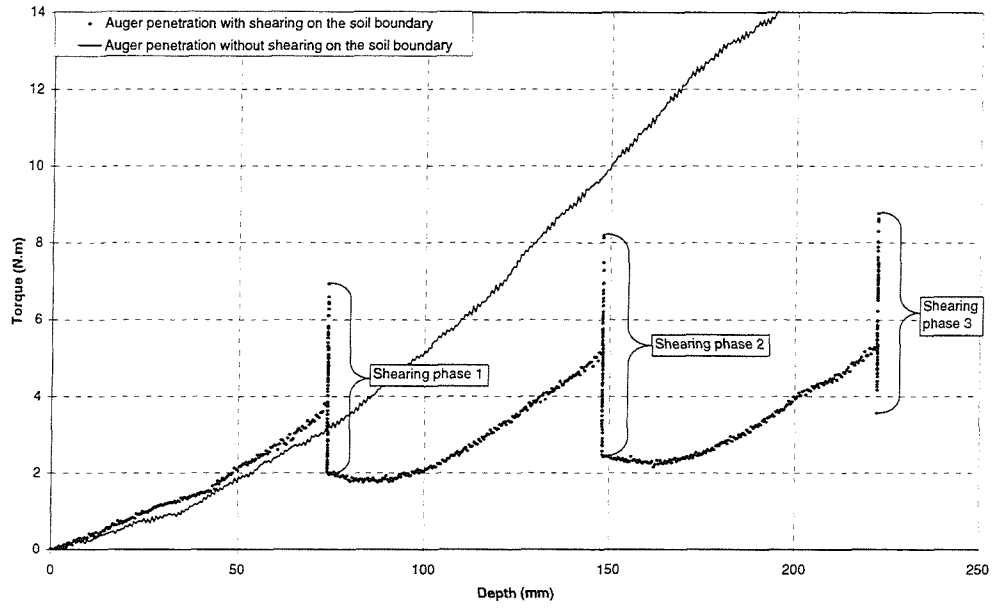

Figure 4.40: Torque measurement from three auger shear tests conducted consecutively in one hole, and an auger penetration test

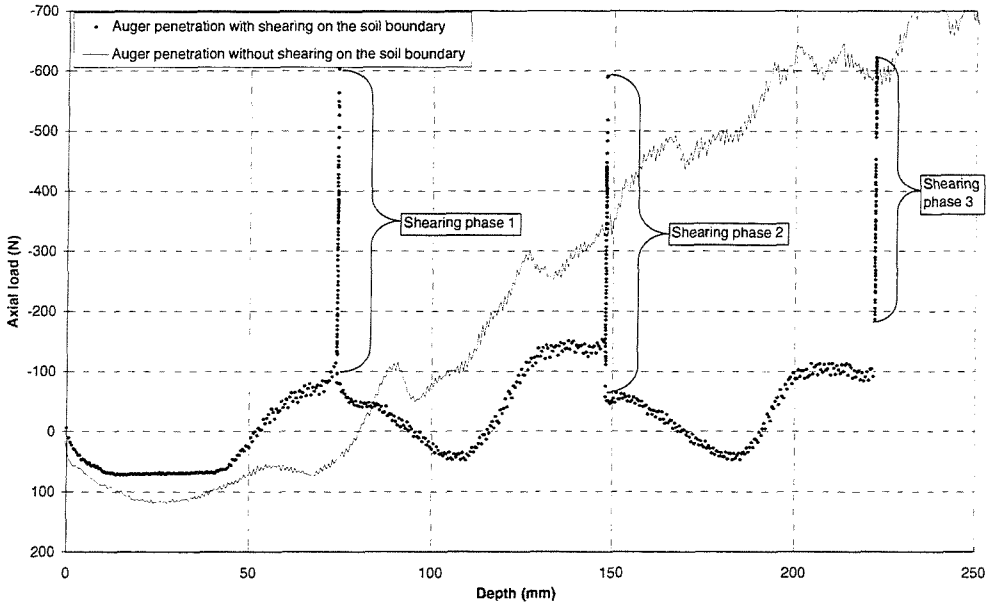

Figure 4.41: Load measurement from three auger shear tests conducted consecutively in one hole, and an auger penetration test

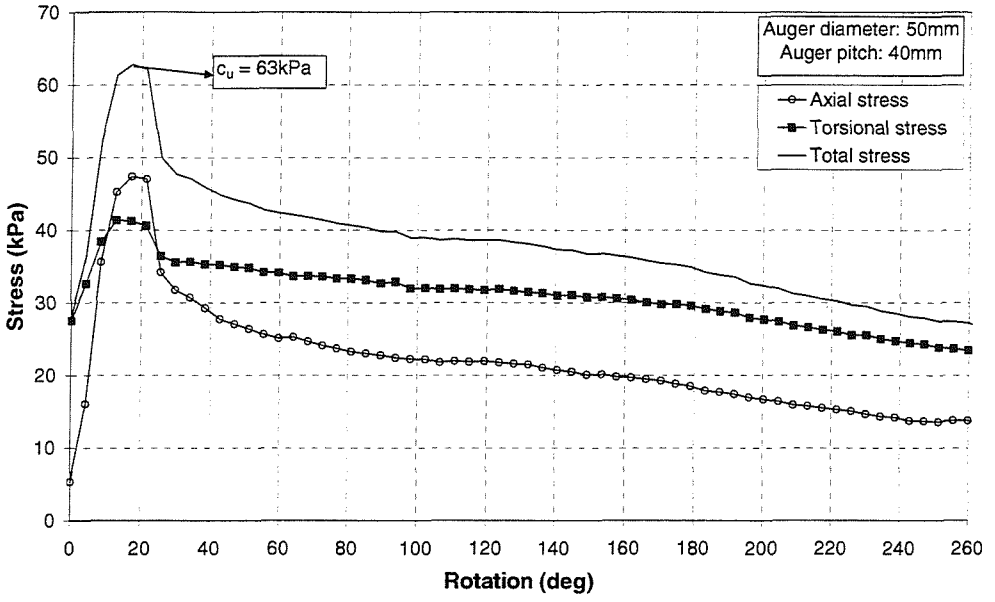

Figure 4.42: Example of the shearing phase of an auger shear test showing shear stresses imposed on the soil boundary

Chapter 5

DISCUSSION

A set of tests on model continuous flight augers has been carried out. The model design and test procedure were based on close observation of the operation of full-scale CFA rigs, as well as a literature review on CFA piling. This chapter discusses of the model test results, and attempts to link the findings from the model test results to site observations and issues highlighted in the literature. The applicability of the model test results to a full-scale CFA rig is discussed and suggestions regarding required rig instrumtation and rig modification are made.

5.1 Bored pile design procedures in the literature

Golder and Leonard (1954) state that "From extensive experience of the construction of bored piles in the London area, the authors consider that an 18-inch-diameter pile bored 30 feet into the London clay should carry satisfactorily a working load of 50 to 60 tons". This was the situation in 1954, when engineers based their designs on experience gained in similar projects. As time progressed however, more assurance was required that pile design was as economical as possible. Skempton (1959) proposed a pile design based on the undrained shear strength (c_u) of the soil. By the 1970's it was well rec-

ognized that this was a semi empirical method, requiring close adherence to the test methods used to measure c_u values. Difficulties in the measurement of this parameter, as well as the development of the principle of effective stress, gave rise to two other methods of pile capacity prediction. Design based on effective stress (Chandler, 1968; Burland, 1973; Parry and Swain, 1977) and design based on in-situ tests (Aoki and de Alencar, 1975; Schmertmann, 1978; Ruiter and Beringen, 1979; Philipponnat, 1980; Bustamente and Gianeselli, 1982; Decourt, 1982; Price and Wardle, 1982; Meyerhof, 1983; Bazaraa and Kurkur, 1986; Lopes and Laprovitera, 1988; Hirayama, 1990) were developed.

An Imperial College study into the scatter of predictions of pile capacity from pile design specialists was conducted in 1999 (Wheeler, 1999). The study asked specialists to predict the pile capacity of a driven steel pile and a driven steel pile with a jet grouted base using site investigation data and pile dimensions. The piles were subsequently constructed and loaded to failure. The results of this study showed a wide range of pile capacity predictions as shown in Figure 5.1. Given the number of pile design methods and formulae available to the pile designer this outcome was not surprising. It is interesting to note that the pile shaft capacity predictions underestimate in 15 of the 16 cases in this study.

The use of effective stress design for piles has proven to be more complex and expensive but still inaccurate and empirical because of the assumptions that have to be made to estimate the horizontal earth pressure after pile installation. "As any effective stress approach to pile design in stiff clays requires a greater knowledge of effective stress conditions around a pile than is at present available, pile design based on currently recommended values of α is likely to be more reliable" (Parry and Swain, 1977). The number and complexity of factors affecting the pile bearing capacity is too great to be taken into account by traditional pile design (Zelikson, 1988).

Peck (1953) stated, "the subject of pile foundations is the most complicated aspect of foundation engineering". To date no method of pile design

that can predict pile performance with sufficient accuracy has been developed, as shown by the study conducted at Imperial College (Figure 5.1).

5.1.1 *CFA pile design methods*

The methods used for the design of CFA piles is the same as those used in the design of bored piles (Hodgon, 1991; McVay, Armaghani and Casper, 1994). No specific design procedure for CFA piles has been developed, although as Fleming (1995) highlights, some authors have suggested that CFA piles have larger capacities than other types of bored piles. Tchepak (1998) suggests the use of an "installation factor" for the design of CFA piles in residual clays. The installation factor is applied to the traditional bored pile design to take into account the effect of CFA pile construction on the pile capacity. The factor is determined from the back analysis of a pile load test. In another paper, van Weele (1988) notes that from his experience with CFA piles in the Netherlands, "the predetermination of CFA pile capacity"... "is not yet possible with sufficient accuracy".

5.1.2 *Variability in soil parameters used for pile design*

Figure 3.9 shows site investigation data used in 1998 to design CFA piles on the Royal Victoria docks in London for the ExCel exhibition centre. A generalized soil profile is provided to the left of the depth axis on all three plots. The first plot shows c_u against depth, where c_u values were measured by unconsolidated undrained triaxial tests on 100mm samples. The second and third plots show cone penetration test results of the cone point and cone sleeve resistance respectively. The wide scatter of results from the site investigation tests is striking, as well as the fact that no corresponding trend can be found for the three. Site investigation data with such a wide scatter of results is commonly used to design piles.

Fleming and England (2001) gave the following criticisms on tools used for pile design procedures as published in a meeting report in Ground Engineering.

- *"Undrained shear strength: does not measure strength or stiffness in any absolute way. Approximately equivalent to an index test.*
- *Standard Penetration Test: a dynamic test with dependence on bore size and which can easily be upset by water inflow, large rock fragments, and even non-standard equipment. Results can be very misleading.*
- *Pressuremeter: should be effective but measures strength in the horizontal direction. Horizontal and vertical soil properties may differ significantly.*
- *Dutch cone: a dynamic and rate affected test. Its depth may be limited in hard ground. It provides much information about local ground variations and can be a reasonable good strength indicator tool. Stiffness cannot normally be measured.*
- *Seismic methods: use bulk response at low strain to infer low strain soil modulus. Directional uncertainty is probable and careful correlation is required. It is a 'young' application of the method in need of further research."*

Furthermore, undrained shear strength test results are affected by sample size and test procedure. In the UK the SPT test does not suffer from the problem of non-standard equipment. Inherent disadvantages of site investigations for bored pile designs include:

- the inability to take into account the local variations in soil conditions on site,
- the inability to predict the influence of pile construction on soil conditions and
- the cost of site investigations both in terms of their actual cost and the fact that they need to be completed before construction commences, often placing them on the critical path of the project.

5.1.3 *Installation effects on bored pile capacity*

Peck (1973) states that the technique of construction is "vital to the success of our installations". This section briefly discusses the installation effects known to affect the capacity of bored piles. Installation effects may affect the integrity of the pile itself, or the properties of the in-situ soil surrounding the pile. Integrity defects to the pile itself are well documented and are not discussed here because these defects are formed during the auger extraction phase of CFA construction (Hodgon, 1991; Tomlinson, 1994; Fleming, 1995), whereas the research in this thesis is concerned with the auger penetration phase of CFA pile construction. During auger penetration the soil surrounding the bore will be disturbed.

The mechanisms known to influence the properties of the soil surrounding bored piles are listed and a short discussion of their relevance to CFA pile construction is outlined. Three mechanisms that may influence the properties of the soil surrounding the bore are given by Milititsky (1983):

- stress relief of the soil surrounding the bore (also discussed by Brons and Kool (1988), Anderson (1988) and van Weele (1988)),
- remoulding of a thin layer of soil directly in contact with the pile shaft and
- water migration from the fresh concrete softening the surrounding soil.

Furthermore, Thorburn, Greenwood and Fleming (1993) and Lacy et al. (1994) have shown that subsidence next to the pile can occur when augering in granular materials.

The remoulding of a thin layer of soil directly in contact with the auger is particularly damaging in soil with variable layers of high and low permeability (for example layers of sand and clay). Excessive rotation of the auger causes these soils to remould and mix on the side of the bore, thereby causing the moisture content in the low permeability soils to increase, which dramatically reduces the shear strength of the soil. CFA pile test results on the highly variable Brackelsham beds in Southampton, as in the case of

the recent construction of the West Quay centre, showed a high variation in pile capacity across the site (Troughton, 2002). A definite cause of the high variability could not be established, but it may well have been due to the remoulding of a thin layer of soil directly in contact with the auger to a greater or lesser extent depending on the installation technique. Schwartz, A'Bear and Strydom (1999) discuss a case history where CFA piles did not perform as expected on a site in Johannesburg, and suggest a small adhesion factor as one of the possible reasons for the lack of pile capacity. This may also be a result of the same mechanism.

Lacy et al. (1994) conclude from a case history on CFA piles that "a contractor's technique for installing this type of pile is more important than small variations in soil density and grain size of the soil in which the pile is installed". The development of specifications for monitoring of CFA pile construction (BS8004, 1986; ICE, 1988; ICE, 1996; ENV1997-1, 1997) shows that the monitoring of the whole construction process has been given greater importance over the past two decades, driven by experience gained during construction. The above specifications stress the increasing importance of monitoring during the installation of CFA piles, driven by the fact that the construction method influences the pile performance.

The lead of the CFA auger has been found to influence pile capacity, especially in granular materials (Lacy et al., 1994). The model auger test results show that the auger lead is dependent on the torque used when augering, and that a rig must have sufficient torque available to be able to advance the auger at a high lead. By using the relationship of torque to the lead measured on the model auger rig, and the lead obtained on site using a particular CFA rig and auger, a recommendation can be made as to how much extra torque would be required to advance the CFA auger at given minimum lead.

Analysis of data recorded on CFA rigs showed that CFA augers are usually advanced at a rate of between 15 and 40% of the auger pitch per revolution. A minimum rate of penetration of 50% has been suggested by Lacy et al. (1994), as severe subsidence of adjacent structures was measured when the

rate of penetration was less than 50%. Other authors such as van Weele (1988) have raised their concern over the use of CFA rigs with low torque capacities.

5.2 Model auger tests

It was decided to carry out tests at model scale because:

- there could be close control of the auger movement;
- accurate measurement of the forces on the auger was required;
- a repeatable and relatively uniform soil could be used and
- a large number of tests could be conducted at relatively low cost.

This section contains a discussion of the model auger test results. A comprehensive description of the model auger test procedures and a complete set of results have been given in Chapter 4 and Appendix A. Detailed derivations of the equations used in the following sections are given in Appendix B.

5.2.1 *Auger penetration test results*

The auger penetration test procedure is described in Section 4.6. Variation in the rate of rotation of the auger at a given lead by more than an order of magnitude did not yield any clear relationship to the measured torque, as shown in Figure 4.31. Therefore there appeared to be a small rate effect if any at all. This contradicts work by Brons and Kool (1988) which suggested that an auger would require less torque at a low rate of rotation. This result may be due to undrained conditions prevailing in the soil even at the lowest rate of rotation used.

Variation of the lead of the auger severely affected the amount of torque and load measured. Figures 5.2 and 5.3 are representations of the results of a large set of auger penetration tests carried out at varying auger leads. The surface in Figure 5.2 represents the torque measurement results and the surface in Figure 5.3 represents the load measurement results on a 40mm

diameter auger. The lead axis shows auger lead as a percentage of the pitch of the auger (i.e. an auger penetrating the soil at a lead equal to its pitch was said to be penetrating at a lead of 100%). Lines were drawn on the surfaces in Figures 5.2 and 5.3 to distinguish different parts of the surfaces for discussion. The *'zero load contour line'* is drawn on Figure 5.3 through the points where the axial load on the auger is zero. The *'maximum torque'* and *'maximum load'* lines are drawn through the maximum values for torque and axial load respectively, measured at the depths shown on the depth axis. The *'full auger'* line is drawn at the lead of:

$$L_{full} = 100(1 - \frac{V_{aug}}{V_{bore}}) \tag{5.1}$$

where: L_{full} = *'full auger'* line value (%),
V_{aug}[1] = volume of the auger and
V_{bore} = volume of the bore (assuming that the bore diameter is equal to the outer diameter of the auger).

It is assumed that at a lead greater than or equal to L_{full}, the auger flight will be filled with soil (i.e. soil is in contact with the top and bottom of the auger flight as illustrated in Figure 5.4). This is because the auger will displace a volume of soil equal to its own volume, preferentially onto the auger flight if the auger flight is not completely filled with soil. Once the flight is full, lateral and vertical displacement can be expected.

Lead in excess of the full auger, maximum torque and maximum load lines

Figure 5.4 is an illustration of an auger penetrating at a lead greater than the full auger line, maximum torque and maximum load lines. When the auger is penetrating as shown in Figure 5.4, the following is assumed:

[1] auger volumes were measured by measuring their water displacement

- the flight of the auger is completely filled with soil (i.e. soil is in contact with the top and the bottom of the auger flight as discussed before) and
- the soil on the soil boundary has not been sheared.

The second assumption is based on the belief that soil on the soil boundary shears only when the lead is less than the values given by the maximum torque and maximum load lines for a given depth. This belief is motivated by the reversal in the auger torque and load to the auger lead relationship when the auger lead reduces below the maximum load and torque lead values.

Given the two assumptions, the only surface on which soil is sheared at the specified lead is on the surface of the auger. Force and moment equilibrium equations were derived and are discussed in Section B.3. Because of the number of unknown variables in these equations they could not be used and an approximate solution was formulated. A conclusion that could be drawn from the force equilibrium equation was that stresses normal to the auger surfaces cannot be equal on the different surfaces of the auger. Details of how the approximate solution was derived are given in Section B.4. The equation derived was

$$\frac{T}{r_t} cos\psi + F sin\psi = A_{aug}\tau_{aug} + f \tag{5.2}$$

where: τ_{aug} = shear stress on the auger surface;
A_{aug}= surface area of the auger in contact with soil (Section B.1);
T = torque applied to the auger in the direction of auger rotation;
r_t = the weighted distance of area from the auger polar axis (Section B.2);
ψ = angle representing the ratio of axial to rotational movement (Section B.4);
F = axial load applied to the auger and

f = constant resistance at the tip of the auger taking into account: the cutting action at the tip of the auger flight, and the resistance to the penetration of the solid inner stem.

The value of f can be calculated iteratively if it is assumed that the shear stress on the auger surface (τ_{aug}) is constant. At the first iteration, it is assumed that f is equal to zero and the shear stress on the auger flight is calculated using Equation 5.2. By iteratively choosing values for f it is then possible to determine a unique value for f that yields a constant shear stress on the auger surface (τ_{aug}) for any depth of the auger.

Figure 5.5 shows τ_{aug} back calculated from nine auger penetration tests on the 40mm outer diameter auger for a range of penetrations per revolution from 92.1% to 99.7% (full auger line value (Equation 5.1) = 86.7%).

The shear stress on the auger flight calculated by assuming f equal to zero is shown in Figure 5.5, labelled 'Uncorrected shear stress ($f = 0N$)'. A correction was then applied to the shear stress by determining a value for f which resulted in a constant shear stress on the auger surface. The value of f for this case was a force of 34N, implying that a constant force of 34N was required at the tip of the auger for the cutting action of the tip of the auger flight and the penetration of the solid inner stem of the auger. The average value of τ_{aug} was 24kPa, with a standard deviation of 6.5kPa. The shear stress correction due to f declines to approximately 5% of τ_{aug} at 250mm, 6.4 times the auger pitch.

Potyondy (1961) investigated the skin friction between various soils and construction materials. Since τ_{aug} is a measure of c_a, we may compare these values to those found by Potyondy (1961). The value of c_a/c_u for two clay moisture contents (22.8% and 26.1%) on smooth steel was found to be 0.27 and 0.30, respectively and on rough steel the values were 0.47 and 0.58 respectively. The back calculated value for c_a/c_u for this experiment is 0.30 (the clay moisture content was approximately 40.5%). This value is therefore within the boundaries found by Potyondy (1961) and therefore seems rea-

sonable. The conclusion may be drawn that the undrained behaviour of soil sufficiently explains the behaviour of the auger when auger lead values are between 92.1% and 99.7% of the auger pitch.

Values of shear stress on the auger have only been computed for a depth greater than or equal to 40mm as the assumption that f is constant does not hold at the start of penetration. This is because there is less constraint for soil being displaced to the surface at the start of penetration (40mm is approximately a penetration of one auger pitch, therefore the section of auger flight directly above the cutting tip will have penetrated the soil restraining the upward displacement of soil). Results from the back analysis converge at approximately this depth.

Lead not exceeding the full auger, maximum torque and maximum load lines

Figure 5.6 is an illustration of an auger penetrating at a lead less than the full auger, maximum torque and maximum load lines. When the auger is penetrating in this manner the following is assumed:

- the flight of the auger is not filled with soil (i.e. soil is not in contact with the bottom of the auger flight and only in contact with a part of the inner stem and the top of the auger flight as shown on Figure 5.6) and
- soil on the soil boundary has been sheared.

The assumption that under these conditions the auger flight was not filled with soil was observed in the laboratory. The void develops as more soil is being transported (flighted) to the soil surface than is being displaced by the auger. The second assumption is based on the belief that soil on the soil boundary sheared when the lead was less than the maximum torque and maximum load lines. As the bore was stable, soil was not being drawn in from the side of the bore to fill the auger flight. Since the tests were conducted under normal gravity conditions (1g), this is an inaccurate modelling of the

full-scale procedure. At full-scale the value of the stability number N given in Equation 5.3 may exceed 4, a value determined empirically at which, if exceeded, a bore may become unstable (Taylor, 1948). The value of N for the model tests did not exceed 0.1.

$$N = \frac{\gamma H}{c_u} \tag{5.3}$$

where: N = 'stability number' (Taylor, 1948);
γ = soil unit weight in kN/m^3 and
H = depth of bore in m.

The torque and axial load applied to the auger had to be great enough to overcome:

- the resistance of the soil to the cutting action at the tip of the auger flight,
- the resistance of the soil to the penetration of the solid inner stem of the auger and
- the shear stress developed on the soil boundary.

Force and moment equilibrium equations were derived for the free body representing the auger partially filled with soil. Details of the derivation are given in Section B.5.

Force equilibrium yields

$$W + W_s - F - f_s - f_{cut-v} + \tau_{so} A_{soil} sin\alpha = 0 \tag{5.4}$$

and moment equilibrium yields

$$T - \tau_{so} A_{soil} cos\alpha (D/2) - f_{cut-t}(d/2 + (D/2 - d/2)/2) = 0 \tag{5.5}$$

where: W = the weight of the auger;
W_s = weight of soil on the auger;
F = axial load applied to the auger;
f_s = resistance of the inner stem to penetration;
f_{cut} = resistance to the cutting action at the tip of the auger;
A_{soil} = the contact area between the soil on the auger and soil surrounding the bore (Equation 5.6);
α = the angle of movement of the soil relative to horizontal; (Equation 5.7);
T = torque applied to the auger and
τ_{so} = the shear stress between soil on the auger flight and soil surrounding the bore.

and subscripts '-v' and '-t' denote vertical and torsional components respectively.

As the lead of the auger decreases the surface contact area on the soil boundary reduces and may be calculated using the following equation:

$$A_{soil} = \pi D l \left(1 - \frac{(L_{full} - L_{\%})}{100}\right) \tag{5.6}$$

where: $L_{\%}$ = Lead of the auger as a percentage of the auger pitch.

The angle of soil movement with the horizontal, α, is

$$\alpha = tan^{-1}\left(\frac{L}{\pi D}\right) + tan^{-1}\left(\frac{V_{aug}}{V_{bore}}\right) \tag{5.7}$$

where: L = the lead of the auger (vertical advance per revolution).

This equation takes into account the fact that soil will move in the opposite direction to the edge of the auger flight plus a vertical amount because of the displacement of the auger volume into the soil matrix. It does not however take into account any bulking effect of the soil, which was assumed to be small

for the kaolin sample. This assumption was based on the observation in the laboratory that the sampled was sheared as a continuous ribbon, therefore no extra voids were formed in the sample to increase the voids ratio. Furthermore no outward displacement of the soil was assumed because the cutting action of the auger would have favoured soil being cut onto the auger flight as opposed to being displaced laterally into the surrounding soil.

As the auger penetrates deeper into the soil, the proportion of applied torque required to overcome the cutting resistance at the tip of the auger will diminish. The term f_{cut-t} in Equation 5.5 will therefore become less significant with depth. If it is assumed that f_{cut-t} is equal to zero and solve Equation 5.5 for τ_{so}, it should be found that τ_{so} approaches an asymptote as the depth of the auger increases. Figures 5.7(a) to 5.7(d) show some of the auger test results, indicating that the τ_{so} does approach an asymptote as the auger depth increases. Figure 5.8 shows the value of τ_{so} approximated at 250mm depth using the 40mm auger at different lead values. Back calculated values of τ_{so} from moment equilibrium for auger lead values between 6% and 87% of the auger pitch showed an average value of 12kPa, with a standard deviation of 3.2kPa. Interestingly the estimate of τ_{so} declines with declining auger lead value. This may show that f_{cut-t} diminishes with decreasing lead value because restraint to soil being cut by the auger will diminish.

Similarly the significance of W, W_{so}, f_s and f_{cut-v} in Equation 5.4 should diminish with depth. Therefore when solving Equation 5.4 with these values equal to zero, τ_{so} should approach an asymptote as the auger depth increases. Values for τ_{so} are also shown on Figures 5.7(a) to 5.7(d). The back calculated values for τ_{so} from force equilibrium are greater than those found using Equation 5.5. These values also seem to be less reliable due to the scatter of results. This may be a result of the sum of W, W_{so}, f_s and f_{cut-v} requiring a larger proportion of the applied axial load than f_{cut-t} does of the applied torque.

Analysis of the auger penetration test results in terms of energy use

The following equations were used to calculate from the test results the amount of energy dissipated by the auger:

$$E_{Rot} = \sum \overline{T} \cdot \delta\overline{\theta} \tag{5.8}$$

$$E_{Ax} = \sum \overline{F} \cdot \delta\overline{l} \tag{5.9}$$

$$E_{Tot} = E_{Rot} + E_{Ax} \tag{5.10}$$

where: E_{Rot} = energy dissipated by rotational movement of the auger;
$\overline{\theta}$ = vector of angle of rotation of the auger in radians;
E_{Ax} = energy dissipated by vertical movement of the auger;
$\overline{l}$ = vector of vertical distance moved by the auger;
E_{Tot} = total energy dissipated by the auger and
$\overline{T}$ = vector of torque applied to the auger and
$\overline{F}$ = vector of axial load applied to the auger.

Figures 5.9 to 5.12 are representations of the energy dissipated by the augering process. Total energy dissipation results from two augers (40 and 50mm outer diameters) are included to show repeatability of the results.

Note that the magnitude of energy dissipated by the axial load on the 40mm diameter auger (Figure 5.10) is much smaller than that dissipated by torque applied to the 40mm diameter auger (Figure 5.9), and furthermore that the energy dissipated by axial load on the auger has a negative value for most readings. The smaller quantity of energy dissipated by axial load is partially because the vertical movement ($\sum \delta\overline{l}$) is less than the rotational movement ($\sum \delta\overline{\theta}$). The energy dissipated by the axial load on the auger is negative for the majority of the readings because in the model auger tests,

the axial load was usually applied to the auger in a direction opposite to the direction of movement of the auger causing the force and displacement vectors to be in opposite directions to one another (i.e. the auger was pulled upward while moving downward).

The total energy dissipated by the augering process is shown in Figures 5.11 and 5.12. Note that at any given depth, the total energy dissipated is almost constant over the range of auger leads from 15% to 90% of the physical auger pitch.

5.2.2 *Auger shear test results*

Figures 4.40 and 4.41 show the torque and load measurement results from three auger shear tests where a 40mm diameter auger was allowed to penetrate for 74mm at 37mm per revolution (penetration phase), penetration was then stopped and rotation was continued for one more revolution (shearing phase). Also in Figures 4.40 and 4.41, is the result of the 40mm diameter auger penetrating the soil at 37mm per revolution into the same sample box, but without the shearing phase (an auger penetration test result). The test results given in Figure 4.40 show that the torque required to advance an auger into the soil when shearing the soil on the soil boundary after the first shearing phase is less than is required when not shearing the soil on the soil boundary. The difference between the torque measured during the two tests became greater with every subsequent shearing phase. The reduction in torque when penetrating with incremental shearing phases is mostly due to the reduction in soil shear strength on the soil boundary but also due to soil being transported to the surface (flighted). This result explains why rig operators regularly rotate the CFA auger without penetration when advancing the CFA auger into the soil.

Figure 4.42 shows an example of the torque and axial load measured during the shearing phase of the auger shear tests, converted to shear stresses on the soil boundary using equations 4.4 to 4.6. Calculation of the undrained shear strength (c_u) by assuming that the maximum shear stress on the soil

boundary is equal to c_u yielded lower values than those measured by the hand vane apparatus (Table 4.8) however, the standard deviation of the results are comparable. If this test is therefore to be used for pile design it will have to be calibrated by comparisons to measurements of pile capacity. Also observe in Figure 4.42 that the stress resulting from torque and axial load on the soil boundary reduces after post peak rotation and does not reduce to a constant value, suggesting that the required torque could be lowered further by further rotation during the auger shearing phase.

5.2.3 *Comparison between the auger penetration and auger shear test results*

This section is aimed at comparing results from the two different types of auger tests (auger penetration and auger shear tests). In effect this section investigates the possibility of fitting the auger shear test results onto the three dimensional surfaces shown in Figures 5.2 and 5.3, obtained from the auger penetration tests, therefore showing that Figures 5.2 and 5.3 are unique regardless of the path of the auger. Figures 4.34 and 4.35 in Chapter 4 show cross sections through the data used to produce Figures 5.2 and 5.3. An auger shear test result is added to Figures 4.34 and 4.35 for comparison. In these two figures the vertical axes show torque or load measurement at particular depth intervals represented by the different lines, at the auger lead values shown on the horizontal axes.

In order to make this comparison the average lead of the auger (L_{ave}) has been defined as the depth of the auger tip (l) divided by the number of revolutions the auger has been turned through to reach l. The lead value has been expressed as a percentage of the pitch of the auger (Equation 5.11).

$$L_{ave} = 100\left(\frac{l}{R}\right)/P \tag{5.11}$$

where: L_{ave} = average lead as a percentage of the
physical auger pitch and

R = total number of revolutions of the auger.

For example if an auger with a physical pitch of 40mm is allowed to penetrate at 95% of the auger pitch per revolution (38mm per revolution) for two revolutions, the value of L_{ave} is equal to 95% $(100\left(\frac{76}{2}\right)/40)$. If this auger is then turned through another revolution without any penetration, L_{ave} reduces to 63% $(100\left(\frac{76}{3}\right)/40)$.

Figures 5.13 and 5.14 show a comparison of torque and axial load, respectively, measured in an auger shear test and the auger penetration tests. The auger shear test was conducted at a depth of 72mm ($l = 72mm$) whereas the auger penetration test results are plotted for every 50mm to a depth of 250mm. If the auger shear test results were equivalent to the auger penetration test results, then the auger shear test result would plot between the auger penetration test results obtained at 50mm and 100mm penetration.

In general the test results seem comparable however, there is a definite discrepancy. Both torque and load measurement results on the auger shear test exceed values measured at 100mm depth on the auger penetration tests. For the case of the load measurement this occurs only at the peak value, but for torque measurement this is true for most of the test. The discrepancy may be due to the fact that the soil at the bottom of the auger (i.e. horizontal face of the soil boundary) is sheared during the auger shear test and not during the auger penetration test, resulting in a higher torque and load requirement.

5.3 Proposed methods of capacity prediction for CFA piles

Some authors have suggested that monitoring of the CFA pile construction procedure may produce valuable information on the soil conditions and pile performance (Derbishire et al., 1989; O'Neill, 1994; Tomlinson, 1994). This section proposes two possible methods of obtaining pile capacity by such

monitoring. If proven useful these methods would have inherent advantages over traditional pile design methods, most notably:

- the data used for pile design would be pile specific and
- a detailed site investigation would not be required as the pile design data could be captured during construction.

The first design method is based on the measurement of c_u using the CFA rig. The second design method is based on the relationship between the energy dissipated by the auger whilst penetrating the soil and the pile capacity.

Neither of the methods suggested predict the end bearing capacity of the pile. It is believed that the end bearing capacity of CFA piles is unreliable and unlikely to be fully mobilized because of the inability to clean the pile base, and the large strains required to mobilize end bearing resistance (Whitaker and Cooke, 1966; Price and Wardle, 1982). Instead an accurate method of shaft capacity prediction is sought.

The instrumentation currently on most CFA rigs has been added to the rig mainly for the purpose of monitoring the concreting (auger extraction) phase of CFA construction (see Section 3.1.2). The design procedures described in this section require accurate measurement of both torque and axial load on the auger. These are not currently available on CFA rigs. New instrumentation for the CFA rig is being developed jointly with Stent Foundations and Lancaster University. A short section of un-flighted, instrumented auger stem is to be added between the auger and the rotary table to measure the required parameters. The software on the on-board computer will need to be updated to use the measurement of torque and axial load for the estimation of the pile capacity in real time.

This section will be concluded by an investigation into the possibility of using the measurements currently available on CFA rigs for pile capacity prediction.

5.3.1 *CFA pile capacity prediction using c_u as measured by the CFA rig*

This section describes the method proposed for estimating c_u using the CFA rig. The following procedure must be followed:

1. Penetrate the soil at a high lead so as not to shear the soil on the soil boundary.

2. Stop the auger penetration using the winch attached to the top of the auger, but continue rotation so as to shear the soil on the soil boundary.

3. While the soil on the soil boundary is shearing (Step 2), measure the axial load and torque on the auger to obtain peak and remoulded values. Use the measurements to determine c_u and pile capacity for the specific section of the pile.

4. Restart auger penetration, and repeat steps 1-3 until the required pile capacity is reached.

Steps 1-3 define a single test. To obtain actual values for peak load and peak torque for each test, the load and torque values measured at the remoulded soil state from the previous (higher) test need to be subtracted from the peak values measured in step 3. By assuming that the maximum stress on the soil boundary is equal to c_u, traditional total stress pile design can then be applied as described in Chapter 2. Accuracy would be greatly improved if torque and axial load could be measured further down the auger since the measurement can be expected to become increasingly inaccurate the further the auger penetrates into the soil. The reason for this is that the amount of shear stress on the rest of the auger will increase, therefore the required measurement at the tip will be a lower percentage of the total measured signal (i.e. the signal to noise ratio will become less).

The method described above uses the auger for conducting an in-situ test measuring the average c_u along the pile shaft. In his 1984 Rankine lecture,

Wroth discussed different in-situ tests by which c_u may be measured. He showed how the tests were fundamentally different and compared them to the unconsolidated undrained triaxial test. Differences such as the directions and freedom of rotation of the three principal stresses were highlighted. He described the different test results as a hierarchy of c_u and concluded that "it is imperative for a designer to recognize this hierarchy, and to select a strength which is appropriate to the analysis or the design procedure being used" (Wroth, 1984). Results from the model auger tests show that the values back-calculated from the auger tests were as repeatable as results from standard test methods.

5.3.2 *CFA pile capacity prediction using energy dissipated by the CFA auger*

A number of systems have been designed to monitor drilling equipment, with the aim of obtaining additional objective data from the borehole drilling process. Teale (1965) used such a system to monitor exploratory drilling carried out for the mining industry. Other systems have been used to provide supplementary information on ground conditions whilst carrying out ground improvement or geotechnical processes. For example, Gui, Soga, Bolton and Hamelin (2002) showed how soil strata may be distinguished using additional instrumentation, when drilling holes for compensation grouting above NATM tunnels in soft ground.

Figure 5.15 shows how energy measured during the augering process may be used to estimate pile shaft capacity. The figure incorporates the results from 14 model auger tests with lead values between 15% and 90% of the physical auger pitch per revolution, carried out on three different sample boxes using two different augers. A theoretical pile shaft capacity was calculated using Equations 2.2 and 2.3, an α value of 0.45 and c_u as measured by the hand vane. The total energy dissipated by the auger to reach a depth is plotted against the theoretical shaft capacity for this depth. The mean of the results, as well as shaded areas showing offsets of between 1 and 2 times

the standard deviation, are shown in Figure 5.15.

As seen in Figure 5.15 the relationship between energy dissipation and pile capacity is non-linear despite the fact that strength was considered constant with depth. The non-linearity can be explained by the fact that as the auger drills deeper into the soil, the energy required to advance a unit distance increases, since energy is dissipated all along the section of the auger that has penetrated the soil. In other words the increase in energy consumption can be attributed to energy being dissipated along the longer section of the auger that has penetrated the soil.

Regressions using different formulae on Figure 5.15 showed the closest correlation to the measured data when using the empirical equation:

$$\text{Pile capacity (N)} = (27 * \text{Energy dissipated (J)})^{\frac{1}{1.26}} \tag{5.12}$$

within the range tested by the model auger rig. This formula was obtained by performing least square regressions on a variety of different formulae, and selecting the formula with the best fit.

In general the relationship between pile capacity and energy dissipated by an auger rig may be described by the equation:

$$\text{Pile capacity} = (m * \text{Energy dissipated})^{\frac{1}{r}} \tag{5.13}$$

however it is important to note that c_u was approximately the same in all the sample boxes. The influence of c_u on the auger energy use has not been quantified.

A database with pile test results and energy dissipated by a particular rig will allow the determination of values for r and m for that particular CFA rig and auger.

This design procedure is not based on traditional soil mechanics, and is totally empirical however, Tomlinson (1994) states that the current prediction of the load carrying capacity of a pile is also based "mainly on empirical methods based on experience".

5.3.3 *The use of measurements currently available on CFA rigs for pile capacity prediction*

On the CM48 CFA rig, discussed in Section 3.1.3, measurements of the following parameters were made during auger penetration:

- time (s);
- depth (m);
- pressure in the hydraulic system (bar) and
- the number of rotations of the auger.

An approximate estimate of energy used by the CM48 rig was made using the time and pressure measurements, and the fact that the maximum power output of 73kW was used when the pressure in the hydraulic system was 350bar (Section 3.1.3). It was assumed that the pressure in the hydraulic system was directly proportional to the rate of energy dissipation.

An estimate of pile capacity may be made using the measurement of depth, site investigation data from the sites concerned and a study into properties of the London clay by Skempton (1959). Figure 3.12 shows the estimate of pile capacity against energy used on the CM48 rig with a 350mm CFA for 8 piles constructed on the ExCel site in the London dockyards. Figure 3.13 shows the distribution of pile capacity predictions for an energy use of 8MJ using all available construction records on the ExCel site with a 350mm auger. The skewness[1] of the distribution is -0.8, indicating a moderate skewness to the left. The kurtosis value[2] is 3.7, where 3.0 indicates a normal distribution. This kurtosis value indicates that the data is more peaked than

[1]Skewness is a measure of symmetry, or more precisely, the lack of symmetry. A distribution, or data set, is symmetric if it looks the same to the left and right of the center point.

[2]Kurtosis is a measure of whether the data are peaked or flat relative to a normal distribution. That is, data sets with high kurtosis tend to have a distinct peak near the mean, decline rather rapidly, and have heavy tails.

a normal distribution. If it is assumed that a normal distribution of data, then the standard deviation is 12.9% of the mean (The mean is 1040kN and the standard deviation is 128kN).

An investigation was then conducted into the effect of auger size on the pile capacity prediction. Figure 5.16 shows the average pile capacity predictions for auger sizes of 300, 350 and 450mm on both the Brentford and ExCel sites in London for 8MJ energy dissipation, indicating that the results are influenced by auger diameter. Figure 5.17 shows the distribution of the combination of all the pile capacity prediction results for an energy use of 8MJ. Data from both the Brentford and ExCel sites are included. The skewness of the distribution is 0.5, indicating that the data is moderately skewed to the right. The kurtosis value is -0.33, indicating that the data set has a very flat peak. The combined data set does not therefore appear to follow a normal distribution, indicating that the pile capacity prediction is statistically dependent on auger diameter (as the individual data sets do follow a normal distribution).

It may be noted that there are several discrepancies between the model test results and the results from the CFA rig data concerning auger energy use. Most notably:

- For the model rig the relationship of energy use to pile capacity seemed to be independent of auger diameter (Figure 5.15), whereas on the full scale rig auger diameter influenced the relationship (Figure 5.16).

- The model test results showed clearly that as the auger progressed further into the soil, more energy was required to increase the pile capacity by a unit value. The full-scale results seem to suggest the opposite.

- If Equation 5.12, obtained from the laboratory model, is used to estimate pile capacity for 8MJ energy dissipation, a prediction of 4118kN is obtained. This value is approximately 4.6 times the average value predicted on the full-scale CFA rig. Figure 5.18 is a plot of the energy-

capacity correlation found on the model rig and estimated from the full-scale data. Note that both axes are on a logarithmic scale.

These discrepancies are mainly due to the inaccurate estimation of both energy dissipation and pile capacity for the full-scale situation, as well as the gross extrapolation of the auger model test results (approximately four and a half orders of magnitude). Furthermore the energy used by axial load on the full-scale rig was not available, and therefore not taken into account. However the results are encouraging because of the narrow spread of results for a given auger (Figures 3.13 and 3.18).

5.3.4 *Factors of safety*

In Table 2.1 partial factors of safety are suggested for soil parameters and shaft and end bearing capacity of piles using traditional design methods. For the case of the pile shaft resistance the lowest combined factor of safety is 1.84 (design using angle of internal friction of the soil with a high level of confidence on the soil parameters) and the highest is 3.00 (design using c_u with a low level of confidence on the soil parameters). The probability of failure acceptable for permanent works is given in Table 2.2 as being in the region of 0.05% to 0.01% (the probability of failure is small to ensure that the foundation performs within serviceability limits). If it is assumed that the factors of safety used in industry are commonly designed to yield this probability of failure, the results of design by auger energy can be compared with those from conventional design procedures. If it is assumed that pile capacity predictions follow a standard normal distribution, and the required probability of failure is from 0.05% to 0.01%, the design values need to be from 3.29 to 3.69 standard deviations lower than the predicted pile capacity.

For a standard deviation of 11%, as found in the variation of energy dissipation results in the laboratory, the factor of safety required to ensure a probability of failure of 0.05% to 0.01% lies between 1.6 and 1.7. The small coefficient of variation has however been achieved in laboratory conditions

and accurate full-scale tests would be required to assess the variability of results obtained in the field. The data currently available on the CFA rig showed a standard deviation of 12.5% for a given auger (as shown in Section 5.3.3). A factor of safely of 1.7 to 1.9 would be required if this data was to be used. The effect of installation on pile capacity has not been taken into account and would increase the variability of the results and therefore the required factor of safety.

An estimate of the coefficient of variation in current pile capacity predictions can be found in the literature. Neely (1991) compares the results of several design methods to measured pile capacities for CFA piles. The standard deviation of the ratio given by $\frac{calculated\ capacities}{measured\ capacities}$ was between 25% ('Meyerhoff's method') and 35% ('Douglas's method'). A factor of safety to ensure a 0.05% probability of failure using these design methods would have to be in excess of 12. The reason why these methods do not produce a large number of pile failures is that the mean of the predicted values is much lower than the mean of the measured results (predicted values were on average 54% of measured values for the 'Meyerhoff method'). A general underestimation of pile shaft capacity was also noted in the study conducted by Imperial College which was presented earlier in this chapter (Figure 5.1).

5.4 Shortcomings of the model test procedure and data analysis

It is well appreciated that a model will never perfectly simulate a full-scale situation, and it is important to understand what the shortcomings are and how they affect the relevance of the model results to full-scale augering. The following shortcomings are listed for this set of tests, and the results need to be seen in light of these:

- The soil sample was an overconsolidated sample of reconstituted Speswhite kaolin clay. Natural soils all have their own unique characteristics and

the auger may perform differently in different soils.

- The ratio of bore depth to c_u in the model tests was much lower than would be expected at full-scale, which made the bore in the model tests more stable than would be the case at full scale. This effect was more significant in the cases where the auger was partially-loaded as material could potentially have fallen onto the auger flight if the bore was unstable.
- Several geometries of augers are available for CFA piling rigs. The model augers did not simulate all the different geometries, although the most common CFA augers have been modelled.
- The procedure used to create the three dimensional graphs averages the data results, and therefore do not perfectly reflect the full variability of data. These graphs are used as illustrations of the results.
- The design procedure proposed using energy dissipation on the auger is compared to a calculated, rather than a measured, pile capacity.

5.5 Alternative design for the auger used on CFA rigs for piling in clay

Having studied CFA rigs, the author proposes an alternative design for their augers. Figure 5.19 is an illustration of the suggested auger design, in which the auger is only flighted for a short section at its bottom end. This auger penetrates the soil by using the following procedure:

1. The auger is advanced into the soil for the length of its flighted section at a lead large enough to ensure that soil on the soil boundary is not sheared.

2. Auger penetration is stopped by application of the brake to the winch, but with continued rotation so as to shear the soil on the soil boundary.

3. The torque and axial load measurements are used to obtain a value for c_u for the soil section penetrated by the auger.

4. Steps 1 and 2 are repeated until the cumulative values of c_u predict the required pile capacity.

Friction on the auger stem and the top of the cylinder being sheared need to be taken into account when calculating c_u. The torque measurement position closer to the tip of the auger will yield more accurate results because friction on the auger stem does not have to be taken into account.

This process should result in a series of cylinders one below the other being sheared as the auger progresses. These cylinders would be left in place so as to support the soil surrounding the bore. When the auger is extracted the soil on the soil boundary will have been sheared, causing the cylinders to move upward with little resistance. The auger in combination with the procedure above, has the following advantages:

- less torque and energy would be required for a given pile length and diameter because of the reduced surface area on this auger in contact with the soil (or a given rig should be able to manufacture a larger pile);
- over rotation of the auger would only affect the section of the bore surrounding the area where the flighted auger is situated at the time;
- it may be possible to socket the end of the pile in soft rock as the over-rotation required to penetrate the rock will not affect soil surrounding the upper section of the bore;
- a more accurate measurement of c_u can be made than in the case of a continuously flighted auger because the ratio of signal to noise will be larger;
- this auger could be fitted onto conventional CFA rigs with minimal modification required to the rig (instrumentation to measure torque and load on the auger would be required if pile capacity were to be assessed);
- the auger would be cheaper to manufacture than traditional continuous flight augers because it only requires a short flighted section and

- since the sheared cylinders are on top of one another with little resistance to axial movement, the collective weight of the cylinders will counter the flighting of soil if the bottom of the auger is rotated excessively.

The proposed auger design suffers from the following disadvantages:

- it is commonly believed that the auger flight of the CFA lends extra support to the bore and
- the auger flight provides resistance to soil sliding down the flight and contaminating the concrete when the auger is withdrawn.

The belief that the outside edge of the auger flight lends support to the auger bore has not been proved and may not be correct as the surface area of this outside edge is small in comparison to the area of the bore. Moreover, in the proposed procedure, if the soil cylinders are sheared without excessive remoulding of the soil, they will provide adequate support to the soil surrounding the bore to counter stress relief. Natural soils will have a greater tendency to bulking than those tested in the laboratory, and therefore some soil may start moving up the auger bore as the auger drilling process is in operation. Soil contaminating the concrete when the auger is extracted is a more serious issue for this type of auger design. The following measures may be taken to help prevent the contamination from occurring:

- high concrete pressure at the bottom of the auger (the larger the inner diameter of the hollow stem, the higher the pressure at the tip of the auger will be, care should be taken not to cause hydrofracture of the soil);
- a low pitch angle on the auger (a small ratio of pitch to diameter) and
- slow rotation of the auger during extraction (in the same direction as used for penetration).

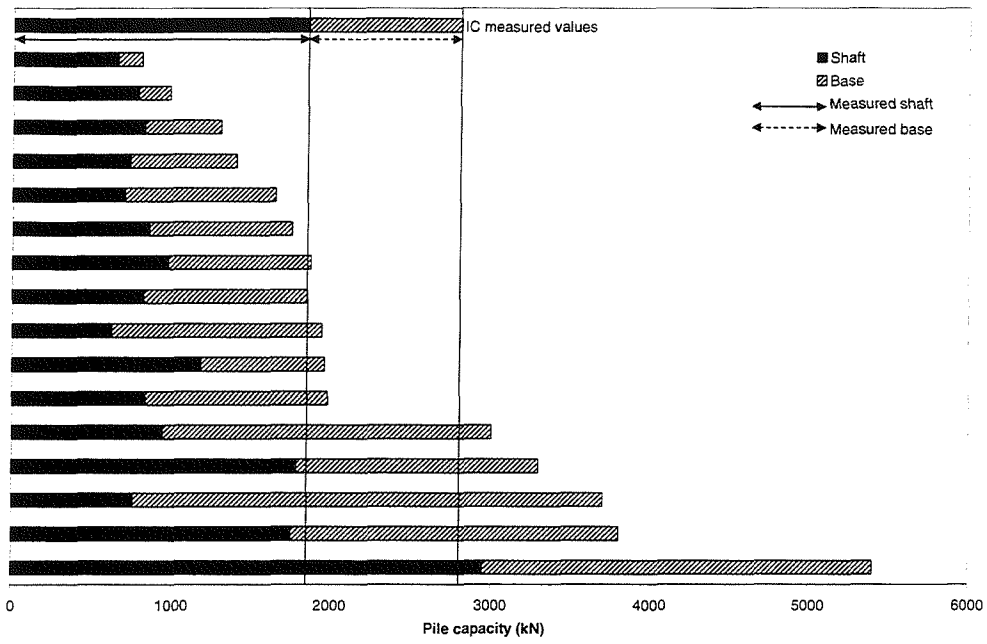

Figure 5.1: Predicted load capacity and measured results from an Imperial college study (redrawn, after Wheeler (1999))

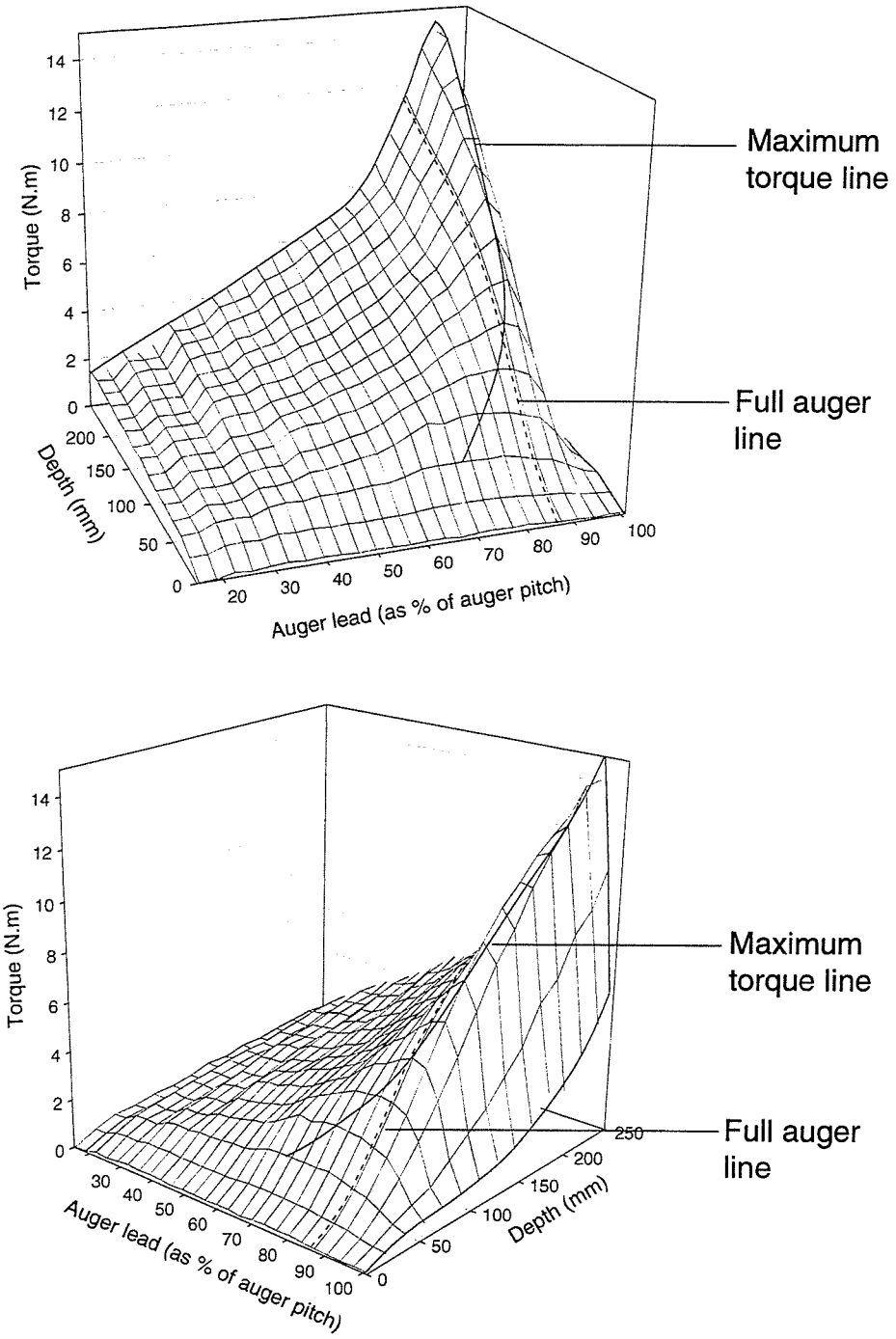

Figure 5.2: Typical torque measurement result from a set of auger model tests (graph from 2 different angles)

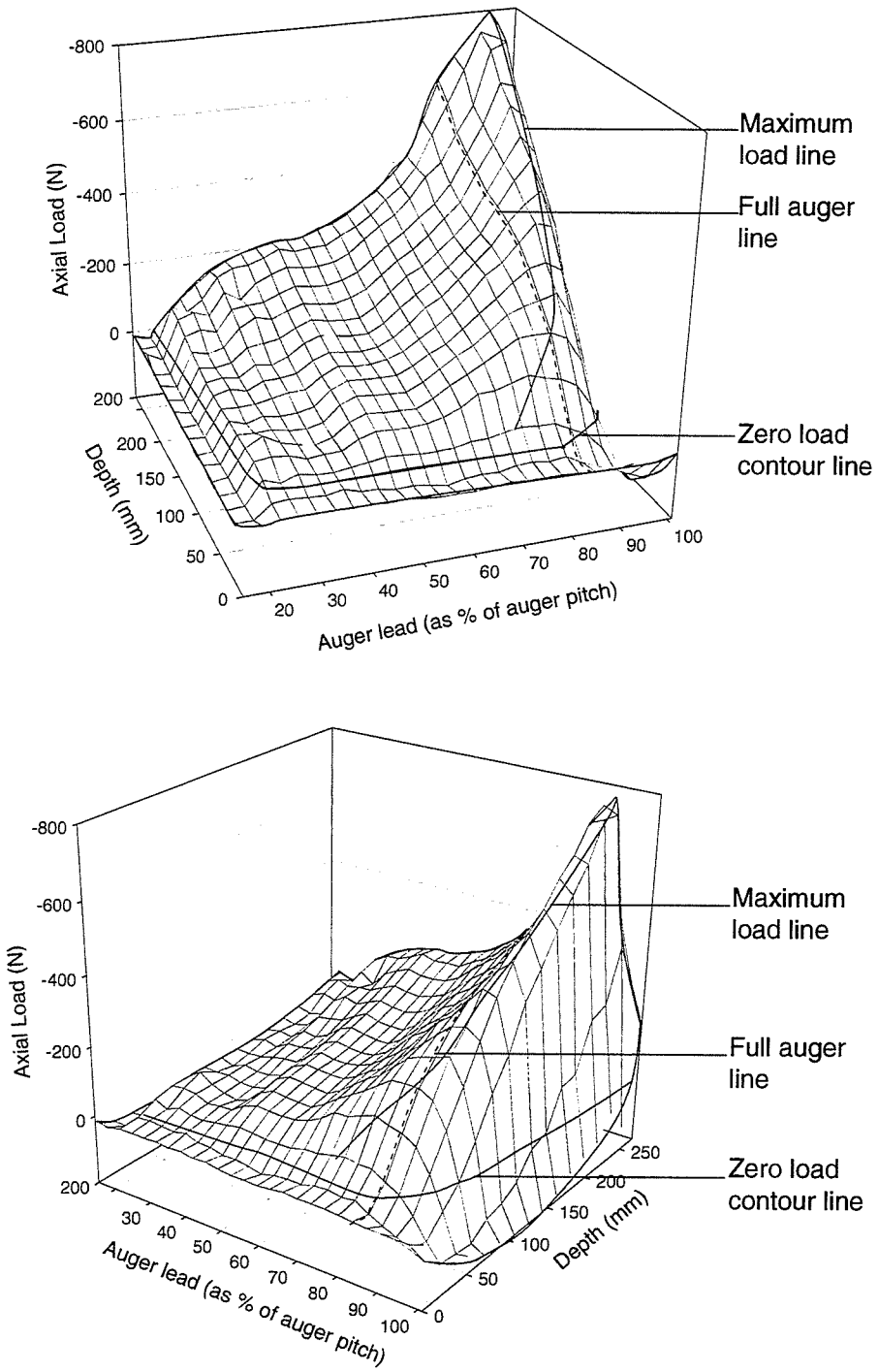

Figure 5.3: Typical load measurement result from a set of auger model tests (graph from 2 different angles)

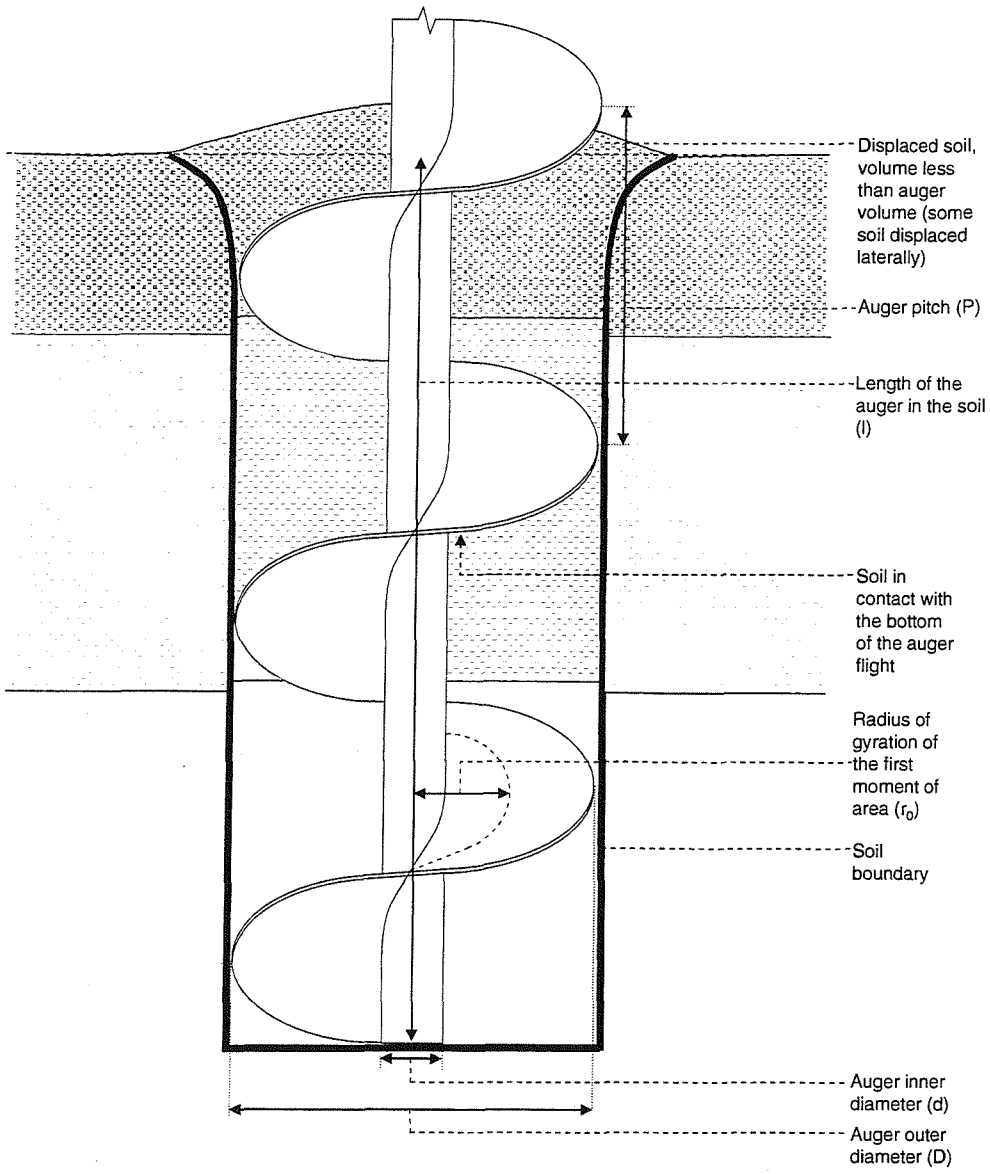

Figure 5.4: Illustration of an auger penetrating at a lead value in excess of the full auger value

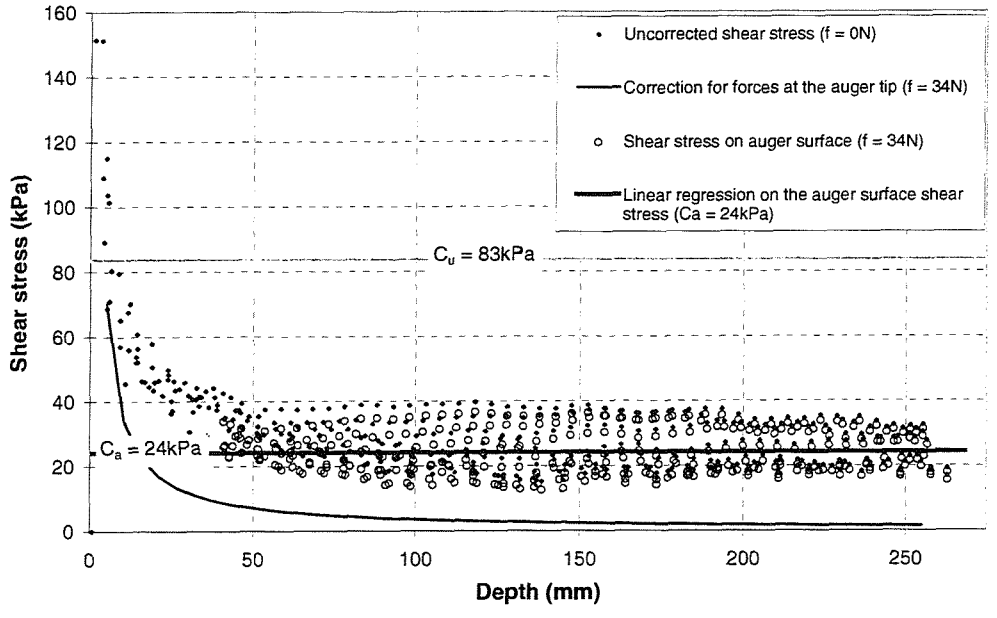

Figure 5.5: Shear stress on the auger surface during nine auger penetration tests at lead values in excess of the full auger value

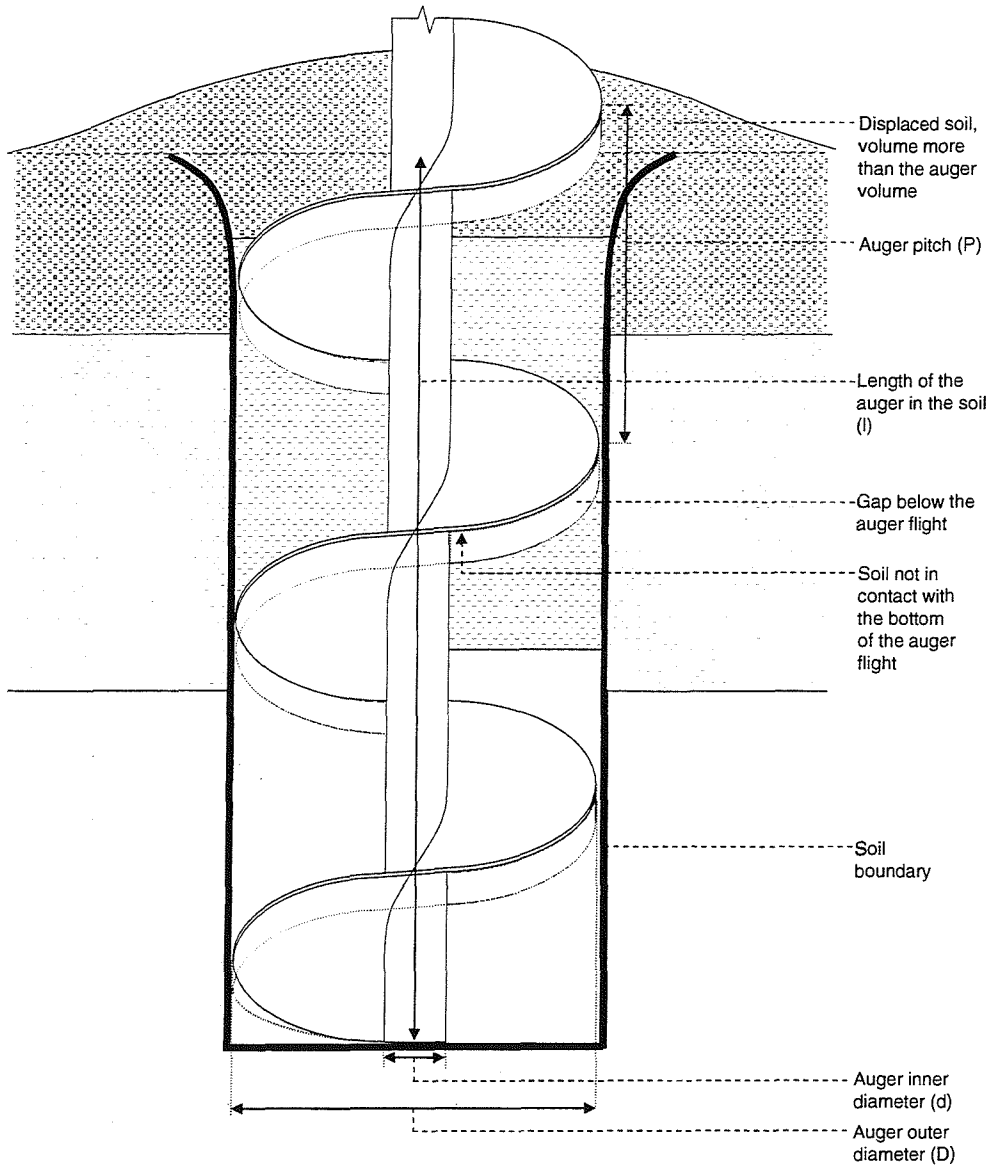

Figure 5.6: Illustration of an auger penetrating at a lead value less than the full auger value

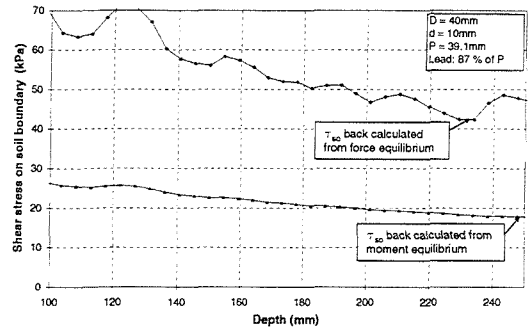

(a) Lead value 87% of auger pitch

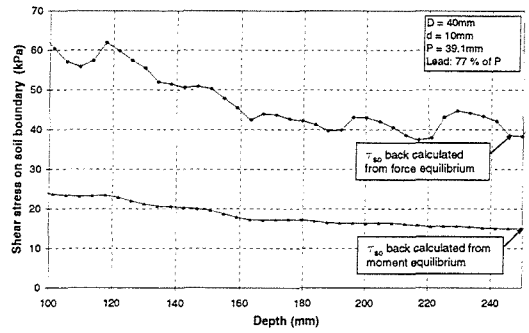

(b) Lead value 77% of auger pitch

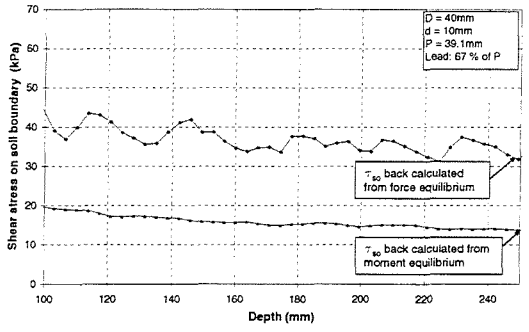

(c) Lead value 67% of auger pitch

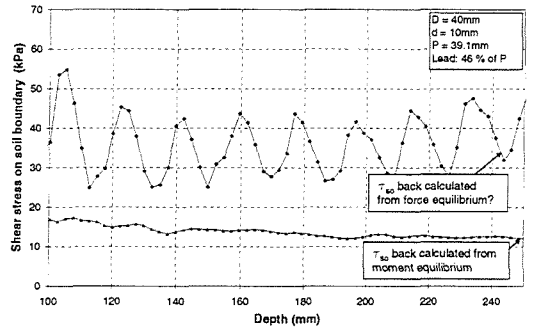

(d) Lead value 46% of auger pitch

Figure 5.7: Values of τ_{so} back calculated from force and moment equilibrium

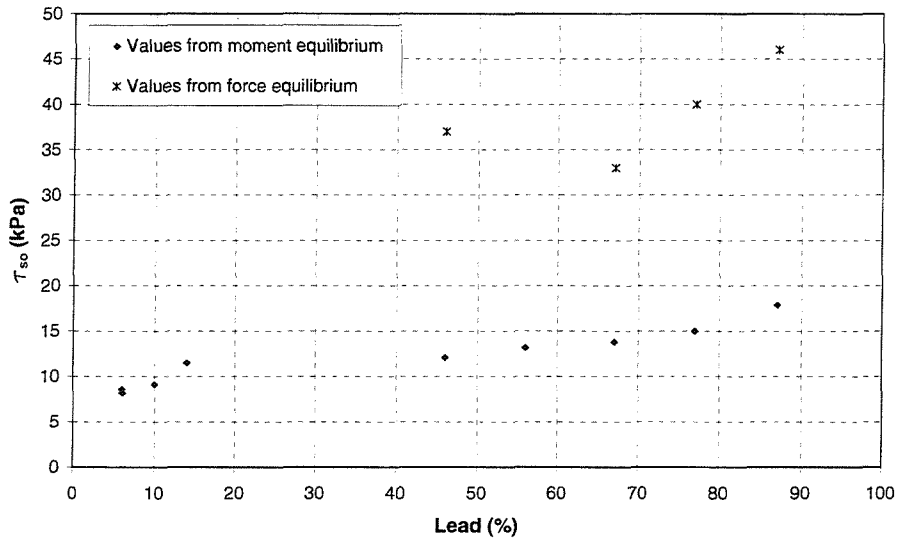

Figure 5.8: Values of τ_{so} back calculated from Force and Moment equilibrium equations

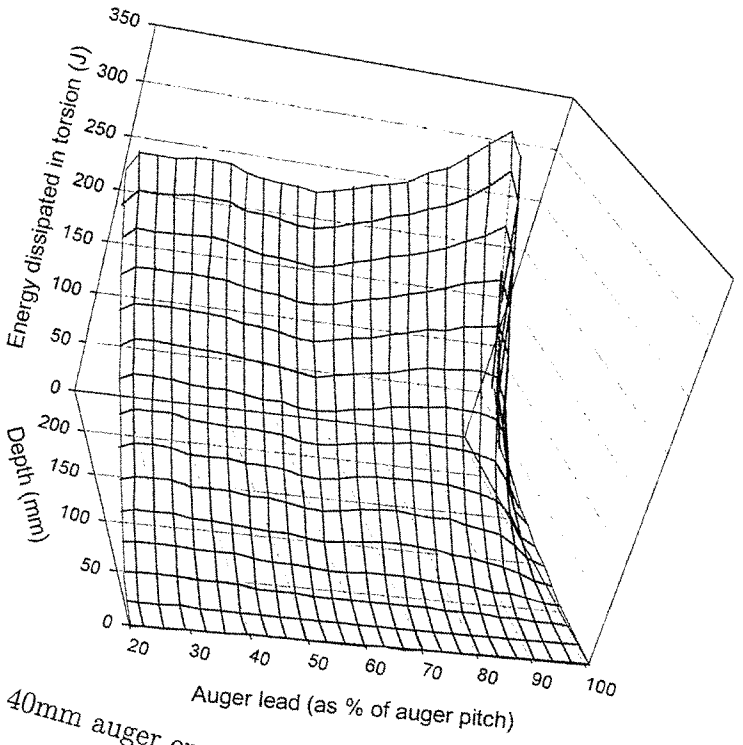

Figure 5.9: The 40mm auger energy dissipation by torque (rotation)

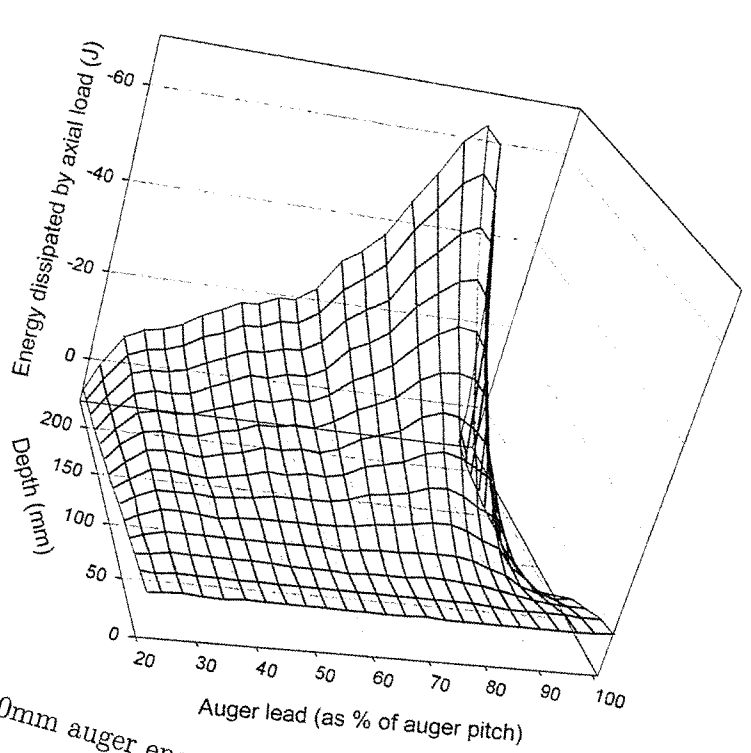

Figure 5.10: The 40mm auger energy dissipation by axial load (translation)

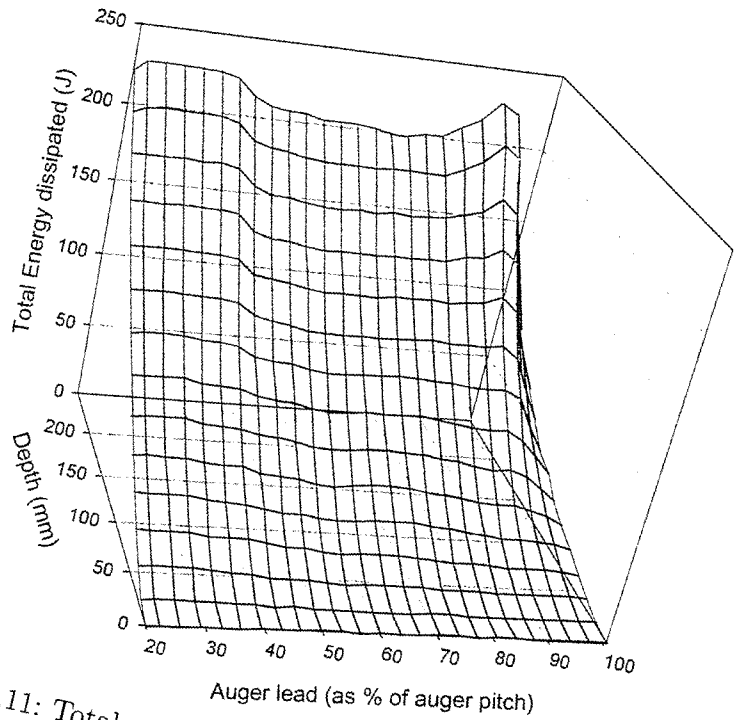

Figure 5.11: Total energy dissipation on the 40mm auger

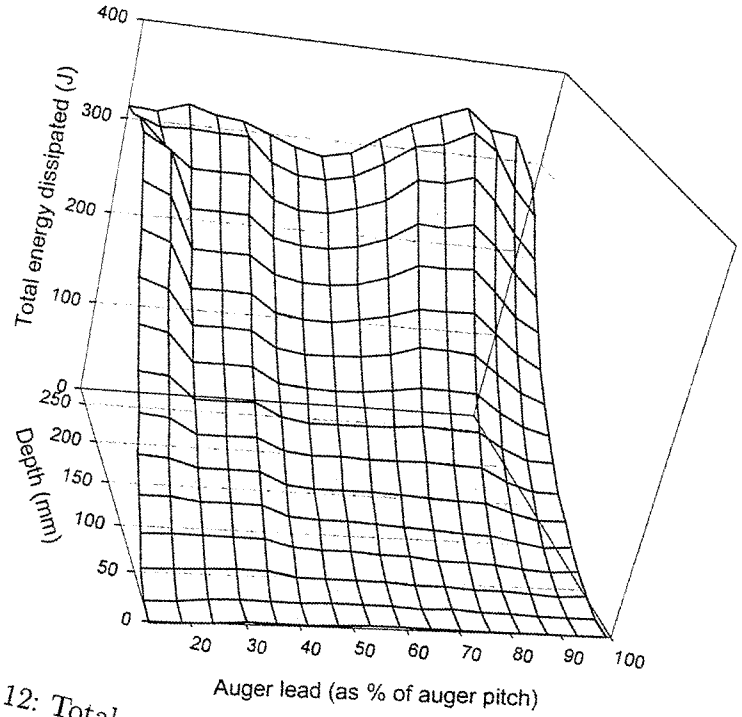

Figure 5.12: Total energy dissipation on the 50mm auger

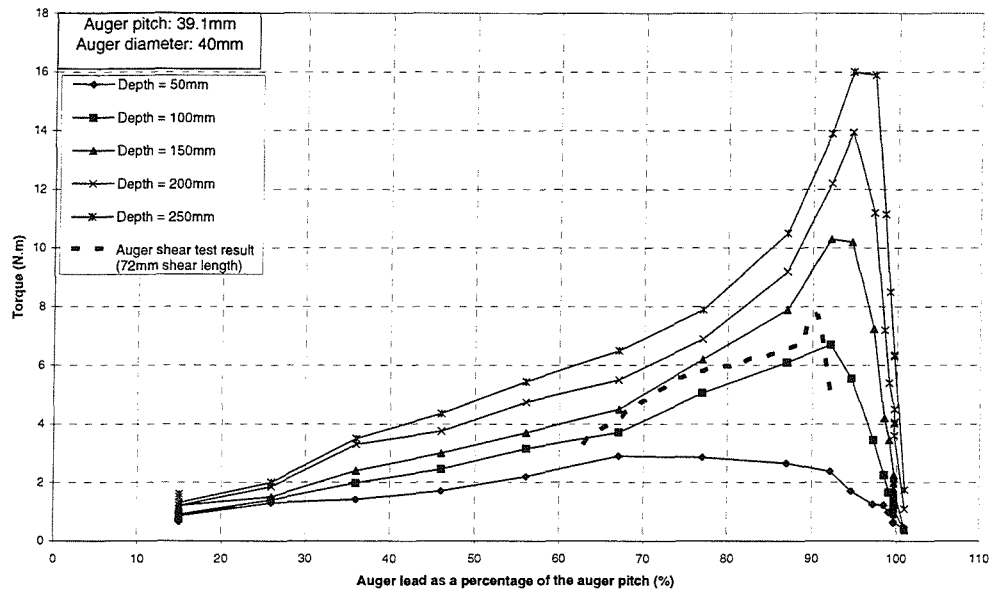

Figure 5.13: A comparison between torque measured on the auger penetration tests and auger shear tests

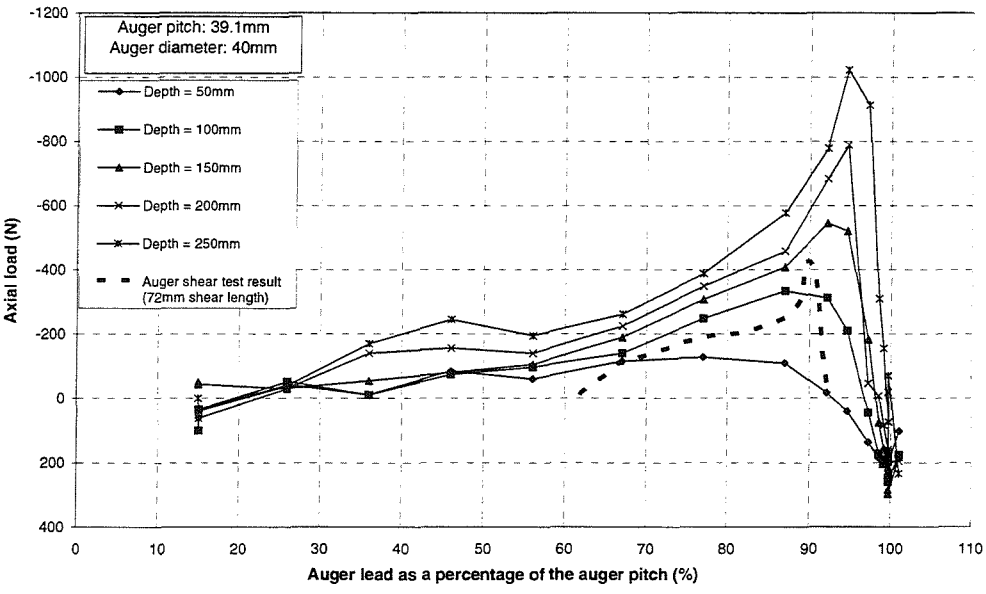

Figure 5.14: A comparison between axial load measured on the auger penetration tests and auger shear tests

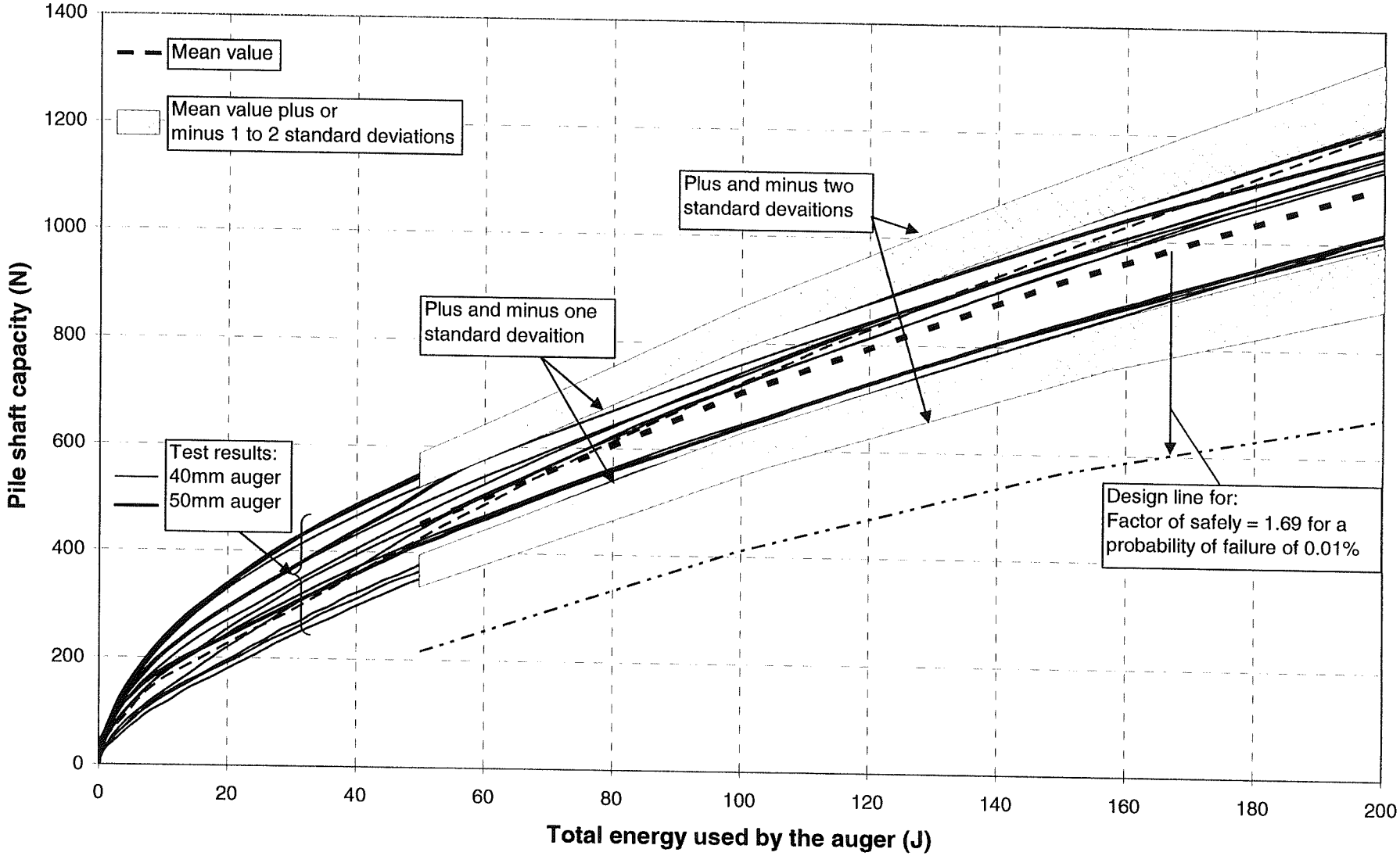

Figure 5.15: Energy dissipation results for auger penetrations from 15% to 90% of the pitch per revolution against predicted pile capacities

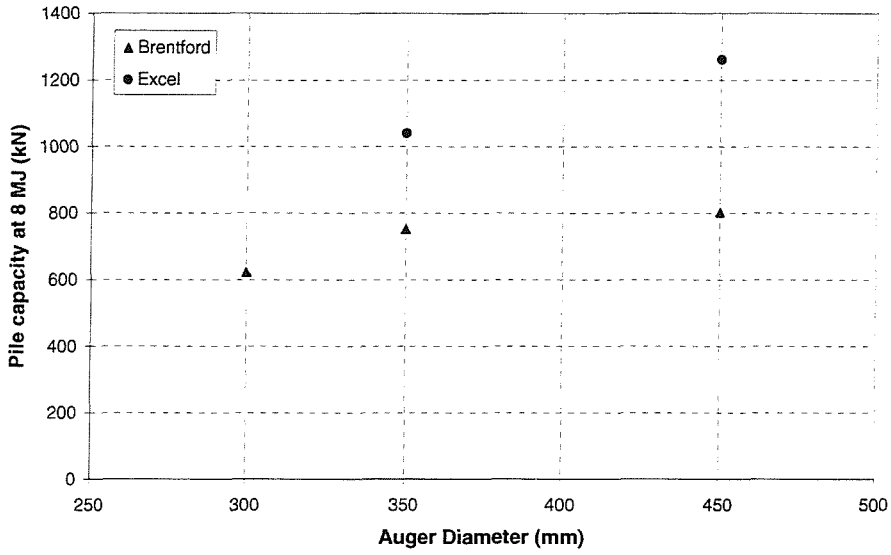

Figure 5.16: Average pile capacity predictions for the CM48 CFA rig on the Brentford and ExCel sites in London for 8MJ energy dissipation

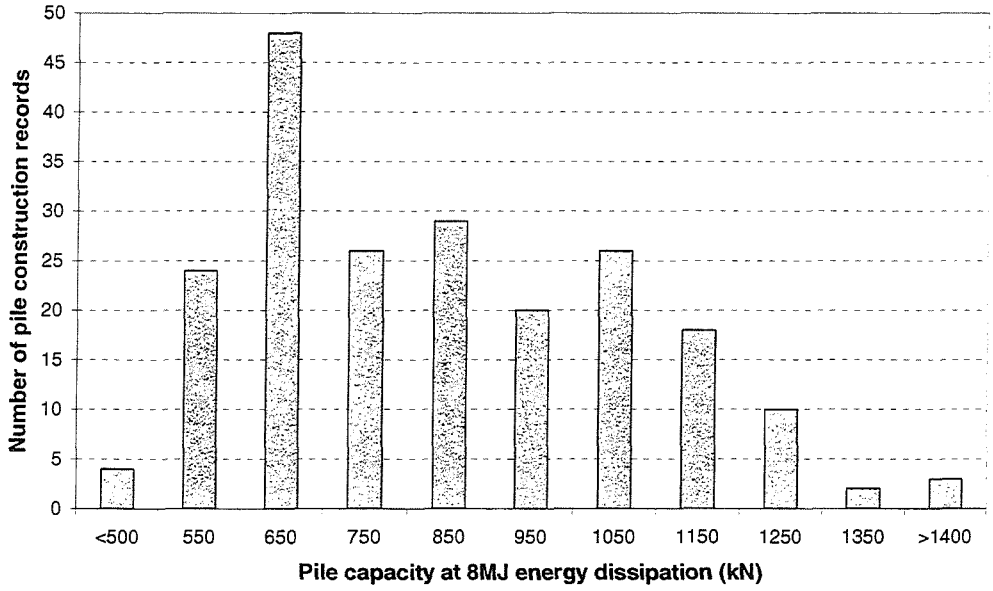

Figure 5.17: The distribution of pile capacity prediction results using the CM48 CFA rig with augers ranging from 300mm to 450mm in diameter for 8MJ energy dissipation

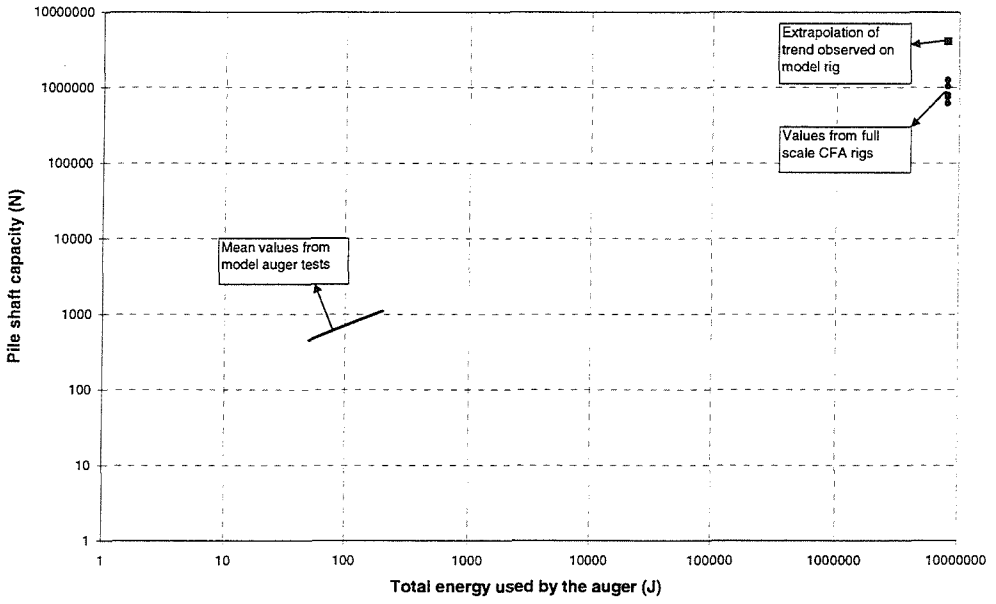

Figure 5.18: Energy-capacity correlation observed on the model and the full-scale CFA rigs

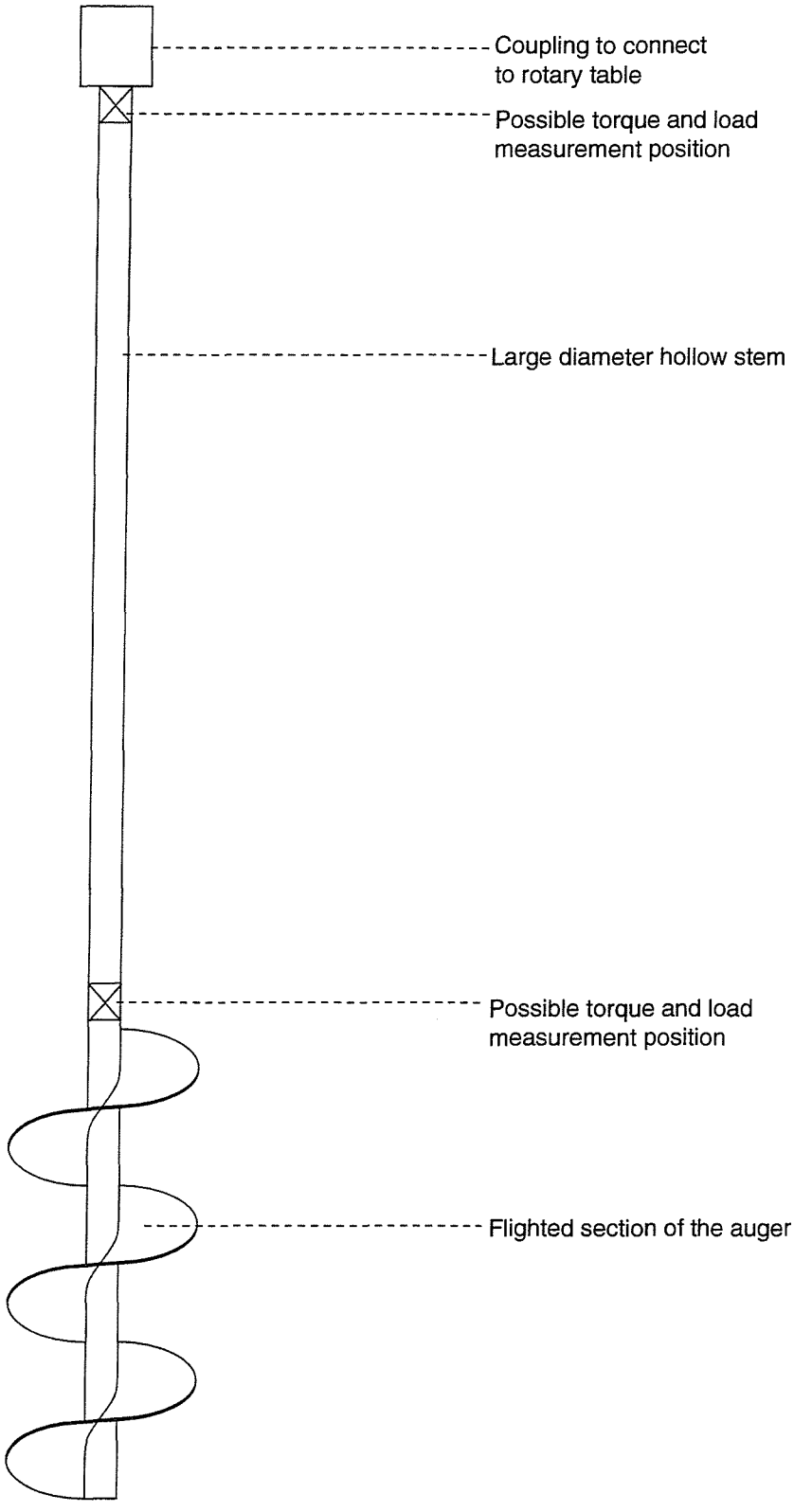

Figure 5.19: Suggested new design for augers used on CFA rigs

Chapter 6

CONCLUSIONS AND RECOMMENDATIONS

6.1 Conclusions

A large part of this thesis has been concerned with the development of an instrumented CFA rig model. The rig model was based on a literature review of CFA rig operation, close observation of the full-scale rigs in operation, analysis of data recorded on full-scale rigs and preliminary tests in the laboratory to ascertain design values for torque and axial load capacity of the model.

The development of this model rig has made it possible to produce a sufficient amount of data to investigate the mechanics of an auger penetrating clay. In-depth data analysis has shown that the forces measured on the augers may be explained using the undrained behaviour of clay. Model test results designed to simulate the observed behaviour of full-scale CFA rigs helped explain why these rigs were being operated in the manner observed.

Specific conclusions drawn from different parts of the research will now be discussed.

6.1.1 *The state of current CFA pile design and construction procedures*

CFA pile design is based on traditional bored pile design, frequently used with no adaptation of the design procedure to account for the effect of the method of installation on pile capacity. A large set of different design formulas and factors of safety are available to the designer to estimate ultimate state and serviceability requirements. Results from in-situ and laboratory tests routinely used to derive the variables used in these formulas have been found to yield a high variability. Furthermore design formulas have been verified by using a range of different pile tests which have also been shown to influence the measured pile capacity.

It is well appreciated that better installation practices for CFA piles result in better pile performance. As a result of this observation piling specifications have become more stringent in terms of the monitoring of CFA pile construction. Case histories have shown that over rotation of the auger causes reduced pile capacity but also that increased rig torque capacity decreases the amount of over rotation of the auger. There is however no guideline available for the required CFA rig torque capacity for given pile size and soil conditions. Field observations and data analysis from existing CFA rigs showed that CFA rigs commonly over rotate severely. Because of the complexity of the factors that are to be taken into account, it may be concluded that the prediction of CFA pile performance is currently not possible to acceptable levels of accuracy.

6.1.2 *Laboratory model design*

Considerable effort was put into producing a repeatable clay sample in the laboratory to make it possible to compare the results from different samples.

Preliminary auger tests gave repeatable results and provided required torque and axial load capacity values on which to base the CFA model rig design.

The model CFA rig was designed to have, and achieved, close control of

the rotational and translational movement of the auger. The torque measurement transducer was designed to compensate for axial loads on the transducer however, the load measurement transducer was not compensated for torsional loads. Torsional and axial loads had to be separated mechanically to ensure accurate measurement of the axial load by the load transducer.

6.1.3 *Laboratory test results*

General findings from the analysis of model auger tests were that:

- the rate of rotation of the auger seemed to have little, if any, effect on the torque required to turn the auger within the boundaries tested,
- the torque required to turn the auger is highly dependent on the auger lead and
- the axial load required to ensure the auger moves at a specific lead is highly dependent on the auger lead.

For every auger at every depth a lead value was found where the auger required a maximum positive torque and negative axial load to penetrate the soil (torque sign convention was chosen to be positive in the direction of auger rotation and axial load positive in the downward direction). Lines of maximum load and maximum torque were drawn on graphs of the test results to indicate the position of these lead values. Both torque and axial load requirements reduced if the lead values deviated from these lines. Back calculation of residual adhesion values between the auger and clay or the residual cohesion values at the bore wall as well as cutting forces at the tip of the auger showed that the torque and load measurements could be explained using the undrained behaviour of a clay.

The test results explained why a small amount of torque is required if the auger is rotated excessively. It is also shown that the torque required to turn an auger reduces when a rig applies an axial load in the direction of the auger movement (thus pushing the auger into the ground).

Further analysis of the data showed that the energy required for augering was independent of auger lead value. A comparison of theoretical pile shaft capacity to energy used by the auger showed a low spread of results, indicating that energy used by the auger may yield a good indication of pile shaft capacity.

Auger tests conducted to mimic a stop-start penetration procedure employed by some CFA rig operators, showed that the maximum amount of torque required by the rig decreases if the auger is advanced in such a way. Back calculation of the undrained shear strength values on the bore wall yielded values that were of similar repeatability as those measured by hand vane and unconsolidated undrained triaxial tests. Mean values of these three tests differed and any use of these measurements need to take into account these differences.

6.1.4 *Analysis of data logged on a full-scale CFA rig*

General findings from the analysis of data logged on a full-scale CFA rig were that:

- a large scatter of data was observed both for the rate of auger rotation and the rate of auger penetration and
- auger lead values and auger diameter were inversely proportional on a given CFA rig and site.

It could not be established whether the scatter of data was a result of a rapid variation in the auger rate of rotation and rate of penetration or inaccurate measurement techniques.

The measurement of pressure in the hydraulic line enabled a rough estimation of the energy used by a full-scale auger rig to be made. As with the model tests, a comparison of rig energy use to a theoretical pile shaft capacity was made for hundreds of piles constructed on two sites in London. A reasonably small variance of results was found, comparing favourably to

values of variance found for pile design methods in the literature. There was a significant difference between predicted pile capacity based on the energy use for augers with different diameters. A possible reason for this is the very low lead values at which the augers penetrate at (as was found from the analysis of data on the rigs). On the model rig it was found that the energy required to advance the auger when penetrating at lead values lower than 15% of the auger pitch was more than for higher lead values. The other possibility is that the differences are only due to the low accuracy of the methods used to produce both the pile capacity and energy use values.

6.2 Recommendations

An investigation into the effect of c_u on the energy required to auger into a sample would ba a valuable addition to this work. Samples can be prepared in a similar manner to those prepared for this research. By using different consolidation pressures, different values for OCR and c_u can be obtained.

It is recommended that CFA piling specifications should include guidance of the torque capacity required on a CFA rig for given auger diameter and soil type.

Transducers currently installed on CFA rigs were designed to monitor the concreting phase of CFA pile construction. Further instrumentation would be required to obtain an accurate measurement of energy use on the CFA rig. Measurement of axial load and torque placed on the auger as well as time will yield an accurate estimate of energy used by the auger.

If the measurement of torque and load were available on the auger then a more fundamental approach to the pile capacity prediction might be attempted by using the auger to measure the soil undrained shear strength (only applicable to clays), and then deducing pile capacity using the relevant design formula. To achieve this the auger would be required to advance using a stop-start procedure (as described in Section 5.3.1). A high rate of data logging will be required to obtain the maximum values of torque and load.

An analysis of the decay of shear stress on the bore wall when the soil is being sheared on this surface might also be useful for estimating soil sensitivity or the remoulded undrained shear strength of the soil. These values might provide a more accurate estimate of pile bearing capacity as some of the effects of pile installation on pile capacity could be taken into account.

Augers traditionally used for bored cast-in-place piling are similar in design to the auger proposed in this section (except for the hollow stem). Therefore to test the feasibility of a partially flighted auger design (Chapter 5), an auger with a solid stem normally used for bored cast-in-place pile construction could be employed on a CFA rig.

Bibliography

Al-Tabaa, A. (1987). *Permeability and stress-strain response of Speswhite kaolin*, PhD thesis, Cambridge University.

Anderson, W. F. (1988). Effective stresses on the shafts of bored cast-in-situ piles in clays, *Proc. 1st Int. Geotech. Sem. on Deep foundations on Bored and Auger piles* pp. 387–394. Balkema, Ghent, Holland.

Aoki, N. and de Alencar, D. (1975). An approximate method to estimate the bearing capacity of piles, *Proc. 5th Pan-American conf. of SMFE* pp. 367–376. Buenos Aires, Argentina.

ASTM (1974). Standard method of testing piles under axial compressive load, *Annual book of ASTM standards* pp. 178–188. Part 19 Designation D 1143-74.

Bandini, P. and Saldago, R. (1998). Methods of pile design based on cpt and spt results, *Proc. 1st Int. Conf. on site characterization* pp. 967–976. Atlanta, Georgia.

Barden, L. (1972). The influence of structure on deformation and failure in clay soil, *Geotechnique* **22**: 159–163.

Barker, W. R. and Reese, L. C. (1970). Load-carrying characteristics of drilled shafts constructed with the aid of drilling fluid, *Research report 89-9*, U.S. Dept. of Transport, The University of Texas. Project 3-5-65-89.

Bazaraa, A. R. and Kurkur, M. M. (1986). N-values used to predict settlements of piles in egypt, *Use of in-situ tests in geotech. eng. ASCE Geotech. special publication* **6**: 462–474.

Bjerrum, L. (1973). Problems of soil mechanics and construction on soft clays, *Proc. 8th ICSMFE, Moscow* **3**: 111–159.

Boardman, D. I., Glendinning, S. and Rogers, C. D. F. (2001). Development of stabilisation and solidification in lime-clay mixes, *Geotechnique* **50**(5): 533–543.

Brons, K. F. and Kool, A. F. (1988). Methods to improve the quality of auger piles, *Proc. 1st Int. Geotech. Sem. on Deep foundations on Bored and Auger piles* pp. 269–272. Balkema, Ghent, Holland.

BS1377 (1990). British standards: Soils for civil engineering purposes, *BS 1377: Part 2.*

BS8004 (1986). British standards: British standard code of practice for foundations, *BS 8004.*

Burland, J. B. (1973). Shaft friction of piles in clay - a simple fundamental approach, *Ground engineering* **6**(3): 30–40.

Burland, J. B. and Twine, D. (1988). The shaft friction of bored piles in terms of effective strength, *Proceedings of the seminar on deep foundation on bored and auger piles* pp. 411–420. Balkema, Ghent, Holland.

Burland, J., Butler, F. and Dunican, P. (1966). The behaviour and design of large diameter bored piles in stiff clay, *Proc. Symp. on large bored piles* pp. 51–71. The Institution of Civil Engineers, London.

Bustamente, M. and Gianeselli, L. (1982). Pile capacity prediction by means of static penetrometer CPT, *Proc. 2nd European Symposium on penetration testing* **2**: 493–500.

Butler, H. D. and Hoy, H. E. (1977). Users manual for the Texas quick-load method for foundation load testing, *FHA office of development.*

Byrne, G., Everett, J. and Schwartz, K. (1995). *A guide to practical geotechnical engineering in Southern Africa*, 3 edn, Franki, South Africa.

Casagrande, A. (1948). Classification and identification of soils, *ASCE* **113**: 783–810.

Chandler, R. J. (1968). The shaft friction of piles in cohesive soils in terms of effective stress, *Civ. Eng and Pub. Wks. Rev.* **63**: 48–51.

Chiesura, G. (1998). Some dynamic parameters of drilled piles under low- and high-energy tests. correlation with the static pattern., *Deep foundations*

on bored and auger piles, BAP III : Proc. of the 3^{rd} *Int. Geotech. Seminar on Deep Foundations on Bored and Auger Piles, Balkema, Ghent.*

Clayton, C. R. I., Matthews, M. C. and Simons, N. E. (1995). *Site Investigation*, 2 edn, Blackwell Science Ltd.

Couldery, P. A. J. and Fleming, W. J. K. (1986). Continuous flight auger piling at St. Enoch square, Glasgow, *Ground Engineering* **19**(1): 17–28.

Decourt, L. (1982). Prediction of bearing capacity of piles based exclusively on N-values of the SPT, *Proc.* 2^{nd} *European symposium on Penetration testing* **1**: 29–34.

Derbishire, P. H., Turner, M. J. and Wain, D. E. (1989). Recent developments in continuous flight auger piling, *Proc.* 1^{st} *Int. Geotech. Sem. on Deep foundations on Bored and Auger piles* pp. 33–42.

England, M. (1994). New techniques for reliable pile installation and pile behaviour design and analysis, *Transportation Research Record* (1447): 39–48.

England, M. and Fleming, W. G. K. (1994). Review of foundation testing methods and procedures, *Proc. Instn. Civ. Eng. Geotechnical Engineering* **107**: 135–142.

ENV1997-1 (1997). Eurocode 7: Geotechnical design.

Fellenius, B. H. (1980). The analysis of results from routine load tests, *Ground Engineering* **13**(6): 19–31.

Fenoux, G. Y. and de Buysere, G. (1988). Starsol enbesol procedure, *Proc.* 1^{st} *Int. Geotech. Sem. on Deep foundations on Bored and Auger piles* pp. 325–331. Balkema, Ghent, Holland.

Fleming, W. G. K. (1995). The understanding of continuous flight auger piling, its monitoring and control, *Proc. Instn. Civ. Eng. Geotechnical Engineering* **113**: 157–165.

Fleming, W. G. K. and England, M. (2001). Locking pile behaviour, *Ground Engineering* **January**: 30–33.

Fleming, W. G. K. and Simpson, B. (1988). Auger injected piles, *Proc. Instn. Civ. Eng.* **84**(1): 1316–1319.

Golder, H. Q. and Leonard, M. W. (1954). Some tests on bored piles in London clay, *Geotechnique* **4**: 32–41.

Gui, M., Soga, K., Bolton, M. and Hamelin, J. (2002). Instrumented borehole drilling for subsurface investigation, *ASCE Journal of Geotechnical and Geoenvironmental Engineering* **128**(4): 283–291.

Hirayama, H. (1990). Load settlement analysis for bored piles using hyperbolic transfer function, *Soils and Foundations, JSSMFE* **1**(30): 55–64.

Hodgon, R. M. (1991). *A review of the design and construction of continuous flight auger piles*, Master's thesis, University of Surrey. MSc.

Hounsel, W. S. (1966). Pile load capacity estimates and test results, *Proc. ASCE* **92**: 1–30.

ICE (1988). *Specification for piling*, Thomas Telford. ISBN: 0 7277 1304 3.

ICE (1996). *Specification for piling and embedded retaining walls*, Thomas Telford. ISBN: 0 7277 2566 1.

Jaky, J. (1944). The coefficient of earth pressure at rest, *Journal for Society of Hungarian Architects and Engineers* pp. 355–358.

Jamiolkowski, M. and Lancellotta, R. (1988). Relevance of in-situ test results for evaluation of allowable base resistance of bored piles in sand, *Proc. 1^{st} Int. Geotech. Sem. on Deep foundations on Bored and Auger piles* pp. 107–119. Balkema, Ghent, Holland.

Kantartzi, C. (1993). *Ground movements during diaphragm wall installation in clays*, PhD thesis, Queen Mary and Westfield College, University of London.

Kirkpatrick, W. M. and Rennie, I. A. (1972). Directional properties of consolidated kaolin, *Geotechnique* **22**: 166–169.

Kirkpatrick, W. M. and Rennie, I. A. (1973). Clay structure in laboratory prepared samples, *Proc. Int. Symp. on Soil Structure* pp. 103–111.

Lacy, H. S., Moskowitz, J. and Merjan, S. (1994). Reduced impact on adjacent structures using augered cast-in-place piles, *Transportation research record* (1447): 19–26.

Lizzi, F. (1988). The load bearing capacity of bored piles, a problem not yet satisfactorily solved - some proposals, *Proc. 1st Int. Geotech. Sem. on deep foundations on bored and auger piles* pp. 443–450.

Lopes, F. R. and Laprovitera, H. (1988). On the prediction of the bearing capacity of bored piles from dynamic penetration tests, *Proc. 1st Int. Geotech. Sem. on Deep foundations on Bored and Auger piles* pp. 537–540. Balkema, Ghent, Holland.

McVay, M., Armaghani, B. and Casper, R. (1994). Design and construction of Auger-Cast piles in Florida, *Transportation Research Record* (1447): 10–18.

Meigh, A. C. (1987). Cone penetration testing methods and interpretation, *Ground engineering report: In situ testing*, CIRIA.

Menzies, B. K. and Merrifield, C. M. (1980). Measurements of shear stress distribution on the edges of a shear vane blade, *Geotechnique* **30**: 314–318.

Meyerhof, G. C. and Murdock, L. J. (1952). An investigation of the bearing capacity of some bored and driven piles in London clay, *Geotechnique* **3**: 267–282.

Meyerhof, G. G. (1956). Penetration tests and bearing capacity of cohesionless soils, *Journ. of the Geotech. Eng., ASCE* **82**(1): 1–19.

Meyerhof, G. G. (1976). Bearing capacity and settlement of pile foundations, *ASCE Jour. Geot. Eng. Div.* **102**: 197–228.

Meyerhof, G. G. (1983). Scale effects of ultimate pile capacity, *Journ. of the Geotech. Eng., ASCE* **109**(6): 797–806.

Milititsky, J. (1983). *Installation of bored piles in stiff clays: an experimental study of local changes in soil conditions*, PhD thesis, University of Surrey.

Modhorst, C. (1988). The ultimate bored pile load capacity in granular soils: A case history against the current effective stress design theory in comparison to a penetration based method, *Proc. 41st Int. Geotech. Sem. on Deep foundations on Bored and Auger piles* pp. 451–456.

Mohan, D. and Chandra, S. (1961). Frictional resistance of bored piles in stiff clays, *Geotechnique* **2**: 294–301.

Mohan, D., Jain, G. S. and Jain, M. P. (1967). A new approach to load tests, *Geotechnique* **17**: 274–283.

Neely, W. J. (1991). Bearing capacity of auger-cast piles in sand, *Journal of Geotechnical Engineering* **117**(1): 331–345.

O'Neill, M. W. (1994). Review of augered pile practice outside the united states, *Transportation Research Record* (1447): 3–9.

Parry, R. H. G. and Swain, C. W. (1977). A study of skin friction on piles in stiff clays, *Ground engineering* **10**(8): 33–37.

Patel, D. C. (1992). Interpretation of results of pile tests in London Clay, *Piling Europe.* Thomas Telford.

Peck, R. (1973). Discussion, *Proc. 8th. Int. Conf. S.M.F.E.* pp. 73–77.

Philipponnat, G. (1980). Methode practique de calcul d'un pieu isole a l'aide du penetrometre statique, *Revue Francaise de Geotechnique* **10**: 55–64.

Potyondy, J. G. (1961). Skin friction between various soils and construction materials, *Geotechnique* **11**: 339–355.

Price, G. and Wardle, I. F. (1982). Comparison between cone penetration test results and the performance of small diameter instrumented piles in stiff clay, *Proc. 2nd Euro. Symp. on penetration testing* **2**: 775–780.

Reese, L. C. and O'Neill, M. W. (1988). Field load tests of drilled shafts, *Proc. 1st Int. Geotech. Sem. on Deep foundations on Bored and Auger piles* pp. 145–191. Balkema, Ghent, Holland.

Rogers, C. D. F., Glendinning, S. and Roff, T. E. J. (1997). Lime modification of clay soils for construction expediency, *Proceedings of the Institution of Civil Engineers, Geotechnical Engineering* **125**: 242–249.

Ruiter, J. D. and Beringen, F. L. (1979). Pile foundations for large north sea structures, *Marine Geotechnology* **3**(3): 267–314.

Schmertmann, J. H. (1978). Guidelines for cone penetration test, performance and design, *U.S. Dept. of Transportation, FHWA-TS-78-209.*

Schwartz, K., A'Bear, A. G. and Strydom, J. H. (1999). Capacity of Continuous Flight Auger piles in the Johannesburg CBD, *Proc.* 12^{th} *regional Conf. for Africa on soil mechanics and geotechnical engineering: 'Geotechnics for developing Africa'.*

Seward, D. W., Scott, J. N., Dixon, R., Findlay, J. D. and Kinniburgh, H. (1997). The automation of piling rig positioning using satellite GPS, *Automation in Construction* **6**(3): 229–240.

Sherwood, P. T. (1993). *Soil stabilisation with cement and lime*, London: HMSO.

Skempton, A. W. (1959). Cast in-situ piles in London Clay, *Geotechnique* **9**: 153–173.

Smith, E. A. L. (1960). Pile driving analysis by the wave equation, *ASCE Journal of Soil Mechanics and Foundations* **86**: 36–61.

Snow, R. (Fall 1965). Telltales, *Foundation facts, Raymond International* pp. 12–13.

Svinkin, M. R. and Woods, R. D. (1998). Accuracy of determining pile capacity by dynamic methods, *Proc. of* 7^{th} *Int. Conf. and exhibition on piling and deep foundations* pp. 121–128. Vienna, Austria.

Taylor, D. W. (1948). *Fundamentals of soil mechanics*, Wiley, New York.

Tchepak, S. (1998). The performance of CFA piles in residual clays, *Proc.* 3^{rd} *Int. Geotech. Sem. on Deep foundations on Bored and Auger piles* pp. 349–354.

Teale, R. (1965). The concept of specific energy in rock drilling, *Int. Jour. on Rock Mechanics and Mining Science.*

Terzaghi, K. (1944). *Theoretical soil mechanics*, Wiley, New York.

Thorburn, S., Greenwood, D. A. and Fleming, W. G. K. (1993). The response of sands to the construction of CFA piles, *Proceedings of the international conference on deep foundations on bored and auger piles* pp. 1–15. Balkema, Rotterdam.

Tomlinson, M. J. (1994). *Pile design and construction practice*, 4^{th} edn, E & F N Spon.

Troughton, V. (2002). Case history of the west quay centre, southampton, Presentation given to the Southern Group of the British Geotechnical society.

van Impe, W. F., van Impe, P. O., Viggiani, C., Russo, G. and Bottiau, M. (1998). Load settlement behaviour versus distinctive α pile execution parameters, *Deep foundations on bored and auger piles* pp. 335–366.

van Weele, A. F. (1988). Cast-in-situ piles: Installation methods, soil disturbance and resulting pile behaviour, *Deep foundations on bored and auger piles* pp. 219–226.

Wheeler, P. (1999). Scattering predictions, *New Civil Engineer* **2**: 34.

Whitaker, T. (1957). Experiments with model piles in groups, *Geotechnique* **7**: 147–167.

Whitaker, T. (1963). The constant rate of penetration test for determination of the ultimate bearing capacity of a pile, *Proc. Int. Civ. Eng.* **26**: 119–123.

Whitaker, T. and Cooke, R. W. (1961). A new approach to pile testing, *Proc. 5th Int. Conf. on S.M.F.E* **2**: 171–176. Paris.

Whitaker, T. and Cooke, R. W. (1966). An investigation of the shaft and base resistances of large bored piles in London Clay, *Large bored piles.*

Wright, S. J. (1979). Design of large diameter bored piles, *Ground engineering* **112**(8): 17–23.

Wroth, C. P. (1984). The interpretation of in-situ soil tests, *Geotechnique* **34**(4): 449–489. Rankine lecture.

Zelikson, A. (1988). Examination of some common rules for bored piles against hydraulic gradient model results, *Proc. 1st Int. Geotech. Sem. on Deep foundations on Bored and Auger piles* pp. 507–519. Balkema, Ghent, Holland.

Appendix A

Results from a set of experiments aimed at assessing the influence of auger lead on torque and load measured on the auger (auger penetration test results)

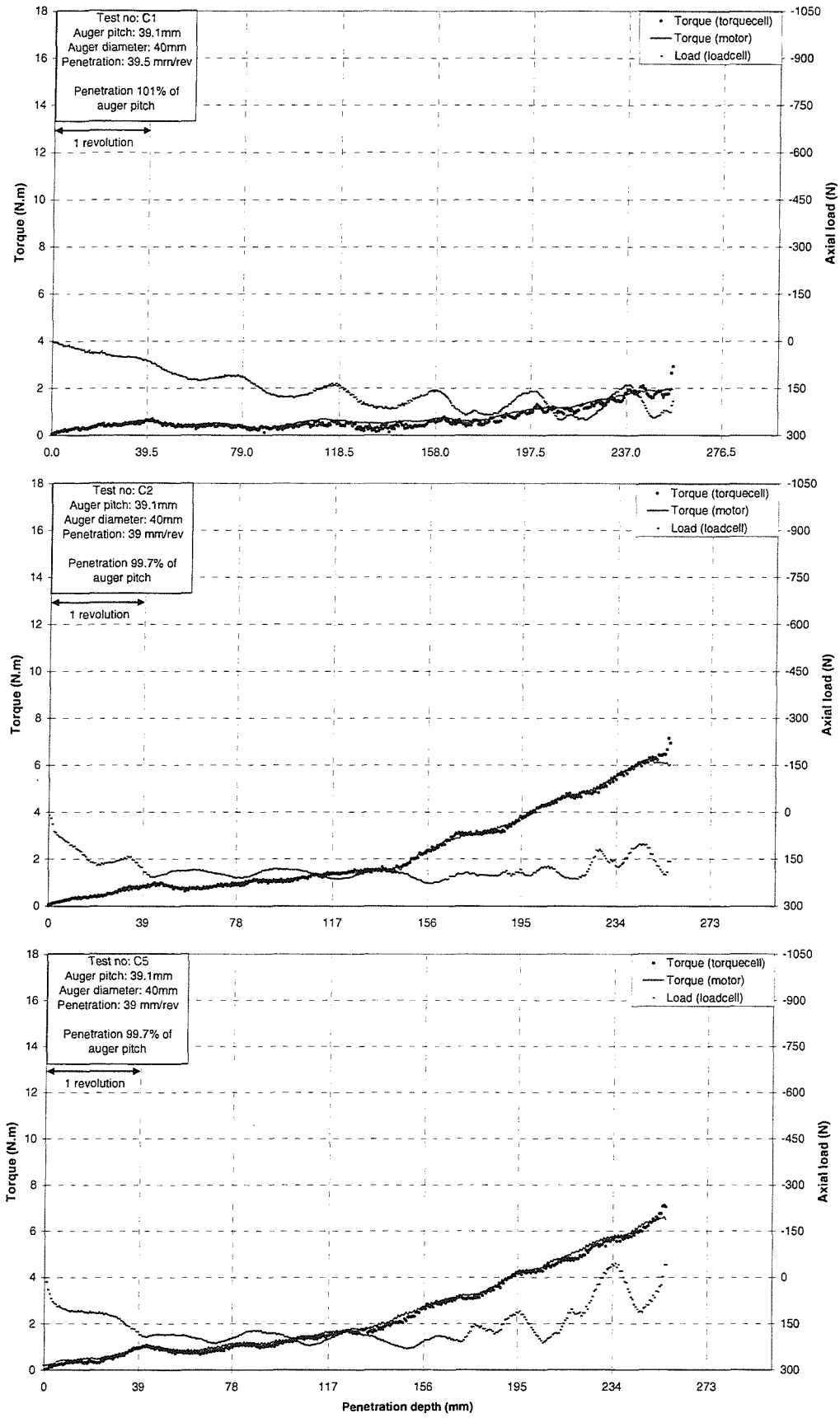

Figure A.1: Test C1, C2 and C5 on the 40mm OD auger

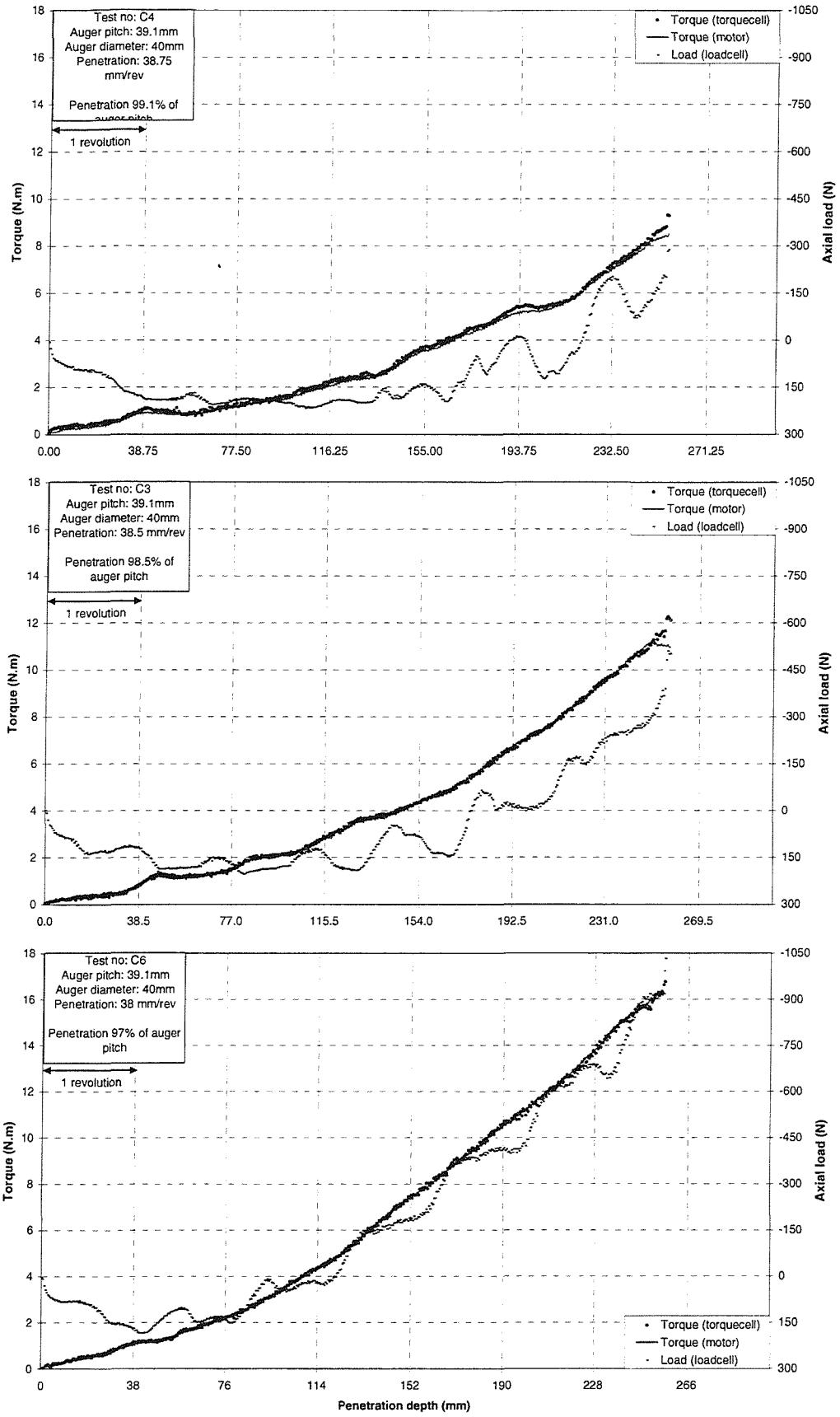

Figure A.2: Test C4, C3 and C6 on the 40mm OD auger

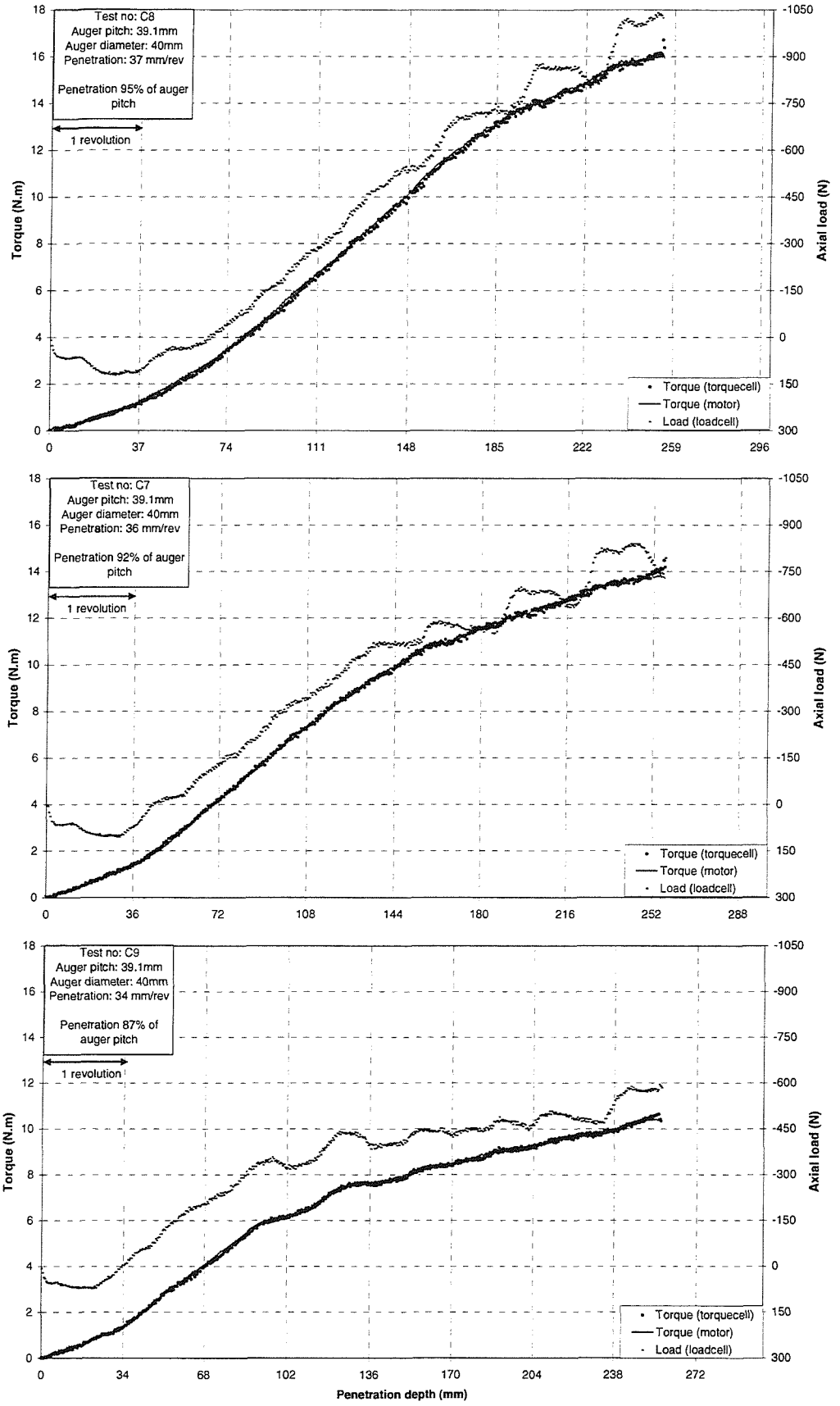

Figure A.3: Test C8, C7 and C9 on the 40mm OD auger

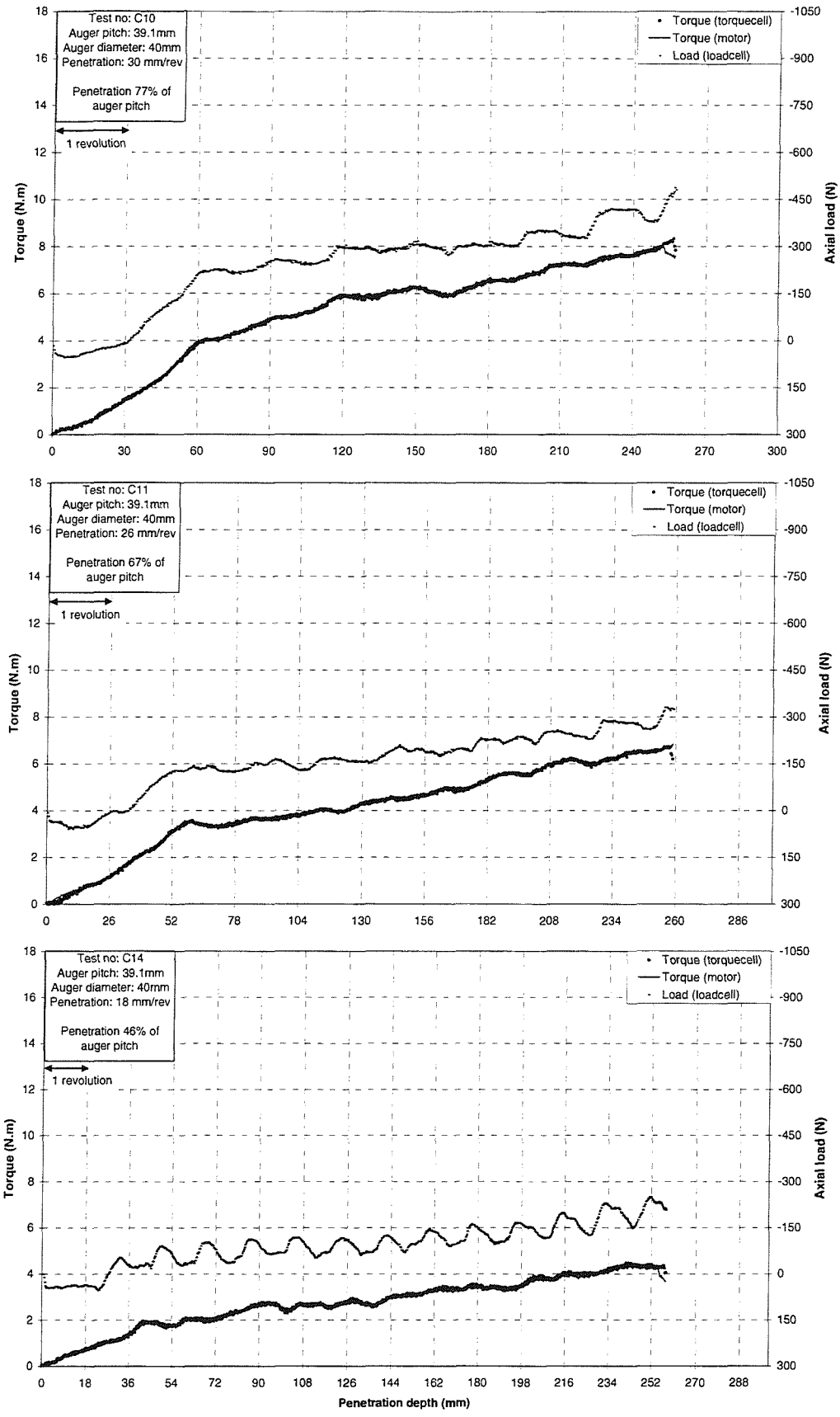

Figure A.4: Test C10, C11 and C14 on the 40mm OD auger

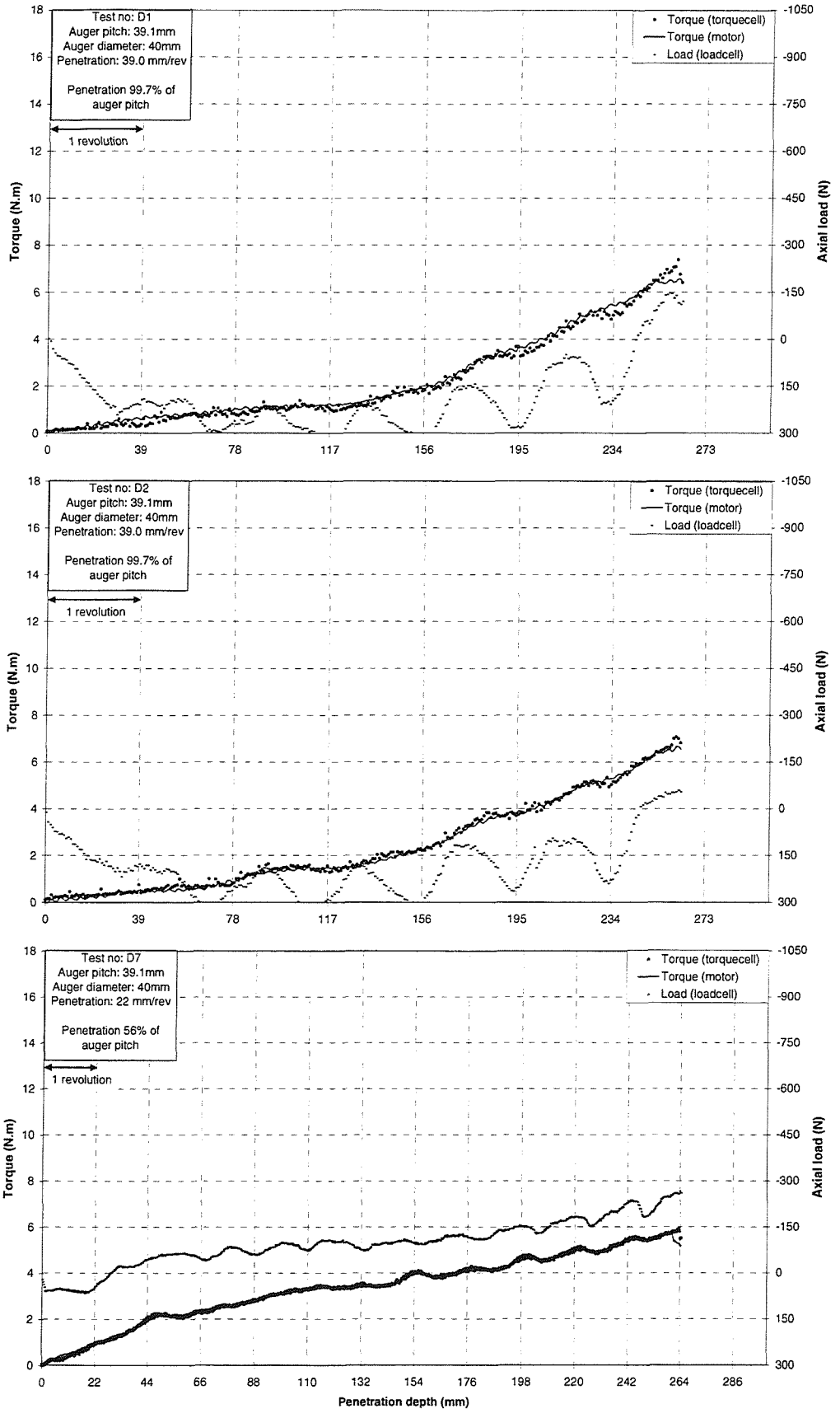

Figure A.5: Test D1, D2 and D7 on the 40mm OD auger

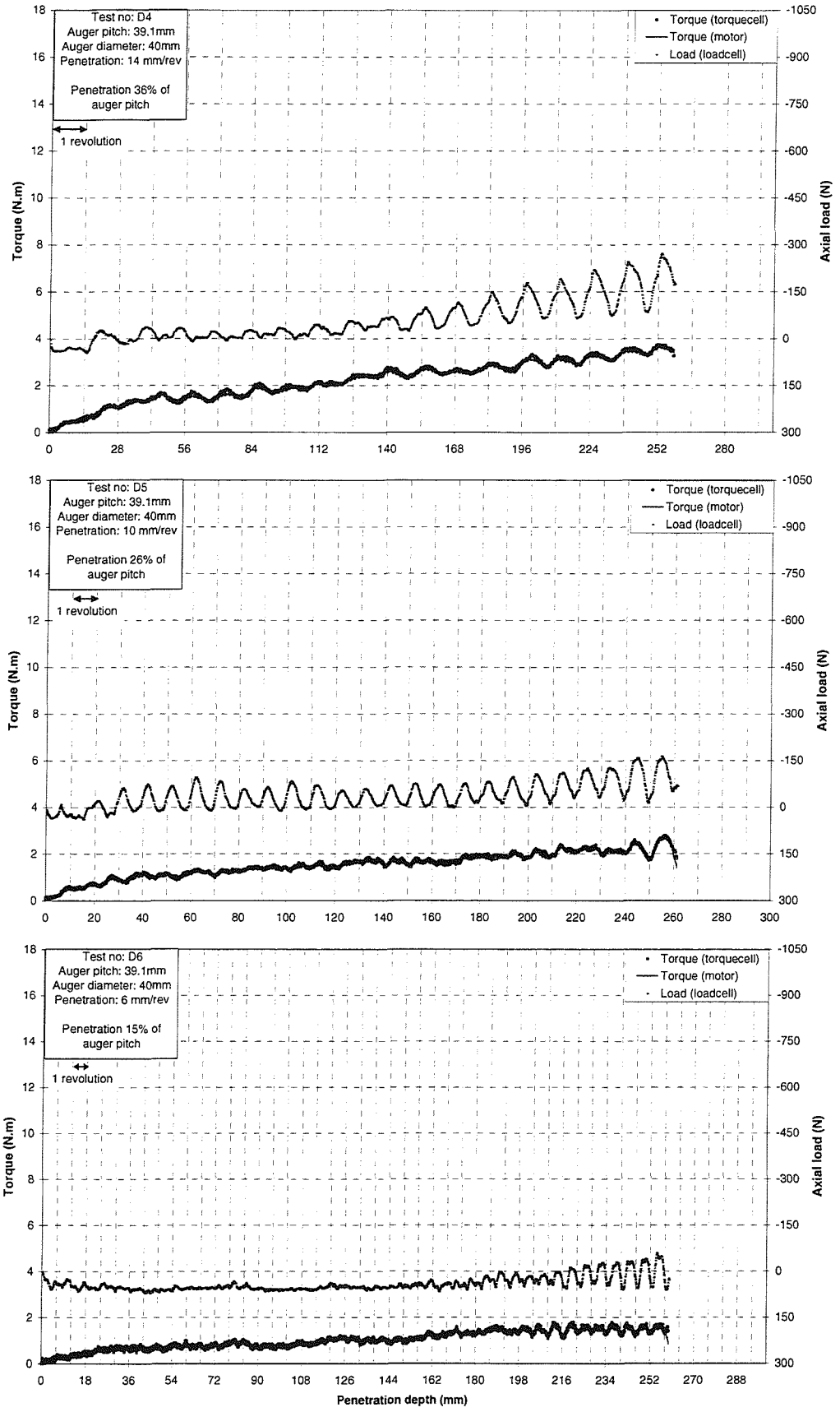

Figure A.6: Test D4, D5 and D6 on the 40mm OD auger

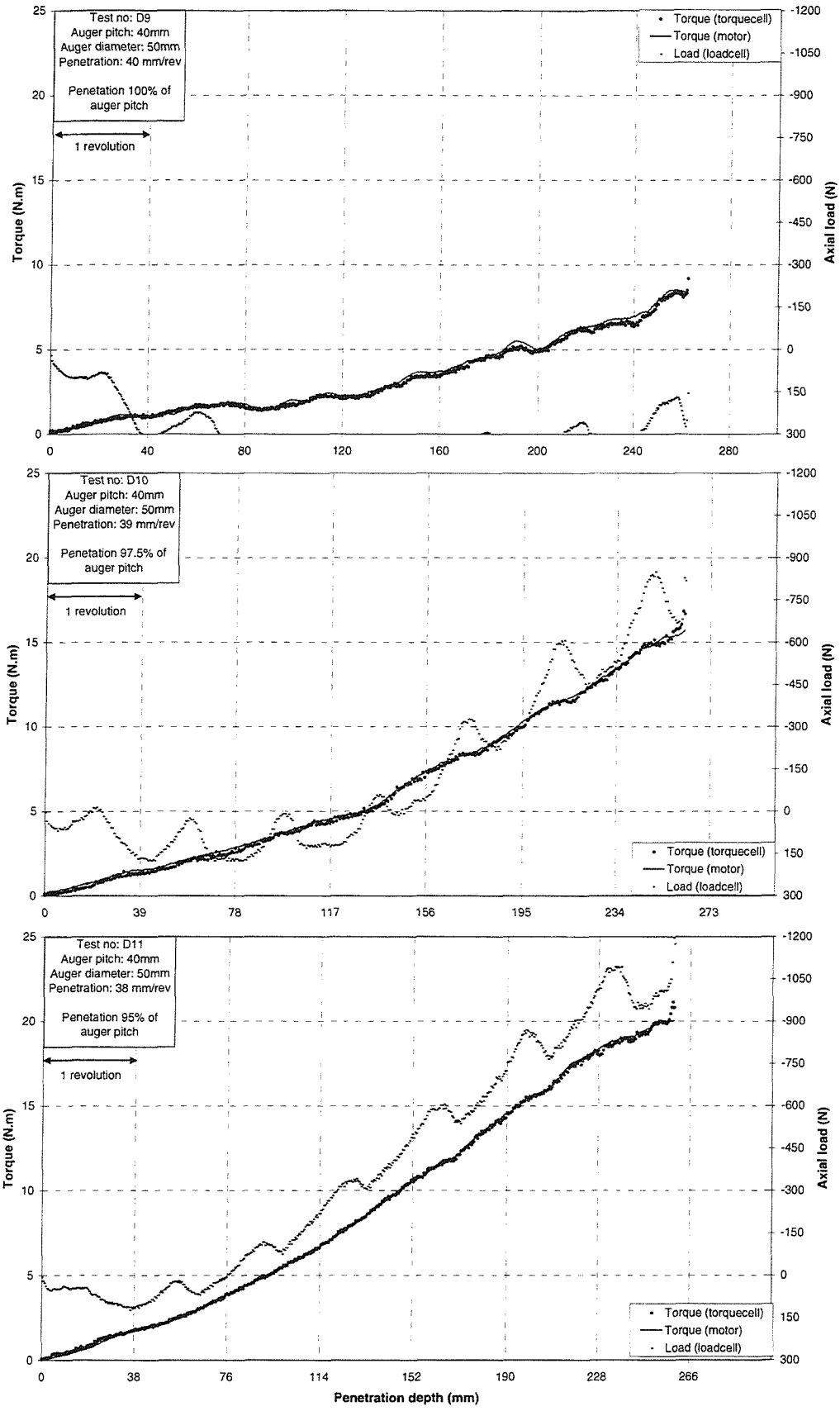

Figure A.7: Test D9, D10 and D11 on the 50mm OD auger

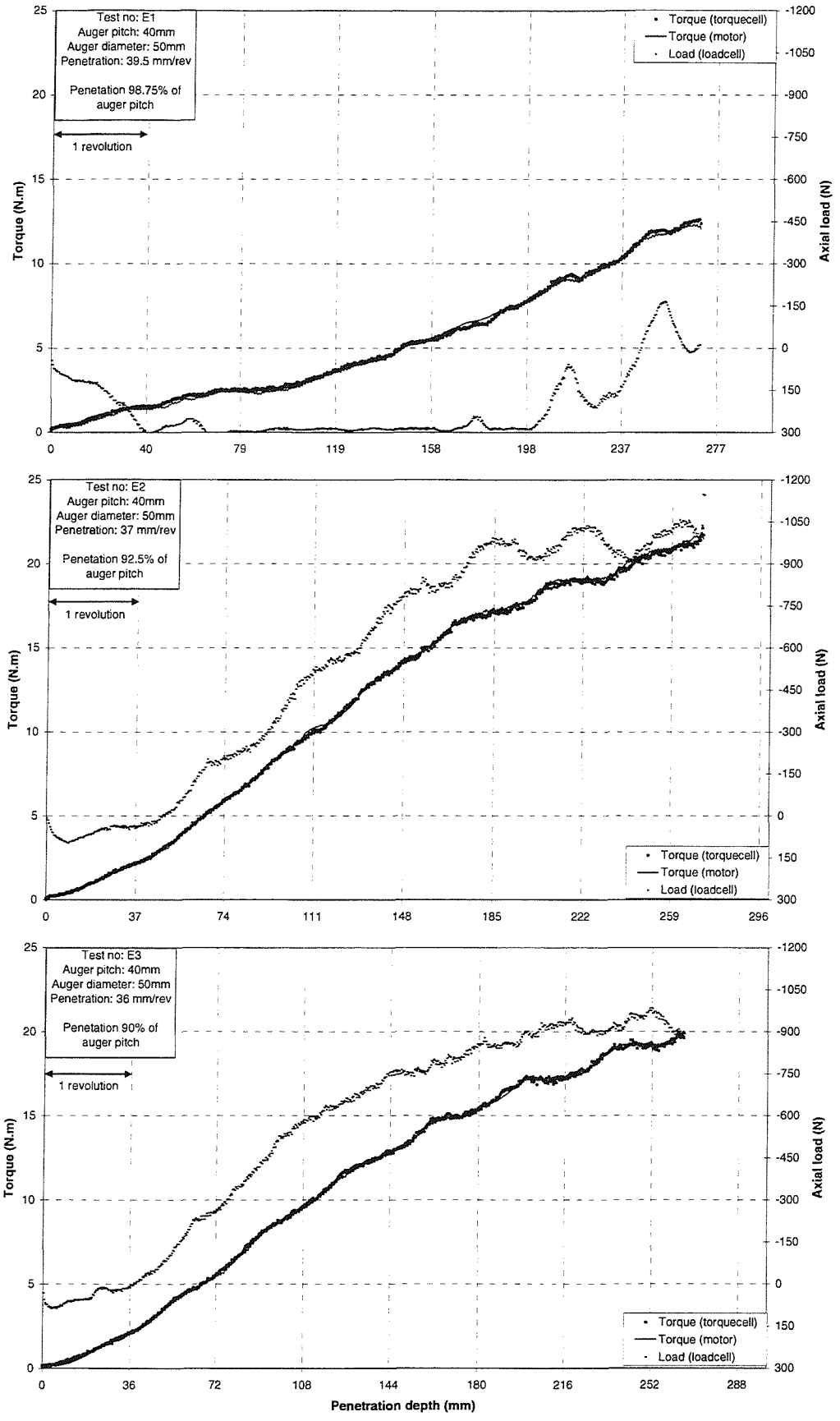

Figure A.8: Test E1, E2 and E3 on the 50mm OD auger

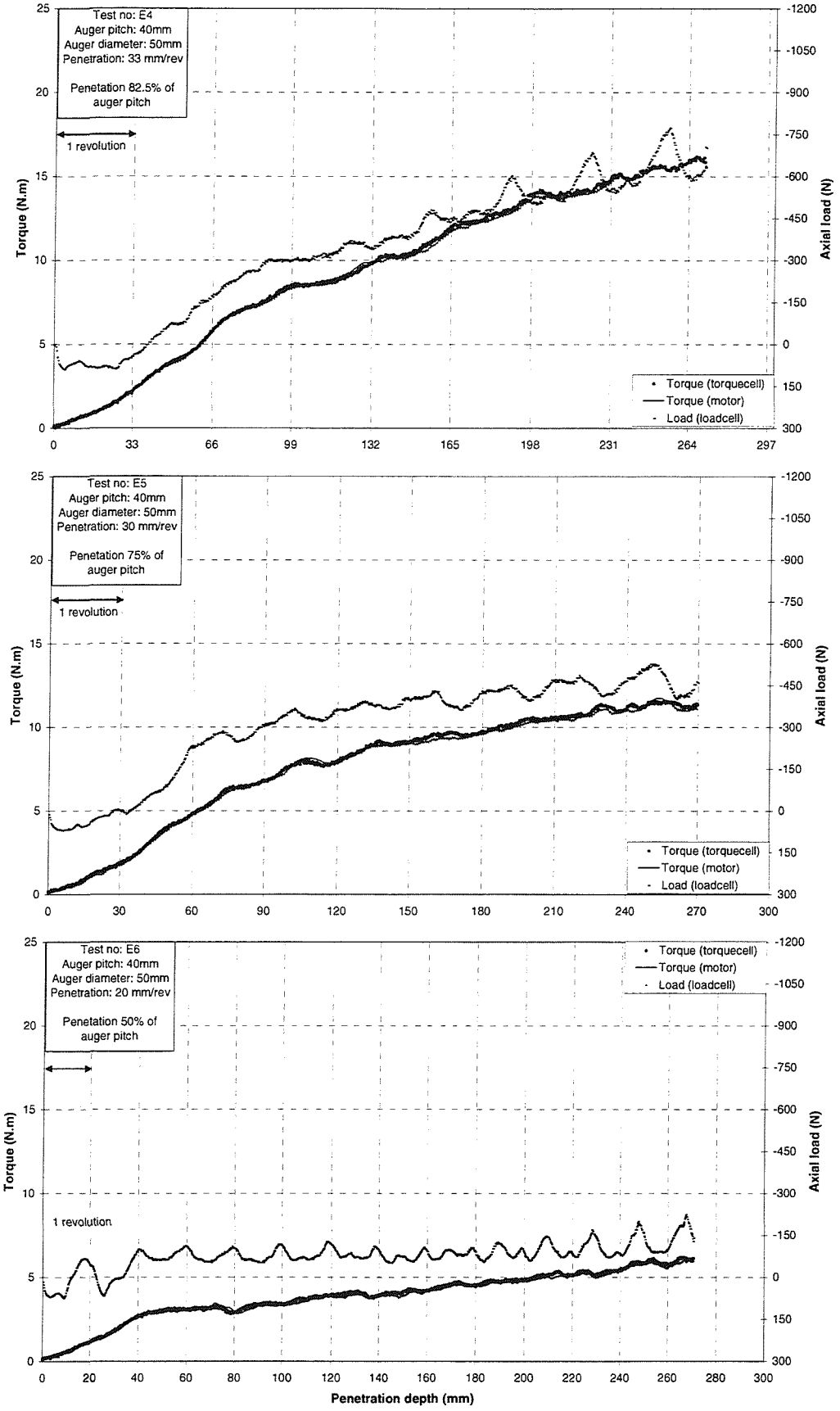

Figure A.9: Test E4, E5 and E6 on the 50mm OD auger

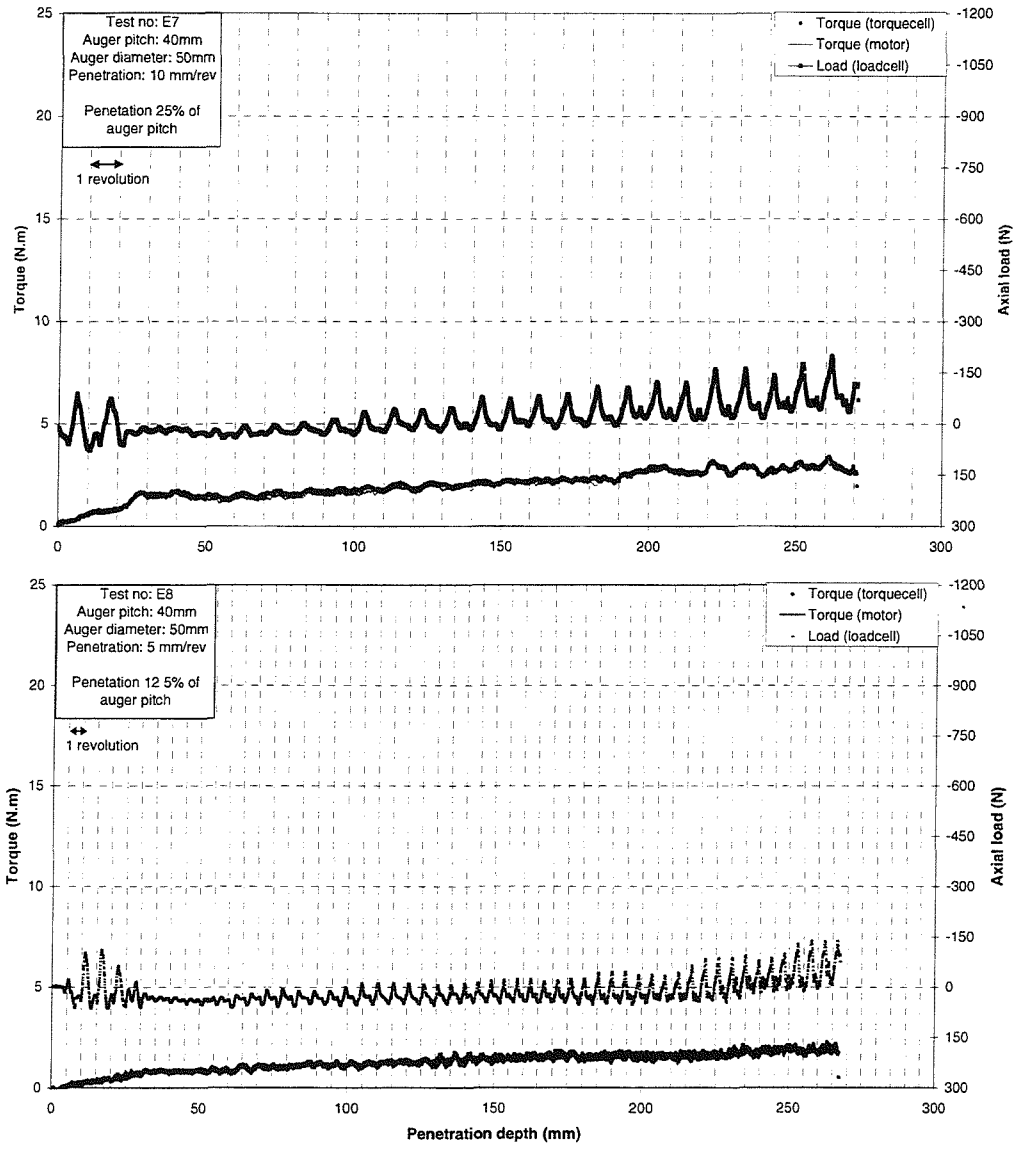

Figure A.10: Test E7 and E8 on the 50mm OD auger

Appendix B

Derivation of the formulae used in the thesis

Figures B.1(a) and B.1(b) illustrate the basic geometry of an auger with a single flight. The variables P, D, d and l uniquely define the auger geometry

where: P = the pitch of the auger;
D = the outer diameter of the auger;
d = the inner diameter of the auger and
l = the length of the auger.

B.1 The surface area of the auger (A_{aug})

We start by calculating the surface area of an auger one pitch long (A_p). The surface area of the auger is a composite area, consisting of the auger flight (A_{fl}) and the auger stem (A_{st}). At any radius r_0 (from $d/2$ to $D/2$) we may calculate the *circumference* of the auger L_0 by

$$L_0 = \sqrt{(2\pi r_0)^2 + P^2} \tag{B.1}$$

In order to calculate A_{fl} we choose a differential ring as shown in Figure B.2. A_{fl} is thus

$$A_{fl} = \int_{d/2}^{D/2} \sqrt{(2\pi r_0)^2 + P^2} dr_o \tag{B.2}$$

which, when integrated, becomes

$$A_{fl} = \left(\frac{D}{4}\sqrt{\pi^2 D^2 + P^2} + \left(P^2 log(2\pi D + 2\sqrt{\pi^2 D^2 + P^2})\right)/4\pi\right) - \left(\frac{d}{4}\sqrt{\pi^2 d^2 + P^2} + \left(P^2 log(2\pi d + 2\sqrt{\pi^2 d^2 + P^2})\right)/4\pi\right) \quad \text{(B.3)}$$

and A_{st} is equal to

$$A_{st} = \pi d P \quad \text{(B.4)}$$

A_p is equal to two times A_{fl} (top and bottom flight surface) plus A_{st}

$$A_p = 2A_{fl} + A_{st} \quad \text{(B.5)}$$

Finally the surface area of an auger of length l (A_{aug}), is calculated by

$$A_{aug} = \frac{l}{P} A_p \quad \text{(B.6)}$$

B.2 The torque lever arm on the auger (r_t)

The lever arm of the torque applied to the auger is calculated by determining a weighted distance of the area of the auger from the polar axis, z-z. The first moment of area around the polar axis (I_z) is calculated using an integral of the form

$$I_z = \int r dA \quad \text{(B.7)}$$

In order to calculate I_z of the auger, the values of I_z of all the surfaces that the auger is composed of are calculated separately and then added together. Calculations are again done on a section of auger length equal to P. Care is taken to calculate all of the I_z values around the same axis (i.e. the polar axis z-z on Figure B.1(a)). I_z for the inner stem of the auger (I_{z1}) is simply

$$I_{z1} = (\pi d P)\frac{d}{2} \quad \text{(B.8)}$$

We choose a differential ring, as shown in Figure B.2, to calculate I_z for one side of the auger flight (I_{z2}), and thus

$$I_{z2} = \int_{d/2}^{D/2} r_0 \sqrt{(2\pi r_0)^2 + P^2} dr_o \quad \text{(B.9)}$$

which, when integrated, becomes

$$I_{z2} = (\frac{P^2}{12\pi^2} + \frac{D^2}{12})\sqrt{P^2 + \pi^2 D^2} - (\frac{P^2}{12\pi^2} + \frac{d^2}{12})\sqrt{P^2 + \pi^2 d^2} \quad \text{(B.10)}$$

By using Equations B.8 and B.10 we may now calculate I_z as

$$I_z = I_{z1} + 2I_{z2} \quad \text{(B.11)}$$

The weighted distance of area of the auger is

$$r_t = \frac{I_z}{A_p} \quad \text{(B.12)}$$

B.3 Force and moment equilibrium of a fully-loaded auger

Figure B.3 is a free body diagram showing all the forces and stresses imposed on the auger. The following forces and stresses have been identified:

- the axial load on the auger (F),
- the torque applied to the auger (T),
- the weight of the auger (W),
- resistance to penetration of the inner stem (f_{st}),
- resistance to the cutting action of the auger (f_{cut}),
- normal stresses:
  - on the top of the auger flight (N_t),
  - on the bottom of the auger flight (N_b),
  - on the auger stem (N_{st}),
- shear stresses:
  - on the top of the auger flight (τ_t),
  - on the bottom of the auger flight (τ_b) and
  - on the auger stem (τ_{st}).

The angle of the auger flight with the horizontal, β, as a function of r_0 is

$$\beta = tan^{-1}\frac{P}{2\pi r_0} \tag{B.13}$$

In the force and moment equilibrium equations '-v' or '-t' will be added to the subscript of terms to indicate wether the vertical or torsional components are being referred to (for example the vertical component of the force normal to the top of the auger flight (N_t) is referred to as N_{t-v}).

Force equilibrium: $[\sum F_p = 0]$

$$F + N_{t-v} + W - N_{b-v} - \tau_{t-v} - \tau_{b-v} - \tau_{st}A_{st}sin\beta_r - f_{st} - f_{cut-v} = 0 \tag{B.14}$$

where: $N_{t-v} = \frac{l}{P}\int_{d/2}^{D/2} N_t L_0 cos\beta dr_0,$

$N_{b-v} = \frac{l}{P}\int_{d/2}^{D/2} N_b L_0 cos\beta dr_0,$

$\tau_{t-v} = \frac{l}{P}\int_{d/2}^{D/2} \tau_t L_0 sin\beta dr_0,$

$\tau_{b-v} = \frac{l}{P}\int_{d/2}^{D/2} \tau_b L_0 sin\beta dr_0,$

$\beta_r = tan^{-1}\frac{P}{2\pi r}$ and

and f_{cut-v} is

$$f_{cut-v} = f_{cut}sin\left((tan^{-1}(P/\pi D) + tan^{-1}(P/\pi d))/2\right) \tag{B.15}$$

Moment equilibrium: $[\sum M_p = 0]$

$$\begin{aligned} &T + N_{t-t}(r_{fl}) - N_{b-t}(r_{fl}) - \tau_{t-t}(r_{fl}) - \tau_{b-t}(r_{fl}) \\ &-\tau_{st}A_{st}cos\beta_r(d/2) - f_{cut-t}(d/2 + (D/2 - d/2)/2) = 0 \end{aligned} \tag{B.16}$$

where: $N_{t-t} = \frac{l}{P}\int_{d/2}^{D/2} N_t L_0 sin\beta dr_0,$

$N_{b-t} = \frac{l}{P}\int_{d/2}^{D/2} N_b L_0 sin\beta dr_0,$

$\tau_{t-t} = \frac{l}{P}\int_{d/2}^{D/2} \tau_t L_0 cos\beta dr_0,$

$\tau_{b-t} = \frac{l}{P}\int_{d/2}^{D/2} \tau_b L_0 cos\beta dr_0,$

$$r_{fl} = \frac{\int_{d/2}^{D/2} r_0 \sqrt{(2\pi r_0)^2 + P^2} dr_o}{A_{fl}}.$$

and f_{cut-t} is

$$f_{cut-t} = f_{cut} cos\left((tan^{-1}(P/\pi D) + tan^{-1}(P/\pi d))/2\right) \quad \text{(B.17)}$$

We may assume that the shear stress on the auger surface is constant, therefore $\tau_t = \tau_b = \tau_{st} = \tau_{aug}$. We may however *not* assume that the stresses normal to the surfaces are equal. Stresses in the soil matrix will cause these to be different. It is after all possible to advance the auger into the soil when applying an axial load in the direction opposite to auger movement. In Equation B.14 the sense of F will then reverse and the only positive axial loads will be the weight of the auger and the component of the normal load on the top of the auger flight in the vertical direction (N_{t-v}). As F has often been measured to be much larger than the weight of the auger (see model test results for magnitude of F), the magnitude of N_{t-v} must be larger than N_{b-v} to satisfy equilibrium. We are therefore left with the following variables:

- resistance to penetration of the inner stem (f_s),
- resistance to the cutting action of the auger (f_{cut}),
- the weight of the auger (W),
- normal stresses:
  - on the top of the auger flight (N_t),
  - on the bottom of the auger flight (N_b)and
- shear stress on the auger surface (τ_{aug}).

The fact that the six variables exceed the two equations make the system statically indeterminate. An approximate solution was therefore used.

B.4 Approximate solution: Calculation of the shear stress on the auger surface of a fully-loaded auger

As the force and moment equilibrium equations could not be solved due to the number of variables in the equations exceeding the number of equations,

an approximate solution was attempted. The results from the model auger tests were used to check the validity of the approximate solution. This section is only applicable to auger lead values in excess of the maximum load and torque lines, therefore:

- the flight of the auger is completely filled with soil (i.e. soil is in contact with the top and the bottom of the auger flight) and
- the soil on the soil boundary has not been sheared.

In the preliminary auger tests it was shown that when no axial load is applied to the auger, the amount of torque required to turn the auger at a certain depth is fixed. There should therefore be a function $T(l)$ that describes the torque required to turn a specific auger if no axial load is applied. As the surface area of the auger increases linearly with increase in depth, we expect $T(l)$ to be of the form

$$T(l) = c_1 l + c_2 \tag{B.18}$$

where $c_1 l$ describes a linear increase of torque with increase in auger depth, and c_2 describes a constant amount of torque that needs to be applied to the auger to overcome the constant resistance at the tip of the auger.

Results from the model tests showed that as axial load on the auger was increased (downward), the torque required to turn the auger decreased (see for example test C1 in Appendix A). There should therefore be a function $F(l)$ that describes the axial load required to turn a specific auger if no torque is applied to the auger. Again the surface area of the auger increases linearly with depth, and therefore we expect $F(l)$ to be of the form

$$F(l) = c_3 l + c_4 \tag{B.19}$$

where $c_3 l$ describes a linear increase of axial load with increase in auger depth, and c_4 the constant amount of axial load that needs to be applied to the auger to overcome the constant resistance required to advance the tip of the auger.

A combination of torque and axial load can also be applied to the auger to overcome the resistance of the auger. Again the increase in resistance of the auger with depth should be linear and therefore

$$f(T) + f(F) = c_5 l + f \tag{B.20}$$

and again $c_5 l$ describes the linear increase of auger resistance with depth, and f describes the constant resistance at the auger tip. The moment applied to the auger may also be described by a force and lever arm.

Because of the nature of the undrained behaviour of clay, shear stress on the auger surface will be constant over the surface area of the auger. If we therefore assume that the resistance of the auger is directly proportional to the surface area of the auger [1], we may calculate an approximate value for the lever arm as r_t (see Section B.2). This value for the lever arm is approximate because it does not take into account the resistance at the tip of the auger.

Next we estimate $f(T)$ and $f(F)$ by calculating the components of the torque and axial load in the direction of movement of the auger. We begin by defining the angle of direction of movement of the auger (ψ)

$$\psi = tan^{-1}(\frac{L}{2\pi r_t}) \tag{B.21}$$

where L is the lead of the auger (vertical advance of the auger per revolution). Again this equation ignores the forces at the tip of the auger and will therefore be inaccurate especially at the start of penetration. The component of axial load in the direction of auger movement ($f(F)$) is

$$f(F) = Fsin\psi \tag{B.22}$$

where F is the axial load applied to the auger. Note that the direction of the force needs to be taken into account as the direction of movement is often opposite to that of the applied load (as before we have chosen positive notation as downwards). The component of torque in the direction of auger movement, converted to a load by using the lever arm is

$$f(T) = \frac{T}{r_t} cos\psi \tag{B.23}$$

where T is the torque applied to the auger. Note that the direction of the torque also needs to be taken into account. Positive torque notation corresponds to the direction of rotation required to advance the auger (clockwise for the augers used in the experiments).

We therefore find that

$$\frac{T}{r_t} cos\psi + Fsin\psi = c_5 l + f \tag{B.24}$$

[1] This assumption will be inaccurate at the start of penetration as the resistance at the tip of the auger will be a significant proportion of the total resistance of the auger

It is possible to check the validity of the equation with the model auger test results. Figure B.4 shows that the increase of $\frac{T}{r_t}cos\psi + Fsin\psi$ (named 'Auger resistance (N)' on the graph) with depth is approximately linear, indicating that the assumptions made deriving Equation B.24 were reasonable.

If we define τ_{aug} as the shear stress on the auger surface, we may estimate the value of $c_5 l$ as $A_{aug}\tau_{aug}$, and by using the model test results, obtain a value for both τ_{aug} and f. Equation B.24 may now be written as

$$\frac{T}{r_t}cos\psi + Fsin\psi = A_{aug}\tau_{aug} + f \tag{B.25}$$

As shown in Figure 5.5 a unique value for f (34N) exists that yields a constant and unique value for τ_{aug} (24kPa) for the 40mm diameter auger. This value for τ_{aug} seems reasonable compared to values found in the literature, once again indicating that the assumptions made were reasonable.

B.5 Force and moment equilibrium on a partially-loaded auger

When the auger lead is significantly less than the auger pitch, the following assumptions are made:

- the flight of the auger is not filled with soil (i.e. soil is not in contact with the bottom of the auger flight and only in contact with a part of the inner stem and the top of the auger flight) and
- soil on the soil boundary has been sheared.

Figure B.3 is a free body diagram showing all the forces and stresses imposed on the auger partially-loaded with soil. The following forces and stresses have been identified (Figure: B.5):

- the axial load on the auger (F),
- the torque applied to the auger (T),
- the weight of the auger (W),
- the weight of the soil on the auger (W_s),
- resistance to penetration of the inner stem (f_s),
- resistance to the cutting action of the auger (f_{cut}),

- normal stress on the bore wall or soil boundary (N_{so}) and
- shear stress on the bore wall or soil boundary (τ_{so}).

An auger will be fully-loaded when penetrating at a lead value equal to or greater than

$$L_{full} = 100\left(1 - \frac{V_{aug}}{V_{bore}}\right) \tag{B.26}$$

where: V_{aug} = the volume of the auger,
V_{bore} = the volume of the bore and

This equation takes into account the fact that the auger must displace its own volume into the soil matrix. This volume will preferentially be displaced onto the auger flight if the auger flight is only partially-loaded because of less restraint to displacement in that direction. The angle of soil movement with the horizontal, α, is

$$\alpha = tan^{-1}\left(\frac{L}{\pi D}\right) + tan^{-1}\left(\frac{V_{aug}}{V_{bore}}\right) \tag{B.27}$$

where: L = the lead of the auger (vertical advance per revolution).

This equation takes into account the fact that soil will move in the opposite direction to the edge of the auger flight plus a vertical amount because of the displacement of the auger volume into the soil matrix. In the force and moment equilibrium equations -v or -t will be added to the subscript of the terms to indicate wether the vertical or torsional components are being referred to.

Force equilibrium: $[\sum F_p = 0]$

$$W + W_s - F - f_s - f_{cut-v} + \tau_{so}A_{soil}sin\alpha = 0 \tag{B.28}$$

where f_{cut-v} is described by Equation B.15.

Moment equilibrium: $[\sum M_p = 0]$

$$T - \tau_{so}A_{soil}cos\alpha(D/2) - f_{cut-t}(d/2 + (D/2 - d/2)/2) = 0 \tag{B.29}$$

where f_{cut-v} is described by Equation B.17.

Next we calculate the contact area on the boundary between soil on the auger and soil surrounding the auger (the soil boundary)

$$A_{soil} = \pi D l \left(1 - \frac{L_{full} - L_{\%}}{100}\right) \tag{B.30}$$

The following variables are left:

- resistance to penetration of the inner stem (f_s),
- resistance to the cutting action of the auger (f_{cut}),
- the weight of the auger (W),
- the weight of soil on the auger (W_{so}) and
- shear stress on the soil boundary (τ_{so}).

Although the number of variables exceed the number of equations, we may make an assumption in order to approximate the values of τ_{so}.

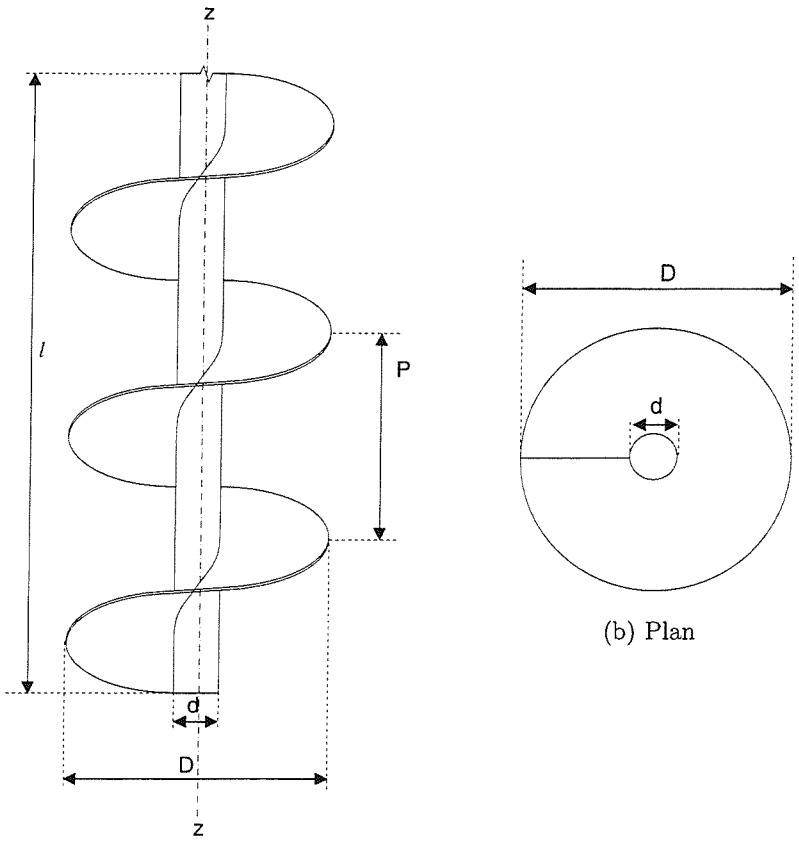

(a) Elevation

(b) Plan

Figure B.1: Basic geometry of a single flight auger

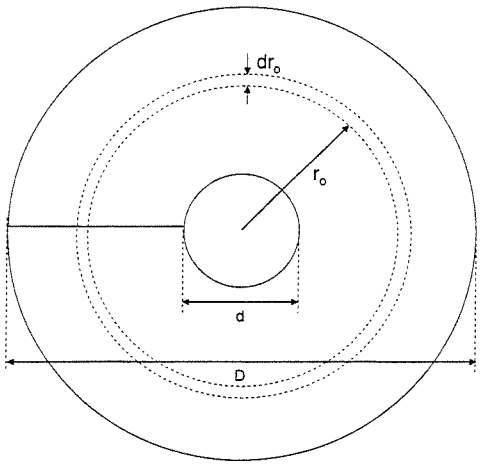

Figure B.2: Illustration of the differential element used to calculate A_{aug} and I_z

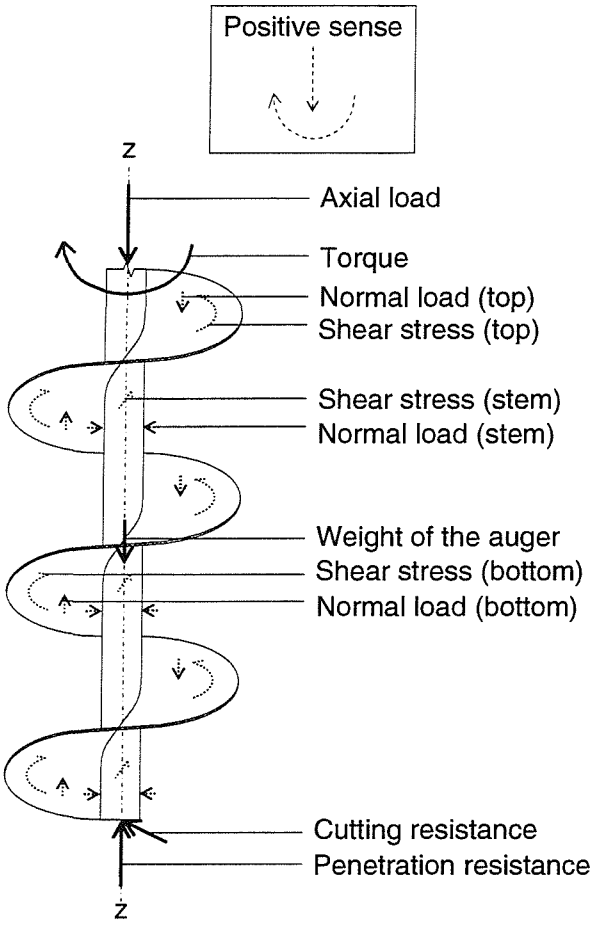

Figure B.3: Free body diagram of the auger

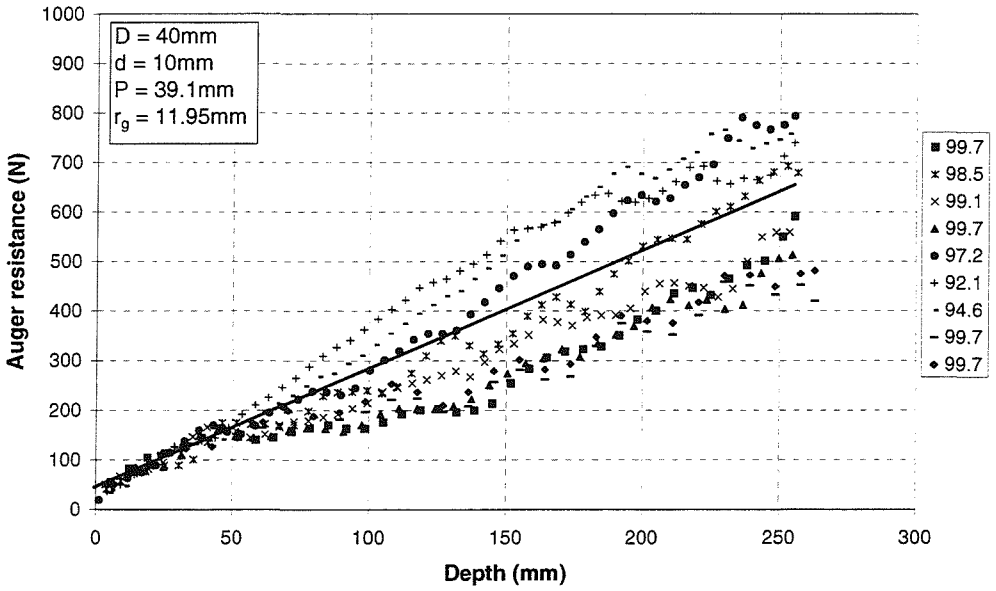

Figure B.4: Data from the auger test results showing the increase in auger resistance with depth

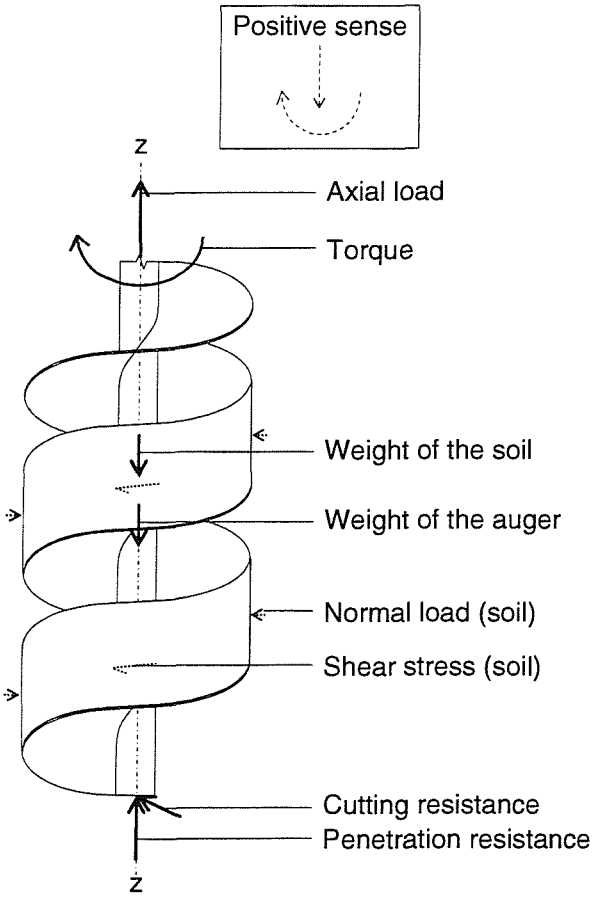

Figure B.5: Free body diagram of the auger partially filled with soil